Durham University

Durham E-Theses

Integrated characterisation of mud-rich overburden sediment sequences using limited log and seismic data: Application to seal risk

SEYEDHAMID KARIMI

How to cite:

KARIMI, SEYEDHAMID (2015) Integrated characterisation of mud-rich overburden sediment sequences using limited log and seismic data: Application to seal risk. Doctoral thesis, Durham University.

Use policy

The full-text may be used and/or reproduced, and given to third parties in any format or medium, without prior permission or charge, for personal research or study, educational, or not-for-profit purposes provided that:

- a full bibliographic reference is made to the original source
- a https://etheses.durham.ac.uk/id/eprint/11285/ is made to the metadata record in Durham E-Theses
- the full-text is not changed in any way

The full-text must not be sold in any format or medium without the formal permission of the copyright holders.

Please consult the full Durham E-Theses policy for further details.

Academic Support Office, The Palatine Centre, Durham University, Stockton Road, Durham, DH1 3LE
e-mail: e-theses.admin@durham.ac.uk Tel: +44 0191 334 6107
https://etheses.durham.ac.uk

Durham E-Theses

Integrated characterisation of mud-rich overburden sediment sequences using limited log and seismic data: Application to seal risk

KARIMI, SEYEDHAMID

How to cite:

KARIMI, SEYEDHAMID (2015) Integrated characterisation of mud-rich overburden sediment sequences using limited log and seismic data: Application to seal risk, Durham Theses, Durham University. Available at Durham E-Theses Online: http://etheses.dur.ac.uk/

Use policy

The full-text may be used and/or reproduced, and given to third parties in any format or medium, without prior permission or charge, for personal research or study, educational, or not-for -profit purposes provided that:

- a full bibliographic reference is made to the original source
- a link is made to the metadata record in Durham E-Theses
- the full-text is not changed in any way

The full-text must not be sold in any format or medium without the formal permission of the copyright holders.

Please consult the full Durham E-Theses policy for further details.

Academic Support Office, Durham University, University Office, Old Elvet, Durham DH1 3HP
e-mail: e-theses.admin@dur.ac.uk Tel: +44 0191 334 6107
http ://etheses.dur.ac.uk

Integrated characterisation of mud-rich overburden sediment sequences using limited log and seismic data: Application to seal risk

Seyedhamid Karimi

A thesis submitted in partial fulfilment of the requirements for the degree of Doctor of Philosophy at Durham University

Department of Earth Sciences, Durham University

2015

Abstract

Muds and mudstones are the most abundant sediments in sedimentary basins and can control fluid migration and pressure. In petroleum systems, they can also act as source, reservoir or seal rocks. More recently, the sealing properties of mudstones have been used for nuclear waste storage and geological CO_2 sequestration. Despite the growing importance of mudstones, their geological modelling is poorly understood and clear quantitative studies are needed to address 3D lithology and flow properties distribution within these sediments. The key issues in this respect are the high degree of heterogeneity in mudstones and the alteration of lithology and flow properties with time and depth. In addition, there are often very limited field data (log and seismic), with lower quality within these sediments, which makes the common geostatistical modelling practices ineffective.

In this study we assess/capture quantitatively the flow-important characteristics of heterogeneous mud-rich sequences based on limited conventional log and post-stack seismic data in a deep offshore West African case study. Additionally, we develop a practical technique of log-seismic integration at the cross-well scale to translate 3D seismic attributes into lithology probabilities. The final products are probabilistic multiattribute transforms at different resolutions which allow prediction of lithologies away from wells while keeping the important sub-seismic stratigraphic and structural flow features. As a key result, we introduced a seismically-driven risk attribute (so-called Seal Risk Factor "SRF") which showed robust correspondence to the lithologies within the seismic volume. High seismic SRFs were often a good approximation for volumes containing a higher percentage of coarser-grained and distorted sediments, and vice versa.

We believe that this is the first attempt at quantitative, integrated characterisation of mud-rich overburden sediment sequences using log and seismic data. Its application on modern seismic surveys can save days of processing/mapping time and can reduce exploration risk by basing decisions on seal texture and lithology probabilities.

Declaration

I declare that this thesis, which I submit for the degree of Doctor of Philosophy at Durham University, is my own work and not substantially the same as any which has previously been submitted at this or any other university.

Seyedhamid Karimi

Durham University

January 2015

The copyright of this thesis rests with the author. No quotation from it should be published without prior written consent and information derived from it should be acknowledged.

Acknowledgements

Firstly, I would like to thank my supervisor, Professor Andy Aplin, for his guidance, support and encouragement throughout. I've learnt a lot from him in the project and through discussion, and he has always been willing to discuss my thoughts and ideas for the project. Having a good supervisor is the key to a positive PhD experience. Thanks for everything Andy.

Many thanks also to Dr Kuncho Kurtev and Dr Frans Kets who have significantly contributed to this work. Your technical advices in seismic interpretation and log analysis really helped me get through this PhD. Thank you for enthusiastic discussions and for sharing your great ideas with me.

The PhD project has been funded by the Caprocks Project which allowed me working with a multidisciplinary team of researchers from three other universities in the UK: Heriot-Watt, Cardiff and Leeds Universities. Special thanks to Caprocks colleagues in Cardiff University, Professor Joe Cartwright, Dr Tiago Alves, Dr Tuviere Omeru and Dr Iqbal Hajana, for their kind support and for opening my mind for new approaches and aspects in seismic interpretation of mudstones.

During this PhD I have benefited hugely from several software packages. So I must thank Dave and Mathew in Durham University and Graham and Iain in Newcastle University for their continuous support regarding software licensing, installation and maintenances.

I must also thank all my friends for their unending support. To all those in Newcastle and Durham, thank you for keeping me sane! Thanks especially to Ciprian, Majid, Tom, Eliza and Reza. Thank you for your unfailing support and encouragement through thick and thin.

Finally, to my incredibly supportive and wonderful family, I'm so grateful for your love. In particular I express my everlasting gratitude to my beloved wife Behnaz, for her constant encouragement, support and inspiration.

A big thank you to all of you that have contributed so much. I genuinely couldn't have done this without you. Thank you!

Table of Contents

List of Figures

Chapter 2: Recognition of logfacies in mud-rich overburden sediment sequences with limited core and log datasets

List of Tables

Chapter 1: Introduction

Chapter 2: Recognition of logfacies in mud-rich overburden sediment sequences with limited core and log datasets

Chapter 3: Seismic Characterisation of Seal Quality using Volumetric Attributes

1 Introduction

1.1 Rationale

Muds and mudstones are the commonest sediment types and considerably control the fluid flow in sedimentary basins. In a petroleum system they can be a source rock, a shale gas reservoir, a seal, and determine the primary and secondary migration processes in most geological contexts. Furthermore, by restricting fluid flow, they can influence the development of overpressure in sedimentary basins (e.g. Aplin et al., 1999). In addition, the sealing properties of mudstones have been recently used for clay-lined landfill sites and carbon capture storage (CCS) to restrict the leakages over centuries. Despite the growing importance of mudstones, their subsurface geological properties are still poorly understood and clear quantitative studies are needed to address reservoir-modelling-scale heterogeneities in their lithology and flow properties.

The key issues in this respect are the high degree of small-scale (<5 m) vertical heterogeneity in mudstones and the alteration of lithology and flow properties with time and depth by physical or chemical processes and fluid-rock interactions. It has been common practice in the last decade to build geomodels according to a two-step process: geostatistical facies modelling followed by geostatistical petrophysical property modelling. This approach requires that the facies are understood in terms of their mutual genetic-spatial relationships and accurately characterised as far as their relevant petrophysical properties are concerned (Ruvo et al., 2005). In mudstones, thin, mm-sized alternating horizons of silt and clay cannot be resolved by conventional wireline logs. In order to petrophysically characterise such kinds of logfacies it is usually necessary to also define, for instance, the net-to-gross (NTG) which is an important but difficult parameter for geostatistical simulations, depending strongly on the choice of cut-off parameters (e.g. Martin, 2008).

In the framework of quantitative seismic interpretation, quality control is important to analyse data loading parameters, SEGY brick format, noise and spatial resolution, and it is desirable to improve signal by filtering or by wavelet modifications. For instance, thin-bed spectral inversion is a novel way of removing the wavelet from the seismic data and extracting reflectivity. For data with a high signal-to-noise ratio, thicknesses far below tuning can be resolved. The highly

resolved seismic data retrieved in the form of reflectivity data is very useful for making accurate quantitative interpretations and for seismic-log integration (Chopra et al., 2006). On the contrary, the spectral decomposition techniques are not applicable to mudstones because of low acoustic impedance contrasts (White et al., 2015), and mud-rich sequences have to be interpreted in full seismic bandwidth. Therefore, a physically sound quantitative interpretation paradigm is needed to address these technical issues and to control the quality of subsequent geomodelling.

There has been always a gap of incompatible resolution between core, well log and seismic data. This is especially challenging in mudstone sequences where there are considerable small scale petrophysical and sedimentological heterogeneities. To date, there is no well-known approach for log-seismic integration in mud-rich sequences. Stochastically building synthetic data sets with compatible resolution based on both log and seismic data can be helpful (Doyen, 2008; Ruvo et al., 2005). In addition, high or ultra-high density seismic datasets can facilitate the integration problem in this context.

The overall objectives in this study were to analyse quantitatively the fluid-flow-related characteristics of heterogeneous mud-rich sequences based on post-stack seismic attributes, to study attributes-well tie with mud-rich logfacies and to develop a step-wise technique for creating facies probability cubes which capture the stratigraphic and structural features that influence flow in mud-rich context at the subseismic-scale. In this project we aimed to perform explicit probabilistic modelling which could address the limitation of log and seismic data quality and availability in seal formations. We focussed on the pick-trough time interval scale (defined by successive picks and troughs along seismic amplitude traces) as the way of bridging the scales in 1D (vertical direction) between different data types (i.e. core, log and seismic). The final products, 3D facies probability models, can be used for studying the impact of reservoir-modelling-scale heterogeneities on basin-modelling-scale flow mechanisms, i.e. leakage, migration or recovery. The work presented in this thesis has been carried out on sample, core, log and seismic data from an offshore oil field in West Africa, where deep-water sandstone reservoirs are encased in hemipelagites and mass-transport deposits.

1.2 Background

1.2.1 Logfacies recognition in heterogeneous mudstones

A sedimentary facies that is characterised by a set of electrical responses extracted from wireline measurements is called an electrofacies or logfacies (Serra and Abbott, 1982). Several approaches to logfacies recognition have been applied using multiple log and core data. These include artificial intelligence methods: artificial neural networks (ANN) (Qi and Carr, 2006; Ma 2011; Tang et al., 2011), and fuzzy logic (Wong et al., 1997; Cuddy, 2000; Siripitayananon et al., 2001; Saggaf and Nebrija, 2003). Multivariate statistical classification methods include discriminant and cluster analysis, regression analysis (Lee et al., 2002; Tang et al., 2004; Tang and White, 2008; Enikanselu and Ojo 2012), statistical tree-based analysis (Perez et al., 2005), and Bayesian analysis (John et al., 2005; Li and Anderson-Sprecher, 2006; Lindberg et al., 2014). In addition to these conventional approaches, other researchers transformed well log responses into signal form and applied signal processing techniques to recognise patterns of logfacies (Alvarez et al., 2003; Maiti and Tiwari 2005; Hruska et al., 2009). In contrast to the conventional approaches, these techniques are systematic and self-determining, but they require manipulation of raw data (Soliman et al., 2003) and are not suitable recognition tools where the quality of the wireline response is poor.

Given the importance of shale in unconventional reservoirs, facies interpretations of fine-grained sediments using sample, core and log analysis has recently received more attention (Dawson and Almon, 2002, 2006; Passey et al., 2010; Mitra et al., 2010; Hammes and Frebourg, 2012; Wang and Carr, 2012, Gould et al., 2014). Nevertheless, despite several facies interpretation studies in mud-rich sediments, there is still very little research aimed at logfacies pattern recognition in these sediments.

Variants of multifractal techniques have been introduced that can be adapted to different sedimentary contexts by changing fractal properties (Khue et al., 2002; Lopez and Aldana, 2007; Hernandez-Martinez et al., 2013). However, their facies prediction results showed no meaningful relation with seismic. More recently, Grana et al. (2014) applied the Expectation Maximisation (EM) statistical algorithm to classify facies in the Marcellus Shale in the Appalachian Basin, using well log data.

The facies classifications were checked against regional stratigraphy. Despite the promising result, the method is based on Gaussian mixture models of petroelastic properties and relies on availability of both well log and rock physics analysis data.

In this study a modified SOM algorithm, the so-called Indexed and Probabilised Self-Organising Map (IPSOM), is used to achieve a core and seismically correlatable logfacies recognition result. The basic SOM or Kohonen network method was introduced by Kohonen (1982, 1984) for speech recognition. Numerous variants of SOM have been widely developed for data exploration purposes to analyse the experimentally derived high-dimensional data (Kaski et al., 1998; Oja et al., 2003; Pöllä et al., 2007). In petroleum geoscience, the SOM is also one of the most effective unsupervised pattern recognition techniques for the automatic identification and mapping of seismic-scale facies in different depositional contexts (Matos et al., 2007; Roy et al., 2010, 2013; Chopra and Marfurt, 2014). The IPSOM can outperform the EM algorithm in computation and learning speed (Chang and Chong-xiu, 2013) and can improve the decisiveness of the model complexity (Yin, 2008).

1.2.2 3D seismic texture analysis in heterogeneous mudstones

Seismic attributes are properties that can be quantitatively extracted from seismic data to filter or illustrate geological and geophysical characteristics of the subsurface (Chopra and Marfurt, 2005). In the 1960s, 1970s and 1980s, attribute technology gradually developed by introducing several 2D attributes (and applications) to help geoscientists in petroleum exploration: reflector dip attribute (Picou and Utzman, 1962; Simpson et al., 1967), bright-spot (Churlin and Sergeyev, 1963), seismic opacity (Balch, 1971), seismic inversion (Lavergne, 1975; Lindseth, 1976), seismic stratigraphy (Taner and Sheriff, 1977; Vossler,1988), complex trace attributes (Taner et al., 1979), seismic attenuation (Taner et al., 1979), and interval attributes (Dalley et al., 1989; Sonneland et al., 1989). In the 1980s, attributes proliferated and became popular, but 2D seismic stratigraphy was not still successful in many cases (e.g. in chaotic features such as slump and turbidites, or subtle discontinuities) because of the 3D nature of geological features and artefacts (Love and Simaan, 1984).

The emergence of 3D seismic technology led to the development of volumetric attributes which made significant subsurface interpretational and characterisation impacts: coherency attribute (Bahorich and Farmer, 1995), texture attribute (Vinther et al., 1995; West et al., 2002; Gao, 2004), pattern recognition attributes (Russell et al., 1997), spectral decomposition (Peyton et al., 1998; Partyka et al., 1999) and elastic inversion (Connolly 1999; Whitcombe, 2002).

As the very first seismic textural analysis in the 2D domain, Sangree and Widmier (1976) demonstrated the relationship between seismic-signal pattern and constituent sediments of geobodies; later, Love and Simaan (1984) extracted textural patterns using 2D amplitude templates. In the 1990s, the development of volumetric attributes, multi-attribute techniques (Russell et al., 1997) and statistical measures (Vinther, 1997; Whitehead et al., 1999; West et al., 2002; Gao, 2004) opened new perspectives for the classification of textures. By far, the majority of seismic texture detection efforts have been focused on delineating the distribution, quality and connectivity of reservoir pay zones in different sedimentological environments: deep marine (e.g. Prather, et al., 1998; Gao, 2007, 2008), fluvial deposits (e.g. Yenugo and Marfurt, 2010; de Matos et al., 2011), carbonates (e.g. Carrillat, et al., 2002), submarine turbidites (e.g. Gao, 2004), etc. Seismic texture analysis has not been commonly applied to fine-grained sediment sequences and the research has often been limited to either qualitative seismic facies analysis (e.g. Droz et al., 2003; Power et al., 2014), bypass detection (e.g. Heggland et al., 1999; Meldhal et al., 2001; Tingdahl et al., 2001) or semi-quantitative classification at the geobody scale (e.g. Corradi et al., 2009). In this work, an automatic, quantitative approach is proposed to link seal quality with the 3D seismic texture of mud-rich sequences by setting a physically sound, *a priori* texture model (Gao, 2004). In fact this work extends the recent study by Alves et al. (2014) in which multiple surface attributes were used to delineate different MTD textures.

1.2.3 Lithofacies modelling in heterogeneous mudstones

Lithofacies modelling requires an integrated approach, and the use of seismic attributes can reduce the uncertainty of spatial modelling and sometimes provides direct information about the distribution of sedimentary bodies such as channels (Biver et al., 2002, 2009; Hass and Formery, 2002) and mass transport deposits

(Frey-Martinez et al., 2006; Moscardelli and Wood, 2008; Alves et al., 2010). Discrete facies parameters must therefore be constrained with continuous seismic attribute results. This is conducted by either deterministic or stochastic geostatistical methods. Deterministic approaches (Chiles and Delfiner, 1999; Coleou, 2002; Xu et al., 2010) apply kriging principles to interpolate facies data. They are good at honouring the statistics, but often poor at capturing the sedimentary bodies (Amour et al., 2012; Park and Jang, 2014). In contrast, stochastic facies modelling - conditional simulation - generates models representing more realistic depositional features and honouring the existing data and/or the *a priori* model (Dubrule et al., 1998, 2003; Falivene et al., 2006).

Both Bortoli et al. (1992) and Haas and Dubrule (1994) introduced geostatistical inversion (GI), which generates joint realisations of facies and acoustic-impedance, all directly constrained by seismic data. GI is largely dependent on seismic quality; thus the algorithm was used in the case of a faulted reservoir (Lamy et al., 1998; Rowbotham et al., 2000) and a salt tectonised region (Shrestha and Boeckmann, 2002) to discriminate facies and link the uncertainty to seismic quality variations. Despite these advances in geostatistical simulations, the relatively homogeneous, low signal:noise seismic data in fine-grained sediment sequences limits the efficiency of GI in modelling seal facies. The alternative conditional simulation approaches are probabilistic and constrained by facies occurrence probabilities derived from seismic attributes at well locations. The algorithms are not controlled by seismic quality or assumptions used for statistical relationships between facies and seismic attributes (Dubrule, 2003). Macdonald et al. (1995), Skare et al. (1996) and Yarus et al. (2000) also described an application of this method to stochastically model the distribution of bar and channel facies bodies within a shaly background in a Tertiary reservoir in the Gulf of Thailand. Although constraining object-based models with seismic data can effectively capture geological bodies with characteristic geometries such as crevasse splays and channels (Haldorsen and Damsleth, 1990), it is less useful for predicting more subtle variation of facies in laterally extensive, muddy seal units.

Gomez-Hernandez and Journel (1990) and Doyen et al. (1994) proposed probabilistic pixel-based approaches that generalise the indicator simulation methodology developed for continuous variables to be used for discrete variables.

Doyen et al. (1994) successfully applied the methodology in the Ness formation of the Oseberg field (North Sea) to find channel deposits using reflection strength amplitude. Lo and Bashore (1999) proposed a similar approach to obtain a 3D density model and translate it into probabilities of various facies. Insalaco et al. (2001) presented an application of this approach to detailed modelling of a West African turbidite deposit. Due to the increase in interest in shale gas resources, there are also recent case studies utilising similar probabilistic conditional simulations (Wang and Carr, 2012, 2013) to predict shale lithofacies on a regional scale. In this study, the proposed algorithm extended the conventional probabilistic indicator simulation for channel deposits (Doyen et al., 1994) and turbidites (Insalaco et al., 2001) to fine-grained seal deposits. Classic multivariate analysis (Fournier and Derain, 1995; Hart and Balch, 2000) and Bayesian (Buland et al., 2008) techniques have been utilised to establish the likelihood functions of seal facies based on multiple textural attributes with limited well control.

1.3 Thesis structure

This thesis is written in publication style rather than as a monograph, so that individual technical chapters (Chapters 2-4) have their own introduction, aims, data, methods, results, discussion, conclusions and references sections. Thus, materials may repeat in some cases to keep individual technical chapters readable as stand-alone works. In the big-picture view, the technical chapters comprise different steps of an approach to generate lithofacies models in heterogeneous mudstones from limited core, log and seismic data. In this work we utilised all the sample, core, log and seismic data available in a West Africa case study (and partly used sample and seismic data from a North Africa case study for comparison purposes). The second chapter demonstrates a novel neural network approach for logfacies recognition in mud-rich sediment sequences with limited core and log data. In chapter three, we introduce a seal texture model and analyse the corresponding 3D attributes. Finally, in chapter four, the outcomes of logfacies recognition and textural attribute analysis are integrated at the pick-trough time interval scale (in West Africa case study ~ 10 m) to generate a probabilistic seal lithofacies cube in heterogeneous mudstones.

The result of this research work have been partly presented in two international conferences. The first paper has received among the highest ratings from its reviewers and has invited for full paper publication in First Break:

- Karimi, S., Aplin, A.C., Kurtev, K.D. and Kets, F., 2013, Seismic characterization of seal quality using volume attributes. In Proceedings: 75th EAGE Conference & Exhibition incorporating SPE EUROPEC 2013, London. Extended abstract. DOI: 10.3997/2214-4609.20130773.
- Karimi, S., Aplin, A.C., Kurtev, K.D. and Kets, F., 2014, Seismic characterisation of mud-rich sediments - application to seal risk. In Proceedings: Fourth EAGE Shale Workshop, Porto. Extended abstract. DOI: 10.3997/2214-4609.20140031.

1.4 Caprocks project

The research project was embedded in the Caprocks Project (Phase 3), a collaboration of international petroleum companies, the UK Department for Business, Enterprise and Regulatory Reform and researchers at Durham/Newcastle, Cardiff, Heriot-Watt and Leeds Universities. The Caprocks project focused on the fine-grained section of sedimentary basins and developed insights to the related processes of petroleum trapping and leakage. The project was conducted by different teams (in different universities) on various scales of study. Table 1.1 shows the timeline of Caprocks project and Table 1.2 indicates the contribution of different teams in Phase 3 and how my research work fits in the framework of the Caprocks project.

Table 1.1: *Caprocks project timeline*

Project phase	Period	Team	Research theme
Phase 1	2003-2007	Newcastle, Leeds, Cardiff Universities	Mudstone petrophysics: physical properties and log response
Phase 2	2007-2010	Newcastle, Heriot-Watt, Cardiff Universities	Upscaled, effective flow properties of mud-rich, heterolithic rock types

Phase 3	2010-2013	Newcastle/Durham, Leeds, Cardiff and Heriot-Watt Universities	Workflows for basin-scale flow models and seal capacity risking

Table 1.2: *Caprocks project teams and their contribution in Phase 3*

Scale of study	Team	Research theme
Core-scale	Leeds University	Experimental analysis of flow properties in low permeability mudstones
Log-scale	Durham /Newcastle University	Analytical modelling of effective flow properties / logfacies recognition in mudstones
Seismic (voxelgrid)-scale	Durham /Newcastle University	Seismic attribute analysis / seismic-well tie analysis / facies probability cube generation in heterogeneous mud-rich seal sequences
Genetic unit-scale	Heriot-Watt University	Numerical modelling of fluid flow / upscaling of effective flow properties in mudstones
Regional-scale	Cardiff University	Geological interpretation of seal capacity and migration process in mudstones / MTD Atlas

My PhD Research

My PhD study focused mainly on the seismic-scale and partly on the log-scale studies in Caprocks "phase 3". The aim was to integrate the small-scale sedimentological and petrophysical work at Newcastle University (done in phase 1 and 2) with the seismic-scale work at Cardiff University (done in phase 1 and 2) to define the 3D architecture of seal sequences at reservoir-modelling-scale for upscaling and the use in basin-scale flow simulators at Heriot-Watt University. In the log-scale part of the research, Dr Kuncho Kurtev significantly contributed to perform the IPSOM operations in Techlog software and to analyse the available core and sample studies from phase 1 and 2. The horizon surfaces used in this research are mixture of operator mappings and primary mappings at Cardiff University by Prof Joe Cartwright, Dr Mads Huuse (currently Manchester University) and Dr Tiago Alves.

Caprocks "phase 3" was funded by: Anadarko, BHP Billiton, BP, Chevron, ConocoPhillips, ENI, Petrobras, StatoilHydro, Total and BG Group. The case study datasets were provided by the sponsors of the Caprocks project. Due to the confidentiality agreement, the specifications of geological settings and datasets cannot be fully disclosed. Therefore, in this study the aliases are used for the well and surface names, and literature and company names are not stated in the geological settings and data sections.

1.5 References

*Alvarez, G., Sanso, B., Michelena, R.J. and Jiḿenez, J.R., 2003, Litho-logic Characterization of a Reservoir using Continuous-Wavelet Transforms. IEEE Transactions on Geoscience and Remote Sensing, 41(**1**), pp 59–65.*

*Alves, T.M. and Cartwright, J.A., 2010, The effect of mass-transport deposits on the younger slope morphology, offshore Brazil. Marine and Petroleum Geology, 27(**9**), pp 2027-2036.*

*Alves, T.M., Kurtev, K., Moore, G.F. and Strasser, M., 2014, Assessing the internal character, reservoir potential, and seal competence of mass-transport deposits using seismic texture: A geophysical and petrophysical approach. AAPG Bulletin, 98(**4**), pp 793-824.*

Amour, F., Mutti, M., Christ, N., Immenhauser, A., Agar, S.M., Benson, G.S., Tomás, S., Always, R. and Kabiri, L., 2012, Capturing and modeling metre-scale spatial facies heterogeneity in a Jurassic ramp setting (Central High Atlas, Morocco). Sedimentology, 59, pp 1158-1189.

Aplin, A.C., Fleet, A.J. and Macquaker, J.H.S., 1999, Muds and mudstones: physical and fluid-flow properties. Geological Society, London, Special Publications, 158, pp 1-8.

Bahorich, M.S. and Farmer, S.L., 1995, 3D seismic discontinuity for faults and stratigraphic features: The coherence cube. 65th Annual International Meeting, SEG, Expanded Abstracts, pp 93–96.

Balch, A.H., 1971, Color sonograms: A new dimension in seismic data interpretation: Geophysics, 36, pp1074–1098.

Biver, P. and Guillou, O., 2009, Facies and petrophysical model constrained to seismic attributes–impact on hydrocarbon in place uncertainties. In proceeding: 71st EAGE Conference & Exhibition.

*Biver, P., Haas, A. and Bacquet, C., 2002, Uncertainties in facies proportion estimation II: application to geostatistical simulation of facies and assessment of volumetric uncertainties. Mathematical geology, 34(**6**), pp 703-714.*

Bortoli, L.J., Alabert, F., Haas, A. and Journel, A.G., 1992, Constraining stochastic images to seismic data. In Soares A., Ed., In proceeding: International Geostatistics Congress, Troia, Kluwer Academic Publication.

*Buland, A., Kolbjørnsen, O., Hauge, R., Skjæveland, Ø. and Duffaut, K., 2008, Bayesian lithology and fluid prediction from seismic prestack data. Geophysics, 73(**3**), pp 13-21.*

Carrillat, A., Randen, T., Sonneland, L. and Elvebakk, G., 2002, Automated mapping of carbonate mounds using 3D seismic texture attributes. In proceeding: 2002 SEG Annual Meeting, Society of Exploration Geophysicists.

Chang, L. and Chong-xiu, Y., 2013, Modified Self-Organizing Mixture Network For Probability Density Estimation And Classification. In proceeding: Neural Networks (IJCNN), The 2013 International Joint Conference, Dallas, pp 1-6.

Chiles, J.P. and Delfiner, P., 1999, Modeling spatial uncertainty. Geostatistics, Wiley Series in Probability and Statistics. New York: Wiley Interscience.

*Chopra, S., Castagna, J. and Portniaguine, O., 2006, Seismic resolution and thin-bed reflectivity inversion. CSEG Recorder. 31(**1**), pp 19-25.*

*Chopra, S. and Marfurt, K., 2005, Seismic attributes—A historical perspective. Geophysics, 70 (**5**).*

Chopra, S. and Marfurt, K., 2014, Seismic facies analysis using generative topographic mapping. In proceeding: SEG Denver 2014 Annual Meeting, pp 1390-1394.

*Churlin,V.V. and Sergeyev, L.A., 1963, Application of seismic surveying to recognition of productive part of gas-oil strata. Geologiya Nefti I Gaza, 7(**11**), 363 p.*

Coléou, T. (2002). Time-lapse filtering and improved repeatability with automatic factorial co-kriging (AFACK), 64th Mtg. Eur. Assn. Geosci. Eng., Session A, 18

Connolly, P., 1999, Elastic impedance. The Leading Edge, 18, pp 438–452.

*Corradi, A., Ruffo, P., Corrao, A. and Visentin, C., 2009, 3D hydrocarbon migration by percolation technique in an alternate sand–shale environment described by a seismic facies classified volume. Marine and Petroleum Geology, 26(**4**), pp 495-503.*

*Cuddy, S.J., 2000, Litho-Facies and Permeability Prediction From Electrical Logs Using Fuzzy Logic. SPE Reservoir Evaluation and Engineering, 3(**4**)*

*Dalley, R.M., Gevers, E.C.A., Stampfli, G.M., Davies, D.J., Gastaldi, C.N., Ruijtenberg, P.A. and Vermeer, G.J.O, 1989, Dip and azimuth displays for 3D seismic interpretation. FirstBreak, 7(**3**), pp 86–95.*

Dawson, W.C. and Almon, W.R., 2002, Top Seal Potential of Tertiary Deep-Water Shales, Gulf of Mexico: GCAGS Transactions, 52, pp 167-176.

Dawson, W.C. and Almon, W.R., 2006, Shale Facies and Seal Variability in Deepwater Depositional Systems, Proceeding Annual AAPG Convention, April 9-12.

*de Matos, M. C., Yenugu, M., Angelo, S. M. and Marfurt, K. J., 2011, Integrated seismic texture segmentation and cluster analysis applied to channel delineation and chert reservoir characterization. Geophysics, 76(**5**), pp 1-21.*

Doyen, P.M. (2008): Seismic reservoir characterization. An earth modeling perspective (EET II). EAGE publications BV.

Doyen, P.M., Psaila, D.E., and Strandenes, S. (1994), Bayesian sequential indicator simulation of channel sands from 3-D seismic data in the Oseberg Field Norwegian North Sea. In proceedings: SPE Annual Technical Conference and Exhibition. Society of Petroleum Engineers.

*Droz, L., Marsset, T., Ondras, H., Lopez, M., Savoye, B. and Spy-Anderson, F. L., 2003, Architecture of an active mud-rich turbidite system: The Zaire Fan (Congo–Angola margin southeast Atlantic): Results from ZaAngo 1 and 2 cruises. AAPG bulletin, 87(**7**), pp 1145-1168.*

Dubrule, O., 2003, Geostatistics for seismic data integration in Earth models. 2003 Distinguished Instructor Short Course (No. 6), SEG Books.

*Dubrule, O., Thibaut, M., Lamy, P. and Haas, A., 1998, Geostatistical reservoir characterization constrained by 3D seismic data. Petroleum Geoscience, 4(**2**), pp 121-128.*

Enikanselu, A. and Ojo, A., 2012, Statistical Analysis and Evaluation of Lithofacies From Wireline Logs Over Beleema Field, Niger Delta, Nigeria. Journal of Petroleum Gas Engineering, 3, pp 26–34.

*Falivene, O., Arbus, P., Gardiner, A., Pickup, G., Muoz, J.A. and Cabrera, L., 2006, Best practice stochastic facies modeling from a channel-fill turbidite sandstone analog (the Quarry outcrop, Eocene Ainsa basin, northeast Spain). AAPG bulletin, 90(**7**), pp 1003-1029.*

*Fournier, F. and Derain, J.F., 1995, A statistical methodology for deriving reservoir properties from seismic data. Geophysics, 60(**5**), pp 1437-1450.*

*Frey-Martínez, J., Cartwright, J. and James, D., 2006, Frontally confined versus frontally emergent submarine landslides: a 3D seismic characterisation. Marine and Petroleum Geology, 23(**5**), pp 585-604.*

Gao, D., 2004, Texture model regression for effective feature discrimination: Application to seismic facies visualization and interpretation: Geophysics, 69, pp 958–967.

*Gao, D., 2007, Application of three-dimensional seismic texture analysis with special reference to deep-marine facies discrimination and interpretation: Offshore Angola, west Africa. AAPG bulletin, 91(**12**), pp 1665-1683*

*Gao, D., 2008, Application of seismic texture model regression to seismic facies characterization and interpretation. The Leading Edge, 27 (**3**), pp 394-397.*

Gomez-Hernandez, J.J. and Journel, A.G., 1990, Stochastic characterization of grid-block permeabilities: from point values to block tensors. In proceeding: 2nd European Conference on the Mathematics of Oil Recovery.

Gould, K.M., Piper, D.J.W., Pe-Piper, G. and MacRae, R.A., 2014, Facies, Provenance and Paleoclimate Interpretation Using Spectral Gamma Logs: Application to the Lower Cretaceous of the Scotian Basin. Marine and Petroleum Geology, 57, pp 445–454.

Grana, D., Schlanser, K. and Campbell-Stone, E., 2014, Petroelastic and Geomechanical Classification of Lithologic Facies in the Marcellus Shale. Interpretation, 3, pp 51-63.

*Haas, A. and Dubrule, O., 1994, Geostatical inversion-a sequential method of stochastic reservoir modelling constrained by seismic data. First Break, 12(**11**).*

*Haas, A. and Formery, P., 2002, Uncertainties in facies proportion estimation I. Theoretical framework: the Dirichlet distribution. Mathematical geology, 34(**6**), pp 679-702.*

*Haldorsen, H.H. and Damsleth, E., 1990, Stochastic Modeling (includes associated papers 21255 and 21299). Journal of Petroleum Technology, 42(**04**), pp 404-412.*

*Hammes, U. and Frébourg, G., 2012, Haynesville and Bossier Mudrocks: A Facies and Sequence Stratigraphic Investigation, East Texas and Louisiana, Marine and Petroleum Geology,31 (**1**), pp 8-26.*

*Hart, B.S. and Balch, R.S., 2000, Approaches to defining reservoir physical properties from 3D seismic attributes with limited well control: An example from the Jurassic Smackover Formation, Alabama. Geophysics, 65(**2**), pp 368-376.*

Heggland, R., Meldahl, P., Bril, B. and de Groot, P., 1999, The chimney cube, an example of semi-automated detection of seismic objects by directive attributes and neural networks: Part II; interpretation. In proceeding:69th Annual Meeting of SEG, Houston.

*Hernandez-Martinez, E., Perez-Muñoz, T., Velasco-Hernandez, J.X., Altamira-Areyan, A. and Velasquillo-Martinez, L., 2013, Facies Recognition Using Multifractal Hurst Analysis: Applications to Well-Log Data. Mathematical Geosciences, 45 (**4**), pp 471-486.*

Hruska, M., Corea, W., Seeburger, D., Schweller, W. and Crane, W.H., 2009, Automated Segmentation of Resistivity Image Logs Using Wavelet Transform. Mathematical Geosciences, 4, pp 703–716.

Insalaco, E., Marion, D., Michel, B. and Rowbotham, P., 2001, Reservoir-scale 3D sedimentary modelling: Approaches and impact of integrating sedimentology into the reservoir characterization workflow. In proceedings: AAPG Annual Meeting.

John, A., Lake, L. W., Torres-Verdin, C. and Srinivasan, S., 2005, Seismic Facies Identification and Classification using Simple Statistic. Proceeding, SPE Annual Technical Conference and Exhibition, SPE 96577.

Kaski, S., Kangas, J., and Kohonen, T., 1998, Bibliography of Self-Organizing Map (SOM) Papers: 1981-1997. Neural Computing Surveys, 1, pp 102-350.

Khue, P., Huseby, O., Saucier, A. and Muller, J., 2002, Application of Generalized Multifractal Analysis for Characterization of Geological Formations. Journal of Physics: Condensed Matter, 14, pp 2347–2352.

Kohonen, T., 1982, Self-Organized Formation of Topologically Correct Feature Maps. Biological Cybernetics, 43, pp 59-69.

Kohonen T., 1984, Self-Organization and Associative Memory. Springer, Berlin.

Lamy, P., Swaby, P.A., Rowbotham, P.S., Dubrule, O. and Haas, A., 1998, From seismic to reservoir properties using geostatistical inversion. In proceedings: SPE annual technical conference, pp 535-545.

Lavergne, M., 1975, Pseudo-diagraphics de Vitesse en offshore profonde: Geophysical prospecting, 23, pp 695–711.

Lee, S.H., Khargoria, A. and Datta-Gupta, A., 2002, Electrofacies Characterization and Permeability Predictions in Complex Reservoirs. SPE Reservoir Evaluation and Engineering, 5, pp 237–248.

Li, Y. and Anderson-Sprecher, R., 2006, Facies Identification From Well Logs: A Comparison of Discriminant Analysis and Naive Bayes Classifier. Journal of Petroleum Science and Engineering, 53, pp 149-157.

Lindberg, D.V., Rimstad, E. and Omre, H., 2014, Identification of Facies from Multiple Well Logs Accounting for Spatial Dependencies and Convolution Effects. Extended Abstract, 76th EAGE Conference and Exhibition, Amstrdam.

Lindseth, R.O., 1976, Seislog process uses seismic reflection traces, Oil & Gas Journal, 74, pp 67–71.

Lo, T.W. and Bashore, W.M., 1999, Seismic constrained facies modeling using stochastic seismic inversion and indicator simulation a North Sea example. In proceedings: 1999 SEG Annual Meeting. Society of Exploration Geophysicists.

Lopez, M. and Aldana, M., 2007, Facies Recognition using Wavelet Based Fractal Analysis and Waveform Classifier at the Oritupano-A Field, Venezuela. Nonlinear Processes Geophysics, 14, pp 325-335.

Love, P.L. and Simaan, M., 1984, Segmentation of stacked seismic data by the classification of image texture: 54th Annual International Meeting, SEG, session S7.3.

Ma, Y.Z., 2011, Lithofacies Clustering Using Principal Component Analysis and Neural Network: Applications to Wireline Logs. Mathematical Geosciences, 43, pp 401–419.

MacDonald, A.C., Berg, J.I., Skare, Ø. and Holden, L., 1995, Constraining a stochastic model of channel geometries using seismic data. In proceeding: 57th EAEG Meeting.

Maiti, S. and Tiwari, R.K., 2005, An Automatic Method For Detecting Lithologic Boundary Using Walsh Transform: A Case Study From KTB Borehole. Computers and Geosciences, 31, pp 949–955.

*Martin, C.A., 2008, Addressing uncertainty and remaining potential in a mature field. A case study from the Tertiary of Lake Maracaibo, Venezuela. Geological Society, London, Special Publications, 309(**1**), pp 181-192.*

Matos M.C., Osório P.L.M. and Johann P.R.S., 2007, Unsupervised Seismic Facies Analysis Using Wavelet Transform and Self-Organizing Maps. Geophysics, 72, pp 9-21.

*Meldahl, P., Heggland, R., Bril, B. and de Groot, P., 2001, Identifying faults and gas chimneys using multiattributes and neural networks. The Leading Edge, 20(**5**), pp 474-482.*

Mitra, A., Warrington, D.S. and Sommer, A., 2010, Application of Lithofacies Models to Characterize Unconventional Shale Gas Reservoirs and Identify Optimal Completion Intervals. SPE 132513. In proceeding: SPE Western Regional Meeting, Anaheim, California, U.S.A.

*Moscardelli, L. and Wood, L., 2008, New classification system for mass transport complexes in offshore Trinidad. Basin Research, 20(**1**), pp 73-98.*

Oja, M., Kaski, S. and Kohonen, T., 2003, Bibliography of Self-Organizing Map (SOM) Papers: 1998-2001. Addendum. Neural Computing Surveys, 3, pp 1-156.

Park, N.W. and Jang, D.H., 2014, Comparison of geostatistical kriging algorithms for intertidal surface sediment facies mapping with grain size data, The Scientific World Journal, 2014, 11 p.

Partyka, G., Gridley, J. and Lopez, J., 1999, Interpretational applications of spectral decomposition in reservoir characterization: The Leading Edge, 18, pp 353–360.

Passey, Q.R., Bohacs, K.M. and Esch, W.L., 2010, From Oil Prone Source Rock to Gas-Producing Shale Reservoir—Geologic and Petrophysical Characterization of

Unconventional Shale Gas Reservoirs. In proceeding: CPS/SPE International Oil and Gas Conference, Beijing, 8–10 June, SPE 131350.

Perez, H.H., Datta-Gupta, A. and Mishra, S., 2005, The Role of Electrofacies, Lithofacies and Hydraulic Flow Units in

Peyton, L., Bottjer, R. and Partyka, G., 1998, Interpretation of incised valleys using new 3D seismic techniques: A case history using spectral decomposition and coherency. The Leading Edge, 17, pp 1294–1298.

Picou, C. and Utzmann, R., 1962, La coupe sismique vectorielle: Un pointe semi-automatique. Geophysical prospecting, 4, pp 497–516.

Pöllä, M., Honkela, T. and Kohonen, T., 2007, Bibliography of Self-Organizing Map (SOM) Papers: 2002-2005. Addendum. Neural Computing Surveys.

Power, B.A., Covault, J., Sullivan, M. and Posamentier, H., 2014, Bypass-dominated mud-rich channel-fill deposits of the Paleogene Scripps/Ardath formation at Tourmaline Beach, San Diego, CA: An analog for low net-to-gross slope canyon and channel systems. In proceeding: 2014 AAPG Annual Convention and Exhibition, Houston, Texas.

*Prather, B.E., Booth, J.R., Steffens, G.S. and Craig, P.A., 1998, Classification, lithologic calibration, and stratigraphic succession of seismic facies of intraslope basins, deep-water Gulf of Mexico. AAPG bulletin 82 (**5**), pp 701-728.*

Qi, L. and Carr, T.R., 2006, Neural Network Prediction of Carbonate Lithofacies From Well Logs, Big Bow and Sand Arroyo Creek Fields, Southwest Kansas. Computers and Geosciences, 32, pp 947-964.

Rowbotham, S.P., Marion, D., Lamy, P., Swaby, P.A. and Rabary, G., 2000, Detailed reservoir characterisation of the Elgin Field using geostatistical inversion. In proceedings: 62nd EAGE Conference and Exhibition.

Roy, A., 2013, Latent Space Classification of Seismic Facies, Ph.D. Dissertation, University of Oklahoma.

Roy, A., Matos, M. and Marfurt, K.J., 2010, Automatic Seismic Facies Classification with Kohonen Self Organizing Maps - A Tutorial. Geohorizons Journal of Society of Petroleum Geophysicists, pp. 6-14.

Russell, B., Hampson, D., Schuelke, J. and Quirein, J., 1997, Multiattribute seismic analysis. The Leading Edge, 16, pp 1439–1443.

Ruvo, L., Scaglioni, P. and Cozzi, M., 2005, A new approach to the petrophysical characterization of thin layered reservoirs. In proceeding: 67th EAGE conference & exhibition.

Saggaf, M.M. and Nebrija, Ed.L., 2003, A Fuzzy Logic Approach For The Estimation of Facies From Wire-Line Logs. AAPG Bulletin, 87, pp 1223-1240.

Sangree, J.B. and Widmier, J.M., 1976, Seismic interpretation of clastic depositional facies: American Association of Petroleum Geologists Memoir 26, pp 165–184.

Serra, O., Abbott, H.T., 1982, The Contribution of Logging Data to Sedimentology and Stratigraphy. Society of Petroleum Engineers Journal, 22, pp 117-131.

Shrestha, R.K. and Boeckmann, M., 2002, Stochastic seismic inversion for reservoir modeling. In proceeding: 2002 SEG Annual Meeting. Society of Exploration Geophysicists.

Simpson, S.M., Fink, D. and Treitel, S., 1967, Moveout averaging experiments. Geophysics, 32, pp 494–498.

Siripitayananon, P., Chen, H.C. and Hart, B.S., 2001, A New Technique For Lithofacies Prediction: Back-Propagation Neural Network. In proceeding of ACMSE: the 39th Association of Computing and Machinery South Eastern Conference, Atlanta, GA, USA, pp 31-38.

Skare, Ø., Skorstad, A., Hauge, R. and Holden, L., 1996, Conditioning a fluvial model on seismic data. In: Baafi, E.Y. and Schofield, N.A. (Eds.). In proceeding: Fifth International Geostatistics Congress, Wollongong, Australia, pp. 465–476.

Soliman, M.Y., Anseh, J., Stephenson, S. and Mandal, B., 2003, Application of Wavelet Transform to the Analysis of Pressure Transient Data. In: SPE Annual Technical Conference and Exhibition, 6, pp 88–89.

Sonneland, L., Barkved, O., Olsen, M. and Snyder, G., 1989, Application of seismic wave-field attributes in reservoir characterization. 59th Annual International Meeting, SEG, Expanded abstracts, 813.

Taner, M.T., Koehler, F. and Sheriff, R.E., 1979, Complex Seismic Trace Analysis. Geophysics, 44, pp 1041–1063.

Taner, M.T. and Sheriff, R.E., 1977, Application of Amplitude, Frequency, and Other Attributes to Stratigraphic and Hydrocarbon Determination. In: C.E. Payton, ed., Applications to Hydrocarbon Exploration. American Association of Petroleum Geologists Memoir 26, pp 301–327.

*Tang, H., Toomey, N. and Meddaugh, W.S., 2011, Using an Artificial-Neural-Network Method to Predict Carbonate Well Log Facies Successfully. SPE Reservoir Evaluation and Engineering,14(**1**).*

Tang, H. and White, C.D., 2008, Multivariate Statistical Log Log-Facies Classification on a Shallow Marine Reservoir. Journal of Petroleum Science and Engineering ,61, pp 88-93.

Tang, H., White, C.D., Gani, M.R. and Bhattacharya, J.P., 2004, Comparison of Multivariate Statistical Algorithms for Wireline Log Facies Classification. In proceeding: AAPG annual meeting 2004.

*Tingdahl, K. M., Bril, A. H. and de Groot, P. F., 2001, Improving seismic chimney detection using directional attributes. Journal of Petroleum Science and Engineering, 29(**3**), pp 205-211.*

Vinther, R., 1997, Seismic texture classification applied to processed 2D and 3D seismic data: 67th Annual International Meeting, SEG, Expanded Abstracts, pp 721–724.

Vossler, D.A., 1988, Automatic whole section seismic reflection mapping. 58th Annual International Meeting, SEG, session S2.2.

Wang, G. and Carr, T.R., 2012, Methodology of Organic-Rich Shale Lithofacies Identification and Prediction: A Case Study From Marcellus Shale in the Appalachian Basin. Computers and Geosciences, 49, pp 151-163.

*Wang, G. and Carr, T.R., 2013, Organic-rich Marcellus Shale lithofacies modeling and distribution pattern analysis in the Appalachian Basin. AAPG bulletin, 97(**12**), pp 2173-2205.*

West, B., May, S., Eastwood, J.E. and Rossen, C., 2002, Interactive seismic facies classification using textural and neural networks. The Leading Edge, 21, pp 1042–1049.

White, J.C., Williams, G.A., Grude, S. and Chadwick, R.A., 2015, Utilizing spectral decomposition to determine the distribution of injected CO2 at the Snøhvit Field. Geophysical Prospecting, 63 (5), pp 1213-1223.

Whitcombe, D.N., 2002, Elastic impedance normalization: Geophysics, 67, pp 60–62.

Whitehead, P., Fairborn, J. and Wentland, R., 1999, Identifying stratigraphic units by seismic patterns. 69th Annual International Meeting, SEG, Expanded Abstracts, pp 942–945.

Wong, K.W., Wong, P.M. and Gedeon, T., 1997, A State-of-Art Review of Fuzzy Logic for Reservoir Evaluation. APPEA Journal, 43, pp 587-593.

Xu, Y. and Chopra, S., 2010, Deterministic mapping of reservoir heterogeneity in Athabasca oil sands using surface seismic data. Heavy Oils: Reservoir Characterization and Production Monitoring, 13, 165 p.

Yarus, J.M., Yang, K., Sriisraporn, S., Chuemthaisong, N. and Sangwongwanich, K., 2000, Integrating 3d seismic and geostatistics; building a 3D model of a Tertiary deltaic and shallow marine deposit Malay Basin Offshore Gulf of Thailand. In proceeding: Offshore Technology Conference.

*Yenugu, M., Marfurt, K.J. and Matson, Sh., 2010, Seismic texture analysis for reservoir prediction and characterization. The Leading Edge, 29(**9**), pp 1116-1121.*

Yin, H., 2008, The Self-Organizing Maps: Background, Theories, Extensions and Applications. Computational intelligence: A Compendium, Springer Berlin Heidelberg, pp 715-762.

2 Recognition of Logfacies in Mud-Rich Overburden Sediment Sequences with Limited Core and Log Datasets

2.1 Introduction

A sedimentary facies is the set of lithological, geometrical, structural, biological and geochemical features of a sedimentary rock and its depositional environment (Reading, 2009). Individual facies have distinct petrophysical, mechanical and hydraulic characteristics, and the prediction and mapping of sedimentary facies plays an important role in subsurface characterisation in a sedimentary basin. Facies recognition is thus a foundation for the inference of the physical properties of sedimentary sequences (e.g. Gill et al., 1993; Chang et al., 2002).

Facies can be defined using different types of data resources including core, outcrop, seismic and logs. A sedimentary facies that is characterised by a set of electrical responses extracted from wireline measurements is called an electrofacies or logfacies (Serra and Abbott, 1982). The identification of logfacies is carried out by comparing or training pattern recognition with sedimentary interpretation derived from core analysis (John et al., 2005). In exploration and development of a petroleum reservoir, logfacies mapping can help to reduce the risk of drilling a dry well or to improve the efficiency of a production well by delineating reservoir, source and seal sequences (Alvarez et al., 2003).

Several approaches to logfacies recognition have been applied using multiple log and core data, mainly developed to map different reservoir rock types where good quality core and log data are readily available. As an initial approach, Serra and Abbott (1982) applied a clustering technique for logfacies prediction that gave very limited information about real rock properties. Subsequently, various more sophisticated approaches have been developed for logfacies pattern recognition which can be classified into two main groups: artificial intelligence and multivariate analysis (statistical) methods. Artificial intelligence methods include artificial neural networks (ANN) (Qi and Carr, 2006; Ma 2011; Tang et al., 2011), and fuzzy logic (Derek et al., 1990; Chang et al., 1997; Wong et al., 1997; Cuddy, 2000; Siripitayananon et al., 2001; Bhatt and Helle, 2002; Saggaf and Nebrija, 2003). Multivariate statistical classification methods include discriminant and cluster

analysis, regression analysis (Delfiner et al., 1987; Sakurai and Melvin, 1988; Avseth et al., 2001; Lee et al. 2002; Tang et al., 2004; Guo et al., 2007; Tang and White, 2008; Enikanselu and Ojo 2012), statistical tree-based analysis (Perez et al., 2005), and Bayesian analysis (John et al., 2005; Li and Anderson-Sprecher, 2006; Lindberg et al., 2014). In addition to these conventional approaches, other researchers transformed well log responses into signal form and applied signal processing techniques to recognise patterns of logfacies (Alvarez et al., 2003; Maiti and Tiwari 2005; Hruska et al., 2009). In contrast to the conventional approaches, these techniques are systematic and self-determining, but they require smoothing of the raw signals and retention of the details (Soliman et al., 2003). Thus, they are not suitable recognition tools where the quality of the electrical (wireline) response is poor.

Although the development of pattern recognition methods has greatly contributed to the automation of lithology prediction in reservoir rocks, little logfacies prediction work has been undertaken in mud-rich sediments or top seal sequences. The rarity of core acquisition and complete log suites in mud-rich overburden sediment sequences forces us here to look for a new approach to identify fine-grained logfacies. The result can be an important asset for flow properties modelling relevant to seal analysis and basin modelling. Previous research has established sedimentary facies models for fine-grained depositional environments including deep water (Stow and Piper, 1984; Stow, 1985; Pickering et al., 1986; Stow, 1994), turbidites (Porebski et al., 1991; Shanmugam, 2000, 2001; Camacho et al., 2002; Sumner et al., 2012) and fluvial systems (Jackson, 1981; Fielding et al., 2009; Jackson et al., 2013). These studies qualitatively interpreted and modelled the complex distribution of sedimentary facies and architectures based on flow evolution and deposit morphology controls derived from the analysis of outcrop, seismic or physical experiments. Given the importance of shale in unconventional reservoirs, facies interpretations of fine-grained sediments using sample, core and log analysis has recently received more attention (Dawson and Almon, 2002, 2006; Passey et al., 2010; Mitra et al., 2010; Hammes and Frebourg, 2012; Wang and Carr, 2012, Gould et al., 2014). Nevertheless, despite several facies interpretation studies in mud-rich sediments, there is still very little research aimed at logfacies pattern recognition in these sediments.

Variants of multifractal techniques have been introduced that can be adapted to different sedimentary contexts by changing fractal properties (Turcotte, 1997; Khue et al., 2002; Lopez and Aldana, 2007; Hernandez-Martinez et al., 2013). For example, Lopez and Aldana (2007) suggested that a wavelet-based multifractal analysis of mud-dominated zones could be associated with well logs with fractal dimensions of greater than 1.2; nevertheless, the logfacies recognition results obtained from these methods could not correlated with seismic. Moreover, as a signal processing method, subtle electrical responses in mud-rich sediments are very susceptible to the manipulation of raw data in multifractal approaches. More recently, Grana et al. (2014) applied the Expectation Maximisation (EM) statistical algorithm to classify facies in the Marcellus Shale in the Appalachian Basin, using well log data. The proposed method was based on Gaussian distribution of petro-elastic properties and has been only verified against logs and regional stratigraphic data. In this study we focus on a novel artificial neural network (ANN) technique to achieve a core and seismically correlatable logfacies recognition result.

The objective here is to develop a step-by-step, unsupervised Self-Organising Map (SOM) approach to predict lithological variations along wellbores within cored and uncored mud-rich, overburden sediments. The basic SOM or Kohonen network method was introduced by Kohonen (1982, 1984) for speech recognition to explain the spatial organization of the brain's functions. Numerous variants of SOM have been widely developed for data exploration purposes to analyse the experimentally derived high dimensional data (Kaski et al., 1998; Oja et al., 2003; Pöllä et al., 2007). In petroleum geoscience, the SOM is also one of the most effective unsupervised pattern recognition techniques for the automatic identification and mapping of seismic-scale facies in different depositional contexts (Kohonen, 2001; Matos et al., 2007; Roy et al., 2010, 2013; Chopra and Marfurt, 2014). Here the aim is to use a modified SOM algorithm, the so-called Indexed and Probabilised Self-Organising Map (IPSOM), to show how mud-rich electrofacies can be recognised on logs.

The IPSOM approach integrates SOM principles, nonlinear Principal Component Analysis (PCA) rules and a maximum likelihood probability approach (Yin, 2008) to improve computation time and the decisiveness of model complexity. Moreover, the IPSOM outperformed the above-mentioned EA algorithm in computation and learning speed (Chang and Chong-xiu, 2013). In this study, the

IPSOM algorithms have been iteratively applied on mud-rich logfacies defined using different classification schemes based on key sedimentological and/or physical properties. The successful algorithm generates correlatable knowledge about the vertical variability of logfacies which can then be incorporated into a seismic-scale analysis of mud-rich sequences, thus defining and upscaling flow properties. In addition, this method has the advantage of avoiding the manipulation of real log data in mud-rich sediments. On the weak side, similar to other artificial intelligent methods, the approach is subjective and requires parameter tweaking by the interpreter. Moreover, to train a reliable network a complete conventional log suite is required, which is not always possible in mud-rich overburden intervals. Here, we try to optimise the procedure by setting up the parameterisation rules and also reducing the requirement for log data. The approach is checked against core, seismic and log data from a regional seal formation in a case study from offshore West Africa. Nevertheless, we expect that the methodology and all the rules derived from the work can be applied as a generic approach to the recognition of mud-rich logfacies, using any ANN-based tool with functionality for unsupervised recognition using multi-layer inputs with elements having linear transformation functions and which use self-organizing maps based on Kohonen algorithms.

The chapter is organised as follows. First, an overview of the terminologies widely used in the chapter is presented in Section 2.1.1. In Section 2.2 an overview of the geological settings of case study area is given, which is followed by detailed descriptions of analysed data in Section 2.3. In Section 2.4, the proposed IPSOM methodology is explained. The approach is organised into three basic modules: Data Preparation, Data Quality Control (QC), Corrections and Facies Recognition. Each module is presented with a brief theory description and the reasoning for the presence of its sub-steps and their importance. In addition, parameterisation and optimisation rules are given to illustrate how to perform each module. In Section 2.5, the application of proposed IPSOM approach in different wellbores of West Africa case study is explained. Finally, discussion remarks and common conclusions on recognising mud-rich logfacies from conventional logs are presented in Section 2.6.

2.1.1 Terminology:

Throughout this chapter we use the terms facies, texture and lithology. Here, we provide our working definitions of those terms:

Complete Conventional Log Suite: Typically it is a set of wireline logs that contains responses from conventional logging tools including spontaneous potential, gamma ray, resistivity, acoustic, neutron, and density logs.

Electrofacies (Logfacies): A sedimentary facies that is characterised by a specific set of electrical responses extracted from wireline measurements.

Facies Classification Scheme: A way of grouping sedimentary facies according to one or more of their lithological, textural and physical (/flow) properties.

Lithology: A relatively homogeneous and visually distinctive volume of sediment formed from sedimentary particles with a given grain size distribution. Lithology is a facies attribute and controls the physical properties (e.g. porosity, permeability, compaction behaviour) of sub-domains of the facies.

Sedimentary Facies: A visually distinguishable volume of sediment with a pattern of variability which is the combined product of sediment supply, deposition, re-working and diagenesis. It has a characteristic set of lithological, geometrical, sedimentary structural, biological and geochemical features.

Texture: A visually distinguishable spatial architecture of sediments built from one or more lithological sub-domains. Texture is a facies attribute and represents its "lithological geometry". The generalisation of the texture of a given sediment volume defines the anisotropy of its lithological and physical properties.

2.2 Geological setting

Case study A is located approximately 140 km off the coast in one of the major deep offshore petroleum exploration and development blocks in West Africa. In the area of study, the average water depth is 1350 m. It has proven reserves of over 500 million barrels equivalent of oil in two prominent oil field discoveries associated with deep water, Tertiary channel sands. The hydrocarbons are mainly charged from Upper Cretaceous–Tertiary marine shales and accumulated in Miocene and Oligocene slope channel sandstone reservoirs associated with evolving river systems. The reservoir sedimentary facies are mainly turbidite channel and sheet sand deposits. Structurally, the case study is located in a regional-scale turtle

structure with global 5-10° southward structural dip associated with movement of Aptian salt. There are sets of normal faults, mainly north-east and south-east trending, cutting most of the Tertiary and Upper Cretaceous sediments. Thus both structural and stratigraphic elements control trap formation and fluid flow movement. There are five regional seal units within the Tertiary, numbered 1 to 5 (mixture of operator mapping and primary mapping at Cardiff University by Caprocks team in "Phase 1, 2 and 3"). The seal units, comprising hemipelagic shale and mass transport deposit (MTD) successions, are fine to coarse mudstone sediments with a range of sedimentary textures. In this study, we analysed electrofacies in regional seal unit 4 because it is located between the reservoir channels of two major oil field discoveries, so that defining the vertical variability of facies can contribute in understanding potential hydrocarbon migration between the accumulations. Moreover, conventional log suites were typically acquired along this seal unit. Seal unit 4 was deposited in the Aquitanian, has an average thickness of 150-200 m and a range of seismic and sedimentary textures (Huuse and Cartwright, 2007 (Caprocks "Phase 1")).

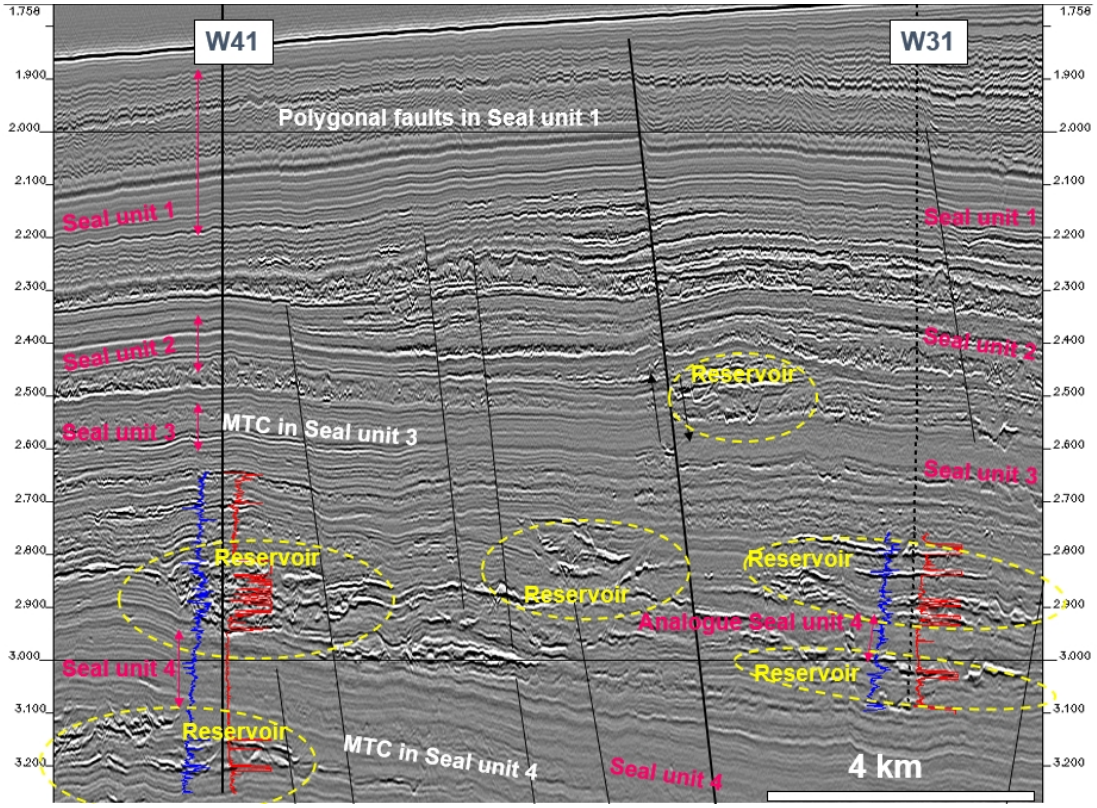

Figure 2.1: *Overview of the regional seal units in West Africa case study: seal unit 1 to 4 (seal unit 5 is out of the section scope). Black lines represent the major normal faults crossing the seal units. Well W31 does not cross seal unit 4 and an equivalent fine-grained depth-interval is used as analogue for seal unit 4. The gamma ray and P-sonic logs are*

shown by red and blue curves, illustrating the problem of availability of wireline records along the seal unit intervals (after Huuse and Cartwright, 2007 (Caprocks "Phase 1"))

2.3 Data

Case study A contains 11 wells with wireline measurements. The well logs were all acquired by logging tools of the same service company, Schlumberger, in the late 1990s. In this research, the log suite includes gamma ray (GR), resistivity (RT), p-wave sonic (DT), neutron porosity (NPHI) and bulk density (RHOB). The list of well log availabilities throughout seal unit 4 interval is given in Table 2.1, with wireline measurement gaps highlighted. The wellbores of W41 and W42 with complete conventional log suites are used to perform pilot studies for the proposed facies recognition algorithm. All original log measurements were subjected to quality control, core gamma ray matching and detrending processes prior to facies recognition analysis. These processes will be explained in detail in Sections 2.4.2 and 2.4.3.

Here, the functionality of conventional well log tools are briefly explained according to Theys (1991) with a focus on their potential ability for fine-grained sediment characterisation. The gamma ray log (GR) measures the background natural electromagnetic radiation from minerals or fluid(s) in the rock. This is mainly due to existence of three radioactive isotopes in the rocks: Potassium (^{40}K), Uranium (^{238}U) and Thorium (^{232}Th). There is usually a tendency to have concentration of ^{238}U in the clay-rich rocks deposited in reducing environments or ^{40}K in smectite/illite-rich sediments; however, clean sandstone with feldspars, silicates and heavy minerals (e.g. Zirconium, Titanium, Thorium, etc.) or even with $^{40}K^{17}Cl$ in the fluid content can be radioactive. Therefore, the GR log cannot be directly used as a measure of clay content. The vertical resolution of GR log is also variable and depends on the logging speed due to fluctuation of minerals' radiation.

The resistivity log (RT) is the inverse of the electrical conductivity of the rock. Since most minerals are electrically resistant, the RT log is usually used to indicate fluid type and saturation. However, RT log also reflects a relative estimation of rock permeability by considering drilling fluid invasion effects (providing the well is drilled with a conductive fluid). Moreover, the geometry of the rock can change the orientation of conductive elements and hence resistivity. Thus, in the fine-grained

context, the RT log might be an effective tool in discriminating silty and muddy facies and/or layered and distorted muddy facies.

The sonic transit time log (DT) is an estimate of the travel time of a compressional wave through the rock along the wellbore. The log resolution varies according to the spacing of the first and last receivers in the logging tool. In contrast to the electrical current, the compressional wave is mainly sensitive to the rock's solid phases so that the DT log can reflect lithology and also the pore pressure of the rock. Moreover, there are several empirical relationships to calculate porosity using DT log in different sediments. At a specified cementation and compaction degree in clean, coarse-grained sediments, there are often non-linear inverse relationships between DT log and porosity (e.g. Raymer et al., 1980; Dvorkin and Nur, 1996). However, the presence of significant clay, with higher transit time, in fine-grained sediments, can result in an overestimation of porosity from DT logs. Apart from clay volume, the distribution of clays also affects transit time. The presence of clay can be corrected for neutron porosity, density, spontaneous potential and gamma ray logs prior to any direct porosity estimation using DT log in fine-grained sediments (e.g. Fertl, 1981). Therefore, in mud-rich sediments DT log is expected to be a reliable measure only for the qualitative prediction of the contribution of acoustically fast components (sand, silt, heavy minerals and carbonates).

The bulk density log (RHOB) measures electron density in the sedimentary rock as an estimation of bulk density. As a nuclear logging tool, the measurement is based on transformation of emitted high energy gamma rays to low energy signals according to Compton scattering phenomena. The neutron porosity log (NPHI) has a similar design but identifies the hydrogen density, indicating liquid-filled porosity in clean formations. The NPHI tool emits fast neutrons into the formation and the sensors measure the difference of resulting slowed down thermal neutrons. The vertical resolution of both tools is variable and depends on receiver spacing. In fine-grained sediments, the integration of NPHI and RHOB can give significant lithological information. Negative (inverse) RHOB-NPHI separation commonly indicates interbedded sandy/silty units in a muddy matrix. Similarly, the amount of positive RHOB-NPHI separation characterises the clay content of fine-grained sediments.

In addition to logs, cores were acquired in six wells (W31, W41, W42, W43, W44 and W45) at and close to reservoir intervals (Table 2.1). Since core was taken mainly within reservoir intervals, there is a general lack of fine-grained sediments, increasing the uncertainty of logfacies recognition results. Moreover, the fine-grained facies are often reworked in the examined cores. For this reason, we focus on the wellbores having the most complete conventional log suite in seal unit 4 interval and core description data in the reservoir level, i.e. wells W41 and W42. Although well W31 is not crossing seal unit 4, an equivalent depth-interval (fine-grained) of well W31 (2373.0-2540.5 m TVDSS, 2443.0-2656.0 m MD) has been considered as an analogue for seal unit 4 in this study because it is the best placed well in the dataset for the purpose of seismic facies calibration (Huuse and Cartwright, 2007 (Caprocks "Phase 1")) and located in the vicinity of wells W41 and W42, and has high quality sample, core and log data. The derived IPSOM approach can be extended/cross-validated to uncored wellbores with incomplete log suites within the seal interval, with a higher degree of uncertainty.

Table 2.1: *Core and wireline availability at seal unit 4 in West Africa case study (*Note: Well W31 is not crossing seal unit 4 and an equivalent fine-grained depth-interval is used as an analogue for seal unit 4)*

Well	Seal interval (m TVDSS)	Core data (m TVDSS)	Wireline measurements	Wellbore type
W31	2373.0-2540.5*	2215-2376.2	out of wireline range *	Deviated
W41	2372.9-2506.9	2598-2624.35	complete log suite	vertical
W42	2306.6-2527.3	2002-2214, 2681-2738.8	complete log suite	vertical
W43_PH	2291.1-2518.2	2129.5-2300	out of wireline range	highly deviated
W44_G	2416.3-2598.5	2196.1- 2242.4	out of wireline range	deviated
W45_PH W45_G	2471.2-2634.5	2319-2342.5	no DT log at seal unit 4 interval	highly deviated
W71	2282.4-2398.5	no core data	complete log suite with missed interval at hemipelagite-4	vertical
W71-01	2124.0-2394.9	no core data	no log measurement at hemipelagite-4	slightly deviated
W72_B	2199.8-2358.4	no core data	out of wireline range	deviated

W101	2288.3-2441.2	no core data	complete log suite	vertical
W102	2193.1-2387.0	no core data	complete log suite	deviated

The sedimentologists/petrophysicists of the operating company (a sponsor of Caprocks project) undertook comprehensive core analysis on over 800 m of core including lithology, grain size, physical structure, fracture, diagenesis and X-ray analysis. They described sedimentary facies based on the core and sample data analysis and established a 16 facies scheme, of increasing depositional energy (Insalaco et al., 2001). The scheme subdivisions are in accordance with the most popular turbidite classifications (Bouma, 1962; Stow, 1984). A brief sedimentological description of the facies, along with their characteristic log signatures and potential role in the petroleum system, are presented in Table 2.2.

Table 2.2: *Sedimentary facies descriptions given by sedimentologists/petrophysicists of the operating company (a sponsor of Caprocks project; Insalaco et al., 2001) are based on core/sample analysis at reservoir levels in six wells (W31, W41, W42, W43, W44 and W45) in West Africa case study.*

Sedimentary facies		**Sedimentological description**	**Log signatures**	**Potential role in the petroleum system**
1	**Hemipelagic shales**	hemipelagic muds; in dark green colour; interbedded with muddy turbiditie deposits constituting decametric intercalations of silts	-very high GR (due to increase in ^{238}U) -very low RT -large separation of RHOB-NPHI -high PEF	at reservoir scale: continuous seal
2	**Mud turbidites LP: Lower part of complete turbidite sequence** (~T4, T5 and T6 units in Stow's sequence (Stow, 1984))	graded muddy to silty/muddy thin layers including indistinct or wispy or millimetric silt or laminae or lenses	-GR > 60° API -large RHOB-NPHI separation -low RT -PEF < 3.5	at reservoir scale: waste-zone
3	**Mud turbidites UP: Upper**	graded silty/muddy layers including plurimillimetric basal very fine sand	-GR > 60° API -large RHOB-NPHI	at reservoir scale:

	part of complete turbidite sequence (~ T0, T1, T2 and T3 in Stow's sequence (Stow, 1984))	to silt laminae (~ T0, T1, T2 and T3 in Stow's sequence)	separation -PEF < 3.5 -low RT -good contrast in oil-based mud dip-meter (OBDT) curves	waste-zone
4	**Thin-bedded, cross-laminated silts**	very thin-bedded (centimetric or pluricentimetric scale) silty facies with sharp base and ripples, a traction- / fall-out dominated facies	-too thin to detect individually on conventional logs (e.g. if intercalated with mud turbidites shows a good organisation of OBDT curve, change in GR and RT values and larger DT)	very thin and intercalated with other elements
5	**Silty low-density turbidites**	classical graded silt-dominated turbidites, showing the complete Bouma succession; the thickness of beds ranges from 5 to 50 cm; they occur with the thick muddy turbidites intervals	-easily identifiable on conventional logs -appears as isolated silty beds in a shaly interval -good contrast in OBDT images	poor reservoir
6	**Thin-bedded, cross-laminated sands**	very thin-bedded facies (centimetric or pluricentimetric scale) fine to medium sandy facies with sharp base and ripples, a traction- / fall-out dominated facies	-too thin to detect individually on conventional logs (e.g. if intercalated with mud turbidites shows a good organisation of OBDT curve, change in GR and RT values and larger DT)	very thin and intercalated with other elements
7	**Sandy low-density**	classical graded sand-dominated turbidites, showing the complete	-easily identifiable on conventional	poor reservoir

	turbidites	Bouma succession; the thickness of beds ranges from 5 to 50 cm; they occur with the thick muddy turbidites intervals	logs -appears as isolated sandy beds in a shaly interval -good contrast in OBDT images	
8	**Massive sandy high-density turbidites (massive m-f TB sands)**	high-density well-sorted homogenous sandy turbidite with sharp base and top and without any internal visible structure; pluridecimetric to metric to scale	-low GR<60° -inverse RHOB-NPHI difference -PEF<2 -no visible dips	very good reservoir
9	**Laminated sandy high-density turbidites (laminated m-f sands)**	similar to facies 8 but with planar parallel laminations	-low GR -large RHOB-NPHI separation -low sonic velocity -low PEF -no visible dips	very good reservoir
10	**Massive gravelly high-density turbidites (laminated C-Arac TB sands)**	poorly sorted coarse sands, often exhibiting a bimodal grain-size; beds are amalgamated, often showing an eroded base underlined by mud-clasts and reworked sideritic pseudo-nodules; without internal visible structures; pluridecimetric to metric to scale	-low GR<60° -inverse RHOB-NPHI difference -low DT -PEF<2 -frequent low RT peaks -no visible dips	good reservoir
11	**Laminated gravelly high-density turbidites (laminated C-Arav sands)**	sandy facies with crude planar laminations, sometimes with reverse grading	-low GR -large RHOB-NPHI separation -low velocity -low PEF -no visible dips	good reservoir
12	**Muddy debris-flow deposits**	heterolithic muddy facies with disorganised shaly matrix (mud supported); large thickness (metric to plurimetric scale); interbedded with facies 2	-very high GR (close to facies 1) -low and irregular DT -low RT	at reservoir scale: moderate seal
13	**Muddy-sandy debris-flow deposits**	heterolithic muddy/sandy facies with disorganised shaly matrix (mud supported); large thickness (metric to plurimetric scale); interbedded with	-moderate GR -very low and irregular DT -low RT	at reservoir scale: poor seal

		facies 2		
14	**Sandy debris-flow deposits**	heterolithic sandy facies with disorganised shaly matrix (grain supported); large thickness (metric to plurimetric scale); interbedded with facies 2	-moderate GR -very low and irregular DT -low RT	at reservoir scale: poor seal
15	**Conglomeratic basal lags**	remnant facies made of clast supported conglomerates located at the erosive base of channel sequences; includes armoured clasts	-similar to facies 12,13 or 14, but thinner (metric scale) -high GR -low PEF -high variability in RHOB, NPHI and OBDT logs due to extraclasts	poor reservoir
16	**Sand injectite**	homogeneous medium to find sandstone, very well sorted heterometric; with abnormal contracts and occasional mud clasts	if thick enough: -low GR -negative RHOB-NPHI difference -low DT	good reservoirs with limited extension

In Caprocks "Phase 2", the sixteen facies were reclassified into ten and seven electrofacies by Newcastle University team based on (a) coarseness and (b) parameters controlling fluid flow. The new facies classifications and their interrelationship with the original sedimentological facies classification – described on the reservoir cores - are shown in Table 2.3. The reclassification was done for purpose of modelling the flow properties of facies at log-scale because sedimentological facies may not be directly identifiable on conventional logs (e.g. facies 4 and 6), where they share the same characteristics as electrofacies. In this study, all three facies classifications are used and evaluated for the logfacies recognition and seismic facies calibration.

Table 2.3: *Three facies classification schemes and their interrelationships; the original sedimentological facies are unified based on based on the distinct sedimentological features which influence fluid flow (Kurtev et al., 2010 (Caprocks "Phase 2")).*

Original sedimentological facies		(a) Coarseness-based facies		(b) Flow facies	
1	Hemipelagic shales	1	Hemipelagic shales	3	Isotropic
2	Mud turbidites LP	2	Mud turbidites LP	2	Discontinuous beds
3	Mud turbidites UP	3	Mud turbidites UP	1	Continuous beds
4	Thin-bedded, cross-laminated silts	4	Cross-laminated silts	4	Small vertical structures
5	Silty low-density turbidites	5	Graded silts	1	Continuous beds
6	Thin-bedded, cross-laminated sands	9	Sands	6	Sands
7	Sandy low-density turbidites				
8	Massive sandy high-density turbidites				
9	Laminated sandy high-density turbidites				
10	Massive gravelly high-density turbidites				
11	Laminated gravelly high-density turbidites				
12	Muddy debris-flow deposits	6	Muddy debris flow	4	Small vertical structures
13	Muddy-sandy debris-flow deposits	7	Sandy debris flow	5	Large vertical structures
14	Sandy debris-flow deposits				
15	Conglomeratic basal lags	10	Conglomerate	7	Conglomerate
16	Sand injectite	8	Sand injections	5	Large vertical structures

2.4 Methods

Our aim is to develop a Kohonen algorithm approach that can predict logfacies in mud-rich overburden sediments with minimal wireline and core data requirement. The method will generate knowledge about the vertical variability of

mudstones at the log scale, in order to evaluate seal capacity or fluid flow properties. In fact, we are extending the IPSOM approach that is widely used for reservoir logfacies prediction, modifying it with stepwise conditioning, parameterisation and post-processing operations. This is required to address the data limitation and geological subtlety typically observed in fine-grained sediments. In reservoir studies, petrophysicists usually use over 20-30 log curves and reliable reservoir core descriptions for detailed logfacies recognition, whereas the focus in this methodology is to perform the recognition with minimal conventional log data (five to ten log curves) and extrapolated core data from the reservoir interval. A flowchart illustrating the methodology is shown in Figure 2.2, comprising three main parts: pre-processing, recognition operation, and validation.

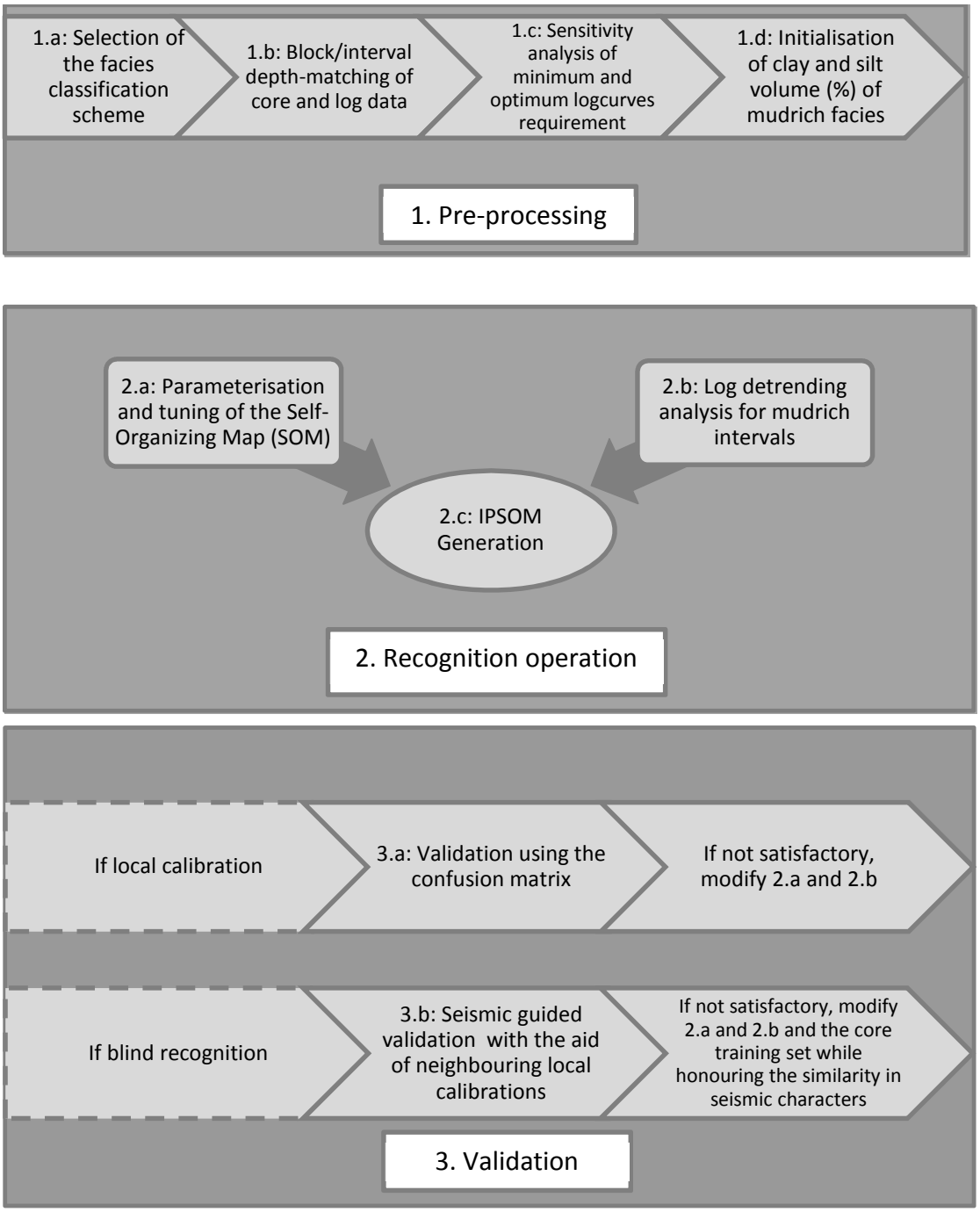

Figure 2.2: *The methodology flowchart for logfacies recognition in fine-grained seal intervals using a supervised probabilistic self-organizing map (IPSOM) approach*

The pre-processing or data preparation and quality control significantly increases the efficiency of the recognition algorithm by controlling the tuning of input data and design of IPSOM algorithm. In contrast to the conventional recognition, the system training here is facilitated by using both knowledge-driven and data-driven information. This includes (a) decisions on the electrofacies classification, (b) core-log depth matching, (c) decisions on the number and type of

predictor log curves, and (d) an initial estimation of clay (%) and silt (%) in mud-rich facies. These are time-consuming but critical precursors to subsequent data analysis.

The logfacies recognition operation attempts to elucidate features or patterns that reflect the nature of well logs. In this study, the probabilistic patterns of logfacies are defined by generating index self-organising maps (MOP), which are two-dimensional, discretized representations of multiple conventional log curves. This approach is based on unsupervised learning from input log curves which have undergone a thorough detrending analysis within fine-grained intervals, prior to mapping. With reference to the research done by Kohonen (1982, 2001) and Pospelov (1988), a brief description of the indexed and probabilised self-organising map (IPSOM) theory is given in Section 2.4.1. The approach can be applied in both cored and uncored wells, but with different validation tasks. In local calibration cases, recognition results are checked by studying confusion matrices, whereas in blind recognition cases, the validation will be guided by seismic data. Both approaches are explained in more detail in Section 2.4.4.

2.4.1 The indexed and probabilised self-organising map (IPSOM) theory:

Despite the numerous advantages, the basic self-organising map (SOM) theory is mathematically cumbersome and only the one-dimensional case has been solved completely by Fort (2006). Thus the SOM is usually adapted for the specified problem (e.g. log facies recognition) by considering modifications and simplifications in the original mathematical theory. It is also recommended to avoid using self-coded software to extend/modify SOM since there are many delicate topological criteria which would affect the convergence, orientation and stability of the results (Pöllä et al., 2007). In the current study, we utilise the commercial "indexed and probabilised self-organising map (IPSOM)" module provided in Techlog software[1]. Further to the advantages of SOM for seal logfacies recognition, IPSOM utilises the linear step index function for the input neurons which prevents generating recognition results in a black-box iterative process. Moreover, the method uses the ANN trained clustering where we can design the optimum clustering parameters (e.g. number of clusters and weighting factor) according to our objective, core descriptions and facies variability.

[1] A Schlumberger software

The IPSOM algorithm was initially developed by Pospelov (1988) by introducing the "method of K average" in order to simplify the basic SOM. Later Chashkov and Kiselev (2011) extended the "method of K average" in order to use it for log data interpretation in IPSOM module of Techlog software. In this approach, the input is a sample set, **x**, consisting of multiple log responses from "s" log types. **x** is in a vector space (sD space) where each coordinate is associated with a log type. The dimension of **x** in each coordinate is determined by the number of log responses, t. In the "method of K average", **x** is split into the given K (an IPSOM design parameter determined by the user) clusters where the intra-cluster and inter-cluster variability are minimum and maximum, respectively. In the present study, we try to use the optimum number of clusters to be able to compartmentalise the main fine-grained lithological/flow features observable using the log-core interrelationships. On the other hand, a large number of clusters could also increase the risk of contributing the prevalent noise/technical logging features in mud-rich units as the geological features. Therefore, K is an important IPSOM design parameter which should be carefully chosen according to the log/core quality and variability of fine-grained sediments at core and seal intervals.

After defining the number of clusters, each entry of the input sample set, $\mathbf{x}_i$, is assigned a random probability $\mathbf{P}_{ji}$, indicating its parent j cluster (j=1,2,…,K). Based on the random probabilities, the centre of mass of each cluster, $\mathbf{M}_j$, is computed (Chashkov and Kiselev, 2011):

$$\mathbf{M_j} = \sum_{\mathbf{i}} \mathbf{P}_{\mathbf{ji}}^{\frac{1}{\mathbf{W-1}}} \mathbf{x_i} \qquad \text{Equation 2.1}$$

Where: **M**: Centre of masses of clusters (a K×1 vector)

P: Probability matrix indicating how likely each sample entry belongs to different clusters (a K×t matrix)

x: Input log sample set (a t×1 vector – in each coordinate)

W is the weighting factor for amplifying the effect of the entries closer to $\mathbf{M}_j$. Chashkov and Kiselev (2011) suggest using the default weighting factor of 1.2. Afterward, the new probabilities are re-calculated, $\mathbf{P}_{mn}$, based on the knowledge of

clusters' centre of masses, $\mathbf{M}_j$. The new probabilities indicates how likely the data entry $\mathbf{x}_n$ belongs to the cluster m (Chashkov and Kiselev, 2011):

$$\mathbf{P}_m = \sum_i \left(\frac{r_m}{r_m}\right)^{\frac{1}{W-1}} \quad \text{Equation 2.2}$$

$$\text{and} \quad r_m = \| \mathbf{M}_m - \mathbf{x}_i \|, \quad r_m = \| \mathbf{M}_m - \mathbf{x}_n \|$$

The r_{mi} and r_{mn} are distance measures between the input data entries and cluster's centre of mass in a sD space. Then $\mathbf{P}_{ji}$ and $\mathbf{P}_{mn}$ are compared, and if different, $\mathbf{P}_{mn}$ are returned to Equation 2.1 for re-calculating/updating the centre of mass of the clusters, $\mathbf{M}_j$. This iterative process continues until reaching the convergence between $\mathbf{P}_{ji}$ and $\mathbf{P}_{mn}$. Finally the converged probabilities $\mathbf{P}_{mn}$ are used for prediction of logfacies along the logging interval. By changing the input design parameters the recognition results may change; thus the best recognition results ought to be obtained through a re-iterative parameter changing, recognition and validation processes. Since there are many different facies classifications, input logs, design parameters and quality control steps, the ordinary process could take few weeks for seal logfacies recognition of wellbores in a typical producing field. To avoid this time-consuming process, we propose a generic stepwise recognition approach which can result in optimum seal logfacies recognition results in fewer iterations without disregarding the key flow features.

2.4.2. Pre-processing

2.4.2.1 Selection of the facies classification scheme

In the recognition process for mud-rich sediments, the number of facies and the type of classification scheme depend on the final aim, which ranges from leakage/secondary migration to enhanced oil recovery (EOR). The correct choice of classification is essential not only to recognise facies from logs, but also to achieve subsequent geological models which adequately capture the sedimentological variability of fine-grained sediments. Whilst a greater range of facies will represent the finer-scale heterogeneities more accurately, the level of recognition uncertainty is likely to increase. On the other hand, minimising the number of facies does not always lead to a better recognition. Thus it is important to determine in advance the criteria for minimising the number of facies. In this study (including the next

chapters, 3 and 4), we aim in detecting lithological and flow property changes within mud-rich overburden sediments at the pick-trough time interval scale (defined by successive picks and troughs along seismic amplitude traces; in case study A ~ 10 m). Therefore, the favourable facies classification scheme would be based on the distinct sedimentological features which most influence fluid flow at the pick-trough time interval scale.

The original sedimentological facies are entirely defined by the depositional factors derived from sample and core analysis, whereas the coarseness-based and flow facies are respectively implicating the dominant lithology, and dominant texture and orientation of the more permeable sedimentological structures. The latter classifications unify various sandy facies into a single sand facies (facies 9 in the coarseness-based scheme and facies 6 in the flow facies scheme), with the focus on lithological variations in fine-grained sediments. In the coarseness-based facies scheme, the facies number increases as the dominant grain size of facies becomes coarser. Similarly in the flow facies classification, facies represented with larger numbers possess higher vertical permeabilities and thus represent a higher risk of leakage. In this study, the seal logfacies recognition process is applied on all three facies classification schemes and the results are compared to evaluate the effect of scheme selection. Therefore, for each recognition process, specific training tables are prepared, which includes: facies top/bottom depth and facies name and number for each member of the selected classification scheme. In this study, we describe the unpreserved core sections as null values to ignore their uncertainty during the training of IPSOM algorithm.

2.4.2.2 Block (interval) depth-matching of core and log data

Since beds are often thin in fine-grained sediments, it is important to depth-match core and logs accurately in order to deliver the highest quality core and log inputs for electrofacies recognition.

A range of techniques have been used in reservoirs to depth-match cores and logs, for example image logs. However, these data are often unavailable in seal intervals. In the current study, Core Gamma Ray-Gamma Ray log (COGR-GR) matching (Morton-Thompson and Woods, 1993) is used which remains exceptionally useful for wells, especially older wells, when only conventional logs

are available. It uses the fact that COGR is performed on the wall of the core while GR is done on the wall of the well. In the wireline operation, the tension and extension of logging tools are accurately calculated and corrected at the well site whilst core displacement and preservation are major issues. Having conventional log data sets in fine-grained seal intervals, COGR-GR matching is used to establish core depth shifts, intervals of core extensions and intervals of core pseudo compaction (as in the case of core mass loss and its representation as shorter core intervals). The core-depth matching process includes three steps: resampling, vertical shifting and biasing the COGR values. This is done with the aid of a tool based on Visual Basic for Applications' (VBA) code (Kurtev, 2003 (Caprocks "Phase 1")). The tool compares the similarity of the average trend of local extremes at each COGR intervals with the corresponding GR local extreme trend. The resampling and vertical shift steps are essential for the recognition purpose, but biasing the COGR curve only modifies its values appropriate to the subsurface condition. The template of the VBA tool is represented in Figure 2.3, where the vertical bulk shift is applied on a resampled COGR result. We implement a practical rule in order to make the best use of COGR and to achieve core depth shift corrections with an accuracy of ±3 cm. We resample COGR with the sampling step smaller by a factor of two than the conventional GR sampling step. For example, in wells W31, W41 and W42, the GR sampling rate is 0.1524 m, so that COGR curves are resampled with sampling steps of 8 cm. In the current case study, the COGR resampling steps range from 8 to 10 cm.

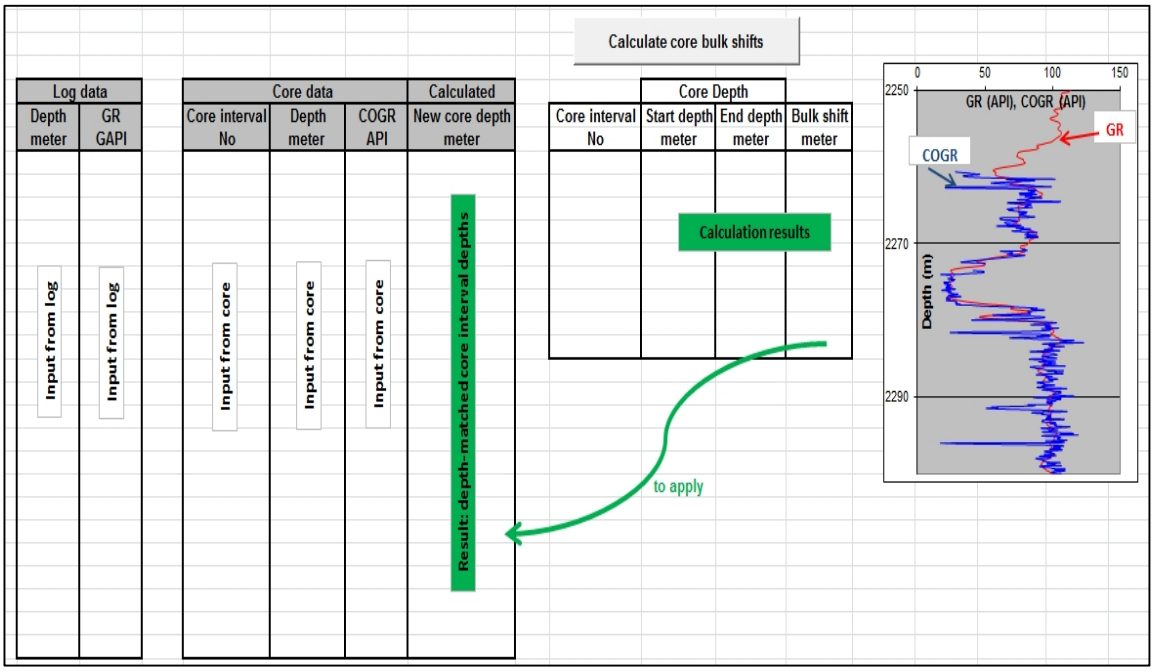

Figure 2.3: *The template of the VBA tool for calculation of vertical bulk shift in COGR after resampling by step smaller by a factor of two than the GR sampling step (after Kurtev, 2003 (Caprocks "Phase 1"))*

Although COGR-GR is a powerful technique to depth-match core with conventional logs, it can be adversely influenced by factors such as drying of the core, core ageing, core loss, etc. To avoid this issue – as described in Section 2.4.2.1 - we ignore the core descriptions in unpreserved intervals.

2.4.2.3 Sensitivity analysis of minimum and optimum log requirements

The quality control (pre-processing) step also includes a sensitivity analysis for the choice of minimum and optimum sets of logs to be used for the recognition of fine-grained logfacies. Although the number of conventional logs is limited, not all are acquired within seal intervals. This step therefore considers the availability of logs as well as the reliability of the resulting recognition. We introduce two sets of log data inputs to recognise fine-grained logfacies: minimum and optimum log suites. The minimum log suite includes the conventional logs which are often acquired within non-reservoir intervals in most modern wellbores and, with local core calibration, can result in the IPSOM recognition in a seal interval of ~ 60-70% or more. Based on our sensitivity analysis, the choice of minimum log suite is presumed to be independent of the context, as they form the essential dimensions of IPSOM maps. We believe the minimum log suite required for mud-rich electrofacies

recognition must include: gamma-ray (GR), compressional slowness (DTCO) and bulk density (RHOB). On the other hand, the recognition can be improved by incorporating further log curves in the mapping process. This new log set is called optimum log suite. The optimum log suite depends on the geological setting and can further improve the local core calibration/blind recognition within a seal interval.

In the wellbores of West Africa case study, within seal unit 4 interval, we have 15 different conventional log types: bulk density (RHOB), compressional wave slowness (DTCO), gamma-ray (GR), gamma-spectrometry (GR-U, Th and K), neutron porosity (NPHI), photo-electric factor (PEF), porosity - effective (PHIE), porosity - total (PHIT), shear wave slowness (DTSM), resistivity – deep (AHT10), resistivity - shallow (AHT90), deep-induction (ILD) logs. According to the sensitivity analysis at recognition targets of two short intervals in hemipelagite-4 and MTD-4 in the cored wells, we categorise the effective log curves as illustrated in Table 2.4. Therefore, given the availability of logs in the well, we apply the appropriate log suite over the full range of seal unit 4 interval. The wellbores without the minimum log suite along seal unit 4 are also removed from the recognition process. Moreover, in the optimum log suite we use the gamma spectrometry (GR - U, Th and K) logs to evaluate their effect on fine-grained facies recognition.

Table 2.4: *Minimum and optimum log suites for IPSOM logfacies recognition at seal unit 4 in West Africa case study (based on the sensitivity analysis on pilot intervals of the cored wells)*

Log suite	Log data		Remarks
Minimum log suite	GR, DTCO, DTSM, RHOB		can work without DTSM, but the results are less accurate
Optimum log suite	GR, DTCO, DTSM, RHOB	AHT90, AHT10, NPHI, PEF	the log suite includes gamma spectrometry (GR - U, Th and K) logs

2.4.2.4 Initialisation of clay and silt percentages of mud-rich facies

In this step, we impose an additional lithological constraint to facilitate the recognition process. Although fine-grained facies have a range of clay:silt:sand

ratios, the ratios can still be correlated to the input log suite to steer the recognition process. Since the proportion of sand is complementary to the silt and clay contents, we only use the two curves of clay and silt contents to avoid excessive calculation. The clay content curve is estimated from the input log suite using the in-house ShaleQuant tool (Yang et al., 2004). On other hand, we have the MICP and SediGraph measurements on 126 core samples, presented in terms of facies groups. The measurements were performed by Newcastle University team in Caprocks "Phase 1 and 2". We cross-plot the clay and silt percentages from the sample data at fine-grained facies to derive their non-linear trend (second-order polynomial) function. Then the silt ratio can be calculated at given log-estimated clay content by applying the established non-linear sample clay-silt correlation. We use a VBA tool (Kurtev, 2007 (Caprocks "Phase 1")) to automate the calculation of the silt content curve. The VBA tool can be adapted to be used for any new group of samples with measured clay% and silt% (Figure 2.4). As a result of this step, we have two knowledge-driven auxiliary curves to increase the robustness of the IPSOM recognition within seal intervals.

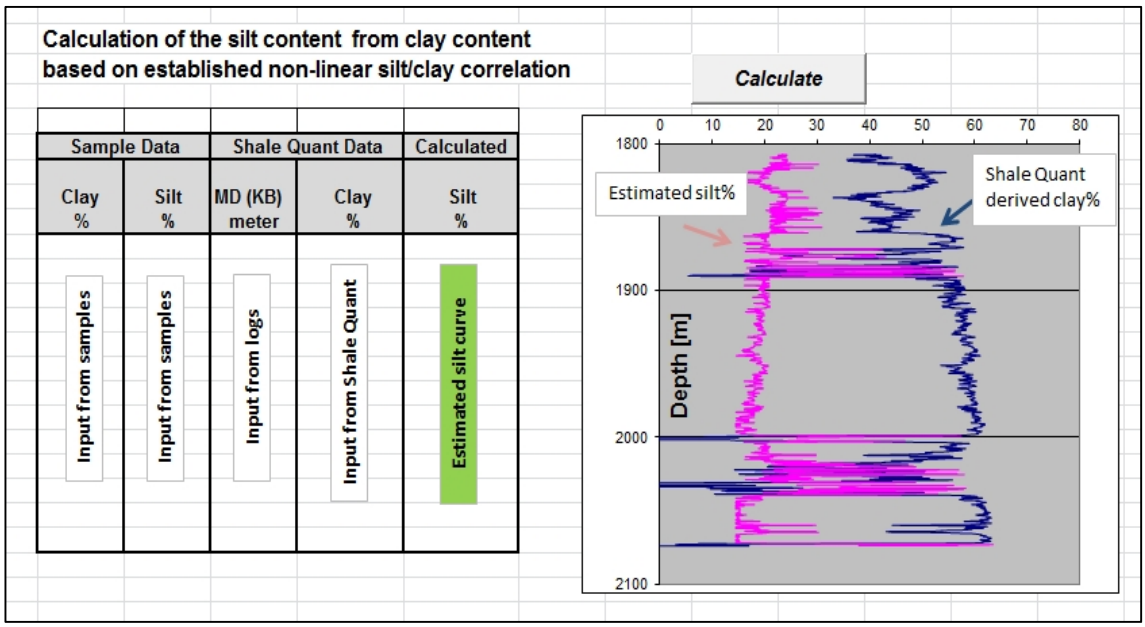

Figure 2.4: *The template of the VBA tool for estimation of silt% from non-linear silt/clay correlation at given ShaleQuant clay content (After Kurtev, 2007 (Caprocks "Phase 1")). The silt/clay correlation is based on core sample analysis performed by Newcastle University team in Caprocks "Phase 1 and 2".*

2.4.3 Recognition operation

2.4.3.1 Parameterisation and tuning of the self-organising map (SOM)

There are several SOM parameters which control the quality of the facies recognition from logs. These include the recognition method, size of the 2D SOM, weight factor, number of learning wells in the log dataset, choice of log data set, etc. Tuning of each of these parameters influences the final quality of facies recognition. The input log suite and the choice of learning wells were discussed earlier in Section 2.4.2. In this step, we only focus on selecting the IPSOM method, map size and weighting factors within fine-grained contexts.

Selecting the grid size is the essential parameter for the IPSOM operation, since the grid modification can provide totally different results with even similar indexation options. In an ideal case (e.g. reservoir studies), a rectangular grid is favourable for visual inspection, since the edges of the array have to be rectangular rather than square (Kohonen, 2001). Moreover, the dimensions of the grid are also expected to be at least equal to the major dimensions (e.g. the principal components) of the distribution of the target parameter/variable. Here we assume that there is no distinct lithological trend along the wellbore from reservoir to seal, so that there is an equi-dimensional distribution of logfacies with respect to logs. We therefore suggest a square grid with dimensions greater than the number of original core facies descriptions. We examine two grid sizes: 50×50 and 16×16 where each grid contains the learning samples with similar rose-diagrams of the input log signals. The bigger map should give higher resolution by achieving good separation of the facies by the input log signals. According to our original core facies descriptions, the grids of size smaller than 16×16 are not recommended as they will be smaller than the major dimensions of the facies.

The SOM can be generated in both supervised and unsupervised manners. If a rich input log database (i.e. ~30-50 log curves along the target) is available, the unsupervised manner will be more generic and effective. Here we utilise the IPSOM as a supervised approach, because the number of learning bases is lower than the number of neurons due to limited input logs within seal intervals. Three different supervised approaches are evaluated to determine the best approach for the

recognition of fine-grained facies: (a) the "quantitative classification" method, which is a more instantaneous pattern detector and the (b) "minimal distance" and (c) "majority vote" approaches which are more sensitive to local-scale pattern changes. By keeping similar all other indexation parameters, the recognition results of these supervised approaches are expected to be complementary.

Finally, we can weight various input logs to generate the best SOM. With the aid of weighting factors, we can honour the most useful logs at each index for equi-probability circumstances. We suggest applying the weighting factors only one curve at a time in order to understand and control the effect. In the present study we individually apply a weighting factor of 1.2 on both the RHOB and PHIT/PHIE log curves, since their log responses are less affected by the mud cake, invasion, wellbore damage and other logging artefacts within muddy seal intervals. In fact, the application of the weighting factor depends on the desired outcome, input logs, context and target. The weighting factor can be also used to magnify or decrease the effect of logs by considering their acquisition and processing quality. The well logs in West Africa case study have undergone similar resampling and environmental corrections and acquired by logging tools of one Service Company.

2.4.3.2 Log detrending effect on the IPSOM recognition of fine-grained facies

Log detrending is an important processing step and is often advised prior to logfacies analysis, for example using neural networks in reservoirs (Delfiner et al., 1987; Roger, 1992). It can be especially helpful to improve the long-range (>300-500 m) cross correlations between well logs (e.g. for seal facies recognition based on the reservoir core descriptions), since it provides the wireline characteristics/fluctuations of lithology which are not associated with the normal compaction trend (Magara, 1986). Therefore we used detrending techniques prior to the generation of IPSOM. In the present study, the linear detrending technique was applied on the minimum log suite including density, p-wave sonic, s-wave sonic and neutron porosity logs. For this purpose, we utilise "detrend" function in the "statistics and random numbers" tool box of *Matlab*. The function removes the average or the best least-squares fit line from the selected log data. This detrending allows us to subtract the systematic increase/decrease from the log responses which are due to the compaction effect. Moreover, this function is a useful tool for detrending multiple logs as it individually

treats different log columns in one go. The tool box offers four different detrending functions:

$$\mathbf{y} = \text{detrend}(\mathbf{x}) \qquad \text{Equation 2.3a}$$

$$\mathbf{y} = \text{detrend}(\mathbf{x},\text{'constant'}) \qquad \text{Equation 2.3b}$$

$$\mathbf{y} = \text{detrend}(\mathbf{x},\text{'linear'},bp) \qquad \text{Equation 2.3c}$$

$$\mathbf{y} = \text{detrend}(\mathbf{x},\text{'constant'},bp) \qquad \text{Equation 2.3d}$$

where **y** (a n×1 vector) and **x** (a n×1 vector) are the detrended and original log values, respectively. n is the number of log samples in a selected interval. Equation (2.3a) removes the best least-squares fit linear trend from the log responses, while Equation (2.3b) only subtracts the mean of the log responses at the given interval. These two equations are useful for intra-litho-unit detrending where the lithology does not change dramatically. However, we can perform similar detrendings using Equations (2.3c) and (2.3d), but within predefined segments by a vector 'bp'. This is illustrated in Figure 2.5 with a full range GR log at well W31. Thus we utilise Equation 2.3c for detrending the minimum input log suite, because it is more effective for the long-range cross correlation between well logs in uncored seal intervals. The break points vector is defined by visual inspection of lithological units which show different local compaction trends. We ignore break points for highly anomalous local trends as this increases the risk of falsifying the input log data. In the default circumstance, we assume that the lithologically-caused log fluctuations are large enough to compensate for the effect of trend removal, so that detrending can improve the long-range cross-correlations between logs. Otherwise, the Mann-Kendall (MK) test for monotonic trend should be performed as described by Gilbert (1987). Hirsch et al. (1982) indicated that this is the most appropriate way to evaluate the significance of removing a monotonic trend from input data. Therefore, in the subtle cases where a compaction trend is not visually clear, detrending was advised only if the MK test statistic (Z_{MK}) was lower than 10.

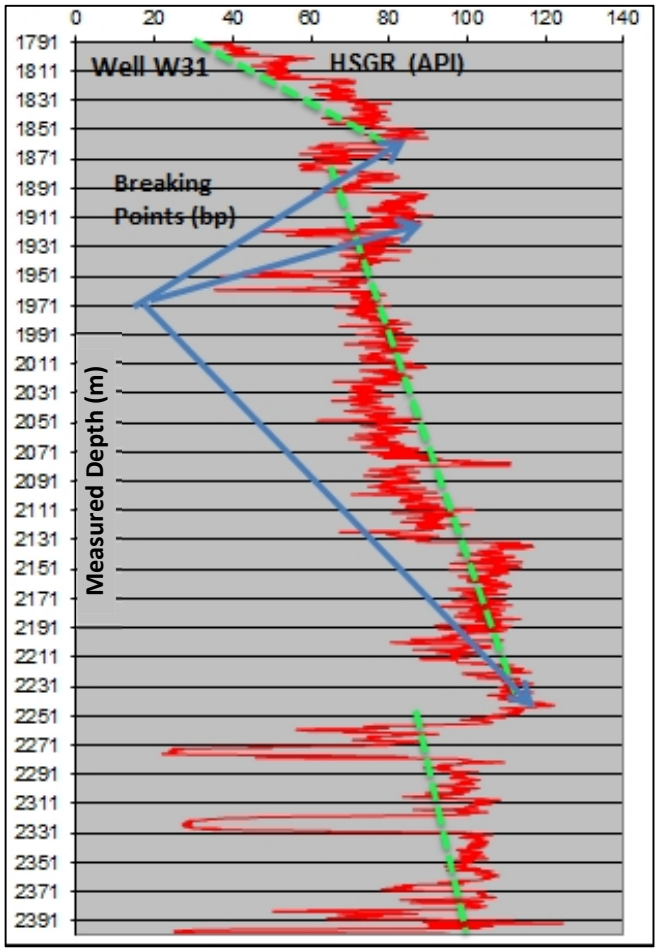

Figure 2.5: *Demonstration of the linear log detrending by using the "detrend" function in Matlab while defining the break points by vectors "bp" at different local compaction trends (Total spectral GR log (HSGR) is represented by the red line along the full wireline range of well W31 which crosses reservoir level A, the analogue seal unit and reservoir level B, respectively).*

2.4.3.3 IPSOM generation

An indexed and probabilised self-organizing map (IPSOM) is an ANN-based method based on the Kohonen algorithm that can be used to predict and propagate facies/rock classifications. The method has been developed over the last decade (e.g. Chashkov and Kiselev, 2011) and been widely used in predicting categorical properties (log and core processing). Here we use the standard algorithm as available in Techlog software. It gives an indexed self-organised map as a result of the log-sample training at cored reservoir interval which is later used to recognise facies at uncored seal interval. In our approach, the results are refined through an iterative

process after the next step, the validation phase. The main steps of the IPSOM operations are briefly described below and illustrated in Figure 2.6:

1. Generation of the initial, unsorted SOM with given parameterisations (including grid size, weighting factor, supervised method and the input log suite)
2. Organisation and sorting of the grid of nodes
3. a) Indexation of grids with facies core descriptions, i.e. a facies as a code is assigned to each neural unit (the key operation); b) Projection (colour coding) of the indexed samples within the SOM nodes (thus transition facies should be clearly identified);
4. Sketching the probability of occurrence of the predicted facies at each depth

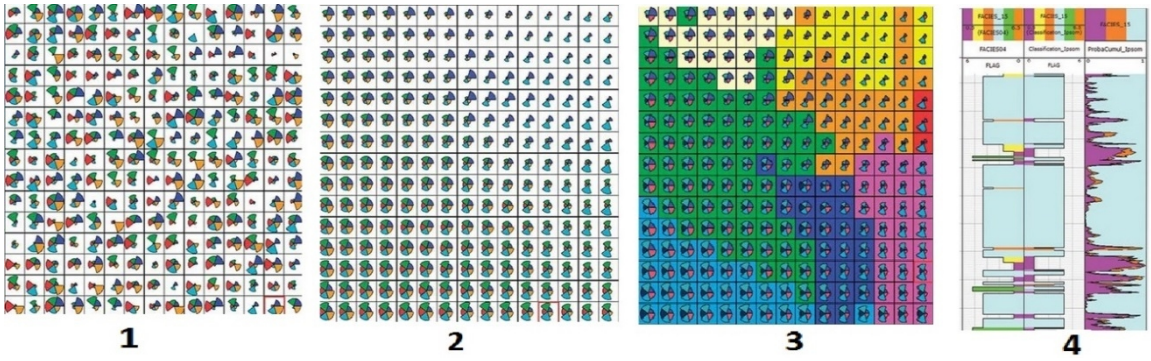

Figure 2.6: *Schematic steps of IPSOM generation (Snapshots are taken from Techlog Manual which are the snapshots available for illustration of algorithm steps)*

2.4.4 Validation

The recognition process is applied on seal units of both cored and uncored wells; thereby the validation of recognition results at different wells is separately handled based on the core availability:

2.4.4.1 Cored wells (local calibration cases):

Although validation of the recognition results with the aid of their corresponding core data or image logs are the most reliable and accurate approaches, mudstone cores and image logs are rarely taken in the overburden formations. Thus our local calibrations in the cored wells are inevitably based on the comparison of the recognition results with the core descriptions at mud-rich sections of the overlying/underlying reservoirs. In both training and validation process, we presume

there is no radical change in the nature of the fine-grained sediments at the juxtaposed reservoir and seal unit.

In local calibration cases, we establish a comparison table, so-called confusion matrix, which allows us to compare quickly two categorical variables (i.e. logfacies). In order to automate the validation of IPSOM recognition results, a VBA tool (Kurtev et al., 2013 (Caprocks "Phase 3")) was used. The template of the tool is represented in Figure 2.7 comprising the input section, VBA action button and confusion matrix. We provide the depth and core/recognition facies data in the input section and by pressing "Calculate Statistics" button, the VBA code computes the entries of confusion matrix. The code compares core facies and recognised logfacies at overlapping depths, calculates the frequencies and provides the relative positive correlations (%) of core-recognised facies for each core facies. The higher diagonal values in the confusion matrix implies the better recognition results. In other words, more core facies are recognised correctly at their overlapping intervals.

The confusion matrix is also very useful tool for analysis of the IPSOM process, since it can illustrate the logfacies with similar characteristics in the SOM (hard to discriminate); or it can be used to compare the effect of different SOM parametrisation, log detrending/QC and logfacies classification schemes. Therefore, in an iterative process, the confusion matrices will be analysed to tune the IPSOM parameters and inputs.

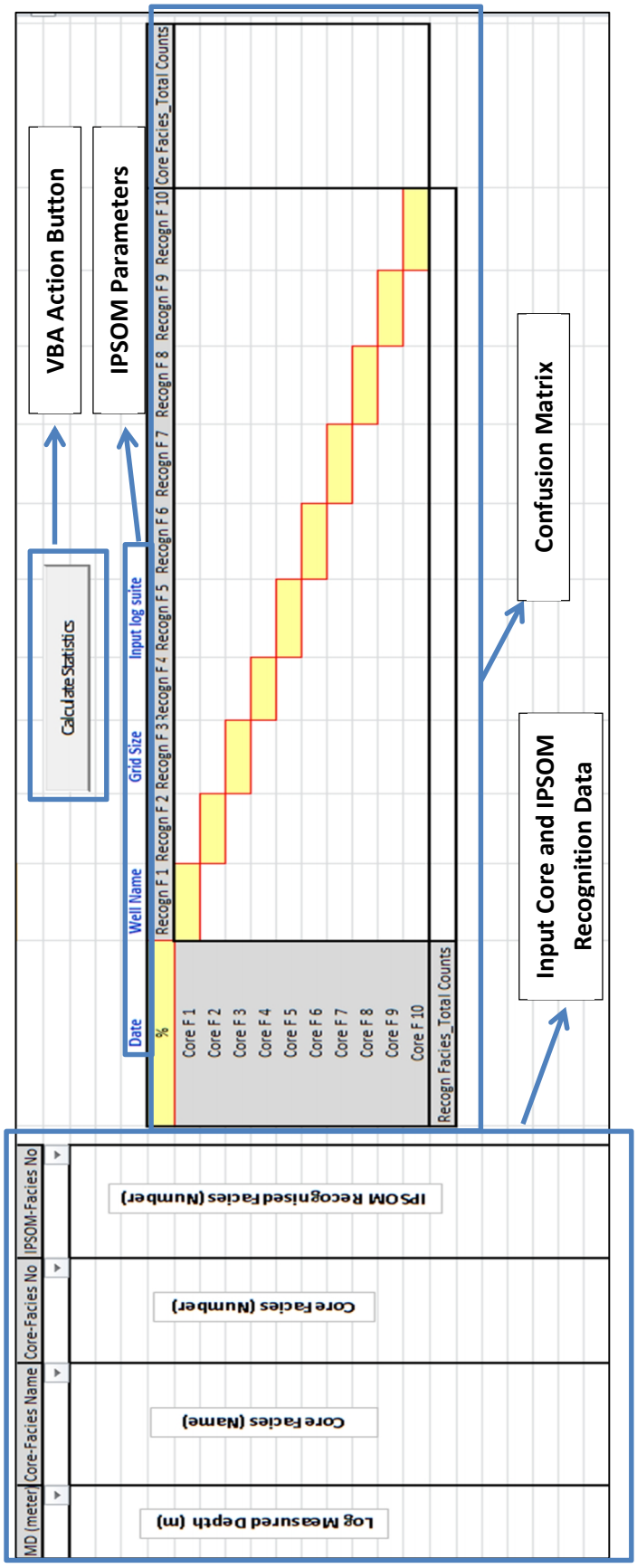

Figure 2.7: *The "confusion matrix" template used for validation of the IPOSM results at local calibration cases (after Kurtev et al., 2013 (Caprocks "Phase 3")). The template is*

supplied by a VBA code which computes the relative positive correlations (%) of core facies with recognised facies at each facies.

2.4.4.2 Uncored wells (blind recognition cases):

Blind recognition means (i) we do not have core facies descriptions along the wellbore even at reservoir level. Therefore, the neural network of IPSOM is trained based on the core descriptions of the nearby well(s). Moreover, (ii) in the cored wells, the blind recognition can be also used to evaluate the efficiency of non-linear correlations derived by the local calibration. An efficient neural network should reproduce acceptable facies recognition results with training set from the adjacent well(s). Validation of case (ii) can be handled by analysis of the confusion matrices and the available core facies descriptions, explained in Section 2.4.4.1. But the question here is how to validate the logfacies recognition results in case (i) where there are not any local core facies descriptions. In the current study, at uncored wells, we utilise seismic responses as the guide for both selecting the training wells and also validating the logfacies recognition results. We believe that there is a qualitative link between the variability of the seismic amplitude and the vertical variability of log facies in finegrained seal intervals, which is a useful for the interpretation of the nature and heterogeneity of these sediments. In addition, the strength of seismic amplitude should implicate the coarseness of the sediments, providing noise, pore-pressure and fluid effects are minimal. Thereby, in case (i) we use the seismic amplitude and frequency to qualitatively validate the trend of the logfacies recognition results and iteratively tune the IPSOM parameters and input training wells. In the mud-rich seal context with marginal effects from pressure and fluid, a reliable facies recognition should honour seismic anomalies as well as the trend of major seismic characteristics. The hypothesis is discussed in more detail in Chapter 3 and 4, where the volumetric seismic attributes are used to predict leakage risk and lithology at fine-grained seal units.

2.5 Results and discussion

The seal facies recognition methodology has been applied on all the wells in West Africa case study with the minimum log suite (Table 2.4) along seal unit 4 (and the analogue seal unit). They are wells W31, W41, W42, W71, W101 and W102, in which the wells W31, W41 and W42 have core data at the reservoir interval (Table

2.1). The fine-grained zones of the cored intervals comprise the training sets for the seal logfacies recognition process (the original/unshifted core depths are provided in Table 2.1). In the present study, the three cored wells are the pilot studies for the recognition with local calibration as well as training sets for the blind recognition networks.

We have implemented the recognition procedure while using three pre-defined facies classification schemes: original sedimentological facies, coarseness-based facies and flow facies (Table 2.3). We compared their logfacies recognition results to evaluate the effect of the facies numbers and unification. As an initial step, all core facies descriptions were tabulated, so that at each core description depth interval, three facies numbers and names were provided corresponding to three different facies classification schemes (sample table for cores K2 and K3 of well W41 is available in Table 2.5). The unpreserved core intervals are ignored by assigning them null values. These intervals are described as core sections where the facies boundaries are not clear in the core images. In these intervals, we used the GR log curve for identifying the facies description boundaries.

Table 2.5: *Tabulated core facies descriptions in three classification schemes for cores K2 and K3 of well W41: the IPSOM algorithm can only work with codes/numbers*

M	M	unitless	unitless	unitless	unitless	unitless	unitless	unitless
Top	Bottom	Core_Sectior	Facies_Sedim_Name	Facies_Sedim_No	Facies_Coars_Name	Facies_Coars_No	Flow_Facies_Name	Flow_Facies_No
2260.7	2261.03	K2	H-Massive m-f TB Sands	8	9-Sands	9	6-Sands	6
2261.03	2261.31	K2	J-Masive c-grav TB Sands	10	9-Sands	9	6-Sands	6
2261.31	2261.62	K2	H-Massive m-f TB Sands	8	9-Sands	9	6-Sands	6
2261.62	2261.74	K2	-9999.25	-9999.25	-9999.25	-9999.25	-9999.25	-9999.25
2261.74	2262.97	K2	-9999.25	-9999.25	-9999.25	-9999.25	-9999.25	-9999.25
2262.97	2263.33	K2	-9999.25	-9999.25	-9999.25	-9999.25	-9999.25	-9999.25
2263.33	2263.4	K2	H-Massive m-f TB Sands	8	9-Sands	9	6-Sands	6
2263.4	2263.69	K2	J-Masive c-grav TB Sands	10	9-Sands	9	6-Sands	6
2263.69	2263.93	K2	H-Massive m-f TB Sands	8	9-Sands	9	6-Sands	6
2263.93	2264.17	K2	-9999.25	-9999.25	-9999.25	-9999.25	-9999.25	-9999.25
2264.17	2264.38	K2	H-Massive m-f TB Sands	8	9-Sands	9	6-Sands	6
2264.38	2264.45	K2	J-Masive c-grav TB Sands	10	9-Sands	9	6-Sands	6
2264.45	2264.81	K2	H-Massive m-f TB Sands	8	9-Sands	9	6-Sands	6
2264.81	2264.9	K2	F-Cross-Laminated Sands	6	9-Sands	9	6-Sands	6
2264.9	2265.03	K2	H-Massive m-f TB Sands	8	9-Sands	9	6-Sands	6
2265.03	2265.13	K2	-9999.25	-9999.25	-9999.25	-9999.25	-9999.25	-9999.25
2265.13	2265.26	K2	C-Mud Turbidites-LP	3	3-Mud-Turbidites LP	3	1-Continuous Beds	1
2265.26	2265.35	K2	-9999.25	-9999.25	-9999.25	-9999.25	-9999.25	-9999.25
2265.35	2265.39	K2	P-Sand Injections	16	8-Sand Injections	8	.arge vertical structur	5
2265.39	2265.79	K2	C-Mud Turbidites-LP	3	3-Mud-Turbidites LP	3	1-Continuous Beds	1
2265.79	2266.17	K2	-9999.25	-9999.25	-9999.25	-9999.25	-9999.25	-9999.25
2266.17	2266.43	K3	C-Mud Turbidites-LP	3	3-Mud-Turbidites LP	3	1-Continuous Beds	1
2266.43	2266.79	K3	-9999.25	-9999.25	-9999.25	-9999.25	-9999.25	-9999.25
2266.79	2266.97	K3	B-Mud Turbidites UP	2	2-Mud-Turbidites UP	2	2-Discontinuous Beds	2
2266.97	2267.06	K3	-9999.25	-9999.25	-9999.25	-9999.25	-9999.25	-9999.25
2267.06	2267.11	K3	-9999.25	-9999.25	-9999.25	-9999.25	-9999.25	-9999.25
2267.11	2267.15	K3	-9999.25	-9999.25	-9999.25	-9999.25	-9999.25	-9999.25
2267.15	2267.29	K3	B-Mud Turbidites UP	2	2-Mud-Turbidites UP	2	2-Discontinuous Beds	2
2267.29	2267.95	K3	L-Muddy Debris Flow	12	6-Muddy Debris Flow	6	mall Vertical Structu	4

In the next step, we have prepared the input log curves according to the wireline availability along seal intervals. We have not used wells W43, W44, W45, W71_01 and W72 in this study, since they do not have the minimum log suite along the seal units for the recognition process. For the rest of the wells, we have plotted all the log curves to make a visual inspection of the log data quality. We can usually have several log curves of the same types, thus we only keep the best quality log curve out of a log family to avoid excessive calculation in the ANN network (due to their linear dependency). Moreover, different log curves can have different sampling intervals which require to be unified prior to the recognition process. Otherwise, the log curves will be automatically resampled during the IPSOM process which can adversely affect the log correlations. As a rule of thumb, we used the best conventional GR log curve in each well as the log reference curve and resampled the rest of the input logs (if different) with GR reference curve sampling depth. This is because we presume the GR log is the most informative conventional log and less affected by the environmental and logging tool features in the fine-grained sediments.

COGR-GR block depth-matching

As explained earlier in Section 2.4.2.2, we apply COGR-GR depth matching technique to put in correspondence the core facies and the recorded input log signals. This is an important step as shifting core training sets can significantly affect the orientation of the topological space in the IPSOM models. We have focused on vertical block shifting of COGR and presumed there is no additional misfit between the GR and the rest of the conventional input logs. We have input the GR and COGR data into the VBA template (Figure 2.3). The algorithm is designed to start from top to bottom so that the bottom part of the COGR curve moves as a block without deformation. This is because the coarser core intervals are located at the upper level in wells W31, W41 and W42 where COGR-GR depth matching is more robust due to larger changes in GR values. Figure 2.8 illustrates the result of COGR-GR depth matching for six core intervals at well W41 in a sandy (Figure 2.8a) and a muddy (Figure 2.8b) sections. In this figure, the red and dotted black curves represent the COGR and GR logs. The misfit between the curves is reduced by applying vertical block shift of COGR; however, they are not completely fitted. This is because first the COGR is acquired at laboratory/surface condition whilst GR responds to the

formation at subsurface condition. Second, we avoid biasing the COGR values, since gamma ray changes in the finer core intervals are smoother than the core scale and COGR value changes can manipulate vertical depth-matching process which is essential for the IPSOM. Table 2.6 illustrates the effect of COGR biasing in increasing the average block misfits along the cored intervals in the studied wells. As shown in the table, the effect of COGR biasing is rather local and it can increase the misfit between COGR and GR curves; hence the risk of wrong correspondence between log signals and core facies (in particular in mud-rich sections).

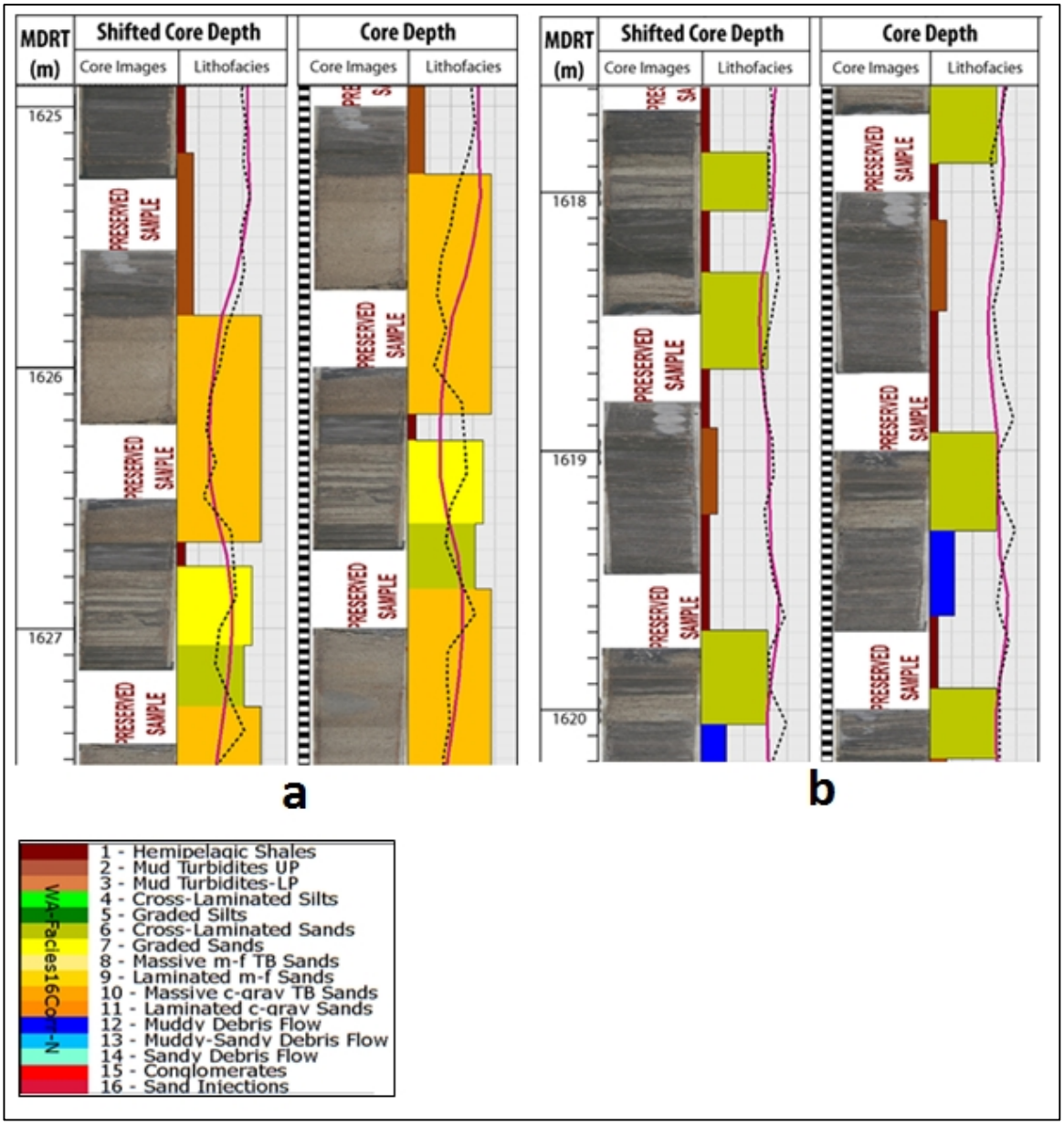

Figure 2.8: *COGR-GR depth match result in sand-rich (a) and mud-rich (b) cored sections in well W41. Only vertical bulk shift is applied, thus minor misfits are expected, mainly in the coarser parts. The red and dotted lines represent the COGR and GR logs.*

Table 2.6: *Average COGR-GR block misfits within the wireline intervals in the pilot wells (W31, W41 and W42)*

Wells	W31	W41	W42
Total core length (m)	189.32	111.06	210.42
Average COGR-GR block misfit (m) – only vertical shift applied	5.11	0.81	1.49
Average COGR-GR block misfit (m) – vertical shift and COGR biasing applied (depth-matched in Techlog)	5.31	0.98	2.03

Estimation of clay and silt percentages of mud-rich facies

In the proposed IPSOM process, the clay and silt curves are added into the input log suite as two knowledge-driven auxiliary curves. For this purpose, we used the sample measurement results (done by Newcastle University team in Caprocks "Phase 1 and 2") at the fine-grained facies. In other words, we only used the results for 40 samples out of the total 126 samples, i.e. 19, 13 and 8 samples from wells W31, W41 and W42. In Table 2.7, the selected core sample analysis (SediGraph analysis) are presented including clay:silt:sand ratios. We have shifted the original sample depths according to the bulk shift obtained during the COGR-GR depth-matching. Then the parent facies of each sample was determined by comparing the sample depth and the core interval description. As indicated in Table 2.7, although the facies can have ranges of clay:silt:sand ratios, they are correlated and we think the mean and variance of the clay/silt contents for each facies help with clustering the log signal-facies correspondence during the IPSOM process.

We cross-plotted the silt content versus clay content using 40 samples (from wells W31, W41 and W42) and derive a second-order polynomial correlation function (Figure 2.9) for the pilot study. We then compared the results with the silt/clay correlation derived in a case study from North Africa, in which 92 fine-grained samples from nine wells had been analysed (by Newcastle University team in Caprocks "Phase 1 and 2"). Although the depositional environment for North Africa case study is deltaic with higher depositional energy, both correlations have approximately similar trend slope (Figure 2.9). Despite of the robustness of the clay/silt correlation (R^2: ~ 0.92) within the pilot area (at proximity of wells W31,

W41 and W42), application of the correlation on full size case study would require further sample information from other wells.

On the other hand, we have derived estimated clay content curve for each well by using the in-house ShaleQuant solution. And finally we have entered the clay content curve and the clay/silt correlation detail in the VBA template (Figure 2.4) to calculate the silt content curve along the pilot wellbores. Figure 2.10 illustrates how the silt content curve was calculated in well W42, in which calculated silt (using sample-based correlation) and clay (using ShaleQuant) contents are represented by pink and blue curves. In this figure, the clay and silt curves clearly indicate two reservoir zones (interval ~1870-1890 m and ~2020-2035 m) and minor lithological changes within the intermediary non-reservoir sequences.

Table 2.7: *Sand:Silt:Clay ratios derived from core sample analysis (SediGraph analysis) of 40 mud-rich samples in wells W31, W41 and W42 (the facies numbers are based on the core descriptions)*

Well name	Shifted sample depth (m)	Facies number	Sand (%)	Silt (%)	Clay (%)
W31	2278.06	2	2.06	18.85	79.10
W31	2278.7	2	4.33	19.26	76.41
W31	2279.43	2	12.14	38.45	49.41
W31	2283.35	14	8.96	21.71	69.33
W31	2288.59	13	8.70	36.60	54.71
W31	2291.56	2	0.47	21.04	78.49
W31	2297.51	2	0.56	18.05	81.40
W31	2301.85	12	28.33	26.69	44.98
W31	2326.62	8	3.05	14.40	82.54
W31	2342.73	2	2.24	14.72	83.05
W31	2361.81	2	15.44	20.81	63.75
W31	2378.28	1	3.16	17.83	79.01
W31	2388.66	3	2.99	15.35	81.66
W31	2401.54	12	0.98	30.84	68.18
W31	2406.62	2	0.13	13.72	86.15
W31	2406.72	2	2.39	57.93	39.68
W31	2410.4	2	0.93	24.08	74.99
W31	2416.73	3	3.14	43.29	53.57

W31	2432.74	2	3.52	16.44	80.04
W41	2279.65	2	1.87	13.69	84.45
W41	2340.35	13	43.23	17.25	39.53
W41	2347.9	12	1.46	14.00	84.54
W41	2358.87	7	0.18	13.17	86.65
W41	2364.9	3	0.21	22.48	77.31
W41	2369.9	10	3.36	14.92	81.72
W41	2599.56	1	0.25	15.78	83.98
W41	2601.45	1	0.38	12.82	86.80
W41	2608.24	1	0.38	14.19	85.43
W41	2613.35	2	0.22	19.85	79.93
W41	2618.16	2	0.17	15.42	84.41
W41	2619.38	2	0.59	17.23	82.18
W41	2623.12	2	0.98	8.10	90.92
W42	2005.58	2	3.85	14.73	81.42
W42	2013.33	12	1.08	15.31	83.60
W42	2016.48	2	0.10	14.51	85.39
W42	2039.57	2	0.15	12.17	87.68
W42	2056.65	1	0.13	12.53	87.34
W42	2173.59	13	1.43	33.36	65.21
W42	2183.4	13	15.53	35.25	49.23
W42	2198.54	2	0.35	14.50	85.15

1 - Hemipelagic Shales
2 - Mud Turbidites UP
3 - Mud Turbidites-LP
4 - Cross-Laminated Silts
5 - Graded Silts
6 - Cross-Laminated Sands
7 - Graded Sands
8 - Massive m-f TB Sands
9 - Laminated m-f Sands
10 - Massive c-grav TB Sands
11 - Laminated c-grav Sands
12 - Muddy Debris Flow
13 - Muddy-Sandy Debris Flow
14 - Sandy Debris Flow
15 - Conglomerates
16 - Sand Injections

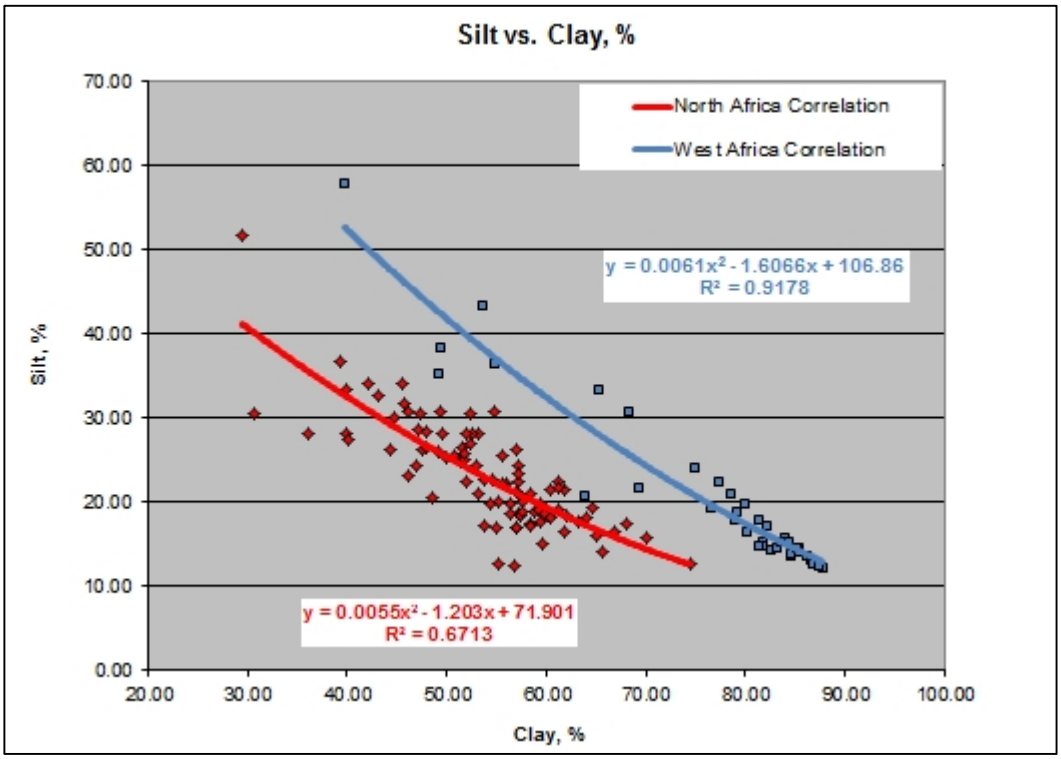

Figure 2.9: *Silt-Clay content correlations in West Africa (Blue) and North Africa (red) case studies. The trend lines have approximately similar slope, and the scatter plots is based on the sand:silt:clay ratios derived from laboratory analysis of mud-rich samples (West Africa: 40 samples; North Africa: 92 samples). The SediGraph measurements were performed by Newcaslte University team in Caprocks "Phase 1 and 2".*

Calculation of the silt content from clay content
based on established non-linear silt/clay correlation

Calculate

Sample Data		Shale Quant Data		Calculated
Clay %	Silt %	MD meter	Clay %	Silt %
16.46	57.928	1804.689	43.6	21.51300102
22.60	44.007	1804.789	44.7	22.04552441
23.67	36.599	1804.889	45.3	27.99329214
27.13	43.291	1804.989	46	28.76160588
29.95	35.247	1805.089	47.2	22.72457887
31.82	38.454	1805.189	46.8	24.73692121
32.68	33.364	1805.289	46.3	27.25234912
33.11	26.69	1805.389	46.7	25.24000679
33.83	24.447	1805.489	46.4	26.74926354
40.03	24.081	1805.589	45.4	28.98458677
44.58	20.812	1805.689	45.3	27.99329214
45.59	30.839	1805.789	44.8	23.03681903
47.40	21.71	1805.889	42.1	22.59104344
51.53	18.849	1805.989	40	24.08248481
52.53	15.873	1806.089	39.8	24.09428779
53.87	21.039	1806.189	40.7	23.59721636
57.87	19.263	1806.289	41.3	23.16599939
59.14	17.831	1806.389	41.6	22.95039091
59.51	18.046	1806.489	41.4	23.0941299
61.11	14.503	1806.589	41.5	23.0222604
61.63	14.402	1806.689	41.5	23.0222604
61.79	15.346	1806.789	41.2	23.23786889
62.93	14.715	1806.889	40.9	23.45347737
64.86	14.508	1806.989	40.8	23.52534687
65.10	17.229	1807.089	41.2	23.23786889
65.65	12.527	1807.189	40.8	23.52534687
65.84	15.313	1807.289	39.5	24.11199227
68.68	14.728	1807.389	37	24.25952953
69.86	11.874	1807.489	36.9	24.26543102
70.92	19.846	1807.589	38.4	24.17690866
70.93	13.718	1807.689	42.2	22.51917394
71.91	15.42	1807.789	41.9	22.73478242

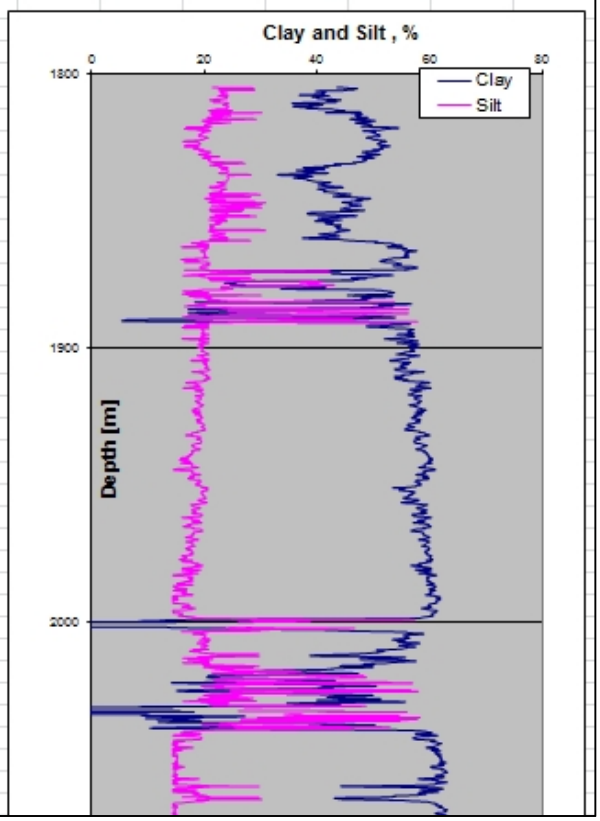

Figure 2.10: *Estimation of Silt (%) from non-linear silt/clay correlation (Figure 2.9) at given ShaleQuant clay contents in well W42. The blue and pink curves represent the ShaleQuant-derived Clay(%) and Silt (%). The silt-rich zones co-exist with sand-rich zones, indicating reservoir level A and B (intervals: ~1870-1890 m and ~2020-2035 m).*

Log detrending / removing the compaction trend

The linear segmented log detrending was applied on seven wells (W31, W41, W42, W71, W101, and W102), in which we have got the minimum input log requirement. The DTCO, DSTM, RHOB, PHIT (if available) and PHIT (if available) logs were detrended as they are expected to be more sensitive to the burial compaction. The operation was coded in the "statistics and random variable" tool box in Matlab. The code includes a step of MK testing in which we determine the significance of removing compaction trend (detrending) in each curve. As a result, the detrending operation was performed on the log curves only if the MK test statistic (Z_{MK}) was greater than 10. In addition, we input the break points vectors "bp" into the code which were visually defined by considering major trend changes in each curve. The "bp" vectors allow segmented (non-linear) detrending in order to

honour different compaction trends through the reservoir to seal unit 4. After obtaining the detrended curves, we performed pilot logfacies recognitions in wells W31, W41 and W42 using original and detrended log curves. This is to evaluate the effect of curves detrending on IPSOM process within seal unit 4 (and the analogue seal unit in well W31).

The detrending operation in well W31 is illustrated in Figure 2.11. In Figure 2.11a, the original log curves (including: DTCO, DTSM, PHIT and RHOB) and the established compaction trends are represented along the full range wireline interval (~500 m). The MK test statistic (Z_{MK}) was 8.1 (<10) for PHIT, thus we operated the detrending only on DTCO, DTSM and RHOB curves. In Figure 2.11b, the result of detending is shown for the DTCO curve, in which the DTCO curve partly bears negative values. Since IPSOM has limited capability in handling negative data, we have shifted any negative-value bearing, detrended curve by adding an appropriate constant value to all log samples (in this case: +30 μs/ft). The pilot IPSOM operations in wells W31, W41 and W42 indicated that the detrending operation generally has negative effect on logfacies recognition in mud-rich intervals (Table 2.8). Detrending of PHIT and DTCO curve created an unrealistic tendency in recognising finer-grained logfacies such as hemipelagic shale and mud turbidites. In contrast, detrending of RHOB caused over estimation of sandy and silty facies within the seal units. Only one exception was established for very clay-rich (dominated by hemipelagic shale and mud turbidites facies) seal unit 4 (e.g. in W42) in which RHOB de-trending coupled with a positive constant shift could improve facies recognition results in average by ~20% (Table 2.8).

Worsening of logfacies recognition could possibly be explained by two facts: first, in IPSOM, ANN input neurons use linear transformation functions whilst the non-linear (segmented) log trend contributes to a broader spread of the log signals on the 2D SOM which effectively leads to a resolution contrast in the topological space of data. Second, the log responses in mud-rich zones often have very short-range variations, hence very susceptible to detrending subtractions and the following shift. Our work clearly showed that removing compaction trend (detrending) from logs such as DTCO, DTSM, PHIE, PHIT and RHOB worsens logfacies recognition within the seal units in most of the wells, thus the a priori assumption in Section 2.4.3.2 is not valid in a mud-rich environment.

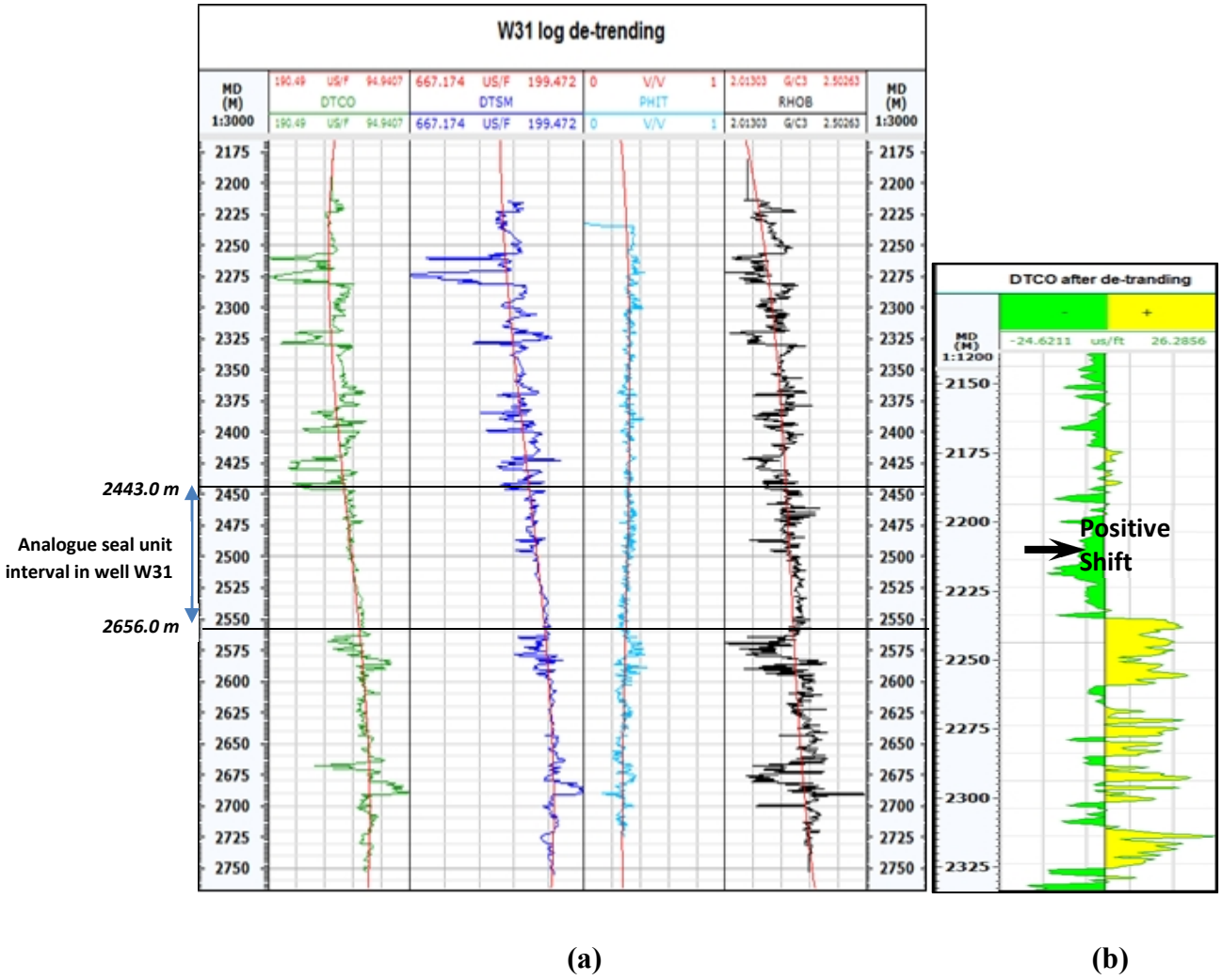

Figure 2.11: *Detrending of logs at well W31: a) the original DTCO, DTSM, PHIT and RHOB log curves are represented with their established compaction trends (red lines). b) detrended DTCO log curve bears negative values; positive shift is proposed applied to avoid adverse effect on the IPSOM (Note that in well W31 an equivalent fine-grained depth-interval is used as an analogue for seal unit 4).*

After the pre-processing steps, the input log and core data are ready to import in Techlog software and implement the IPSOM module. We have created logfacies recognition datasets in two ways: (i) local calibration, where we trained and indexed SOM using the reservoir core descriptions of the same well; (ii) blind recognition, where core descriptions are not available and training/indexing was carried out based on the core data from neighbouring wellbore(s).

2.5.1 IPSOM recognition of seal logfacies using local calibration

The local calibration of IPSOM was carried out in wells W31, W41 and W42, in which we have both minimum log suite and reservoir core descriptions. The input data includes: table of reservoir core facies descriptions (such as in Table 2.5), block shifted non-detrended optimum log suite and clay/silt content curves. The core descriptions were considered as the indexation input and the latter two inputs as the predictors. For the purpose of sensitivity analysis we have run tens of IPSOM iterations and established the optimum parameters of IPSOM which could provide the most efficient recognition of mudstone facies. Figure 2.12 describes the most important parameters in IPSOM recognition of mud-rich facies. For example, we started with SOM size of 50×50, since the bigger maps provide a higher resolution, hence a good separation of the facies by log signals. However, the map size should be proportional to the number of logfacies, number of input log curves and interested resolution. Thereby, we chose the grid size accordingly between 50×50 to 16×16. As recommended (Kohonen, 2001; Kohonen and Somervuo, 2002), the size of SOM cannot be smaller than the distribution dimensions of the input array (facies) i.e. 16. We used the equi-dimensional maps since there is presumably no major lithological trend within the reservoir and seal unit. In addition, the common weighting factor of 1.2 (Equations 2.1, 2.2) was also well accepted in recognition of mud-rich facies. Figure 2.12 illustrates how to set up the optimum IPSOM options/parameters in the “input” and “indexation” panels when recognising mud-rich facies in a local calibration case.

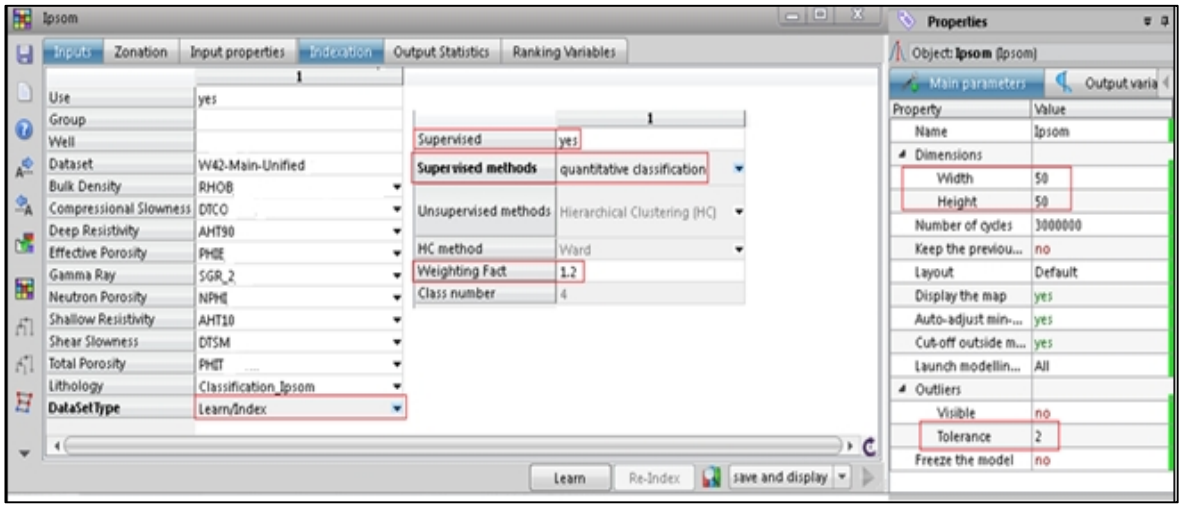

Figure 2.12: *Optimum input and indexation parameters for IPSOM local calibration cases (long range cross-correlations including reservoir and mud-rich units): the most important parameters are highlighted by red rectangles. The grid size, tolerance and number of clusters can change according to the core/log data quality and the number of facies.*

By clicking on "learn" the module calculates an initial unsorted SOM, organises the SOM grids' models and indexes them with core facies data. Depending on the number of input curves and the grid size, the learning process could take up to few minutes. By pressing "save and display" the SOM map is visually displayed in which we can set the number of clusters (K). As explained in Section 2.4.1, this is a parameter which significantly controls the recognition quality/resolution and needs to be proportional to the input data quality and the number of defined facies. Using a high number of clusters could provide a higher recognition resolution, but it also requires high quality core/log data input. In West Africa case study, we have used four to seven clusters depending on well log/core data quality and the applied facies classification scheme. The initial unsorted SOM grid for a local calibration case in well W31 is represented in Figure 2.13, in which the core facies data based on flow facies classification is used for the training. Each cell is the representation of a learning sample, embeds the rose-diagram of log signals for the learning sample, and is indexed/color-coded with core facies data. In addition, the black dots in each cell are the representation of the learning samples with similar rose-diagrams of log signals. The size of the SOM grid is determined by the design parameters. Here we used similar design parameters as in Figure 2.12 and applied seven clusters. In this step, there is a "re-index" option which we used it for IPSOM iterations/sensitivity analysis to optimise the design parameters, hence the SOM trained network, prior to logfacies prediction in the full wireline range.

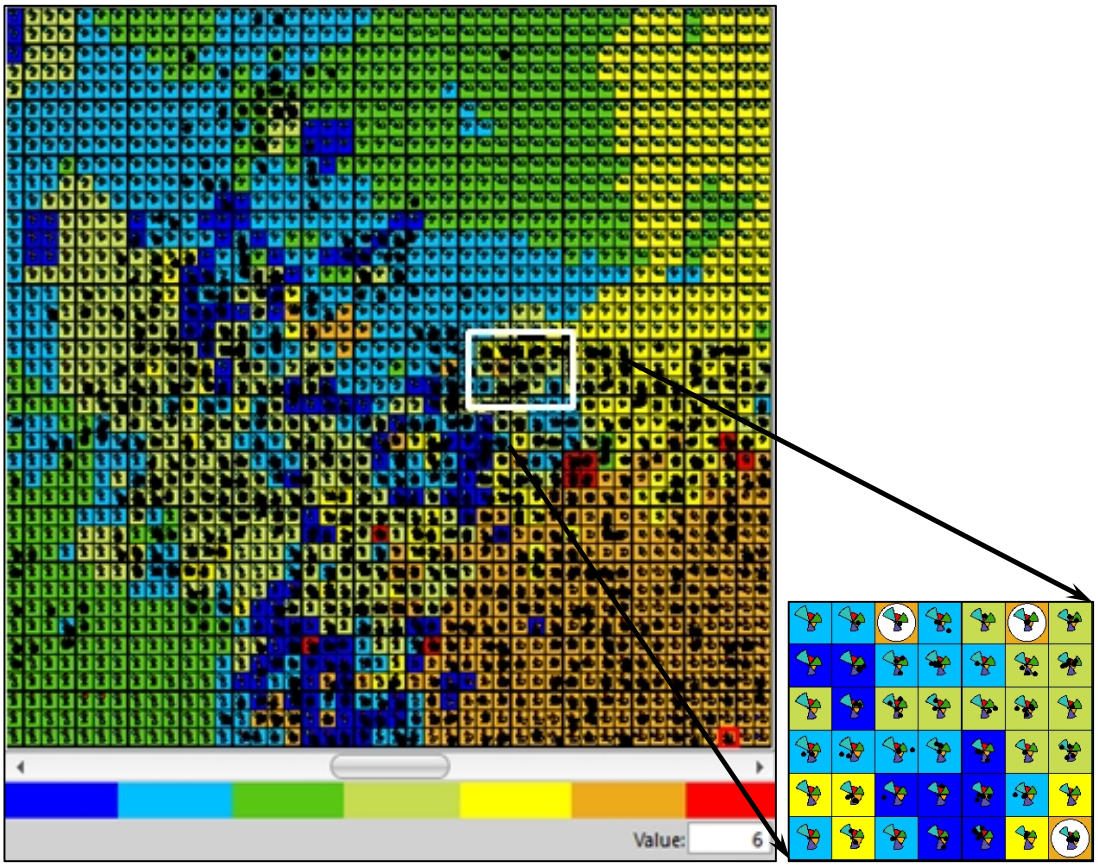

Figure 2.13: *Schematic representation of the initial unsorted SOM grid for a local calibration case in well W31 when using the flow facies classification (7-facies) scheme: each cell is a learning sample, embeds the rose-diagram of log signals for the learning sample, and is indexed/color-coded with core facies data.*

Finally, the generated probabilistic-clustered SOM, IPSOM, was applied to the full wireline range in order to create a logfacies recognition dataset. The recognition dataset covers the whole wireline range including reservoir and non-reservoir formations. In local calibration cases, the validity of generated recognition dataset was evaluated using analysis of the confusion matrix. The confusion matrix provided the ability to compare categorical interval variables, i.e. core facies description and facies recognised by IPSOM. In the matrices, the percentage values in the main diagonal implicated the success of IPSOM and parameterisation. In other words, the ideal confusion matrix would be $100.I_n$, where I_n is an identity matrix of size n. However, this was not possible and we focused on relative accuracy improvement in recognition of fine-grained facies by optimising the inputs and the SOM grid properties. Then we compared the average of diagonal values in different IPSOM runs as a measure of "recognition accuracy".

In Figures 2.14 and 2.15, the logfacies prediction results and confusion matrices are represented for two local calibration recognitions in well W41. The confusion matrices and their statistics have been computed using the VBA-supported template (Section 2.4.4.1). The IPSOM trainings were also operated under the same parameterisations as given in Figure 2.12. In the first operation, Figure 2.14, we applied the flow facies classification scheme, in which the recognition accuracy was approximately 91%. In the other IPSOM operation, Figure 2.15, the coarseness-based facies classification was used and the accuracy of the recognition was slightly reduced by increasing the number of facies in the SOM. Similar efforts under the same IPSOM parameterisation conditions were performed on the other wells while using different classification scheme and log detrendings. In Table 2.8, we provided the average recognition accuracy for the key local calibration recognitions in the three pilot wells (i.e. W31, W41 and W42). In spite of log data quality and core availability issues, in the local calibration cases we have achieved IPSOM recognition accuracy of more than 75% for the key IPSOM operations. In most of the cases, the recognitions with non-detrended logs provided the facies predictions with better core calibration, though the differences are not considerable. The exception was in the highly clay-dominated context (i.e. well W42) where IPSOM recognition with RHOB-detrended input provided better local calibration with original and coarseness-based facies classification scheme. Furthermore, we have not noticed any meaningful dependency between the number of facies (or facies classification scheme) and the recognition accuracy. In other words, the quality of facies classification effect on IPSOM is determined by the geological context at the well location. For example, in well W31, the sedimentary sequences within the wireline line interval (including the cored zone) are relatively coarser with more distinct log responses, thus the unification of the coarse facies in the new facies classification schemes reduced the overall logfacies prediction quality at its fine-grained zones. Thereby the original 16 sedimentological facies provided the best recognition dataset and vice versa for well W42 which is located at much finer-grained sequence.

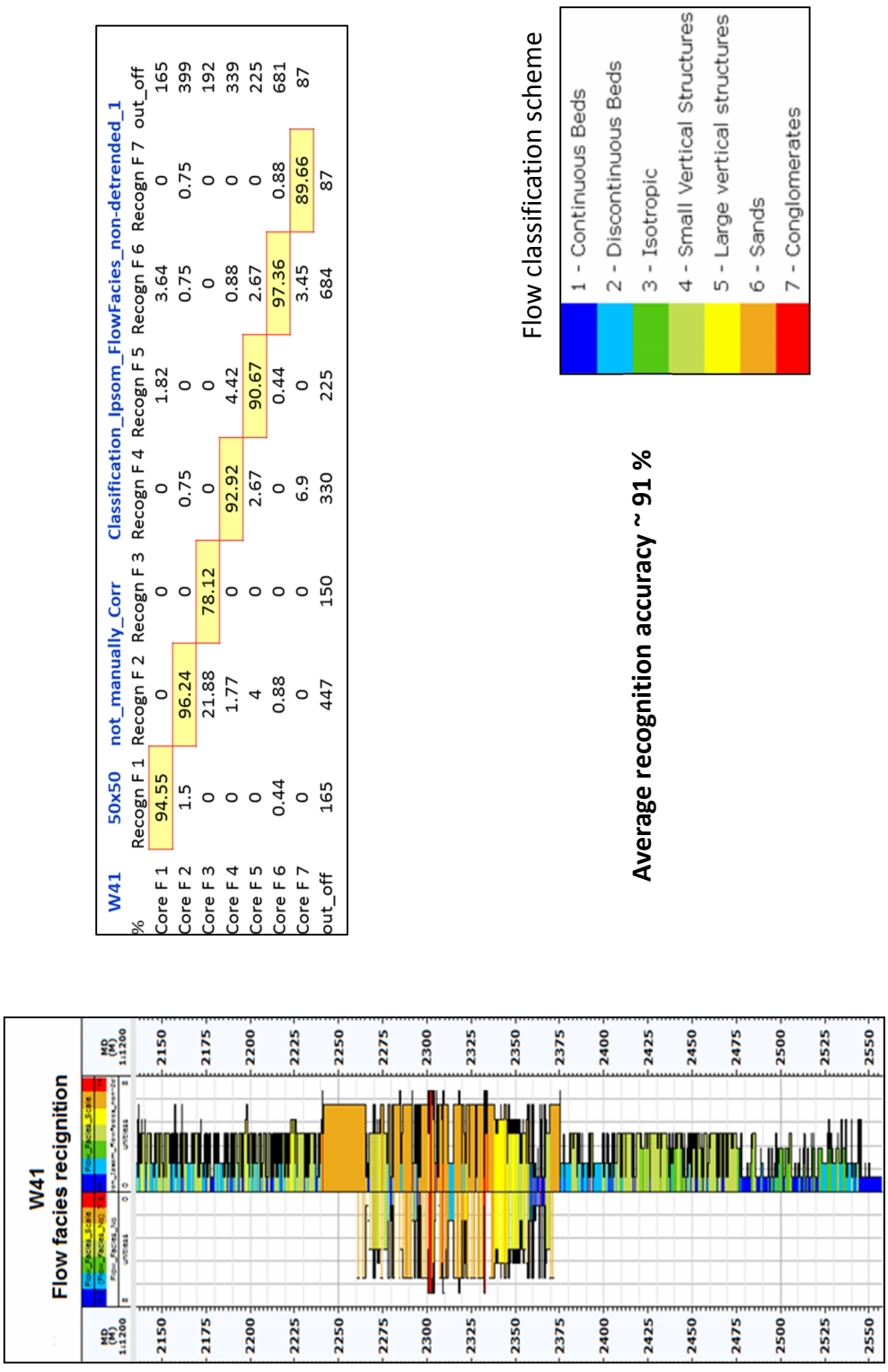

Figure 2.14: *Recognition of flow facies in well W41 using optimum IPSOM parameters with 50×50 grid and non-detrended optimum well log suite. The confusion matrix gives an average recognition accuracy of ~91% which can be visually checked at the well section (at the bottom of the figure) by comparing the recognition data set and the core descriptions along the cored interval.*

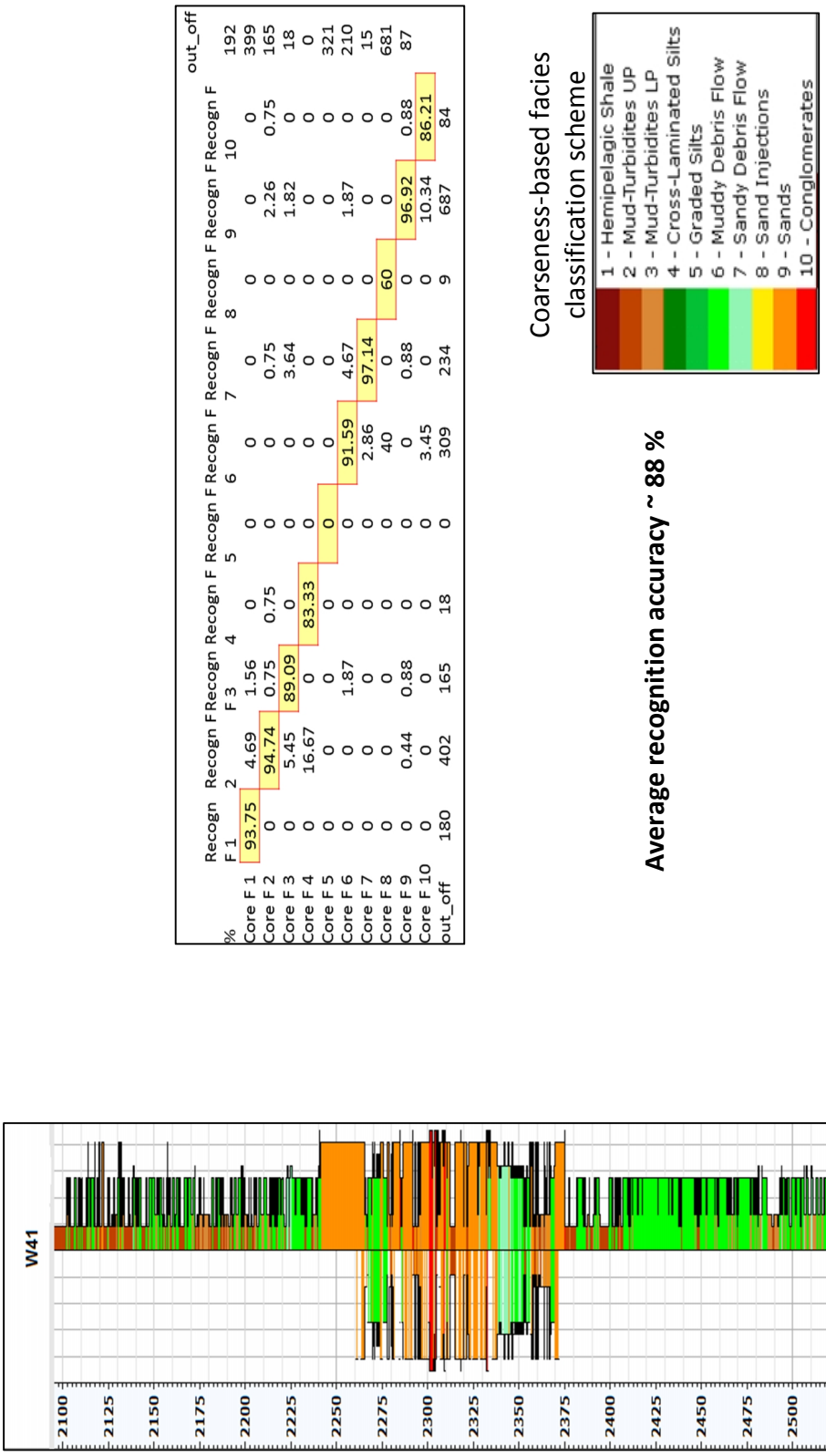

%	Recogn F 1	Recogn F 2	Recogn F 3	Recogn F 4	Recogn F 5	Recogn F 6	Recogn F 7	Recogn F 8	Recogn F 9	Recogn F 10	out_off
Core F 1	93.75	4.69	1.56	0	0	0	0	0	0	0	192
Core F 2	0	94.74	0.75	0.75	0	0	0	0.75	0	0	399
Core F 3	0	5.45	89.09	0	0	0	0	3.64	0	0	165
Core F 4	0	16.67	0	83.33	0	0	0	0	0	0	18
Core F 5	0	0	0	0	0	0	0	0	0	0	0
Core F 6	0	0	1.87	0	0	91.59	2.86	4.67	0	1.87	321
Core F 7	0	0	0	0	0	0	97.14	0	0	0	210
Core F 8	0	0	0	0	0	0	40	0	60	0	15
Core F 9	0	0.44	0.88	0	0	0	0	0.88	0	96.92	681
Core F 10	0	0	0	0	0	0	3.45	0	0	10.34	87
out_off	180	402	165	18	0	0	309	234	9	687	86.21
											84

Figure 2.15: *Recognition of coarseness-based facies in well W41 using optimum IPSOM parameters with 50×50 grid and non-detrended optimum well log suite. The confusion matrix gives an average recognition accuracy of ~88%. The increase in the number of facies slightly reduced the recognition accuracy due to uncertainty growth in clustering.*

Table 2.8: *Summary of the best recognition results in wells W31, W41 and W42 using the proposed IPSOM approach in the local calibration cases: when using three classification schemes and three different detrending practices.*

Well name	Detrended log input(s)	Average recognition accuracy (%)		
		Original sedimentological facies (16-facies)	Coarseness-based facies (10-facies)	Flow facies (7-facies)
W31	Non-detrended	89%	77%	78%
	RHOB detrended	86%	74%	75%
	RHOB, PHIT, PHIE detrended	83%	77%	76%
W41	Non-detrended	87%	88%	91%
	RHOB detrended	83%	84%	86%
	RHOB, PHIT, PHIE detrended	84%	85%	83%
W42	Non-detrended	81%	86%	79%
	RHOB detrended	85%	73%	81%
	RHOB, PHIT, PHIE detrended	79%	78%	79%

Overall, the log detrending and facies classification scheme have not played critical roles in the accuracy of IPSOM recognition of seal facies in the local calibration cases. Instead, the quality of IPSOM recognitions was mainly controlled by specific pre-processing operations (i.e. core shifting and input log selection), SOM grid parametrisation (grid size and number of clusters) and inter-cluster variability of log responses within the seal unit interval. For example, in well logs of well W42, we had the least distinction in the log responses within seal unit 4 and hence achieved the least accuracy for the recognition of mud-rich electrofacies. In another case, we applied an inappropriate input log suite in well W41, which includes spectral gamma ray log (K-U-TH). The improper input log selection imposed a strong negative effect on the recognition of mud-rich facies. The effect is clearly illustrated in Figure 2.16, where we used the optimum IPSOM parameterisation as well as two different classification schemes. In the coarseness-based facies classification case, although the decrease in the accuracy is just 4%, the

application of spectral gamma ray log critically changed the orientation of the topological space and mis-assigned coarse facies within the mud-rich intervals, e.g. muddy debris flow facies replaced the hemipelagic shales at the top seal interval. Furthermore, in the flow facies classification case, the application of this input log suite led to a bigger mistake. The contribution of spectral gamma ray in the input log suite caused the dominant lithology in the top seal changes from isotropic/continuous bed facies to facies with small vertical features. This changed dramatically the preferable flow direction within the seal unit from horizontal to vertical hence could mis-represent the seal risk/quality of seal unit 4 at well W41. The log observations showed that the spectral gamma ray logs respond differently to fine-grained facies in reservoir and mud-rich units; therefore the core (facies)-log interrelationships (IPSOM training) at reservoir cored interval could not be replicated correctly in seal unit 4.

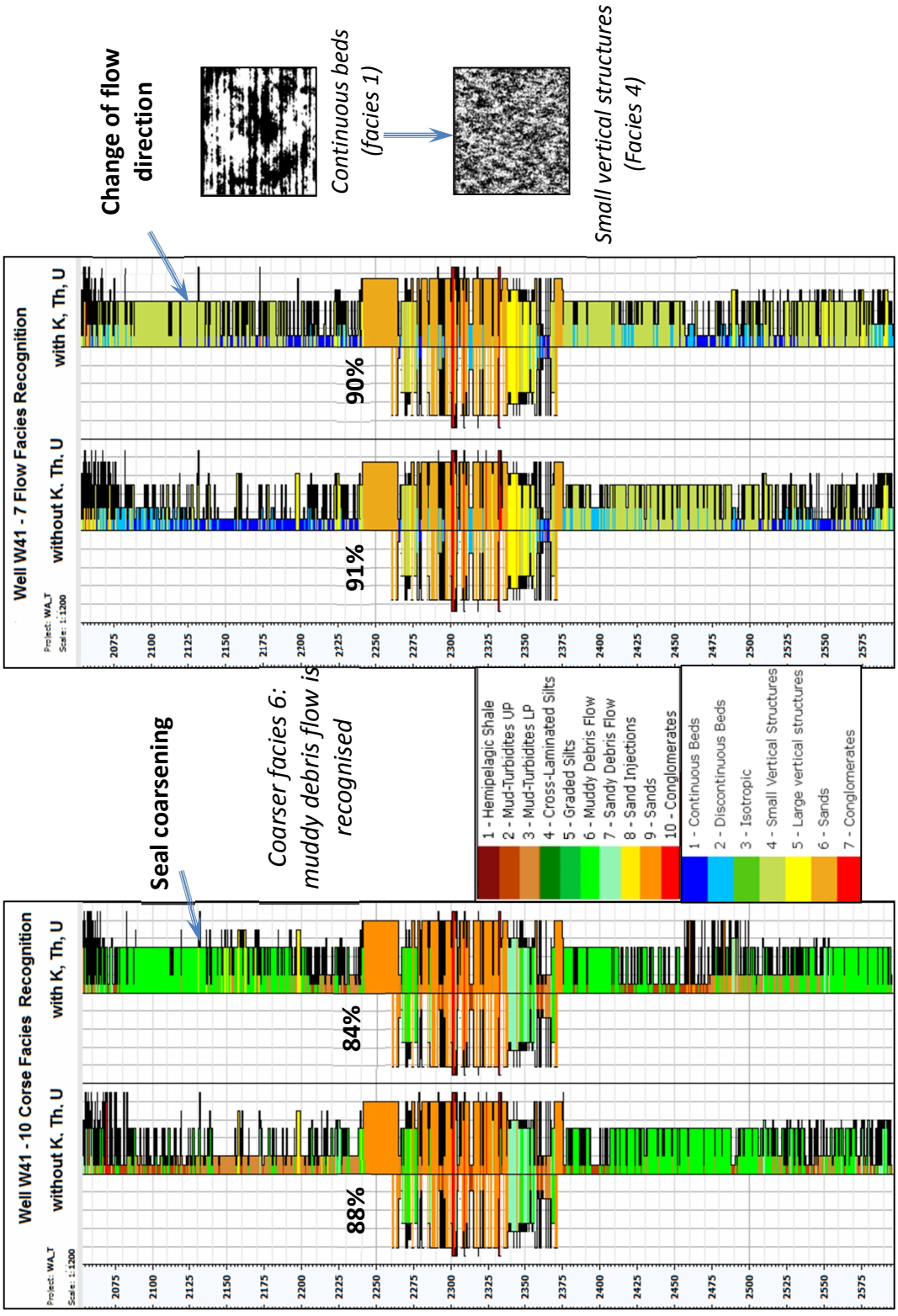

Figure 2.16: *Recognition of coarseness-based and flow facies in well W41 using optimum IPSOM parameters with 50×50 grid and non-detrended spectral gamma ray logs. The average recognition accuracies did not significantly reduce but the qualitative evaluation illustrates the severe mis-assignment of coarser-grained facies to mud-rich units. This is because the spectral gamma ray logs respond differently to reservoir and mud-rich units.*

2.5.2 Blind IPSOM recognition of seal logfacies

In local calibration cases, we have achieved overall accuracy of 75% to 90% for recognition of mud-rich and reservoir logfacies. Although IPSOM contains a probabilistic algorithm, it has a neural network basis. Therefore, as an ANN approach, we have inspected the reliability/robustness of the local calibration results (derived in Section 2.5.1) using blind recognition (or cross-validation). In the first instance, we carried out the blind recognitions on the pilot wells (wells W31, W41 and W42). We ignored the core descriptions of the target well; instead we trained and indexed the SOM based on the core descriptions from the other wells. The trained SOM was then used for recognition of seal/reservoir logfacies at the target well. We compared the match of blind recognition results with the real core facies descriptions at the target well using confusion matrix. As an ANN approach, the accuracy of blind recognition is directly proportional to the number of training sets (cored wells). Since we worked with few distant wellbores (~5-10 km well spacing), the blind recognitions with moderate accuracy could be promoted as good recognitions hence their local calibrations as robust recognitions.

In Figure 2.17, the "Input Panel" of IPSOM is shown where log and core data from wells W41 and W42 set to learn and index the SOM for prediction of logfacies in well W31. The indexation parameters remained the same as in Figure 2.12 and the optimum SOM parameters were used: supervised quantitative classification with four clusters (K) and weighting factor (W) of 1.2. In Figures 2.18, 2.19, 2.20, the results of the blind IPSOM recognition are illustrated when using different facies classification schemes.

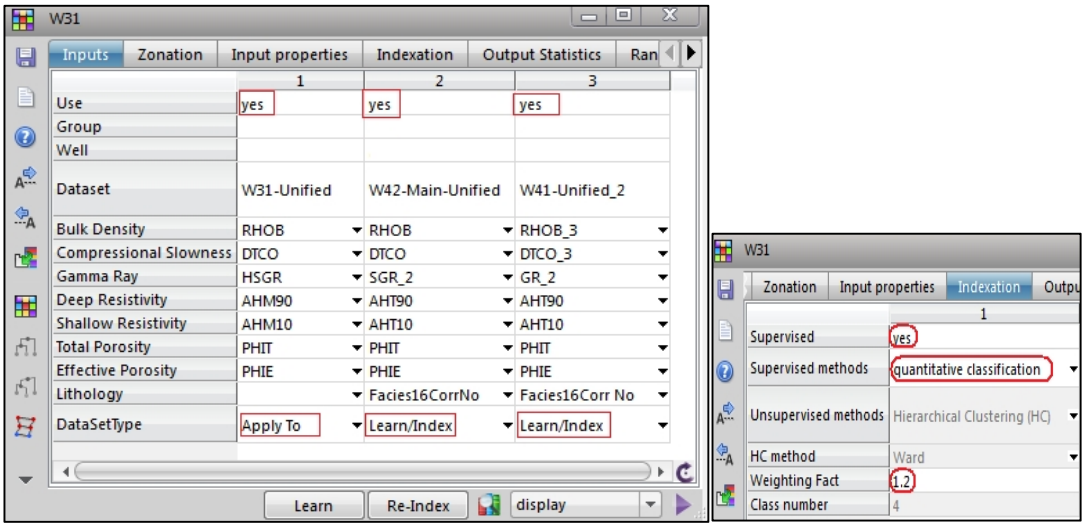

Figure 2.17: *Optimum input and indexation parameters for IPSOM blind recognition cases (long range lateral- and cross-correlations including reservoir and mud-rich units): the most important parameters are highlighted by red rectangles. The choice of learn/index training sets can significantly influence on the recognition accuracy and robustness.*

In Figure 2.18, from top to bottom, you can see the local calibration recognition results for the training wells W41 and W42 (in which only their own core descriptions were used for their recognition) and the blind recognition result for well W31, when using the original sedimentological facies classification scheme. The average recognition accuracies were calculated using the confusion matrices in the VBA-supported template (Figure 2.7). In this case, the single-core local calibrations had acceptable recognition accuracy of 60-70%, whilst the average blind recognition accuracy at well W31 was approximately 20% which is far from the acceptance criteria. Similarly, the results for the other two classification schemes are represented in Figures 2.19 and 2.20. Applying the unified facies classification schemes slightly increased the blind recognition accuracy, but with no major improvement. In fact, the application of flow facies classification scheme mainly improved the single-core local calibrations in wells W41 and W42, whilst using coarseness-based facies classification scheme increased the blind recognitions accuracy (in W31) by 6%.

Since the learning and indexation were carried out using neighbouring well data with different measurements, we repeated the blind recognition operations at well W31 with normalised input logs. The reason was to reduce the effect of potential discrepancies in settings/functionalities of logging tools at different wells. The normalisation of log inputs could solve the problem caused by difference in the

preliminary calibration of logs in the wells. An example of blind recognition with normalised log input is illustrated in Figure 2.21, in which the original sedimentological facies classification scheme was applied. Comparing Figures 2.18 and 2.21, the normalisation of input log suite not only improved the blind recognition but also increased the recognition accuracy in the single-core local calibrations at wells W41 and W42. Thereby, we can say IPSOM would prefer input curves sharing the same range of values.

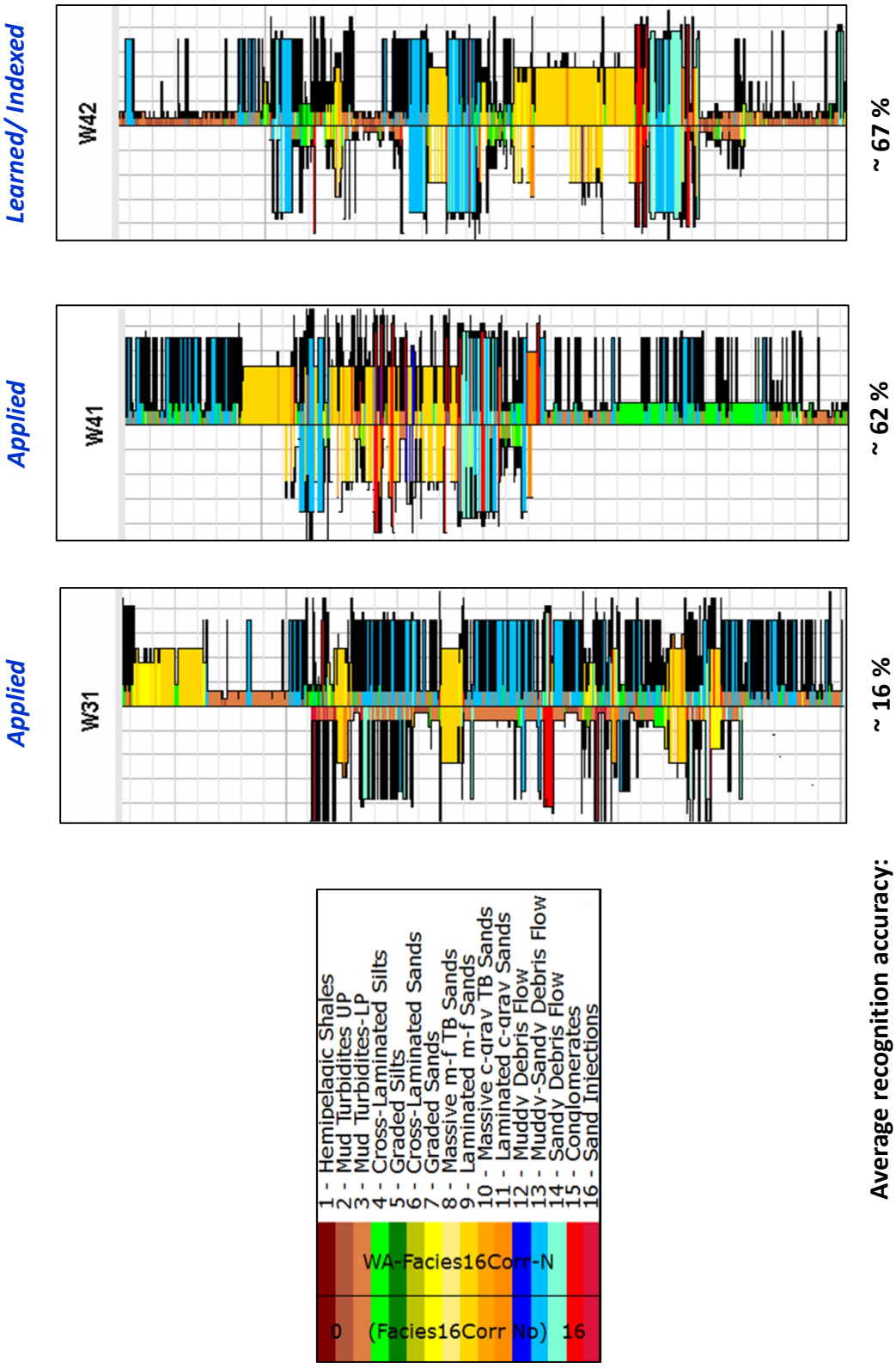

Figure 2.18: *Blind Recognition of original facies in wells W31 and W41 using optimum IPSOM parameters with 50×50 grid and non-detrended optimum well log suite. The SOMs*

are learned and indexed according to corefacies-log correlation in well W42. Successful blind recognition in well W41 suggests similar geological characteristics between reservoir and seal intervals of wells W41 and W42; vice versa for well W31.

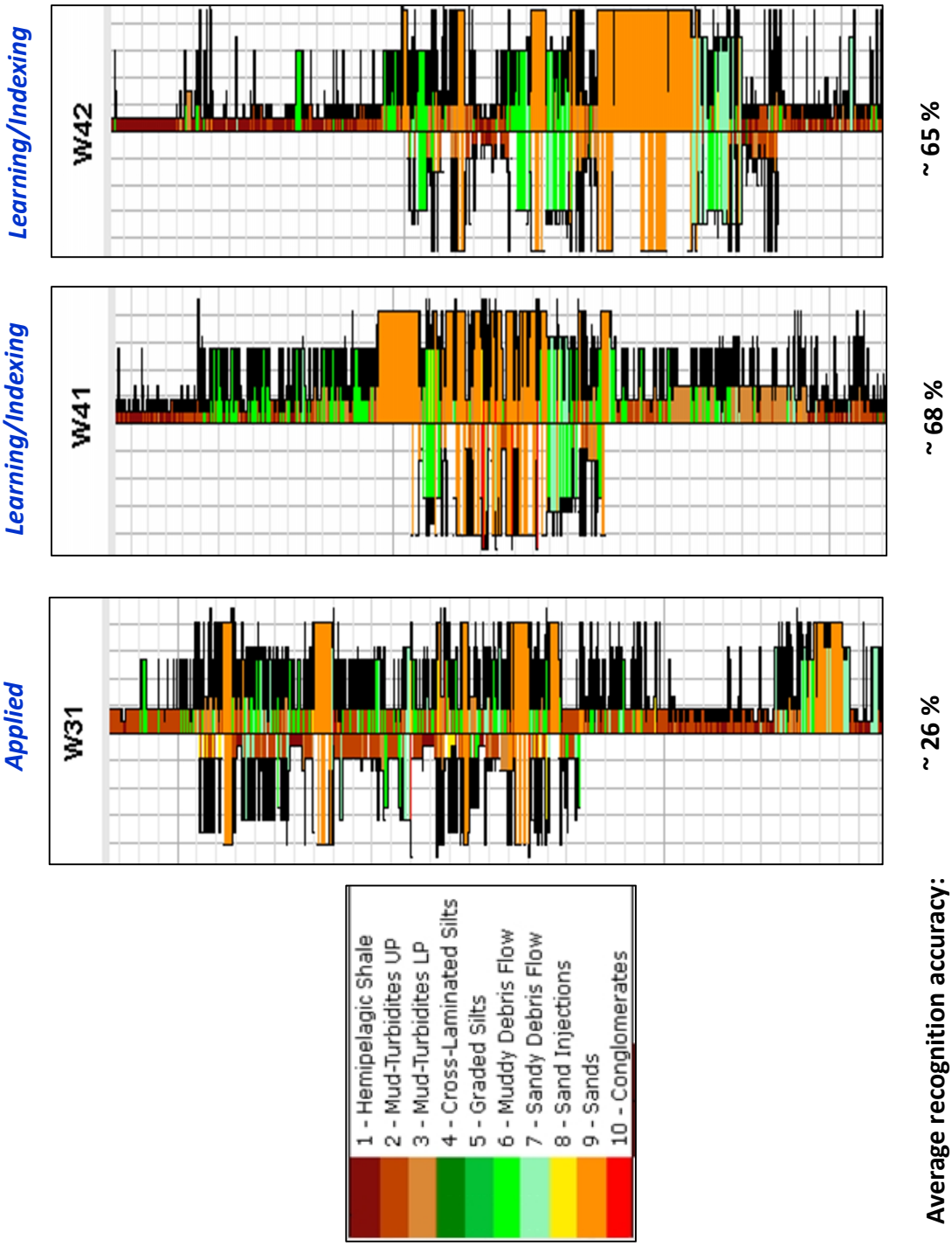

Figure 2.19: *Blind Recognition of coarseness-based facies in wells W31 using optimum IPSOM parameters with 50×50 grid and non-detrended optimum well log suite. The SOM is learned and indexed according to corefacies-log correlations in wells W41 and W42. Difference in lithological characters of training sets and the target interval caused poor blind recognitions.*

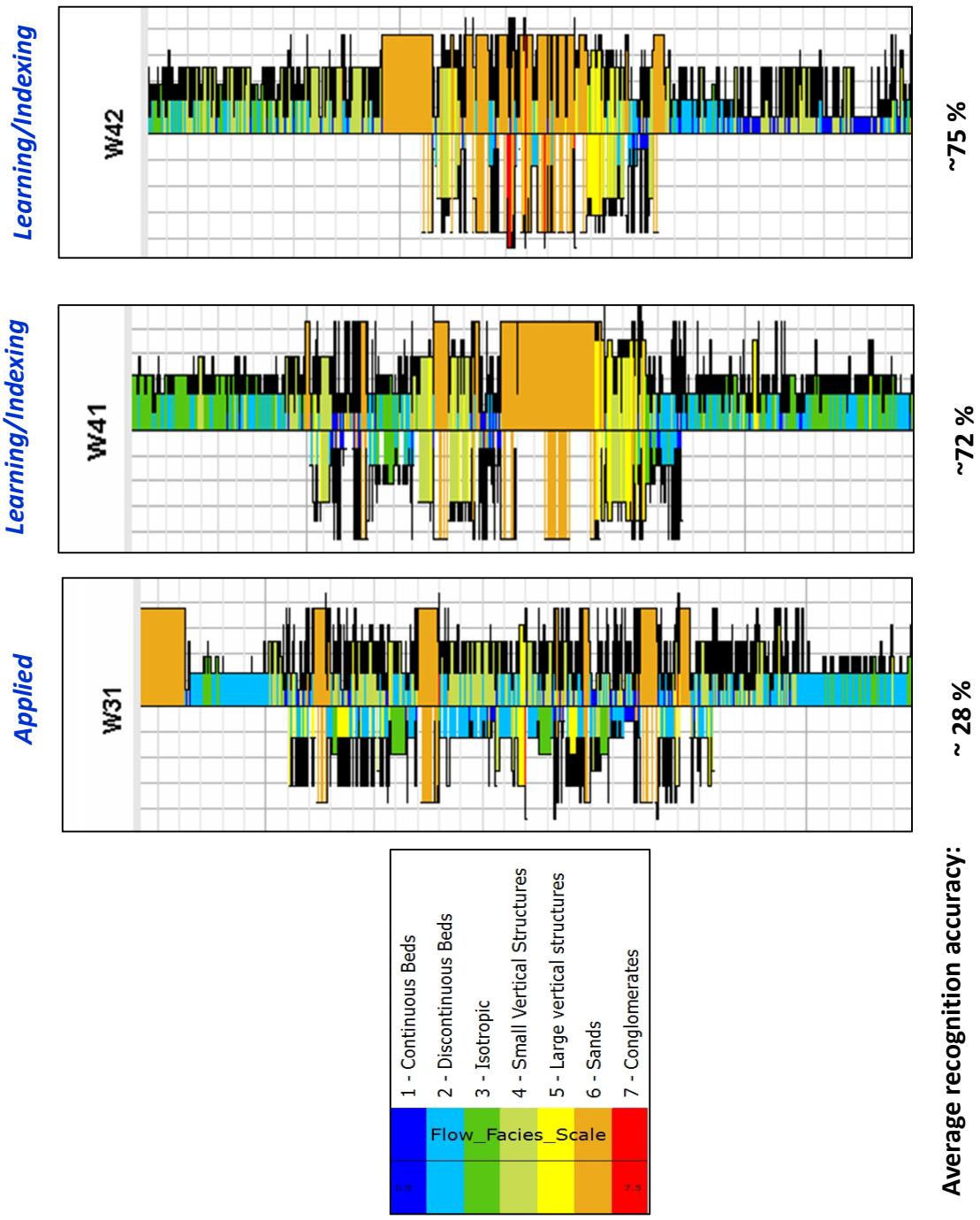

Figure 2.20: *Blind Recognition of flow facies in wells W31 using optimum IPSOM parameters with 50×50 grid and non-detrended optimum well log suite. The SOM is learned and indexed according to corefacies-log correlations in wells W41 and W42. Similar to local calibration cases, the number of facies had intangible effect on blind recognition accuracy.*

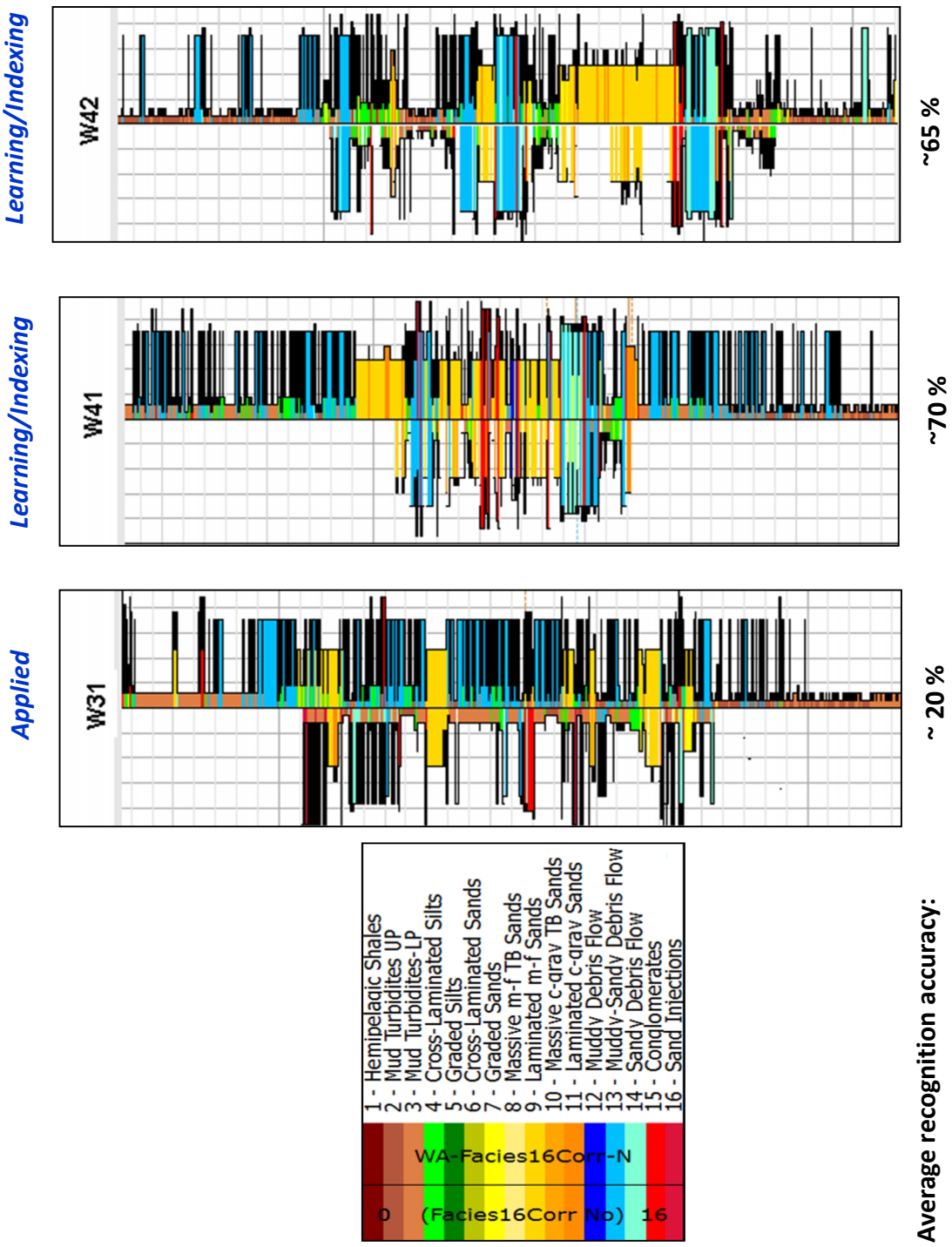

Figure 2.21: *Blind Recognition of original facies in wells W31 using optimum IPSOM parameters with 50×50 grid and non-detrended/normalised optimum well log suite. The SOM is learned and indexed according to corefacies-log correlations in wells W41 and W42. Similar to number of facies, conventional normalisation of log input suite did not significantly improve the blind recognition accuracy.*

The summary of the cross-validation (blind recognition) efforts are given in Table 2.9 while applying three different facies classification schemes, and normalised/original input log suite. Although the overall recognition accuracy has

slightly improved by the normalisation of input logs, the blind recognition results were still very poor. There could be several reasons behind the poor blind recognitions such as the low number of training sets (available logs and cores) and inappropriate selection of training wells. The first point is inevitable as in the majority of seal studies we have very few wells with complete log suite coverage along the seal intervals. Therefore, the selection of training wells for blind recognition of seal logfacies could be a delicate and challenging task. In this study, we used seismic as a guide to select the training wells. In other words, in the training process of a blind recognition, we only incorporated the training well(s) which shared similar seismic characters as the target well in both core and seal intervals. In fact, seismic responses are used as a backward calibration of data. In West Africa case study, the reservoirs (cores) are located in complex/structured sand-rich channels and the reflection seismic data has approximately similar amplitude and frequency characters within these intervals. However, the seismic character (hence sedimentology) changes from seal unit 4 (in wells W41 and W42) to analogue seal unit interval (in well W31). In fact, it is coarsening toward the Southeast, North and Northwest margins of the survey. In Figure 2.22, the NE-SW seismic seal sections at the vicinity of the three pilot wellbores are represented. Seal unit 4 at wells W41 and W42 has similar seismic character, i.e. poor amplitude, and poorly resolved and chaotic reflections, whilst in well W31 the analogue seal unit partly contains blocky/local layered features with moderate amplitude. As a result, we expected incorporation of well W31 for training of blind recognition of W41 and W42 reduces the accuracy of the recognitions. In order to prove it we performed the blind recognitions using single-well training sets. In Figure 2.23, the blind facies recognition in well W41 is shown where we learned and indexed normalised input logs from well W31. As expected, poor blind recognition results were achieved even with normalisation of input log suite. Similar blind IPSOM recognition was carried out on wells W31 and W41, in which we trained the SOM based on the core and log data from well W42 (Figure 2.24). The average recognition accuracy significantly increased compared to the blind recognition case which incorporated well W31 as a training well (Figure 2.21). In contrast, the blind recognition in well W31 remained poor with almost the same accuracy. The same practices were performed using the other training wells and the results are summarised in a clustered column chart in

Figure 2.25. Each column cluster (bin) refers to the core training practices used to recognise the original logfacies along a target wellbore. As expected, the local calibration cases resulted in more accurate logfacies recognition in all wells. In addition, the results confirmed that in a limited well database, we are required to refer to the seismic characters at well locations (throughout the whole cross-correlation interval) prior selecting the training wells for a long-range blind IPSOM recognition of logfacies. Here, for instance well W31 has different seismic character within the analogue seal unit interval, therefore this well should not be used in blind recognition practices (either as training set or target) with W41 and W42 or similar wells. The acceptance criteria could also be used for the blind IPSOM recognition of seal logfacies at non-cored wells; however without core data the validation of their recognition results is not possible. In summary, in a blind IPSOM recognition of seal logfacies, the training wells must pass through all analysed formations and pass through seismic sections having similar characters/variability as that at the target/non-cored well in which facies are to be recognised.

Table 2.9: *Summary of the best blind recognition results in wells W31, W41 and W42 using the proposed IPSOM approach: when using three classification schemes, normalised /non-detrended input log suites and different training wells.*

Target well	Training wells	Normalised log input	Average recognition accuracy (%)		
			Original sedimentological facies (16-facies)	Coarseness-based facies (10-facies)	Flow facies (7-facies)
W31	W41 and W42	No	16 %	26 %	28 %
		Yes	20 %	28 %	31 %
W41	W31 and W42	No	29 %	32%	33 %
		Yes	29 %	35 %	34 %
W42	W31 and W41	No	28 %	27 %	29 %
		Yes	29 %	28 %	31 %

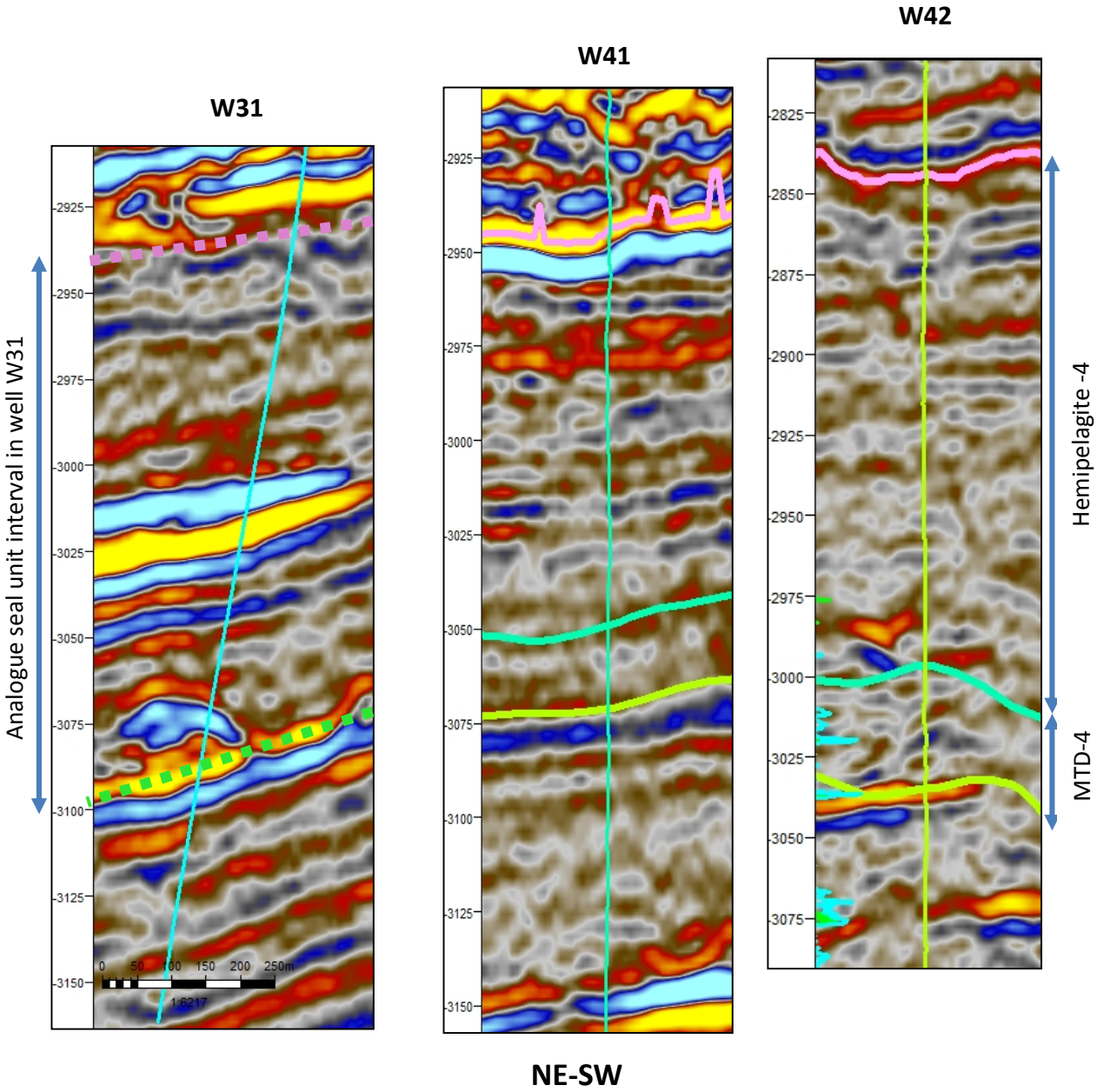

Figure 2.22: *NE-SW seismic section views from three pilot wellbores W31, W41 and W42: In blind recognition of seal logfacies, we suggest using seismic guide (similarity in amplitude and frequency between training and target wells) for selecting training wells; this helps to compensate data limitation issues by integrating knowledge-driven information from another source, i.e. seismic. Pink, cyan and pale green mapped horizons indicate top hemipelagite-4, top MTD-4 and bottom MTD-4. In the reservoir intervals, all three wells share similar channel-related seismic characters, however in seal unit intervals only wells W41 and W42 show similar seismic characters (seismic reflections are better resolved in analogue seal unit in well W31 and have relatively higher amplitudes).*

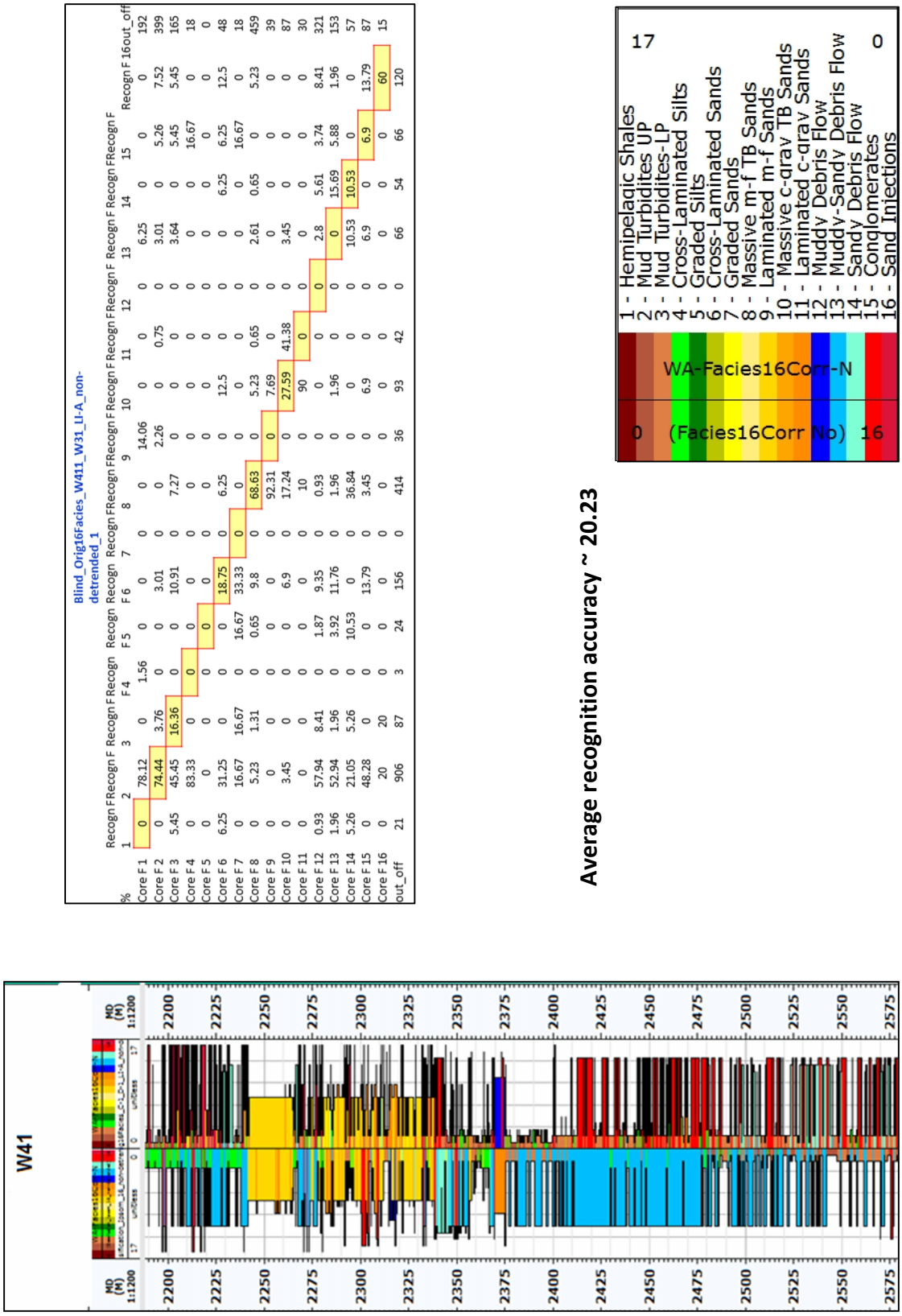

Figure 2.23: *Blind Recognition of original facies in wells W41 and W31 using optimum IPSOM parameters with 50×50 grid and non-detrended optimum well log suite. The SOM is learned and indexed according to corefacies-log correlations in wells W42.*

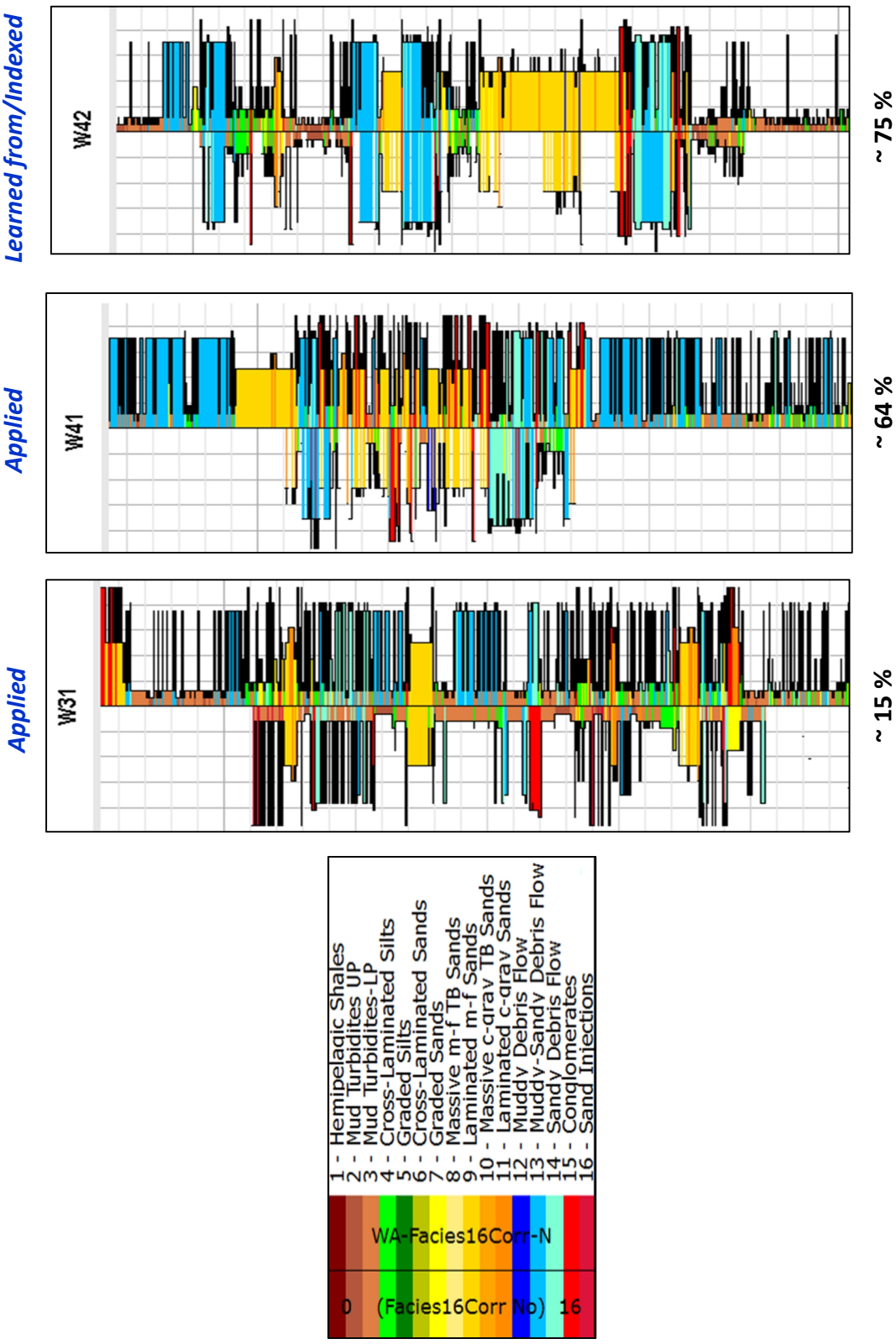

Figure 2.24: *Blind Recognition of original facies in wells W31 and W41 using optimum IPSOM parameters with 50×50 grid and non-detrended/normalised optimum well log suite. The SOM is learned and indexed according to corefacies-log correlations in wells W42. The*

recognition accuracy in well W41 was significantly improved whilst in well W31 the accuracy still remained poor. The results agreed with the proposed seismic-guided selection of training wells.

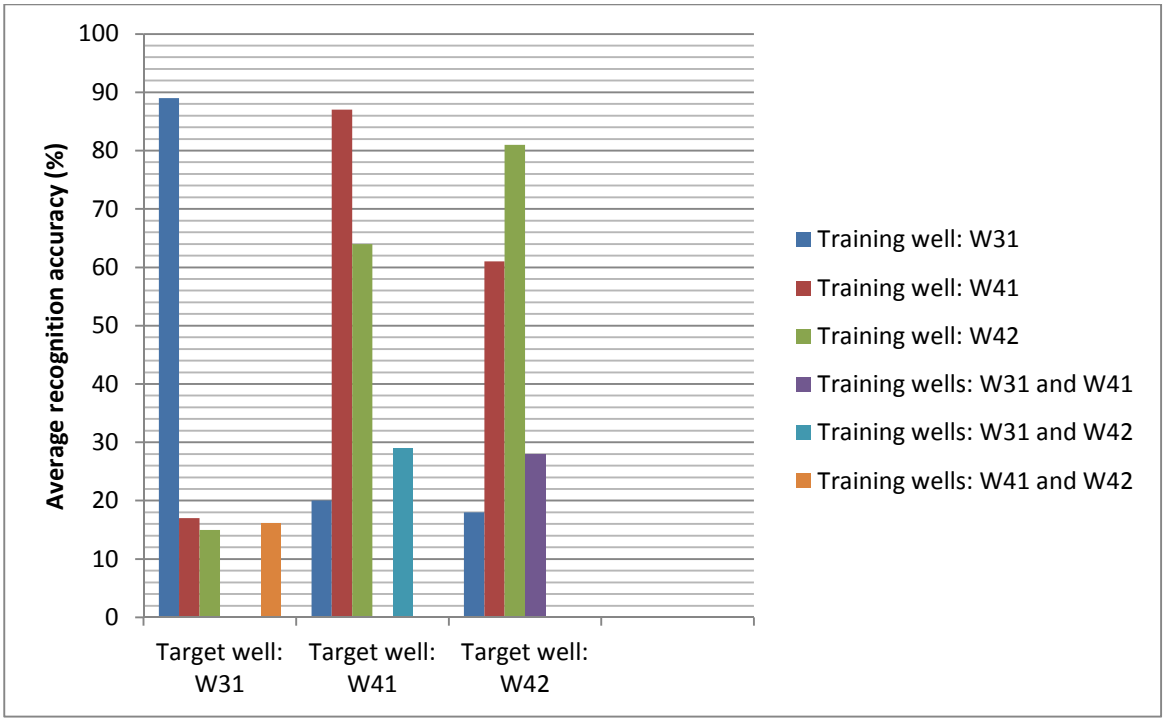

Figure 2.25: *Summary of average recognition accuracies in practices used for recognition of the original logfacies in wells W31, W41 and W42: using optimum IPSOM parameters with 50×50 grid and non-detrended/normalised optimum well log suite. Each column cluster refers to different training sets used for recognition in a target well. Note that the analogue seal unit in well W31 has different seismic character; therefore this well should not be used in blind recognition practices (neither as training nor target) with W41 and W42 or any similar wells.*

2.6 Conclusions

In this chapter, we have presented a new supervised recognition approach which can effectively recognise seal logfacies with different classification schemes and using limited log and reservoir core data. The proposed methodology aimed to supply the IPSOM engine with series of pre-processing, design constraints and validation techniques to offset the core data limitation and log data quality in the fine-grained contexts. The main advantage of the method is that it is applicable to any ANN-based tool with functionality for supervised recognition using multi-layers input with elements having linear transformation functions and which uses self-organizing maps based on Kohonen algorithms. Furthermore, the method gives the

flexibility to combine the data-driven information with knowledge-driven inputs to overcome the seal data limitation issue. As a very first quantitative recognition approach in the seal context, it can be significantly useful to improve our understanding from subsurface lithological distribution within mud-rich sequences, in particular for property modelling hence basin-scale flow simulation.

The method is demonstrated on a deep offshore case study in West Africa where overall recognition accuracy of local calibration and blind recognition cases reached up to 80-90% and 60-70%. The analysis suggested the success of a blind recognition strongly depends on the similarity of seismic character in the target and training wells. Thus qualitative relationships exist between the type and degree of heterogeneity of the vertical distribution of logfacies in mud-rich sections of wells and the amplitude and frequency of seismic at the well location. The link will be investigated further in Chapters 3 and 4.

In addition, the analysis indicated that the typical processes in logfacies recognition in sandstone/reservoir context may not be applicable in the mud-rich environment. The polynomial detrending and the proposed segmented nonlinear detrending changed the nature of log responses and worsened the logfacies recognition results within the seal formations. The inclusion of the spectral gamma log in the input log suite also reduced the predictive power of the IPSOM, resulting in strong coarsening trend in the recognition results. Moreover, the normalization of the log signals only slightly improved the quality of blind recognition cases. The so-obtained recognition method can significantly be improved by incorporating special log inputs, in particular image logs and dip meter information.

2.7 References

*Alvarez, G., Sanso, B., Michelena, R.J. and Jiṁenez, J.R., 2003, Litho-logic Characterization of a Reservoir using Continuous-Wavelet Transforms. IEEE Transactions on Geoscience and Remote Sensing, 41(**1**), pp 59–65.*

Avseth, P., Mukerji, T., Jørstad, A., Mavko, G. and Veggeland, T., 2001, Seismic Reservoir Mapping From 3-D AVO in a North Sea Turbidite System, Geophysics, 66, pp 1157–1176.

Bhatt, A. and Helle, H.B., 2002, Committee Neural Networks for Porosity and Permeability Prediction from Well Logs. Geophysical Prospecting, 50, pp 645–660.

Bouma, A. H., 1962, Sedimentology of Some Flysch Deposits: A Graphic Approach to Facies Interpretation. Elsevier, 168 p.

Camacho, H., Busby, C.J. and Kneller, B.C., 2002, A New Depositional Model For The Classical Turbidite Locality at San Clemente State Beach, California. AAPG Bulletin, 86, pp 1543–1560.

*Chang, H., Chen, H. and Fang, J, 1997, Lithology Determination From Well Logs With Fuzzy Associative Memory Neural Network. IEEE Transactions on Geoscience and Remote Sensing, 35(**3**).*

*Chang, H.C., Kopaska-Merkel, D.C., & Chen, H. C. (2002). Identification of Lithofacies using Kohonen Self-Organizing Maps. Computers and Geosciences, 28(**2**), pp 223-229.*

Chang, L. and Chong-xiu, Y., 2013, Modified Self-Organizing Mixture Network For Probability Density Estimation And Classification. In proceeding: Neural Networks (IJCNN), The 2013 International Joint Conference, Dallas, pp 1-6.

*Chashkov, A.V.and Kiselev, V.M., 2011, Use of the Cluster Analysis and Artificial Neural Network Technology for Log Data Interpretation. Engineering and Technologies, 4(**4**), pp 453-462.*

Chopra, S. and Marfurt, K., 2014, Seismic facies analysis using generative topographic mapping. In proceeding: SEG Denver 2014 Annual Meeting, pp 1390-1394.

*Cuddy, S.J., 2000, Litho-Facies and Permeability Prediction From Electrical Logs Using Fuzzy Logic. SPE Reservoir Evaluation and Engineering, 3(**4**)*

Dawson, W.C. and Almon, W.R., 2002, Top Seal Potential of Tertiary Deep-Water Shales, Gulf of Mexico: GCAGS Transactions, 52, pp 167-176.

Dawson, W.C. and Almon, W.R., 2006, Shale Facies and Seal Variability in Deepwater Depositional Systems, Proceeding Annual AAPG Convention, April 9-12.

Delfiner, P., Peyret, O. and Serra, O., 1987, Automatic Determination of Lithology from Well Logs. SPE Formation Evaluation, 2, pp 303–31.

Derek, H., Johns, R. and Pasternack, E., 1990, Comparative Study of Back-Propagation Neural Network and Statistical Pattern Recognition Techniques in Identifying Sandstone Lithofacies. In Proceedings: Conference on Artificial Intelligence in Petroleum Exploration and Production (1990), College Station, pp 41-49.

Dvorkin, J., and Nur, A., 1996, Elasticity of High-Porosity Sandstones: Theory for Two North Sea Datasets. Geophysics, 61, pp 1363-1370.

Enikanselu, A. and Ojo, A., 2012, Statistical Analysis and Evaluation of Lithofacies From Wireline Logs Over Beleema Field, Niger Delta, Nigeria. Journal of Petroleum Gas Engineering, 3, pp 26–34.

*Fertl, W.H., 1981, Openhole Crossplot Concepts a Powerful Technique in Well Log Analysis. Journal of Petroleum Technology, 33 (**3**), pp. 535-549.*

*Fielding, C.R., Allen, J.P., Alexander, J. and Gibling, M.R., 2009, Facies Models For Fluvial Systems in the Seasonal Tropics and Subtropics. Geology 37(**7**), pp 623–626.*

Fort, J.C., 2006, SOM's Mathematics. Neural Networks, 19, pp 812–816.

Gilbert, R.O., 1987, Statistical Methods for Environmental Pollution Monitoring. Wiley, New York.

*Gill, D., Shomrony, A., and Fligelman, H., 1993, Numerical Zonation of Log Suites and Logfacies Recognition by Multivariate Clustering. AAPG Bulletin, 77(**10**), pp 1781-1791.*

Gould, K.M., Piper, D.J.W., Pe-Piper, G. and MacRae, R.A., 2014, Facies, Provenance and Paleoclimate Interpretation Using Spectral Gamma Logs: Application to the Lower Cretaceous of the Scotian Basin. Marine and Petroleum Geology, 57, pp 445–454.

Grana, D., Schlanser, K. and Campbell-Stone, E., 2014, Petroelastic and Geomechanical Classification of Lithologic Facies in the Marcellus Shale. Interpretation, 3, pp 51-63.

*Guo, G., Diaz, M.A., Paz, F., Smalley, J. and Waninger, E.A., 2007, Rock Typing as an Effective Tool for Permeability and Water-Saturation Modeling: A Case Study in a Clastic Reservoir in the Oriente Basin. SPE Reservoir Evaluation and Engineering, 10(**6**).*

*Hammes, U. and Frébourg, G., 2012, Haynesville and Bossier Mudrocks: A Facies and Sequence Stratigraphic Investigation, East Texas and Louisiana, Marine and Petroleum Geology,31 (**1**), pp 8-26.*

*Hernandez-Martinez, E., Perez-Muñoz, T., Velasco-Hernandez, J.X., Altamira-Areyan, A. and Velasquillo-Martinez, L., 2013, Facies Recognition Using Multifractal Hurst Analysis: Applications to Well-Log Data. Mathematical Geosciences, 45 (**4**), pp 471-486.*

*Hirsch, R.M., Slack, J.R. and Smith, R.A., 1982, Techniques of Trend Analysis For Monthly Water Quality Data. Water Resources Research, 18(**1**), pp 107-121.*

Hruska, M., Corea, W., Seeburger, D., Schweller, W. and Crane, W.H., 2009, Automated Segmentation of Resistivity Image Logs Using Wavelet Transform. Mathematical Geosciences, 4, pp 703–716.

Insalaco, E., Marion, D., Michel, B. and Rowbotham, P., 2001, Reservoir-Scale 3D Sedimentary Modelling: Approaches and Impact of Integrating Sedimentology into the Reservoir Characterization Workflow. In proceedings: AAPG Annual Meeting.

Jackson, M.D., Hampson, G.J., Saunders, J.H., El-Sheikh, A., Graham, G.H. and Massart, B.Y.G., 2013, Surface-Based Reservoir Modelling For Flow Simulation. Geological Society of London, Special Publications, eds. Martinius A.W., Howell J.A. and Good T.R., 387, pp 271-292.

Jackson, R.G., 1981, Sedimentology of Muddy Fine-grained Channel Deposits in Meandering Streams of the American Middle West. Journal Sedimentary Petrology, 51, pp 1169-1192.

John, A., Lake, L. W., Torres-Verdin, C. and Srinivasan, S., 2005, Seismic Facies Identification and Classification using Simple Statistic. Proceeding, SPE Annual Technical Conference and Exhibition, SPE 96577.

Kaski, S., Kangas, J., and Kohonen, T., 1998, Bibliography of Self-Organizing Map (SOM) Papers: 1981-1997. Neural Computing Surveys, 1, pp 102-350.

Khue, P., Huseby, O., Saucier, A. and Muller, J., 2002, Application of Generalized Multifractal Analysis for Characterization of Geological Formations. Journal of Physics: Condensed Matter, 14, pp 2347–2352.

Kohonen, T., 1982, Self-Organized Formation of Topologically Correct Feature Maps. Biological Cybernetics, 43, pp 59-69.

Kohonen T., 1984, Self-Organization and Associative Memory. Springer, Berlin.

Kohonen, T., 2001, Self-Organizing Maps. Third, extended edition, Springer.

*Kohonen, T. and Somervuo, P., 2002, How to Make Large Self-Organizing Maps for Nonvectorial Data. Neural Networks, 15(**8-9**), pp 945-952.*

Lee, S.H., Khargoria, A. and Datta-Gupta, A., 2002, Electrofacies Characterization and Permeability Predictions in Complex Reservoirs. SPE Reservoir Evaluation and Engineering, 5, pp 237–248.

Li, Y. and Anderson-Sprecher, R., 2006, Facies Identification From Well Logs: A Comparison of Discriminant Analysis and Naive Bayes Classifier. Journal of Petroleum Science and Engineering, 53, pp 149-157.

Lindberg, D.V., Rimstad, E. and Omre, H., 2014, Identification of Facies from Multiple Well Logs Accounting for Spatial Dependencies and Convolution Effects. Extended Abstract, 76th EAGE Conference and Exhibition, Amstrdam.

Lopez, M. and Aldana, M., 2007, Facies Recognition using Wavelet Based Fractal Analysis and Waveform Classifier at the Oritupano-A Field, Venezuela. Nonlinear Processes Geophysics, 14, pp 325-335.

Ma, Y.Z., 2011, Lithofacies Clustering Using Principal Component Analysis and Neural Network: Applications to Wireline Logs. Mathematical Geosciences, 43, pp 401–419.

Magara, K., 1986, Thickness of Erosion. In: Geological Models of Petroleum Entrapment, Chapter 7, Elsevier Applied Science Publishers, London, pp. 129-151.

Maiti, S. and Tiwari, R.K., 2005, An Automatic Method For Detecting Lithologic Boundary Using Walsh Transform: A Case Study From KTB Borehole. Computers and Geosciences, 31, 949–955

Matos M.C., Osório P.L.M. and Johann P.R.S., 2007, Unsupervised Seismic Facies Analysis Using Wavelet Transform and Self-Organizing Maps. Geophysics, 72, pp 9-21.

Mitra, A., Warrington, D.S. and Sommer, A., 2010, Application of Lithofacies Models to Characterize Unconventional Shale Gas Reservoirs and Identify Optimal Completion Intervals. SPE 132513. In proceeding: SPE Western Regional Meeting, Anaheim, California, U.S.A.

Morton-Thompson, D. and Woods, A.M. (Eds.), 1993, Development Geology Reference Manual. AAPG Methods in Exploration Series, No. 10. AAPG.

Oja, M., Kaski, S. and Kohonen, T., 2003, Bibliography of Self-Organizing Map (SOM) Papers: 1998-2001. Addendum. Neural Computing Surveys, 3, pp 1-156.

Passey, Q.R., Bohacs, K.M. and Esch, W.L., 2010, From Oil Prone Source Rock to Gas-Producing Shale Reservoir—Geologic and Petrophysical Characterization of Unconventional Shale Gas Reservoirs. In proceeding: CPS/SPE International Oil and Gas Conference, Beijing, 8–10 June, SPE 131350.

Perez, H.H., Datta-Gupta, A. and Mishra, S., 2005, The Role of Electrofacies, Lithofacies and Hydraulic Flow Units in

*Pickering, K.T., Stow, D.A.V., Watson, M., Hiscott, R.N., Permeability Predictions From Well Logs: A Comparative Analysis Using Classification Trees. SPE Reservoir Evaluation and Engineering, 8(**3**).1986, Deep Water Facies, Processes and Models: A Review and Classification Scheme for Modem and Ancient Sediments. Earth Sciences, Rev. 22, pp 75-174.*

Pöllä, M., Honkela, T. and Kohonen, T., 2007, Bibliography of Self-Organizing Map (SOM) Papers: 2002-2005. Addendum. Neural Computing Surveys.

Porebski, S.J., Meischner, D., Gorlich, K., 1991, Quaternary Mud Turbidites from the South Shetland Trench (West Antarctica): Recognition and Implications for Turbidite Facies Modeling. Sedimentology 38, pp 691-715.

Pospelov, G.S., 1988, Artificial Intelligence: the Basis for the New Information Technology. G.S. Pospelov – M.: Nauka.

Qi, L. and Carr, T.R., 2006, Neural Network Prediction of Carbonate Lithofacies From Well Logs, Big Bow and Sand Arroyo Creek Fields, Southwest Kansas. Computers and Geosciences, 32, pp 947-964.

Raymer, L.L., Hunt, E.R., and Gardner, J.S., 1980, An Improved Sonic Transit Time-to-Porosity Transform. SPWLA 21st Anniversary, Logging Symposium, July 8-11, pp 1-12.

Reading, H.G. (Ed.), 2009, Sedimentary Environments: Processes, Facies and Stratigraphy. John Wiley and Sons.

*Rogers, S., Fang, J., Karra, C. and Stanley, D., 1992, Determination of Lithology from Well Logs using a Neural Network. American Association of Petroleum Geologists Bulletin, 76(**5**), pp 731–739.*

Roy, A., 2013, Latent Space Classification of Seismic Facies, Ph.D. Dissertation, University of Oklahoma

Roy, A., Matos, M. and Marfurt, K.J., 2010, Automatic Seismic Facies Classification with Kohonen Self Organizing Maps - A Tutorial. Geohorizons Journal of Society of Petroleum Geophysicists, pp. 6-14.

Saggaf, M.M. and Nebrija, Ed.L., 2003, A Fuzzy Logic Approach For The Estimation of Facies From Wire-Line Logs. AAPG Bulletin, 87, pp 1223-1240.

Sakurai, S. and Melvin, J., 1988, Facies Discrimination and Permeability Estimation From Well Logs for the Endicott Field. Society of Professional Well Log Analysis, 29th Annual Logging Symposium, Transactions.

Serra, O., Abbott, H.T., 1982, The Contribution of Logging Data to Sedimentology and Stratigraphy. Society of Petroleum Engineers Journal, 22, pp 117-131.

Shanmugam, G., 2000, 50 Years of the Turbidite Paradigm (1950s –1990s): Deep-Water/Processes and Facies Models—A Critical Perspective. Marine and Petroleum Geology, 17, pp 285 – 342.

Shanmugam, G., 2001, Deep-Marine Tidal Bottom Currents and Their Reworked Sands in Submarine Canyons: Implications For Sand Distribution. In proceeding AAPG Annual Convention, Denver, Colorado.

Siripitayananon, P., Chen, H.C. and Hart, B.S., 2001, A New Technique For Lithofacies Prediction: Back-Propagation Neural Network. In proceeding of ACMSE: the 39th Association of Computing and Machinery South Eastern Conference, Atlanta, GA, USA, pp 31-38.

Soliman, M.Y., Anseh, J., Stephenson, S. and Mandal, B., 2003, Application of Wavelet Transform to the Analysis of Pressure Transient Data. In: SPE Annual Technical Conference and Exhibition, 6, pp 88–89.

Stow, D.A.V., 1984, Turbidite Facies, Associations and Sequences in the Southeastern Angola Basin. In Hay, W.W., Sibuet, J.-C, et al., Initial Reports, DSDP, 75, Washington (U.S. Government Printing Office), pp 785-799.

Stow, D.A.V., 1985, Deep-Sea Elastics: Where Are We and Where Are We Going? In Brenchley, P.J. and Williams, B.P.J. (Eds.), Sedimentology: Recent Developments and Applied Aspects, Geological Society of London, Special Publication, 18, pp 67-94.

Stow, D.A.V., 1994, Deep Sea Processes of Sediment Transport and Deposition. In Pye, K.(Ed.), Sediment Transport and Depositional Processes, London (Blackwell), pp 257-291.

Stow, D.A.V. and Piper, D.J.W., 1984, Deep-water Fine-grained Sediments: Facies Models. In: Stow, D.A.V. and Piper, D.J.W. (Eds.), Fine Grained Sediments: Deep-water Processes and Facies. Geological Soiety of London, Special Publication 15, pp 611-646.

Sumner, E.J., Siti, M.I., McNeill, L.C., Talling, P.J., Henstock, T.J., Wynn, R.B., Djajadihardja, Y.S. and Permana, H., 2012, Can Turbidites Be Used to Reconstruct a Paleoearthquake Record For the Central Sumatran Margin? Geology, 41, pp 763–766.

*Tang, H., Toomey, N. and Meddaugh, W.S., 2011, Using an Artificial-Neural-Network Method to Predict Carbonate Well Log Facies Successfully. SPE Reservoir Evaluation and Engineering,14(**1**).*

Tang, H. and White, C.D., 2008, Multivariate Statistical Log Log-Facies Classification on a Shallow Marine Reservoir. Journal of Petroleum Science and Engineering ,61, pp 88-93.

Tang, H., White, C.D., Gani, M.R. and Bhattacharya, J.P., 2004, Comparison of Multivariate Statistical Algorithms for Wireline Log Facies Classification. In proceeding: AAPG annual meeting 2004.

Theys, P.P., 1991, Log Data Acquisition and Quality Control, Editions TECHNIP

Turcotte, D.L., 1997, Fractals and Chaos in Geology and Geophysics. 2nd edition, Cambridge University Press, Cambridge.

Wang, G. and Carr, T.R., 2012, Methodology of Organic-Rich Shale Lithofacies Identification and Prediction: A Case Study From Marcellus Shale in the Appalachian Basin. Computers and Geosciences, 49, pp 151-163.

Wong, K.W., Wong, P.M. and Gedeon, T., 1997, A State-of-Art Review of Fuzzy Logic for Reservoir Evaluation. APPEA Journal, 43, pp 587-593.

*Yang, Y., Aplin, A.C. and Larter, S.R., 2004, Quantitative Assessment of Mudstone Lithology Using Geophysical Wireline Logs and Artificial Neural Networks. Petroleum Geoscience, 10(**2**). pp 141-151.*

Yin, H., 2008, The Self-Organizing Maps: Background, Theories, Extensions and Applications. Computational intelligence: A Compendium, Springer Berlin Heidelberg, pp 715-762.

3 Seismic Characterisation of Seal Quality using Volumetric Attributes

3.1 Introduction

Seismic attributes are properties that can be quantitatively extracted from seismic data to filter or illustrate different geological and geophysical characteristics of the subsurface (Chopra and Marfurt, 2005). Seismic attributes were initially extracted from analogue seismic data to optimise the filter settings (Rummerfeld, 1954). Later adopting magnetic analogue recording allowed the production of corrected cross sections and measurement of the basic structural elevation, dip, thickness and discontinuities attributes (Anstey, 2005). By the emergence of digital recording in 1963 and development of the velocity spectrum concept, the most basic attribute in seismic inversion, the interval velocity attribute, was introduced (Taner and Koehler, 1969). In the 1960s, 1970s and 1980s, attribute technology gradually developed by introducing new 2D attributes (and applications) to help geoscientists in petroleum exploration: reflector dip (Picou and Utzman, 1962; Simpson et al., 1967), bright-spot (Churlin and Sergeyev, 1963), seismic opacity (Balch, 1971), acoustic impedance (Lavergne, 1975; Lindseth, 1976), complex trace (Taner et al., 1979), seismic stratigraphic (Taner and Sheriff, 1977; Taner et al., 1979), seismic attenuation (Taner et al., 1979), response (Bodine, 1984), and interval (Dalley et al., 1989; Sonneland et al., 1989) attributes. In the 1980s, attributes proliferated and became popular because they could simplify the interpretation of acoustic impedance data and also the stratigraphic/structural framework. 2D seismic stratigraphic attributes were developed for the interpretation of depositional processes (Vail et al., 1977); however, they were not successful in many cases (e.g. in chaotic features: slump and turbidites or subtle discontinuities) due to the 3D nature of geological features and their strong dependencies to S/N ratio (Love and Simaan, 1984).

In the 1990s, 3D seismic imaging revitalised the seismic attribute world by introducing the concept of 3D (volumetric) attributes (Dalley et al., 1989; Rijks and Jauffred, 1991). The emergence of 3D technology led to development of volumetric attributes which is considered to be the most successful exploration technology so far and made significant subsurface interpretational and characterisation impacts: coherency attribute (Bahorich and Farmer, 1995), texture attribute (Vinther et al.,

1995; Whitehead et al., 1999; West et al., 2002; Gao, 2003, 2004), pattern recognition attributes (Russell et al., 1997), spectral inversion (Partyka et al., 1999; Peyton et al., 1998) and elastic inversion (Connolly, 1999; Whitcombe, 2002).

As the very first seismic textual analysis, in the 2D domain, Sangree and Widmier (1977) demonstrated the relationship between seismic-signal pattern and constituent sediments of geobodies; later, Love and Simaan (1984) extracted textural patterns using 2D amplitude templates. In spite of automation of texture analysis using soft computing techniques, 2D textural analysis was not successful due to the 3D nature of the textural features. In the 1990s, the development of volumetric attributes, multi-attribute techniques (Russell et al., 1997) and statistical measures (Vinther et al., 1995; Vinther, 1997; Whitehead et al., 1999; West et al., 2002; Gao, 2003, 2004) opened new perspectives for the classification of textures. By far, the majority of seismic texture detection efforts have been focused on delineating the distribution, quality and connectivity of reservoir pay zones (Chopra and Marfurt, 2007) in different sedimentological environments: e.g. deep marine (Gao, 2007, 2008), fluvial deposits (Yenugo and Marfurt, 2010; de Matos et al., 2011), carbonates (Carrillat et al., 2002), and submarine turbidites (Gao, 2004). Seismic texture analysis has not been commonly applied to fine-grained sediment sequences and the research has often been limited to either qualitative seismic facies analysis (e.g. Droz et al., 2003; Power et al., 2014), bypass detection (e.g. Heggland et al., 1999; Meldahl et al., 1999, 2001; Tingdahl et al., 2001) or semi-quantitative classification at the geobody scale (e.g. Corradi et al., 2009). In this work, we aimed to automatically and quantitatively link seal quality (or leakage risk) with the 3D seismic texture of heterogeneous mud-rich sequences by introducing an *a priori* seal texture model (Gao, 2004). We believe that this is the first attempt at quantitative 3D seal risk analysis and includes an understanding of the main geological leakage risk elements and their relationships with the volumetric seismic attributes. The proposed procedure generates a seal risk probability cube, delineating suitable seismic seals as well as possible matrix-related leak points and eventually migration scenarios. In fact this study extends the recent work by Alves et al. (2014) in which multiple surface attributes were used to delineate different MTD textures. Similar to any textural analysis, seal texture model and seismic resolution control the pattern detection.

The proposed procedure has been applied on a case study from offshore West Africa with a high-density seismic volume. The pilot cubes contain both regional seals and reservoirs. The structure of this chapter is as follows: introduction, aims, hypothesis, geological settings and dataset, methods, results, discussion, conclusions and references.

3.2 Aims

In the previous chapter, we mainly analysed and predicted different fine-grained facies using core and log datasets; here, the general aim is to capture the lithology and internal texture of sealing units at a seismic scale and to develop a workflow for quantitatively assessing the risk of leakage through the matrix of the seal units. We aim to capture the seismic characteristics important for fluid flow. The study objectives can be divided into three main goals:

1) Signal / noise ratio improvement using trace-based attributes: although mud-rich sediments are often transparent and poorly resolved in the original seismic data, attribute volumes may have better signal content due to the nature of their computation. Therefore, it is important to find the most appropriate attributes which can help with improving signal continuity and identifying structural/stratigraphic features in fine-grained sediment sequences.

2) Seismic estimation of seal risk: find a procedure to automatically estimate seal risk from seismic data based on a conceptual seal texture model and the combination of 3D attributes in the poorly resolved fine-grained seal units.

3) The final objective is to evaluate the results obtained in (2) by correlating the seal risk attribute with the recognised fine-grained log facies at well locations (Chapter 2).

3.3 Hypothesis: Potential seismic characteristics for sealing quality

Cap rocks or seal rocks are sedimentary units with very low permeability that locally or basin-wide restrict or compartmentalise fluid flow in the sedimentary basin. The common seal unit lithologies are mudstone, unfractured carbonates and anhydrites (Kearey, 2001). In this study evaporitic seals have been ignored, since their seismic reflection profiles are extremely poor due to their homogeneous nature,

and hence not feasible for seismic attribute analysis. The main focus here is on siliciclastic seal units. In sedimentary basin analysis, continuous, homogenous, thick, clay-rich mudstones are usually considered as typical good seals, and structured, dipping, thin coarse mudstone and siltstone units as poor seals (Bahorich and Farmer, 1995; Cartwright et al., 2007; Loseth et al., 2009; Seebeck et al., 2015). In this study, a seal texture model (seal quality scheme) has been proposed based on physical reasoning of fluid dynamics (Table 3.1). The scheme is also in accordance with hemipelagite, mass transport deposit (MTD) and leakage atlases recently prepared by Omeru (2014) in different sedimentary basins. In fact, the scheme introduces the potential seal quality components that can link between geological and seismic characters. This is exemplified with seismic sections and their outcrop analogues in Figure 3.1 (Note: the outcrop analogues may not be the exact interpretation of the seismic sections).

Table 3.1: *The scheme of potential sealing quality components (seal texture scheme)*

Seal component	Geological character	Seismic character
1	Sediment sandiness	Reflection strength
2	Sediment verticality	Reflection dip
3	Sediment heterogeneity	Reflection chaoticness

The breach of a seal unit may have a cause that cannot be captured by the seismic data, such as diagenesis, chemical process or sub-seismic feature. Moreover, a seal sequence can be breached through a bypass system such as faults, intrusions and pipes which are out of the scope of this study. The proposed scheme is designed to summarise the seismically observable textural characters in the seals which may link to fluid flow process in these sediments. The focus of this study is on capturing these characteristics using a set of volumetric attributes in fine-grained sediments. We assume the seismic characteristics are mainly controlled by the corresponding geological characteristics. For example, the chaotic nature of reflections is assumed to be only due to the sediments' heterogeneities (Figure 3.1b) and similarly for Reflection Intensity (Figure 3.1a). This may not be a suitable assumption at reservoir environment, but considering the seismic quality limitations for mud-rich units and the required resolution for exploration and basin modelling studies, it cannot be far

from reality in the regional seal units which are laterally uniform and widespread, and show little AVO (Amplitude Versus Offset) effect. At the end of this chapter, we correlate logfacies data with seismic seal risk result to evaluate the geological validity of the current seal texture scheme and the above-mentioned assumption.

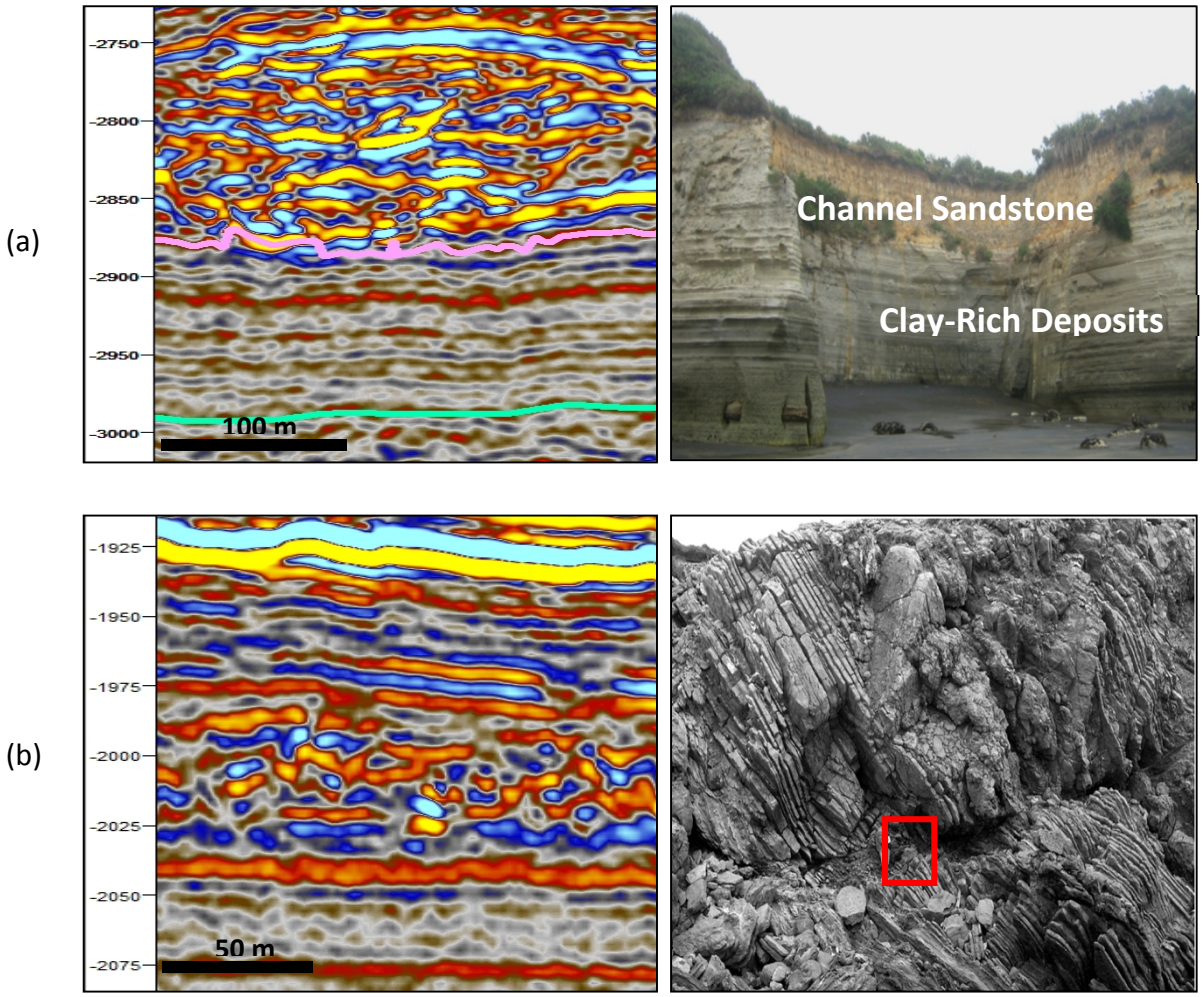

Figure 3.1: *Illustration of potential seal quality components with seismic sections from West Africa case study and the outcrop analogues. Pink and cyan lines are interpretation lines for top hemipelagite and top MTD in the regional seal unit, respectively. We have assumed (a) seismic intensity is controlled by sandiness (channel sandstone and clay-rich deposit sequence, Taranaki Basin, north of New Zealand, Omeru, 2014) where (b) reflection chaoticness depends on sediment heterogeneity (heterogeneous sand_limestone rich MTD in shaly matrix, early Cretaceous MTD, West Portugal, Omeru, 2014).*

3.4 Geological Settings and Dataset

This study uses a high-density 3D seismic (HD3D) volume (bin size: 6.25m × 6.25m) from block X in offshore West Africa (case study A). The block X is operated by a sponsor of Caprocks project and the HD3D seismic were acquired by

CGG in 1999, followed by re-processings in 2001 and 2002. The acquisition and processing parameters are given in Table 3.2. A high-density seismic survey in the oil and gas industry refers to a survey that benefits from tighter array (typical HD3D array parameters in offshore: spread length ~ 1000 m, receiver group length ~ 6.25 m, receiver group interval ~ 6.25 m, airgun displacement ~ 723 in), shorter shot-point interval (~ 12.5 m) and larger source bandwidth (~ 30-150 Hz) than a conventional 3D survey (Boardman and Walker, 1995). The high-density seismic data enables us to interpret the sedimentary facies on a finer level and understand better the internal architecture of the chaotic facies (because of having better spatial/temporal resolutions and preserving the high frequencies) (Calvert et al., 2003). Moreover, the HD3D data can provide a better platform to do seismic well-tie and attribute analysis in a higher resolution.

Table 3.2: *The acquisition and processing parameters of the HD3D volume of case study A*

HD3D volume (case study A)	
Spread type	Orthogonal
Area	402 km^2
Nominal 3D trace density	1,382,400 traces/km^2
Number of streamers	8
Streamers length and depth	2500 m, 4 m
Streamer separation	50 m
Receiver group length	6.25 m
Receiver group interval	6.25 m
Airgun array	2 × 1510 in^3
Airgun depth	3.5 m
Shot interval	12.5 m
Processing procedures	CGG fast-track processing, DMO, standard post-stack migration, geostatistical analysis, high-resolution tau-p demultiple, 4th order NMO
Time sampling	2 ms
Bin size	6.25 m × 6.25 m
Vertical resolution	5 - 10 m
Bandwidth at seal unit 4 level	30 – 110 Hz
S/N ratio at seal unit 4 level	7 - 9 dB

Case study A is located in the flat crest of a Neogene turtle structure in the West African continental margin with a background of active salt tectonics. The liquid hydrocarbon accumulation is significant in its Tertiary deposits and the regional seal units are incised by a set of faults and channels. In addition to the

HD3D seismic volume, reliable mappings (mixture of operator mapping and primary mapping at Cardiff University by Caprocks team in "Phase 1, 2 and 3") and good log suites are provided for the key regional seal unit intervals.

In case study A with approximate dimensions of 23 km by 22 km, there are five main regional seal units. Figure 3.2 reviews the seismic characteristics of the regional seals. Seal units 1, 2, 3 and 5 (located in deeper section) are often out of the wireline range or have very little wireline coverage. This study focuses on seal unit 4 which is laterally extensive and crossed by most of the wellbores. It has the complete log suite coverage in four wells (W41, W42, W101 and W102) and partial log suite coverage in three wells (W45, W71 and W71_01) out of 11 wells (Table 3.3). More importantly, seal unit 4 is located between the two main hydrocarbon accumulations. Note that well W31 does not cross the seal unit 4, however an equivalent fine-grained depth-interval in this well is considered as analogue for the seal unit 4 because it is the best placed well in the case study for seismic facies calibration and has the best quality core and log data.

Seal unit 4 is laterally extensive (~20×20 km) with 170 m-220 m thickness. Reflections from fine-grained seal unit 4 are clearly much weaker than surrounding coarser-grained channel sediments and its seismic character is varying vertically and laterally which may reflect different geological features. Seismic characters of seal unit 4 range from blocky moderate amplitude reflections to very transparent and unresolved noisy reflections (Table 3.3).

Two main seismic facies were interpreted in seal unit 4 by Caprocks team ("Phase 1") at Cardiff University: hemipelagite 4 (upper) and mass transport deposit 4 (MTD 4) (lower) (Figure 3.3). This is a large scale classification of seal unit 4 from a seismic stratigraphic point of view. In other words, lithology cannot be interpreted directly from the seismic facies, and seismic character and lithology vary within each seismic facies. Seal unit 4 has been investigated in both seismic facies. Hemipelagite 4 *mainly* contains low amplitude events with horizontal/low angle seismic reflectors. There are also numerous areas within this seismic facies with local moderate amplitude or distorted reflections. In contrast, MTD 4 often shows variable poor to moderate amplitude reflections with chaotic texture. However the blocky events are the dominant seismic texture in the western part of case study A.

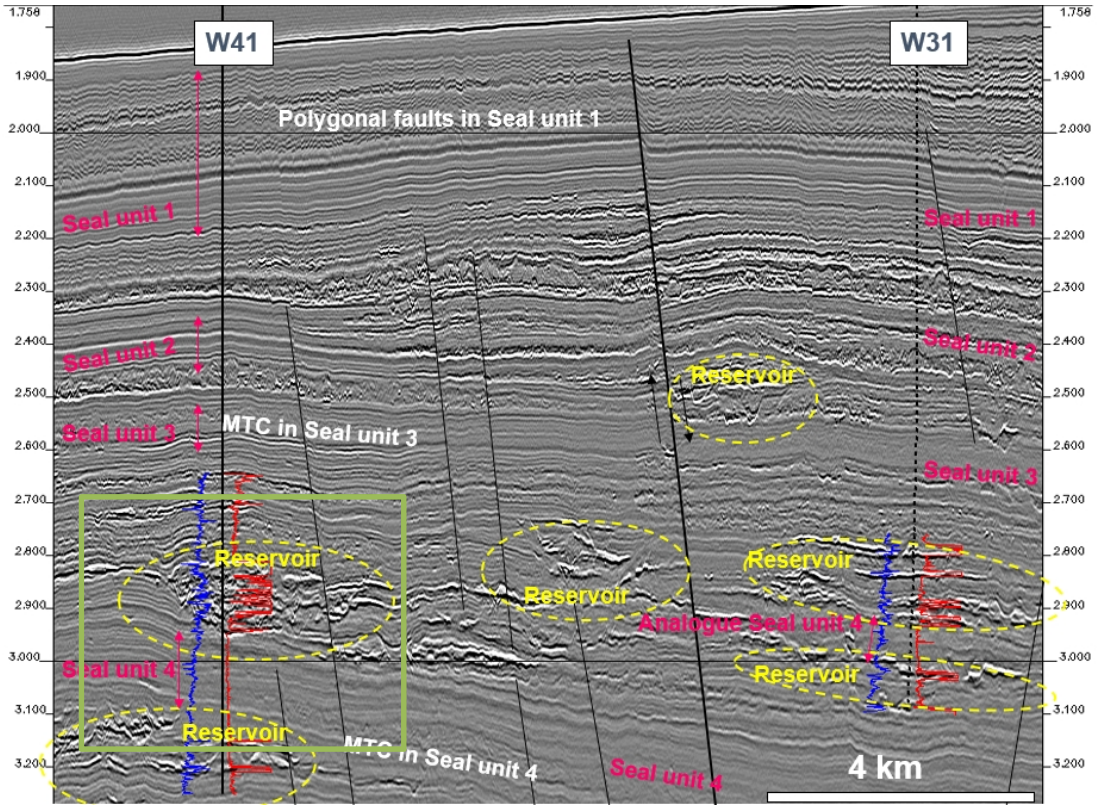

Figure 3.2: *Overview of the regional seal units in case study A. The black lines represent the major normal faults in the seismic profile. Well W31 does not cross the seal unit 4 and an equivalent fine-grained depth-interval is used as analogue for seal unit 4. Gamma-ray (red lines) and P-sonic (blue lines) logs illustrated the problem of availability of wireline records within seal unit intervals. The green box indicates the boundary of the seal unit 4 section view in Figure 3.3. (After Huuse and Cartwright, 2007 (Caprocks "Phase 1"))*

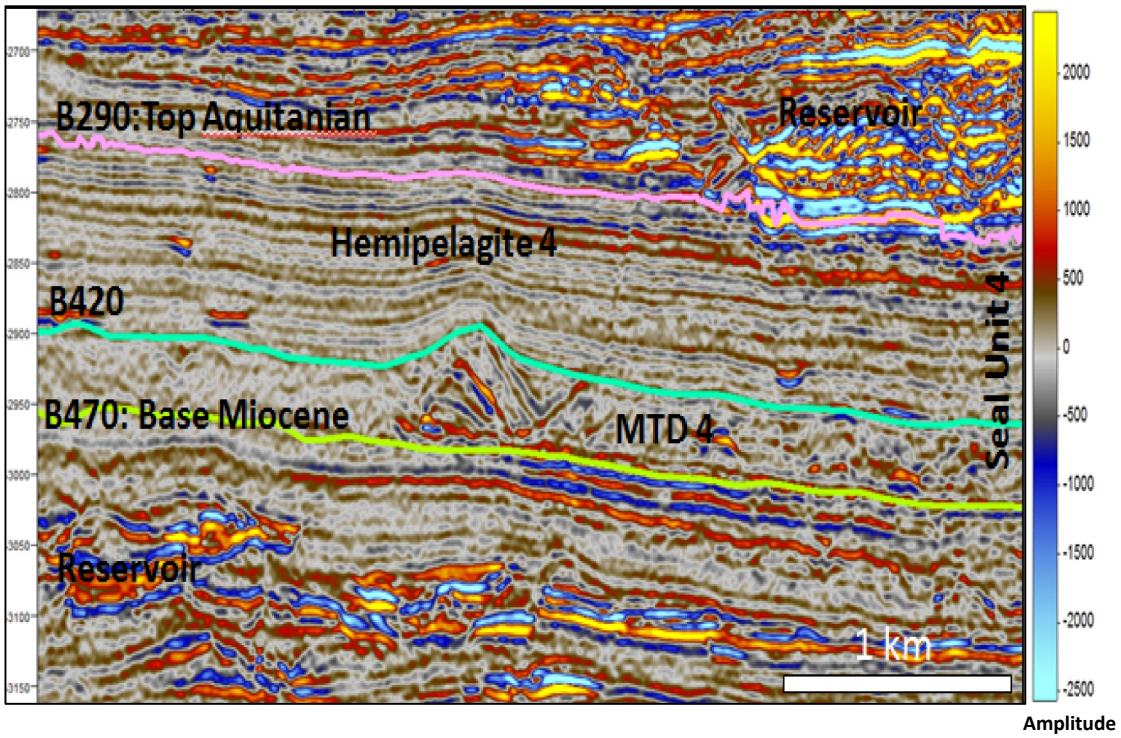

Figure 3.3: *Seismic facies classification of seal unit 4 in case study A: hemipelagite 4 (bounded by pink and cyan interpretation lines) is fairly poor amplitude with continuous reflections whilst MTD 4 (bounded by cyan and pale green interpretation lines) contains variable poor to moderate amplitude reflections with chaotic and/or blocky textures.*

In addition to the seismic data, case study A includes 16 wells, of which five well (W31, W41, W42, W101 and W102) have conventional log suite coverage in the seal unit 4 interval. Table 3.3 shows the availability of wireline records at the seal interval of different wellbores as well as the seismic character within the main seismic facies. It again demonstrates the limitations of studying seal intervals both in terms of log data availability and seismic quality. At the end of this chapter, facies recognition results from wells W31, W41 and W42 (Chapter 2) have been used for correlation with seismic seal quality attribute.

Table 3.3: *Overview of the wireline data and seismic character within two main seismic facies of seal unit 4 (* Conventional well logs are available, including gamma-ray, p-sonic, s-sonic and density logs).*

Well	Seismic character		Wireline data
	Hemipelagite 4	MTD 4	
W31	low to moderate amplitude – continuous reflections	moderate amplitude – chaotic reflections	complete log suite *
W41	Top: moderate amplitude – low frequency continuous reflections Bottom: low amplitude –	low amplitude – chaotic reflections	complete log suite *

	continuous reflections		
W42	Top: low amplitude – continuous Bottom: low amplitude - chaotic reflections	low amplitude – chaotic reflections	complete log suite *
W43 **W43_PH** **W43_G**	low amplitude – fairly continuous reflections	low amplitude – blocky / chaotic reflections	seal unit 4 is out of wireline range
W44 **W44_PH** **W44_SG**	low amplitude – continuous/ chaotic reflections	low to moderate amplitude - chaotic reflections	seal unit 4 is out of wireline range
W45_PH **W45_G**	low to moderate amplitude – continuous reflections (prevalent low frequency at top)	low to moderate amplitude – chaotic reflections	no available acoustic log in seal unit 4
W71	moderate amplitude - continuous reflections	moderate amplitude – blocky / chaotic reflections	complete log suite * (with a missed wireline interval in hemipelagite 4)
W71_01	moderate to high amplitude - continuous reflections	moderate amplitude - blocky reflections	wireline starts just at the top of MTD 4
W72_B	moderate amplitude - continuous reflections	moderate amplitude – chaotic reflections	seal unit 4 is out of wireline range
W101	low to moderate amplitude - continuous reflections	low to moderate amplitude – blocky / chaotic reflections	complete log suite *
W102	moderate to high amplitude - continuous reflections	Moderate to high amplitude – chaotic reflections	complete log suite *

3.5 Methods

In petroleum geoscience, there has always been a gap in resolution between core (cm scale), well log (m scale) and seismic data (deca-metre scale). This is especially challenging in mudstone sequences where there are considerable small-scale petrophysical and sedimentological heterogeneities (Macquaker and Howell, 1999; Macquaker et al., 2007; Aplin and Macquaker, 2011). In the early stage of the study, we performed a primary well-tie analysis in wells W41 and W42 using Petrel[1] Seismic Well Tie module. Different analytical and statistical wavelets were tested and applied to create synthetic seismograms along the seal unit 4 interval.

[1] A Schlumberger software

An example is given in Figure 3.4 for MTD 4 interval of well W42, where the synthetic seismogram is created using a zero-phase, statistical wavelet (calculated in a 3 × 3 trace-neighbourhood using the Bartlett taper and 2 ms sample rate) and a reflection coefficient log (derived from the acoustic impedance log and using 2 ms sampling interval). The synthetic seismogram is stretched and shifted to match the base reflection at TWT = 3036 ms. Although there is a good seismic well-tie for the base seal unit 4 (base MTD 4) reflection, the intra-unit reflections cannot be correlated. For example, at TWT= 3027 ms, no reflection is modelled in the synthetic seismogram (due to the absence of acoustic impedance contrast); or, at TWT=3017 ms, we expected to have stronger reflections at seismic traces. The primary seismic well-tie analysis suggested that poor correlation in seal unit 4 could be caused by the random noise effect on seismic at fine-grained sediment sections (e.g. Brancolini et al., 1994) and/or dependency of weak seismic reflections to other parameters than acoustic impedance contrast (such as sub-seismic vertical variability of facies) (e.g. Pandey et al., 2007).

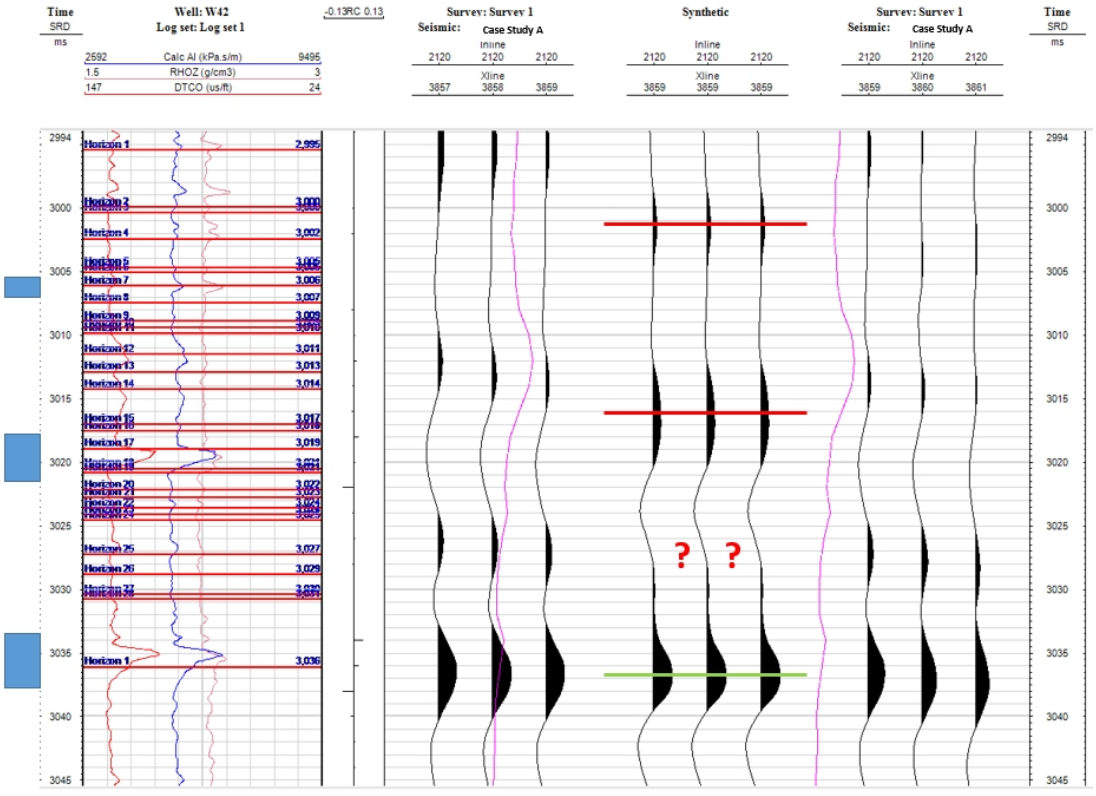

Figure 3.4: *Seismic well-tie analysis at MTD 4 interval of well 42: A good tie was only seen for the base seal unit 4 (base MTD 4) reflection – green line - (at TWT=3036 ms). The red lines indicate the modelled reflections which cannot be matched with seismic. The blue boxes indicate the TWT intervals for the major acoustic impedance contrasts. A statistical wavelet (calculated in a 3 × 3 trace-neighbourhood using the Bartlett taper and 2 ms sample rate)*

and a reflection coefficient log (derived from the acoustic impedance log and using 2 ms sampling interval) were used to create the synthetic seismogram.

We think that in fine-grained sediments achieving a relationship between well data and volumetric attribute or set of volumetric attributes is usually more feasible than conventional single-trace-based well-tie analysis. It is because the level of random noise could be considerably reduced in volumetric attribute calculation. Moreover, geological features are 3D in nature and seismic textural analysis has limited capability using trace-based attributes (Sangree and Widmier, 1977; Love and Simaan, 1984). As a result, we need an explicit, quantitative approach of 3D seismic attribute analysis which considers the sealing quality elements and also develops an automated seal risk cube. The current study proposes a five-step workflow (Figure 3.5): (1) seismic input conditioning; (2) sensitivity analysis of 3D attributes for characterising sealing elements; (3) seismic attributes combination/building seal risk cube; (4) seismic result conditioning (result stabilisation); and (5) validation of estimated seismic seal risk. Each step is now described in detail.

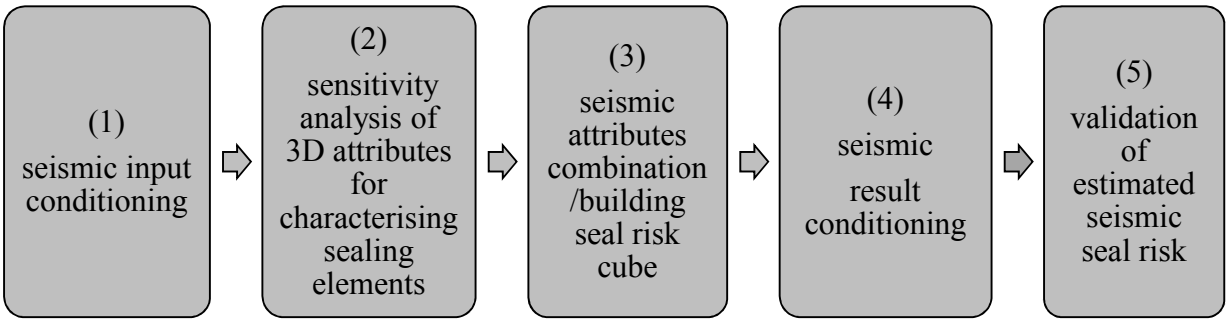

Figure 3.5: *The proposed five-step workflow for an automated seismic seal risk assessment*

3.5.1 Steps 1 and 4: Seismic data conditioning of input/result

The amplitude content of reflections from fine-grained sedimentary facies is relatively low and the stratigraphic/structural mapping of their reflectors is vague and time-consuming in the chaotic or transparent regions. There are selective processing filters which could be utilised for removing multiples and non-coherent noise, such as spectral decomposition (Partyka et al., 1999) and broadband processing techniques (e.g. Zhou et al., 2012). As standard post-processing techniques in reservoir environments, they are mathematically cumbersome and would require even further

delicate adjustment to be used on the commonly transparent seal units. Due to the complexity and extent of the subject, these filtering studies have been excluded from this work, although we recommend them for future research. Here, we utilise trace-based attributes to either pre-condition the seismic within seal intervals at the beginning of the workflow or to help with removing artefacts from the resultant attribute cube. For instance, they can be applied on the original seismic amplitude cube to improve the phase contrast of the reflections.

According to the order of application, we categorise the conditioning attributes into two groups: pre-conditioning and post-conditioning attributes. Seismic data conditioning can simplify the structural interpretation and reduce the interpretation time. This can be done by the stepwise removal of noise and unwanted stratigraphic and structural features to improve the picking stability (Hocker and Fehmers, 2002; Fehmers and Hocker, 2003; Pepper and Bejarano, 2005). In this study, both complex and signal processing attributes from Petrel platform[1] (version 2012.1) were examined for pre-conditioning of the seismic data in the seal interval (Table 3.4). Pre-conditioning attributes are single-trace based and are able to provide a better platform for quantification of seismic character (using structural and stratigraphic attributes) in the resolvable seismic sections. Although some details (e.g. lateral amplitude variation) may be smoothed (Sheriff et al., 1976; Bahorich and Farmer, 1995), these attributes are more effective in visualising chaotic and dipping reflections. Moreover, they can improve continuity of reflections and enhance the visual appearance of edges, such as faults or stratigraphic terminations (Sheriff et al., 1976; Bahorich and Farmer, 1995).

Table 3.4: *The complex and signal processing attributes examined for pre-conditioning of seismic data in seal unit 4 (Petrel 2012.1, exploration geology user guide).*

Attributes analysed for seal seismic pre-conditioning	
Complex attributes	**Signal processing attributes**
Apparent Polarity	First Derivative
Cosine of Phase	Frequency Filter
Dominant Frequency	Graphic Equaliser
Envelope	Original Amplitude
Instantaneous Bandwidth	Phase Shift
Instantaneous Frequency	Reflection Intensity
Instantaneous Phase	Remove Bias
Instantaneous Quality	RMS Amplitude
Quadrature Amplitude	Second Derivative
Sweetness	Time Gain
	Trace AGC
	Trace Gradient

In this study, we examined the efficiency of all the pre-conditioning attributes in Table 3.4 within seal unit 4 context. The successful pre- and post-conditioning attributes will be then included in the overall automatic seal assessment workflow. Here, "Apparent Polarity" and "First Derivative" attributes are described as examples of pre-conditioning attributes:

Apparent Polarity is defined as the sign of the complex seismic trace at the peak or trough of reflection strength. The complex seismic trace can be expressed based on a time-dependent amplitude A(t) and a time-dependent phase θ(t) as: $F(t) = A(t)\, e^{j\theta(t)}$ (Koehler et al., 1976). A specific colour is assigned for positive or negative sign (Figure 3.6), while the intensity of the colour varies based on the value of the reflection strength. The Apparent Polarity is mathematically expressed as:

If Envelope (t-1) < Envelope (t) > Envelope (t+1)

Then Apparent Polarity (t) = sign (F (t))

Else Apparent Polarity (t) = 0 Equation 3.1

where the envelope is the total instantaneous energy of the complex trace.

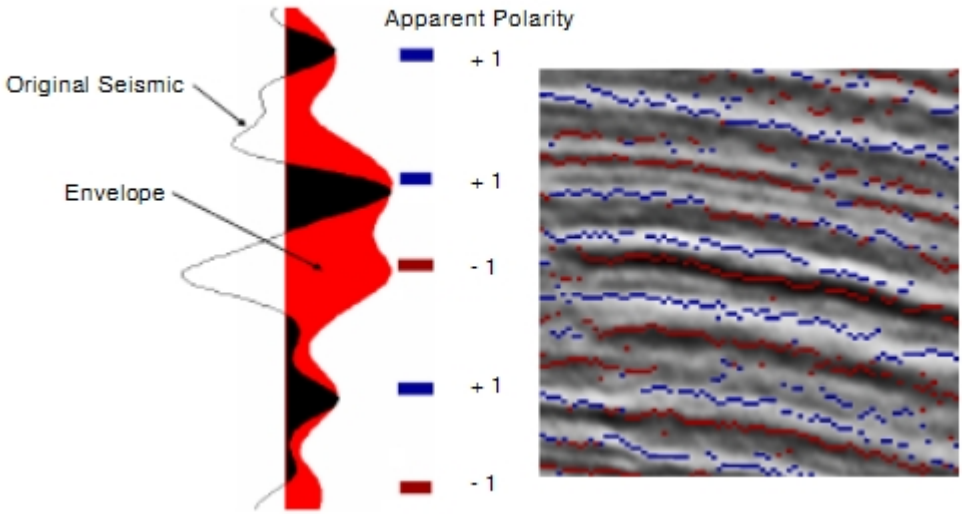

Figure 3.6: *Superimposition of Apparent Polarity attribute on the original seismic. Blue and red colours on the seismic sections represent the positive and negative polarity of the reflections.*

The Apparent Polarity is a practical tool in seismic interpretation because it can increase the event continuity in noisy sections with no effect on waveform. In addition, it illustrates the lateral variation of polarity along a reflection layer (Sheriff et al., 1976).

Similarly, the **First Derivative** attribute allows us to quality control the signal consistency in the picks, as positive or negative should be zero crossing (Yilmaz, 2001). It is defined as the time rate of change of the input real seismic trace f(t):

$$\text{First Derivative} = d\,[f(t)] / dt \qquad \text{Equation 3.2}$$

where real seismic trace is expressed as: $f(t) = A(t) \cos \theta(t)$. The output is equivalent to a + 90° phase shift of the original amplitude cube. Since the boundary of lithological / fluid units are located at the peak or trough (i.e. reflection interfaces) in a zero-phase seismic cube, this phase shift is especially useful for stratigraphic analysis, facies estimation and log-seismic tie studies.

Conditioning attributes act not only as an improved input in the seal risk assessment workflow, but they can also stabilise the attributes combination results at the final stage of the workflow. As an example, **Structural Smoothing** is a multi-trace attribute that can attenuate/filter the vertical artefacts and random noises

resulting from the process of attribute computation and combination. Structural Smoothing is based on a Gaussian weighted filter which is expressed as (Iske and Randen, 2005):

$$h_G(k) = \frac{1}{\sqrt{2\prod\sigma}} \exp\ \left(-\frac{1}{2}\ \frac{k^2}{\sigma^2}\right) \qquad \text{Equation 3.3}$$

where σ is the width of the smoothing filter (the degree of the smoothing or the standard deviation of the Gaussian filter). This scale can be approximately converted to the number of inline/crossline traces (or vertical samples) as:

$$\text{Number of traces/samples} = (2 \times \sigma) + 1 \qquad \text{Equation 3.4}$$

Sigma varies from 0.0 to 5.0 (typical values: 1.0 – 2.5). The larger filter size uses a larger number of samples and traces and delivers smoother results in a longer calculation time. Since the seal risk cube will be automatically smoothed by volumetric attributes, a small filter size (σ: 0.5 – 1.5) is recommended for Gaussian filter to avoid over-smoothing issues.

Structural Smoothing was originally developed to simplify the seismic data (by attenuating random noises and survey imprints) in highly structured geological settings while honouring the prevailing structures (e.g. faults) (Iske and Randen, 2005). We can also benefit from this image analysis advantage to smooth the seal risk cube without degrading the estimated risk values in the original seal risk cube. As a final note, Structural Smoothing in Petrel can be handled in three different ways: without dip guide, dip-guided or edge-enhanced (Petrel 2012.1, exploration geology user guide). In the dip-guided and edge-enhanced options, the visualisation of local structural orientation and discontinuities, respectively, is further enhanced. But in the seal risk assessment workflow, we intend to apply the Structural Smoothing filter only to remove vertical artefacts (noises) from the resultant attribute cube; therefore the dip guiding and edge enhancement options are ignored.

3.5.2 Step 2: Sensitivity analysis of 3D seismic attributes for characterising potential sealing elements

After sensitivity analysis of the pre- and post-conditioning attributes, we aimed to find the most appropriate seismic attributes to quantify the seal quality

components of the proposed texture scheme and to eventually develop automated seismic seal risk detection. A seismic attribute is any information (quantity or property) which is derived or measured from seismic data (Taner, 2001). Thus they can range from complex trace attributes and seismic event geometrical configurations to spatial and pre-stack attributes. They can be analysed in order to enhance information that might be more subtle in an original seismic image. There are now over two hundred attributes in use in some geophysical interpretation software packages, many of which result from slightly differing approaches to determining a specific property, such as frequency or amplitude (Brown, 2004). In reflection seismology, the stacked seismic data volume is commonly used for the interpretation of geologic structure and seismic attributes (Yilmaz, 2001). In this study, we used a 3D post-stack seismic attributes because we believe they are generally more beneficial for detecting orientation and variation of those reflection patterns which may be important indicators of flow/sealing behaviours in fine-grained sediments. Therefore, we performed a comprehensive sensitivity analysis on the industrial standard volumetric post-stack attributes (Table 3.5) in seal unit 4.

In Petrel, volumetric attributes are classified into four main groups: complex trace attributes, signal processing attributes, stratigraphic method attributes and structural method attributes (Petrel 2012.1, Exploration geology user guide). In Table 3.5, Petrel seismic attributes for each group are listed.

Table 3.5: *Volumetric attributes tested/analysed for characterising the potential sealing quality component of the proposed scheme (Petrel 2012.1, Exploration geology user guide).*

Complex Attributes	Signal processing attributes	Stratigraphic method attributes	Structural method attributes
Apparent Polarity	First Derivative	Chaos	3D Curvature
Cosine of Phase	Frequency Filter	Genetic Inversion	Ant Tracking
Dominant Frequency	Graphic Equaliser	Iso-Frequency Component	Dip Deviation
Envelope	Original Amplitude	Local Flatness	Gradient Magnitude
Instantaneous Bandwidth	Phase Shift	Neural Net	Local Structural Azimuth
Instantaneous Frequency	Reflection Intensity	Relative Acoustic Impedance	Local Structural Dip
Instantaneous Phase	Remove Bias	Sweetness	Structural Smoothing
Instantaneous Quality	Rms Amplitude	t* Attenuation	Variance (Edge Method)
Quadrature Amplitude	Second Derivative		
	Time Gain		
	Trace AGC		
	Trace Gradient		

The standard seismic attributes are mainly designed for and applied to the interpretation of geologic structure, stratigraphy and rock/pore fluid properties associated with reservoirs (Chopra and Marfurt, 2005). Here, however, we intend to utilise the post-stack volumetric attribute in the fine-gained seal context, which has a different seismic texture. As a result, the common conventions may not apply or the computation process may require different parameterisation. In this step, we run all the above-mentioned volumetric attributes on the original seismic section of seal unit 4 using all possible (standard / non-standard) parameterisations in Petrel. According to best visualisation performance of attributes, we evaluate the results and rank them for quantification of the seal quality components (i.e. reflection strength, chaoticness and dip). The ranking is qualitative (poor-fair-good) and is entirely based on efficiency of capturing the seismic characteristics indicated in the seal texture scheme. Finally we select the best attributes for each of the three seal quality components and determine the best settings for their computation in seal environments. This is an important and time-consuming part of the seal risk

assessment workflow and the attribute ranking results will guide the choice of the best seal risk attribute(s).

Explaining all the tested attributes (37 attributes listed in Table 3.5) with their parameterisations would not be feasible here. Therefore, we introduce each attribute category with a representative attribute, including the parameterisations and considerations for applying it within the seal context. Please refer to the Petrel manual (Petrel 2012.1, Exploration geology user guide) for the descriptions of other volumetric attributes than the representative attributes.

1. Complex trace attributes: These evolved from the work of Taner et al. (1979), who demonstrated the benefit of thinking of the seismic trace as an analytic signal containing real and imaginary parts, of which only the real part is detected. The applied complex trace attributes in our sensitivity analysis are: Apparent Polarity, Cosine of Phase, Dominant Frequency, Envelope, Instantaneous Bandwidth, Instantaneous Frequency, Instantaneous Phase, Instantaneous Quality, Quadrature Amplitude and Sweetness. In the first step, Apparent Polarity, Instantaneous Phase and Cosine of Phase are used for pre-conditioning the seismic and improving the signal/noise ratio in the more transparent areas of the seal unit. At this stage we analyse the other complex attributes for capturing the seal quality components.

Instantaneous Frequency is one of the most commonly used complex trace attributes for fluid analysis in the reservoir environment. Instantaneous Frequency is defined as the time derivative of instantaneous phase. It is mathematically expressed as (Taner and Sheriff, 1977):

$$\omega_c (t) = \partial \{ \varphi (t) \} / \partial t \qquad \text{Equation 3.5}$$

where $\varphi(t)$ is the Instantaneous Phase and defined as (Taner and Sheriff, 1977):

$$\varphi_c (t) = \tan^{-1} [g(t)/f(t)] \qquad \text{Equation 3.6}$$

where f(t) is the real part of original seismic trace samples and g(t) is the imaginary part of original seismic trace samples or the quadrature trace (from the Hilbert transform). In Petrel, we can set the Hilbert filter window size, ranging from three to eleven samples (Figure 3.7). In addition, the negative values of the frequency

occurred due to the phase reversal are set to zero during the computations (Petrel 2012.1, exploration geology user guide).

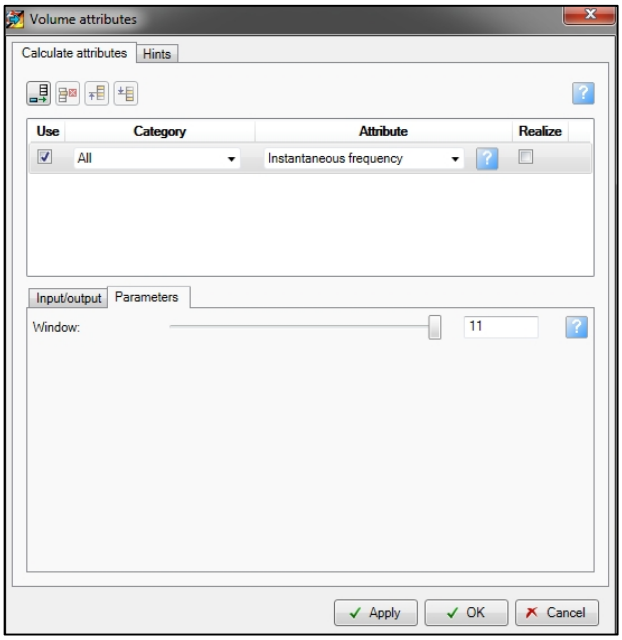

Figure 3.7: *Instantaneous Frequency: Parameters tab for setting the Hilbert filter window size (Petrel 2012.1).*

Instantaneous Frequency is often used in reservoir studies to estimate seismic attenuation as an indicator of fracture zones or hydrocarbon accumulations (Taner and Sheriff, 1977; Taner et al., 1979; Yilmaz, 2001; Castagna et al., 2003). In the seal study perspective, it also has some characteristics which make it a suitable candidate for interpretation. Instantaneous Frequency has an apparent higher resolution than the input amplitude data which is useful for mapping subtle changes. Moreover, it is less affected by the lower amplitudes typically observed in fine-grained sediments (Taner and Sheriff, 1977), but it does tend to be unstable in the presence of noise and is sometimes difficult to interpret. Hence it must be applied with caution in the seal section, where the signal content is relatively poor. This effect can be reduced by choosing a smaller window size and allowing the algorithm to capture more phase changes within the thinner layering of seal unit 4. For the sensitivity analysis, three different Hilbert filter window sizes (i.e. 3, 7 and 11 samples) have been applied in order to calculate the Instantaneous Frequency attributes in seal unit 4.

2. Signal processing attributes: These operate on individual seismic traces within a seismic 2D or 3D volume, producing a new collection of traces based on the signal processing attributes. The following attributes are used for the current sensitivity analysis on seal unit 4: First Derivative, Frequency Filter, Graphic Equaliser, Original Amplitude, Phase Shift, Reflection Intensity, Remove Bias, RMS Amplitude, Second Derivative, Time Gain, Trace AGC and Trace Gradient. Similar to the complex attributes, two signal processing attributes (i.e. First and Second Derivative attributes) are used earlier in the workflow for pre-conditioning of the seismic data. However, there are still other attributes in this group which need to be evaluated for seal quality component characterisation. For example, **Reflection Intensity** is a simple and prevalent signal processing attribute which is related to the energy in the real seismic trace. In Petrel, it integrates and averages the amplitudes along the real seismic trace within a specified moving window using the trapezoidal rule. Petrel manual defines the Reflection Intensity attribute for a real trace function of f(t) as:

$$A_R\,(t) = \sqrt{1/N \sum_{k=-N/2}^{N/2} |f(t+k)|} \qquad \text{Equation 3.7}$$

where t, k and N are time, time step and window size (Petrel 2012.1, exploration geology user guide).

We think the given expression in the Petrel manual (Equation 3.7) is not correct because according to the Fresnel's equations, the "*square*" of amplitude (and reflection coefficient) is proportional to the reflected energy flux per unit area (i.e. intensity) (Jenkins and White, 1957). In addition, Reflection Strength attribute (a complex trace attribute) is also proportional to the sum of "squared" amplitudes (of real and quadrature traces) (Taner et al., 1979). Therefore, the correct expression for Reflection Intensity attribute should be as follows:

$$A_{RI}\,(t) = 1/N \sum_{k=-N/2}^{N/2} f^2(t+k) \qquad \text{Equation 3.8}$$

Although Reflection Intensity is typically utilised to delineate amplitude features implying the presence of hydrocarbons or pay zone thickness changes in the reservoir context (Chopra and Marfurt, 2007), we think it can benefit the seal interpretation too. By using Reflection Intensity on fine-grained units, we can

highlight subtle local amplitude anomalies/variations or pockmarks within transparent seismic facies. In addition, it can be employed to outline the blocky events and moderate amplitude dipping reflectors in the noisy zones or chaotic texture of MTDs. According to our proposed scheme, we suggest that amplitude is controlled mainly by the degree of coarseness of sediments in the seal units (excluding carbonate and evaporite seal rocks). Therefore these higher amplitudes and hence coarser sediments can play an important role in delineating potential features that characterise the flow/sealing behaviour of the seal unit. The default computations in Petrel 2012.1 are based on 3 time samples (here 6 ms). To avoid a smearing effect, smaller window sizes are recommended for seal units due to their greater vertical variation for phase and amplitude. However, Petrel 2012.1 does not allow the user to set the window size; thus Reflection Intensity attribute calculation is parameter-less in this study (the default 3-sample window is used).

3. Stratigraphic method attributes: These are multi-trace based attributes and attempt to isolate seismic textures visible in the data. These include: Structural Orientation Measurements (Chaos and Local Flatness), Frequency Decompositions (Iso-Frequency Component and t* Attenuation), Relative Acoustic Impedance, Sweetness and Seismic Classification (Genetic Inversion and Neural Net).

One of the widely used 3D attributes for stratigraphic analysis in siliciclastic (e.g. channels) and carbonate (e.g. reef) reservoirs is **Chaos**. The Chaos attribute maps the chaoticness of the local seismic signal within a 3D window (Iske and Randen, 2005). Here, chaoticness means the level of inconsistency in the orientation estimate based on Principal Component Analysis (PCA), or in other words it is a measure of the lack of organisation in the structural (dip and azimuth) estimation method.

According to the PCA computation of Local Structural Dip and Azimuth (Randen et al., 2000; Iske and Randen, 2005; Randen and Sønneland, 2005), there are three eigenvectors, $\bar{\boldsymbol{v}}_i$, for each **C**-matrix, each of them associated with one eigenvalue, λ_i. The larger is λ_i, the better $\bar{v}_i$ describes the dip and azimuth. The larger the difference between the dominating λ_i and the two other λ_i's, the more reliable the dip and azimuth estimate is; and assuming $\lambda_1 \geq \lambda_2 \geq \lambda_3$, it can be measured as (Randen et al., 2000; Randen and Sønneland, 2005):

$$J = \frac{2\lambda_2}{\lambda_1 + \lambda_3} - 1 \qquad \text{Equation 3.9}$$

where λ_1, λ_2 and λ_3 are eigenvalues that are associated with $\bar{v_1}$, $\bar{v_2}$ and $\bar{v_3}$ eigenvectors of C-matrix.

By using this measure, regions with low consistency in the estimate typically correspond to regions with chaotic signal patterns. This local chaoticness can be caused by geological features (e.g. faults/discontinuities, reef textures, channel infill), gas migration, salt body intrusions or the chaotic structure of the deposits. This measure is independent of orientation and amplitude values and can produce the same response whether in high or low amplitudes, dipping or non-dipping regions. Thus it can be extremely beneficial to capture the chaotic seismic texture (and according to our proposed texture scheme, the sediment heterogeneity) in the usually low angle and transparent seal seismic context. Moreover, it can also indicate the faults and discontinuities which are potential conduits (if permeable) for fluid migration through the seals.

The Chaos attribute in Petrel is equivalent to J+1 (Equation 3.9) and scaled from 0 (the most organised local signal pattern) to 1 (the most chaotic local signal pattern). We can specify the 3D window size for calculating the Chaos by choosing the radius of neighbourhood in the direction of three main axes (directional sigmas: σ_x, σ_y, σ_z) (Figure 3.8).

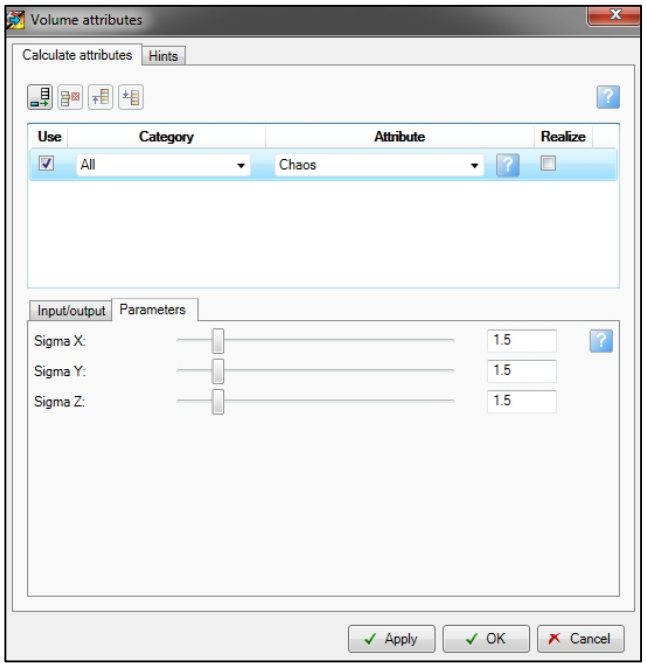

Figure 3.8: *Chaos: Parameters tab for setting the 3D window size for PCA calculations (Petrel 2012.1).*

Similar to the Structural Smoothing, the sigma is related to the number of traces/samples contributed to the computations at certain direction and their relationship is expressed as: number of traces/samples = $2 \times \sigma + 1$. The larger the sigma the smoother the result and also the longer computation time due to the involved PCA of gradient covariance matrix. Typical sigma ranges used for reservoir stratigraphy analysis are 1.0 – 2.5. Regarding the noisy and low signal content of the seal units, larger neighbourhoods are recommended for the fine-grained seal units (typically $\sigma = 2.0 – 3.0$). The smaller 3D window size may lead to misinterpretation of noises or poorly resolved zones as chaotic and discontinuous areas within the seal unit. Figure 3.9 is taken from Iske and Randen's (2005) work which illustrates the effect of the window size on edge/discontinuity detection. In our sensitivity analysis, three different 3D window sizes have been used to calculate the Chaos attributes in seal unit 4, i.e. $\sigma = 0.5$, 1.5 and 4.

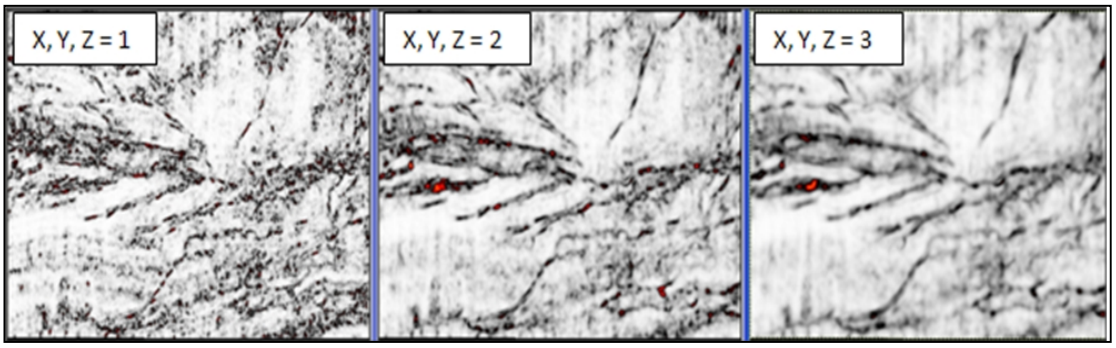

Figure 3.9: *RMS-Chaos time slices computed with different 3D window size. The larger sigma generates the smoother result and also the larger variance in the Chaos values. The black and red colours indicate the areas with relative high and maximum chaoticness (Iske and Randen, 2005).*

4. Structural method attributes: Similar to the stratigraphic method attributes, these are computed in a given 3D window based on analysis of time samples from multiple traces. Structural method attributes are used to isolate the local structural variations in the reflection patterns. These include: Discontinuity or Fault Detection (3D Curvature, Ant Tracking, Dip Deviation and Variance) and Measurement of Local Orientation of Formations (Gradient Magnitude, Local Structural Azimuth and Local Structural Dip). According to the calculation manner, the Structural Smoothing attribute is also placed in this group and is originally developed to enhance event continuity parallel to estimated bedding or to improve the detection of discontinuity (Iske and Randen, 2005). However, as mentioned earlier in the method, we utilised its advantages in contrast recovery and stabilisation for post-conditioning of the seal risk cube and removing noise and vertical artefacts.

The other important attribute of this group is **Local Structural Dip**, which is often used to create dip-constrained seismic volumes for either fault analysis or structural overview of the context (Randen et al., 2000; Randen and Sønneland, 2005). This attribute computes the angle of inclination of seismic events as measured from a horizontal plane. Three methods of Local Structural Dip computation, are made available in Petrel (Figure 3.10), have been tested on seal unit 4:

(i) Event (0° - 90°)**:** calculates the downslope dip of the estimated event in a given neighbourhood. The gradient is assumed to be perpendicular to the event. This method is parameter-less in Petrel 2012.1.

(ii) Gradient (-90° - 90°): measures the dip of the instantaneous gradient (instantaneous dip) of the sample neighbourhood. This method is parameter-less in Petrel 2012.1.

(iii) Principal Component Analysis (PCA) (0° - 90°): computes the local dip estimate from the Principal Component of the gradient covariance matrix (Randen et al., 2000). It is a time-intensive computation involving a local gradient covariance estimate followed by a PCA. Similar to the Chaos attribute, three different (3D) window sizes have been used to calculate the PCA-based Local Structural Dip attributes in seal unit 4 (i.e. σ = 0.5, 1.5 and 4).

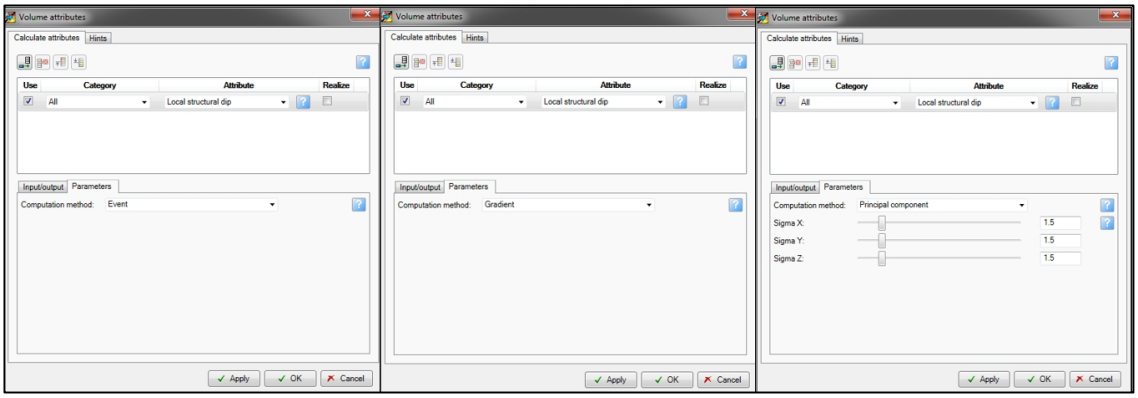

Figure 3.10: *Local Structural Dip: Parameters tab for setting the calculation method, and 3D window size (available only for PCA calculations) (Petrel 2012.1).*

The colour scale is set to +/- 90° for the gradient option while the event and PCA methods have colour a scale of 0° to 90° with wider ranges of colour palette. Regarding the size of captured features, the event and gradient methods are typically used for more detailed studies (e.g. in highly deformed reservoirs), providing the seismic data has an appropriate resolution (Iske and Randen, 2005; Randen and Sønneland, 2005). These two methods compute the local estimate of dip for the seismic events while the PCA method gives a much smoother estimate of the dip. Figure 3.11 illustrates the Iske and Randen's (2005) work where local structural dip was calculated using these three methods with the same parameters. Due to the local gradient covariance matrix, in PCA method dominant orientations of reflections are retained within the sample neighbourhood and instantaneous variations are often ignored. This is useful for dip analysis in fine-grained sediments where the seismic

quality is relatively poor, and the noisy and dipping events are poorly distinguishable on a fine scale. Moreover, regarding the parameterisation of the PCA method, the same recommendations for the sigma values apply as for the Chaos.

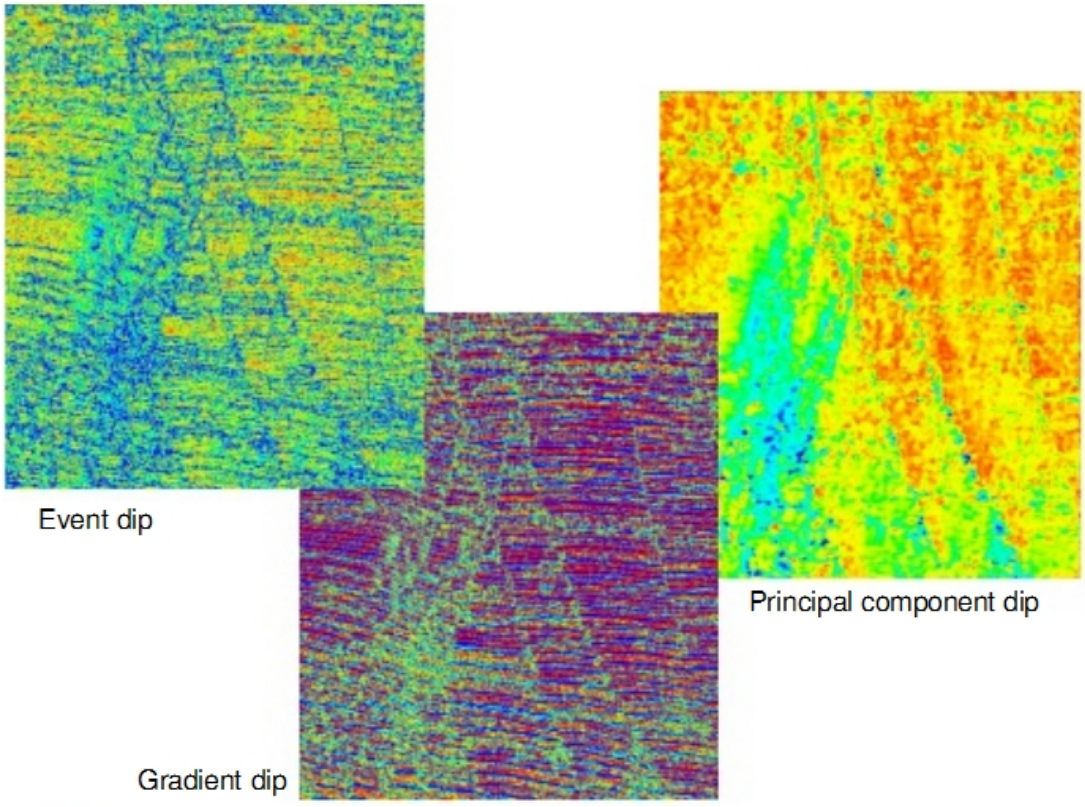

Figure 3.11: *Local Structural Dip attribute calculation using three different methods available in Petrel. Gradient- and Event-based methods give local estimates of dips suitable for more detailed analysis (e.g. in highly deformed reservoirs) while the PCA method calculates much smoother estimates of structural dip favourable for the poorly resolved, noisy seismic context of seal units (Iske and Randen, 2005).*

3.5.3 Step 3: Seismic attributes combination/building seal risk cube

After completion of the sensitivity analysis, the seal risk cube can be developed by proposing a meaningful Seal Risk Factor (SRF) attribute. We know that different attributes will be sensitive to different geologic features of interest (Chopra and Marfurt, 2005). Thereby, at this step, our SRF attribute is formed as a combination of effective 3D attributes, taking into account the three seal quality components. This helps to have a comprehensive view on the sealing quality and also to enhance the contrast between features of interest and their surroundings. In reservoir analysis, soft computing techniques are widely used for a variety of multi-attribute tasks. They are often based on the training of artificial neural networks

(ANN) for combining attributes to delineate specific reservoir features (e.g. Meldahl et al., 2001). However, the ANN approach is not ideal for multi-attribute recognition in the seal context. This is mainly due to the limited diversity of training within the low amplitude/less variable textures of many seal units. Moreover, there is no direct measurement/hard conditioning data for the seal risk and it is very tricky to resemble other measurements as output nodes in the ANN. Therefore, considering the seismic limitations of seal context, the seal quality component attributes are combined in an interactive manner according to physical reasoning regarding the fluid dynamics.

First of all, to define a platform for the SRF attribute, we propose a schematic matrix in Table 3.6 which represents a qualitative – and probabilistic - measure of seismic seal risk (hence flow property) in seal unit intervals in terms of three seal quality components. According to this table, the cap rock with high amplitude, verticality and chaoticness is considered as the riskiest seal and vice versa. Given the importance of the sandiness in the leakage process (as a conduit), the reflection strength received a stronger weight than the reflection dip and chaoticness.

Table 3.6: *The proposed schematic matrix of seismic seal risk in terms of three seal quality components*

Reflection strength	Reflection Dip	Reflection chaoticness	Seismic seal risk
High	High	High	1 (*Riskiest*)
High	High	Low	2
High	Low	High	3
High	Low	Low	4
Low	High	High	5
Low	High	Low	6
Low	Low	High	7
Low	Low	Low	8 (*Safest*)

As it is applied, the Seal Risk Factor (SRF) attribute is assumed to be a mathematical function of seal quality component attributes. Three component attributes contribute to the SRF attribute and the combination should meet the

qualitative measures given by the proposed seal risk matrix. The exact algebraic form (including type of functions, coefficients, etc.) is subjective and should be inferred by physical reasoning or seismic-to-well calibration. This could involve transformation of attributes and weighting factors. For example, we suggest applying exponential or power transformation on the reflection dip attributes to isolate the significant verticality events from a highly structured background. Thus we will examine different combination sets in pilot localities of seal unit 4, but select the attribute combination which also delivers the best distinction on the whole seal unit 4.

3.5.4 Step 4: Validation of estimated seismic seal risk

Since the Seal Risk Factor (SRF) attribute is calculated only from the seismic data, we need to understand the way in which it is related to the geology and whether it can be justified through a link to the logfacies within the seal sections. Typically, core and well test information are used for the validation of seismic attributes in the reservoir context, but they are very scarce in the seal unit intervals. However, in Chapter 2, we introduced an approach for recognition of fine-grained logfacies within uncored seal units. This recognition process was based on extrapolation of core-log interrelationships in cored reservoir interval to the uncored seal interval using index/probabilised self-organising maps. Here, we use the logfacies prediction results within seal intervals as a way of validating the SRF attribute. Therefore, the objective of this step is to investigate and quantify the relationship between the SRF attributes and logfacies frequencies within the studied seal unit. We performed the SRF validation process using logfacies recognition results of wells W31, W41 and W42.

As always, there is a resolution gap between seismic and log data so that an upscaling step is required for log data. Firstly, we converted the logfacies recognition results from depth to time according to available check-shot data. We then divided the whole recognition interval in each well into several sub-intervals where each sub-interval was limited to the two-way-travel times of its corresponding consecutive reflections (consecutive peak and trough). Block curves were finally created for the segmented logfacies results at a seismic observable scale (the pick-trough time interval scale: defined by successive picks and troughs along seismic amplitude

traces) by computing the average frequency (percentage) of each logfacies within the sub-intervals.

For the seismic data, we extracted and derived the same block curves for the SRF attribute along the well locations, at the pick-trough time interval scale (**c**). Having the seismic and log data at the same resolution and unit, we used multivariate statistics to carry out the validation studies for each well. We consider the seismic-derived SRF relevant to the geology providing that it can reflect the frequency variation of logfacies with different sealing quality. Thereby, we assumed the SRF attribute as a linear combination of different facies frequencies in each sub-interval and set the following system of equations for all the sub-intervals throughout seal unit 4 (and the analogue seal unit) in each well:

$$\mathbf{A}\,\mathbf{x} = \mathbf{W}\,\mathbf{c} \qquad \text{Equation 3.10}$$

where: **A**: seal logfacies frequencies – derived from logfacies recognition (predictor),

an n×m-matrix

x: seal logfacies coefficients (unknown), an m×1-column vector

W: an n×n-diagonal matrix where diagonal entries ($w_{i,i}$) are inverse of standard deviations of SRF attributes at the well locations (weighting factors)– derived from seismic

c: SRF attributes at the well locations (measurement/calibrator) – derived from seismic, an n×1-column vector

m and n are the number of seal logfacies and total number of sub-intervals (pick-trough time intervals) in all wells, respectively. The weight matrix is designed to reduce the effect of unstable SRF values which are potentially caused by poor seismic quality (lower S/N ratio). This system of linear equations can be solved through the common weighted least squares method and the r-squared (coefficient of determination) value of the estimated result is a good measure of the link between the seismic SRF and the geological facies variations within the seal unit.

3.6 Results

The five-step workflow was applied on regional seal unit 4 in West Africa case study. In total, 37 volumetric attributes were examined using various parameterisations in the Petrel (Table 3.5). The complex and signal processing attributes mainly involved either conditioning of data or characterising sandiness, while the stratigraphic method and structural method attributes were used to capture the chaoticness and verticality of the sediments.

3.6.1 Effective pre-conditioning seismic attributes

At the first step, 22 commonly used complex and signal processing attributes were tested on seal unit 4 (Table 3.4). Since the majority of operations algorithms were originally designed for well-resolved seismic images, few of them were effective at improving the signal/noise ratio in the fine-grained units. As a result, only five effective pre-conditioning attributes were identified for the seal unit 4 context (Table 3.7). This set of attributes include ones that either improved signal continuity in poorly resolved areas prior to automatic structural/stratigraphic attribute calculations, or conditioned the seismic image for log-seismic integration purpose for Chapter 4.

Table 3.7: *Effective complex and signal processing attributes for signal/noise ratio improvement within seal unit 4.*

Effective seal pre-conditioning attributes
Apparent Polarity,
Instantaneous Phase,
Cosine of Instantaneous Phase,
First Derivative,
Second Derivative

The performance of pre-conditioning attributes is illustrated with two examples. In Figure 3.12 the impact of Apparent Polarity is shown for seal unit 4 using two different computation window sizes: 3ms and 9ms. The Apparent Polarity section shows the continuity of reflections more clearly in the poorly resolved localities of seal unit 4. This effect can facilitate the extraction of structural and

stratigraphic attributes in relatively transparent zones. Although 9 and 33 ms are the default window sizes and typically used for reservoir studies on modern seismic data, the smaller window sizes (i.e. 3 ms) detected weaker continuous reflections within the seal interval. This is mainly due to the relatively rapid changes of subtle competent/incompetent layering in the fine-grained deposits, hence resulting in more vertical polarity variations versus time (Robertson and Nogami, 1984).

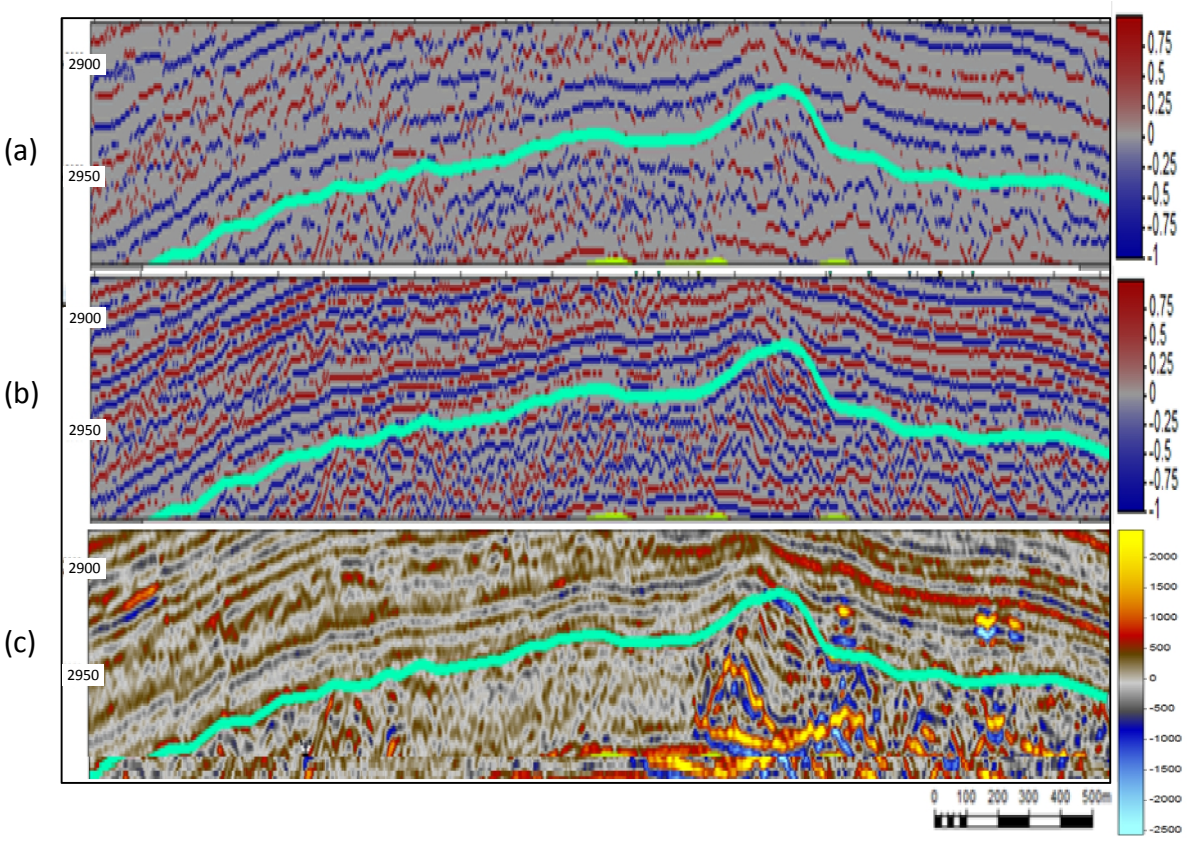

Figure 3.12: *Apparent Polarity effect on the seismic amplitude continuity within seal unit 4 using window sizes of (a) 9ms (software default setting for reservoir studies) and (b) 3ms. Smaller size window gives more realistic result due to the variable and thinner nature of layering at mud-rich sequences thus relatively more rapid vertical polarity changes. (c) Original amplitude section. The cyan interpretation line separates the two main seismic facies: hemipelagite 4 (upper) and MTD 4 (lower).*

Another successful example of pre-conditioning of the seal seismic image is illustrated in Figure 3.13 where we applied the First Derivative attribute on seal unit 4. This is partly a 90 degree phase rotation which makes a zero-phase cube more closely resemble lithological variations. Since the SRF attribute is going to be tied to the lithological data (seal logfacies) in the last step of the workflow, it is recommended to operate this attribute standalone or immediately after the Apparent

Polarity to achieve a more reliable log-seismic integration. In addition to its main application, the First Derivative attribute also sharpens amplitudes and reduces the thickness of reflections. Although this is considered as a drawback in reservoir fluid and thickness analysis, it was advantageous in the poor amplitude seal unit 4 as it more clearly resolved the weak reflections, particularly in hemipelagite 4 facies.

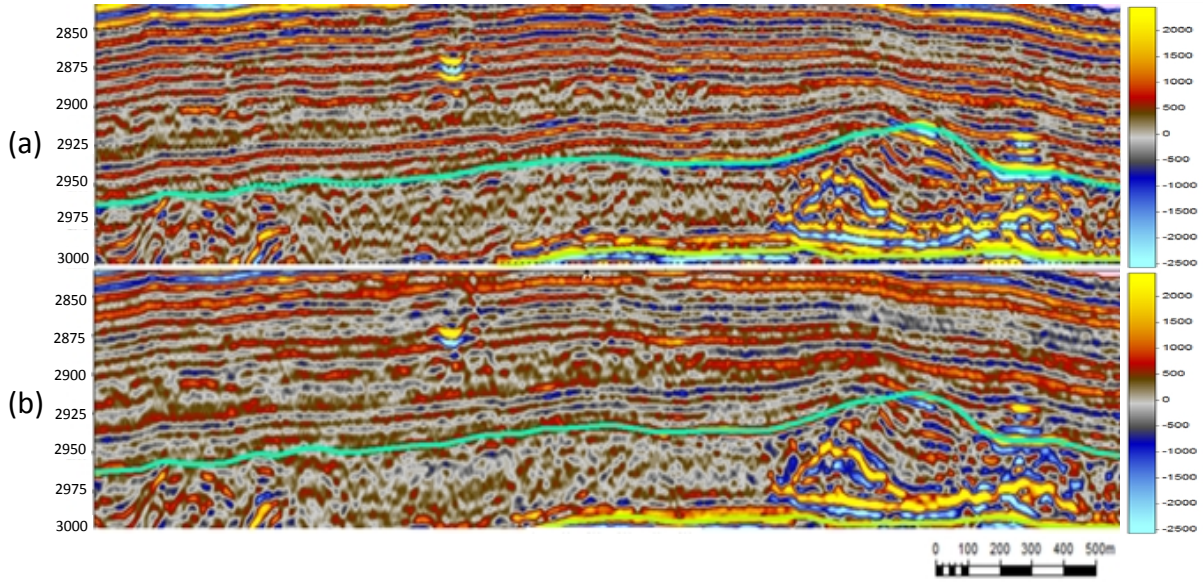

Figure 3.13: *Application of the First Derivative attribute on the original real traces within seal unit 4. (a) First Derivative of the original real traces. This is a direct mathematical operation and does not require a specific computation window size setting. This operation is practical for resolving weak reflections, particularly in hemipelagite seismic facies and also facilitating the log-seismic integration. (b) Original amplitude section. The cyan interpretation line separates the two main seismic facies: hemipelagite 4 (upper) and MTD 4 (lower).*

3.6.2 Effective seal quality/leakage component attributes

Upon completion of pre-conditioning of the seismic input, we performed a sensitivity analysis of the commonly used volumetric attributes with respect to the proposed seal quality components. This is the main and most time-consuming part of the seal risk assessment workflow. 37 attributes were evaluated through an intensive sensitivity analysis process. This included nine complex attributes, twelve signal processing attributes, eight stratigraphic method attributes and eight structural method attributes (Table 3.5). As expected, most attributes were ineffective in capturing the seal texture characters in these low amplitude contexts. This was mainly caused by the instability of volumetric attributes in the presence of noise or the low signal content in seal environments. For example, Instantaneous Frequency,

which is an important attribute for attenuation analysis or mapping in poorly resolved areas, tended to be very unstable in seal unit 4. It could hardly relate to the seal seismic texture, particularly when large Hilbert filter window sizes (> 7 samples) were used (Figure 3.14). Similarly, conventional Relative Acoustic Impedance and Dip Deviation attributes showed significant sensitivity to the low amplitude content in seal unit 4. Relative Acoustic Impedance attribute in seal unit 4 was adversely influenced by the existence of larger (apparent) acoustic impedance contrasts in the overlying channel reservoirs (and replicated their geometry pattern within the seal unit section) (Figure 3.15a). On the other hand, Dip Deviation attribute was incapable of capturing the major dipping events in MTD 4 and acted more as an edge detector indicating the areas with poor and chaotic reflections (Figure 3.15b).

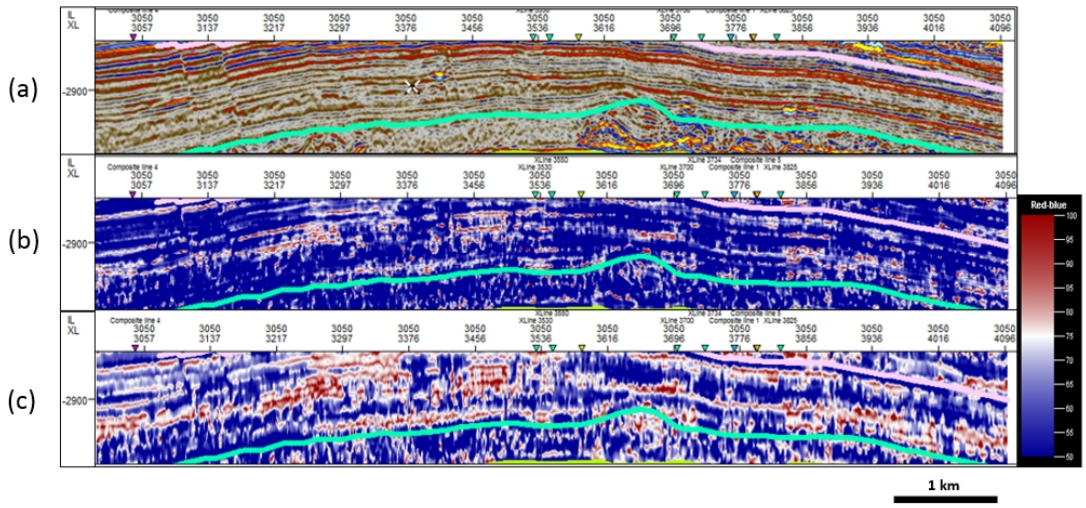

Figure 3.14: *Instantaneous Frequency attributes calculated in seal unit 4 with Hilbert filter window sizes of (b) 3 samples (c) 11 samples. The red and blue colours indicate areas with high and low Instantaneous Frequencies. The calculated Instantaneous Frequencies do not show correspondence with the seal seismic texture in the original amplitude section (a). The pink, cyan and green interpretation lines are top hemipelagite 4, top MTD 4 and bottom MTD 4, respectively.*

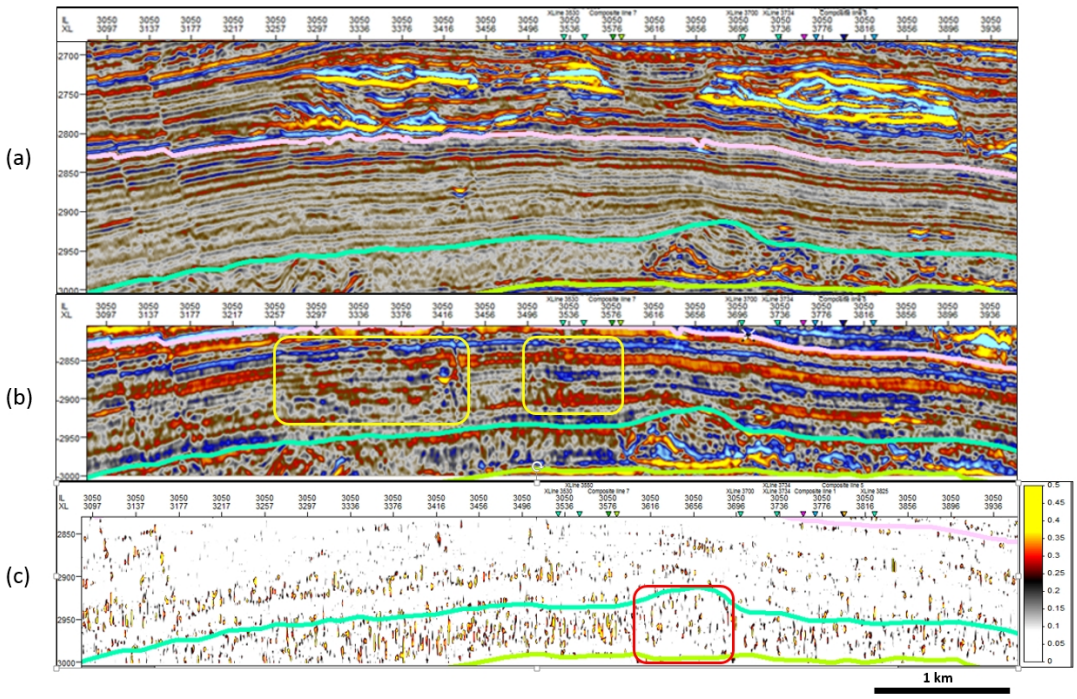

Figure 3.15: *Two examples for ineffective volumetric attributes (in detecting seal quality components): (a) original amplitude section. (b) Relative Acoustic Impedance attribute: The yellow boxes delineate the areas which Relative Acoustic Impedance attribute in seal unit 4 interval have been affected by the presence of the overlying reservoir channels. (c) Dip Deviation attribute (threshold angle=0): The area, which major dipping reflections in MTD 4 are not captured, is indicated with the red box. The pink, cyan and green interpretation lines are top hemipelagite 4, top MTD 4 and bottom MTD 4, respectively.*

Despite this, there were ten attributes which were less influenced by the low signal/noise ratio and were still successful in detection of the seal components. These identified effective attributes are summarised in Table 3.8 according to the extent to which they captured the seal quality components. The characterisation efficiency scales are qualitative measures and were derived by visual investigation of the best performance of each attribute. Although there are a few attributes which can be used to detect reflection strength and chaoticness components, there is only one attribute which successfully captured reflection dip in the seal context. This results from the instantaneous nature of dip attributes which are created for and commonly used in reservoirs. The outputs of such attributes (e.g. dip deviation (Figure 3.15b)) were usually hard to interpret in the seal units and involved a significant amount of pseudo-dipping events caused by noise. On the other hand, it was only the Local Structural Dip with PCA calculations which fits with the low signal content and benefits from covariance analysis of neighbouring traces and samples to reduce the noise effects.

Since we intended to combine the effective attributes and introduce the Seal Risk Factor (SRF) attribute according to Table 3.6, we thus reformed the Table 3.8 into Table 3.9 where each seal quality component is assigned with its most effective volumetric attributes (i.e. with good characterisation efficiency (G)).

Table 3.8: *Summary of identified effective attributes for capturing seal quality components in seal unit 4. The colours represent a qualitative measure of their characterisation efficiency: Poor (*P*): pink, Moderate (*M*): orange and Good (*G*): green.*

Seal quality component attributes	Reflection strength	Reflection Dip	Reflection chaoticness
3D Curvature	P	M	G
Chaos	P	M	G
Envelope	G	P	P
Local Flatness	P	M	G
Local Structural Dip	P	G	M
Magnitude of Gradient	G	P	P
Reflection Intensity	G	P	P
RMS Amplitude	G	P	P
Sweetness	G	P	P
Variance	P	M	G

Table 3.9: *Seal quality components (geological/seismic) and their most effective volumetric attributes (derived from sensitivity analysis of volumetric attributes in seal unit 4)*

	Geological character	Seismic character	Volumetric attribute
Seal quality components	Sediment sandiness	Reflection strength	**Reflection Intensity,** Envelope, Sweetness, RMS Amplitude, Magnitude Of Gradient
	Sediment verticality	Reflection dip	**Local Structural Dip**
	Sediment chaoticness	Reflection Chaos	**Chaos,** Local Flatness, 3D Curvature, Variance (Edge Method)

As shown in Table 3.9, we arbitrarily selected one representative volumetric attribute for each seal quality component out of the attributes which displayed the best characterisation efficiency in seal unit 4. These three representative attributes are: Reflection Intensity (for reflection strength component), Chaos (for reflection chaoticness component) and Local Structural Dip (for reflection dip component). In Figures 3.16-3.21, we review the performance of the representative attributes for seal quality components detection in seal unit 4. Figures 3.16, 3.18 and 3.20 are attributes section views, whilst Figures 3.17, 3.19 and 3.21 are root mean square (RMS) slices of the attributes in hemipelagite 4 and MTD 4 intervals.

In Figure 3.16, the Reflection Intensity attribute clearly isolates the high amplitude features (potential coarser grained deposits) of seal unit 4 which could be potential conduits for fluid leakages through the seal. These features include the moderate amplitude part of MTD 4, local amplitude anomalies in hemipelagite 4 and the top transition zone with the overlying reservoir. Reflection Intensity was not affected by either the waveform or the low signal content in seal unit 4 and very few vertical artefacts were generated during the computation process. In addition, unlike the envelope and RMS Amplitude attributes, the Reflection Intensity had no adverse impact on the frequency contents and did not smooth the seal seismic image.

Similarly, Chaos and Local Structural Dip effectively delineated the distorted and dipping textures (Figures 3.18 and 3.20). Chaotic patterns were mainly detected in the MTD 4 interval; however hemipelagite 4 also showed considerably distorted patterns in the lower part. Chaotic reflections within the seal unit, and hence potential sediment deformation, are considered to decrease seal quality and increase the chance of fluid breakthrough (Praeg et al., 2014). A noteworthy fact is that Chaos is more sensitive to seismic quality (Iske and Randen, 2005) so that a continuous muddy sequence with poorly resolved seismic can be sometimes detected as heterogeneous sediments. This is usually the case in the seal units of the low-density seismic or at the marginal part of the high-density seismic (e.g. NE of case study A). Moreover, the application of Chaos has a by-product which is the detection of discontinuities and faults. Although faults are other potential leakage risk factors and essential to seal bypass analysis, this research work focuses on evaluating textural seal quality. Therefore, it is recommended to subtract the normalized output of an

edge method attribute (e.g. ant tracking) from the result of the Chaos attribute to achieve a better measure of textural seal quality.

The Local Structural Dip attribute was calculated by three methods with different resolutions (Section 3.5.2). The Event- and Gradient-based methods were more instantaneous and edge detectors, and did not realistically capture the dipping layers in seal unit 4 (Figure 3.20). The instantaneous dip detection is an inefficient technique in seal unit 4 where reflection continuity and signal content are relatively low. As a result, the Principal Component Analysis (PCA)-based method was selected for seal quality analysis which estimates the local using the gradient covariance matrix (Randen et al., 2000). Since dipping events are often associated with chaotic patterns in seal units, the Chaos and Local Structural Dip attributes display relatively similar results. However, there are strong differences between them where the organised dipping layers were detected. These are mainly located in the northern part of case study A within MTD 4 where the deposits are influenced by the adjacent active salt tectonics. Furthermore, the Local Structural Dip attribute has the same by-product as the Chaos attribute (i.e. discontinuities and faults), thus the same recommendation is advised to remove the effect of the detected discontinuities from the seal textural analysis.

In order to further illustrate the characterisation efficiency of the representative attributes, we extracted RMS slice maps. These were computed for the representative attributes within hemipelagite 4 and MTD 4 intervals (Figures 3.17, 3.19 and 3.21). The RMS maps are very robust and can present the lateral distribution and also the net effect of the seal quality attributes without the influence of random artefacts (generated during their computation process). Overall, as expected, hemipelagite 4 showed less sandy and a more continuous stratal reflections (Figures 3.17a, 3.19a and 3.21a). However there are still few areas with relatively high amplitude anomalies which may or may not be lower seal quality zones (particularly in the middle and NW part of case study A). The textural seal quality of these areas need to be verified against the well log and rock physics analysis. In contrast, MTD 4 displays much more laterally variable behaviour in reflection strength, chaoticness and dip (Figures 3.17b, 3.19b and 3.21b). MTD 4 contained wider ranges of Reflection Intensity, Chaos and Local Structural Dip values; thus it

requires careful attention on the net effect of the seal quality components at a specified XY location.

As mentioned earlier, fault detection is a by-product of the Chaos and Local Structural Dip attributes. The fault and discontinuity traces are clearly delineated in the hemipelagite 4 RMS maps (Figures 3.19a and 3.21a) while they are smeared by the chaotic patterns in MTD 4 (Figures 3.19b and 3.21b). Moreover, since Chaos is sensitive to noise, a locality with pseudo-chaotic patterns was detected in the NE part of case study A. This was primarily due to the lower fold of seismic and the very poor amplitude content of seal unit 4 at that margin.

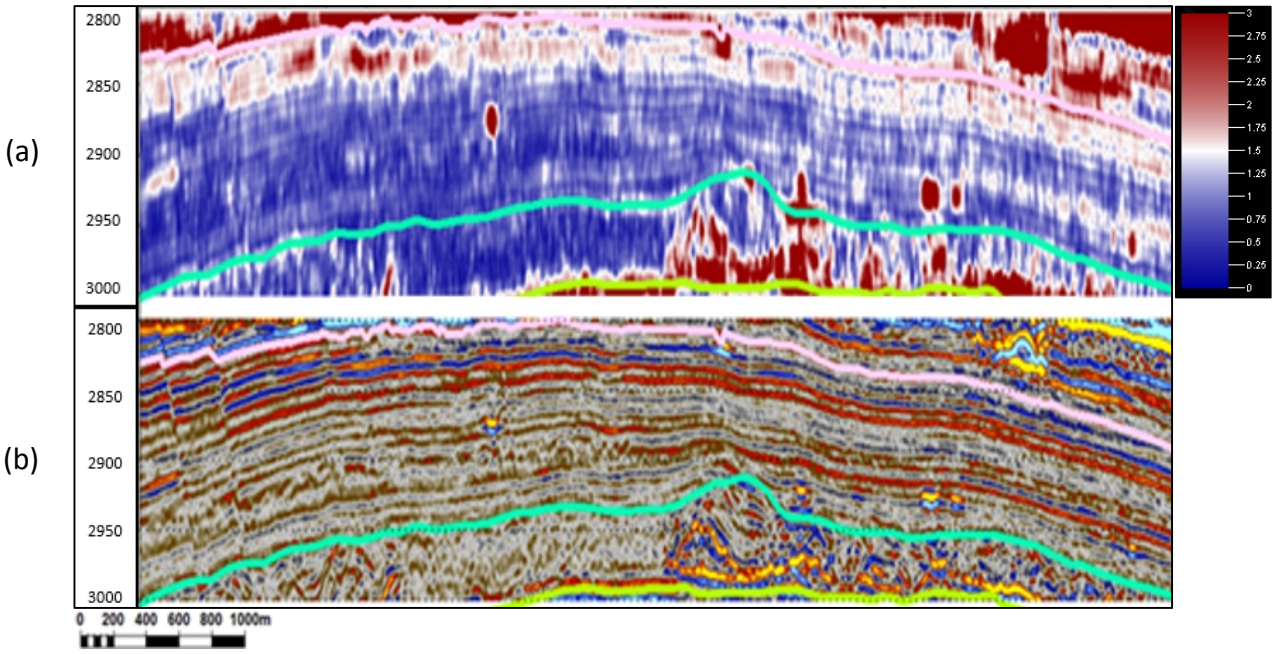

Figure 3.16: *Characterisation efficiency of Reflection Intensity for isolating the higher amplitude features (coarser-grained deposits) in seal unit 4. (a) Reflection Intensity attributes obtained by 3-sample computation. The red and blue colours indicate areas with high and low Reflection Intensity. (b) Original amplitude section. The pink, cyan and green interpretation lines are top hemipelagite 4, top MTD 4 and bottom MTD 4, respectively (The section line location is shown in seismic map views in Figure 3.17).*

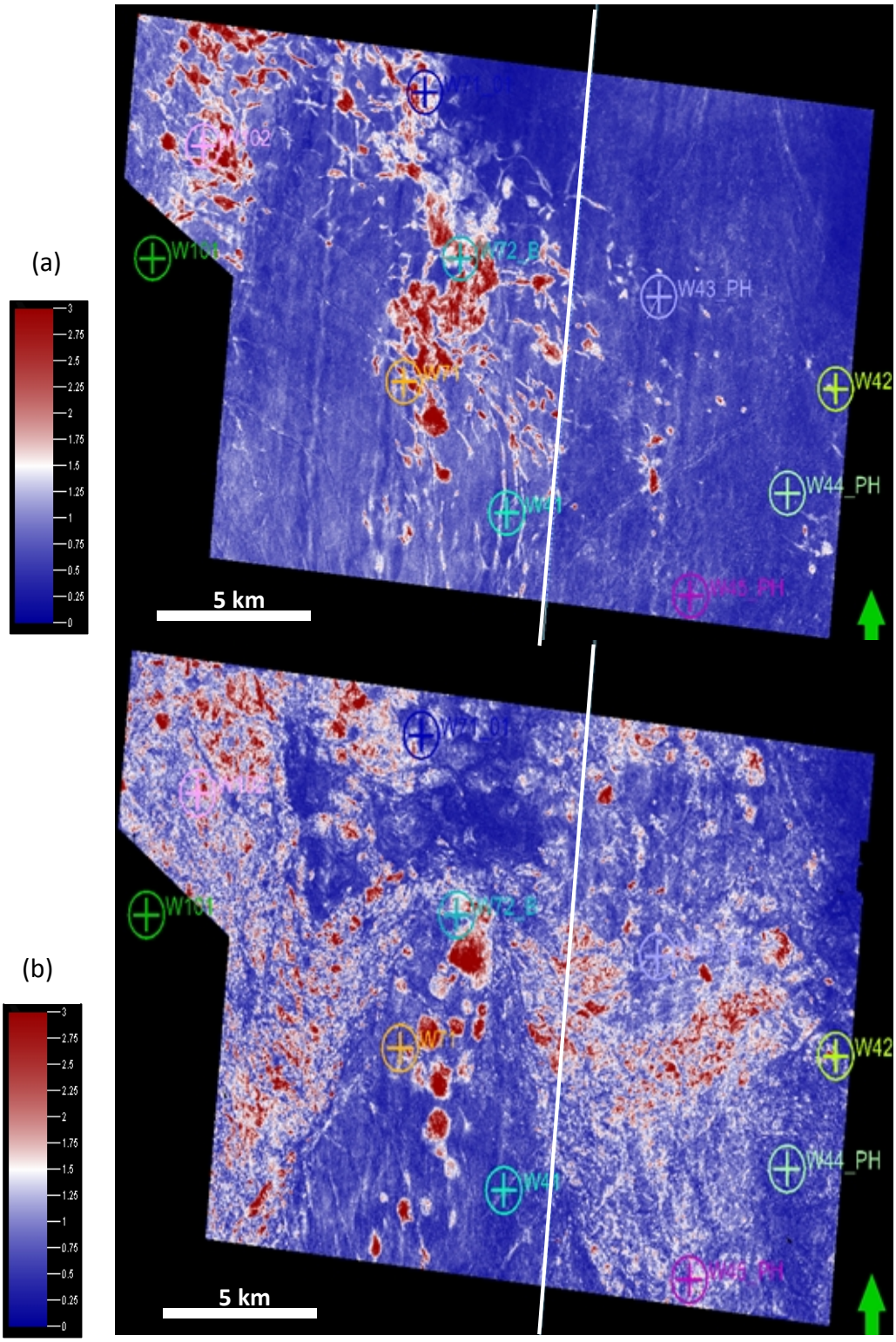

Figure 3.17: *Lateral distribution of the RMS value of the Reflection Intensity attribute in seal unit 4. (a) RMS of Reflection Intensity in hemipelagite 4. (b)RMS of Reflection Intensity in MTD 4 (Reflection Intensity attributes obtained by 3-sample computation). The red and blue colours indicate areas with high and low interval Reflection Intensity (The white line indicates the location of seismic section shown in Figure 3.16).*

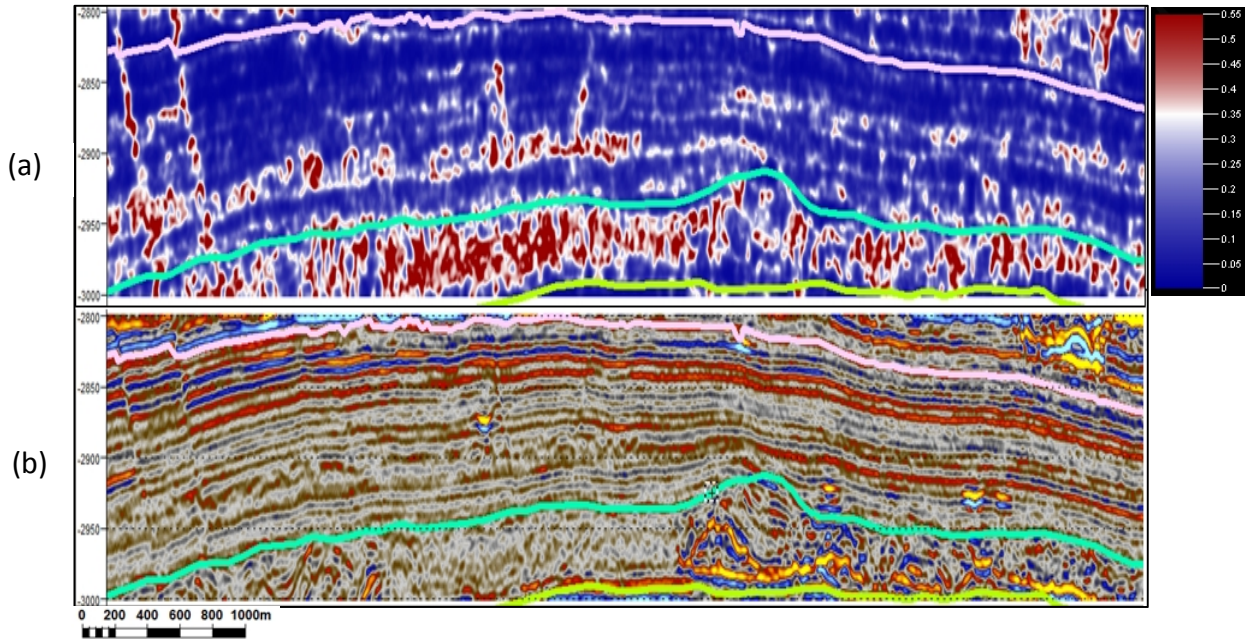

Figure 3.18: *Characterisation efficiency of the Chaos attribute for delineating the distorted reflection pattern (heterogeneous sediments) in seal unit 4. (a) Chaos attribute using a 3D computation window size of σ = 2. The red and blue colours represent the chaotic and organised reflections. (b) Original amplitude section. The pink, cyan and green interpretation lines are top hemipelagite 4, top MTD 4 and bottom MTD 4, respectively (The section line location is shown in seismic map views in Figure 3.19).*

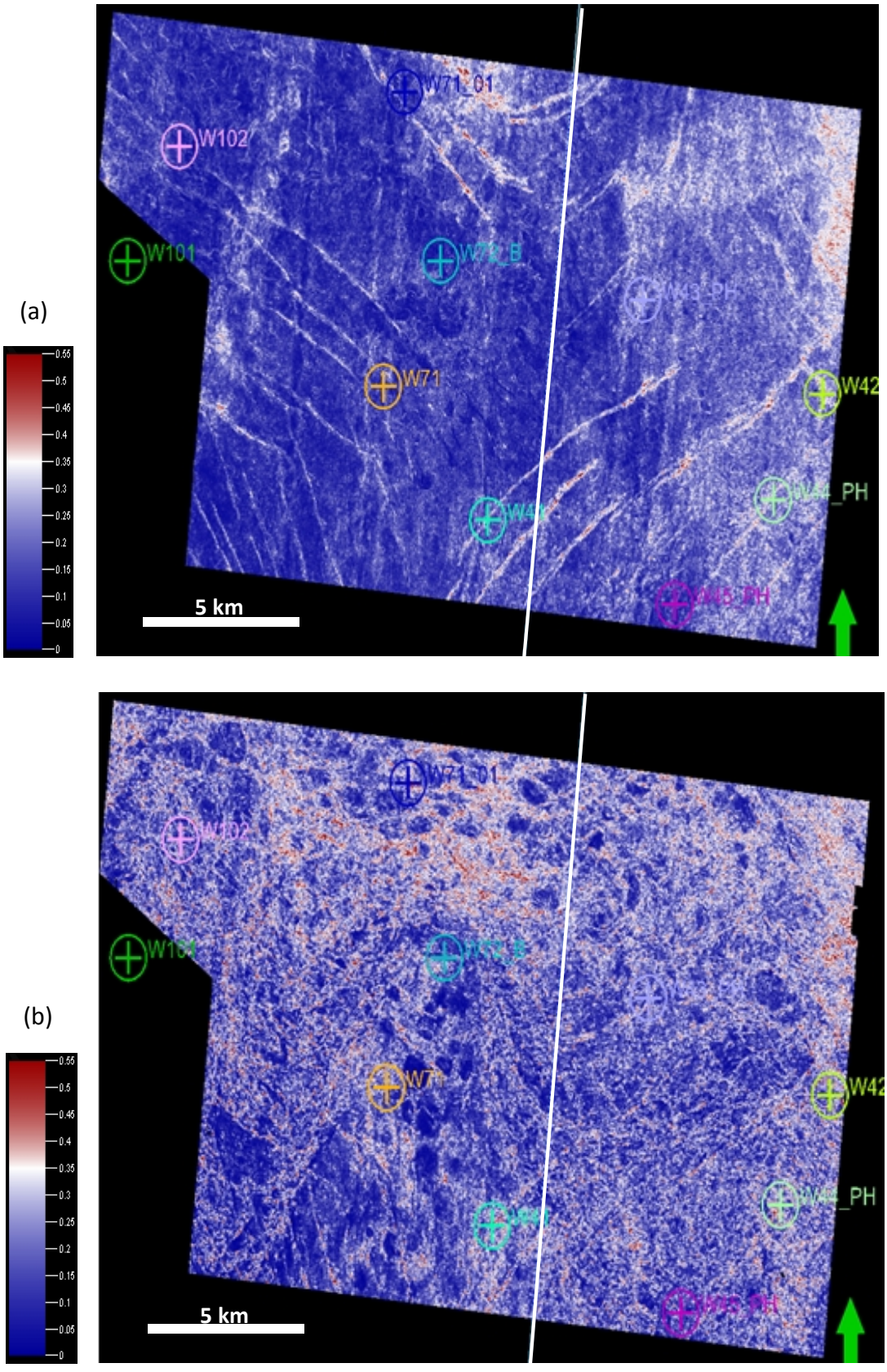

Figure 3.19: *Lateral distribution of the RMS value of the Chaos attribute in seal unit 4. (a) RMS of Chaos in hemipelagite 4. (b)RMS of Chaos in MTD 4 (3D window size used for Chaos computations: σ = 2). The red and blue colours represent the areas with net chaotic*

and organised reflectors in the given interval (The white line indicates the location of seismic section shown in Figure 3.18).

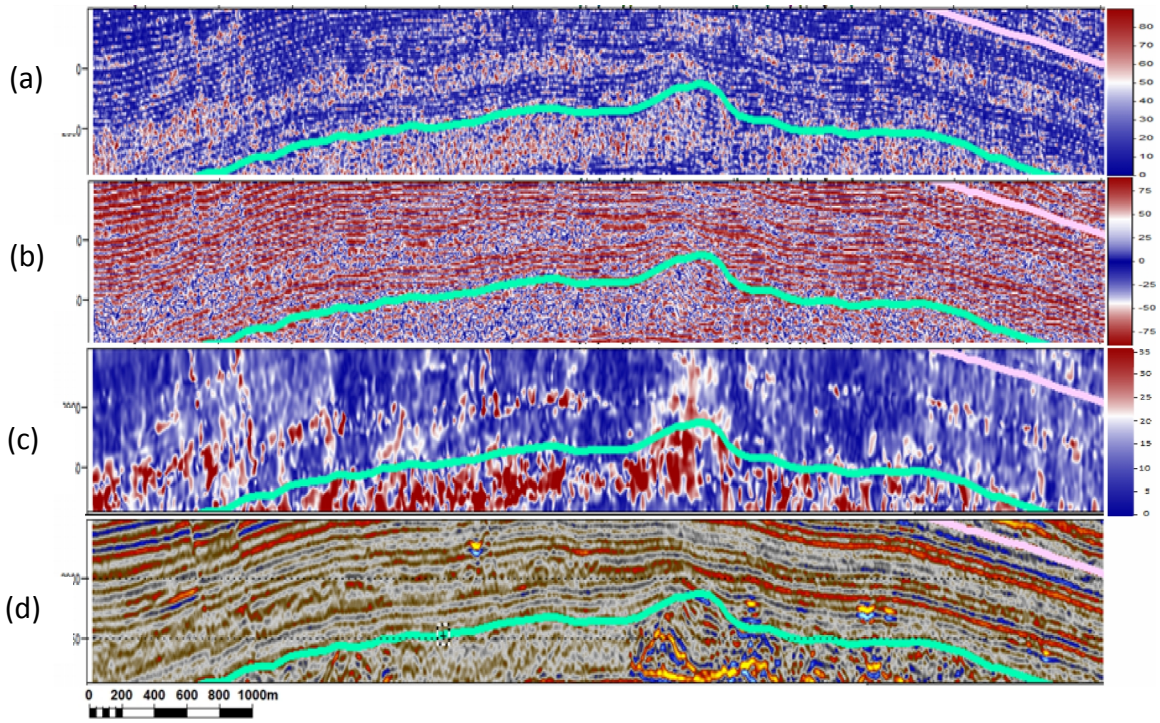

Figure 3.20: *Characterisation efficiency of Local Structural Dip attribute for delineating the dipping reflection events (sediment verticality) in seal unit 4 using three different methodologies: (a) Event-based method, (b)Gradient-based method (c) PCA-based method with 3D computation window size of σ = 2. The red and blue colours indicate the local, relative high and low dip events. (d) Original amplitude section. The cyan interpretation line separates the two main seismic facies: hemipelagite 4 (upper) and MTD 4 (lower) (The section line location is shown in seismic map views in Figure 3.21).*

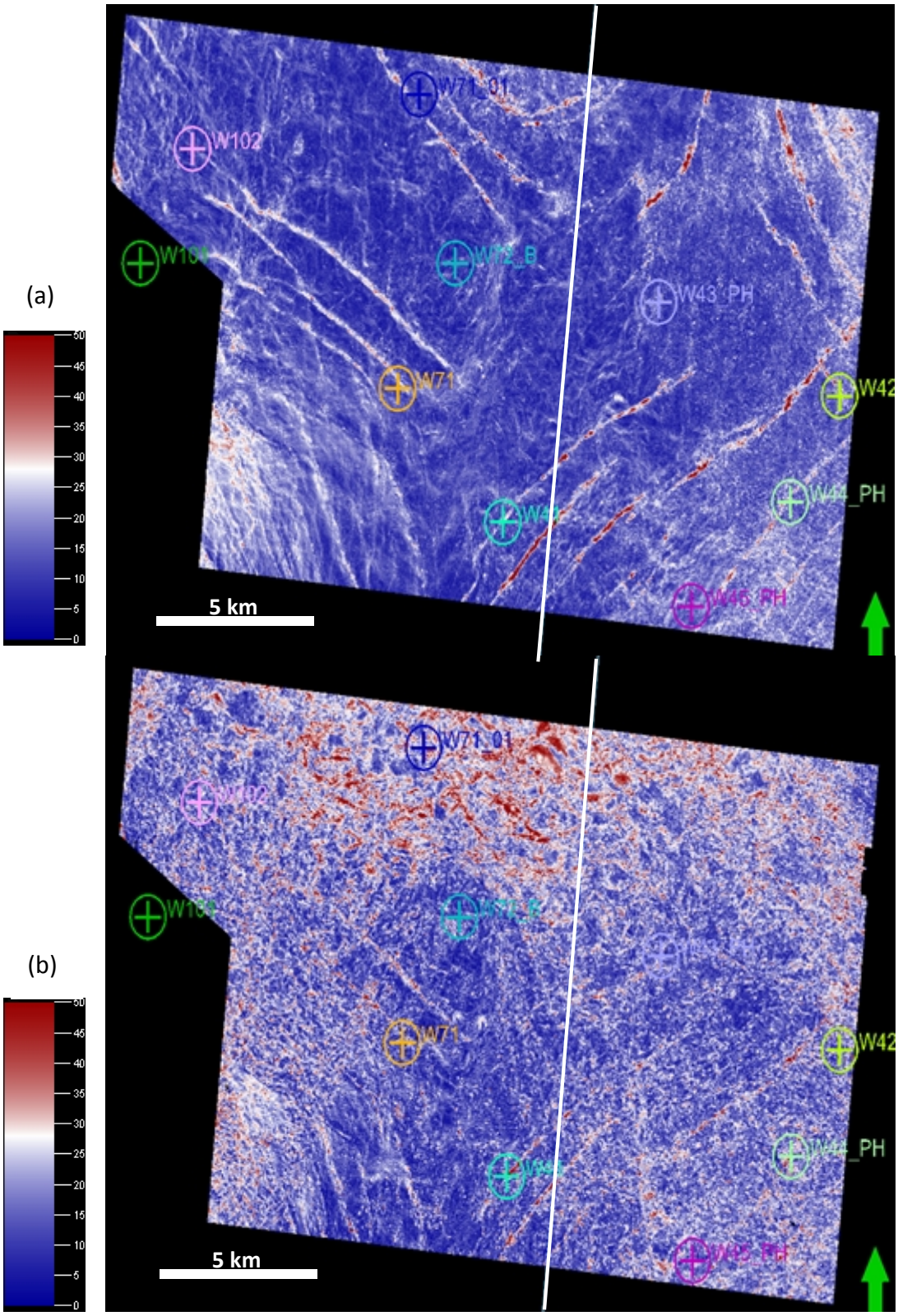

Figure 3.21: *Lateral distribution of the RMS value of the PCA-Local Structural Dip attribute in seal unit 4. (a) RMS of PCA-Local Structural Dip in hemipelagite 4. (b) RMS of PCA-Local Structural Dip in MTD 4 (3D window size used for Local Structural Dip computations: σ = 2). The red and blue colours indicate intervals with more local, relative*

high and low dip events (The white line indicates the location of seismic section shown in Figure 3.20).

To evaluate the reliability of volumetric attribute extraction and calibration in fine-grained seal sequences, the representative volumetric attributes were implemented on a conventional 3D seismic volume from offshore North Africa (provided by a sponsor of Caprocks project) (Figure 3.22). The geological setting here is a major North African deltaic deposit over Messinian salts with a background of Neogene gravity-driven deformation. The deposits mainly contain gas reserves. The North African seismic volume has lower quality in all acquisition and processing aspects compared to the HD3D volume of case study A (Table 3.10). In particular, it suffers from a considerable amount of acquisition footprints and from significant loss of high frequencies in fine-grained sediments in pre-Pliocene (Pliocene imaging was the primary objective of this survey).

Table 3.10: *Comparison of some acquisition and processing parameters of HD3D volume of case study A with the North African conventional 3D volume*

Parameters	HD3D volume (case study A)	Conventional 3D volume from offshore North Africa
Area	402 km^2	907 km^2
Nominal 3D trace density	1,382,400 traces/km^2	~ 48,000 traces/km^2
Time sampling	2 ms	4 ms
Bin size	6.25 m × 6.25 m	25 m × 25 m
Vertical resolution	5 - 10 m	25 – 40 m
Bandwidth at seal unit level	30 – 110 Hz	20 - 50 Hz
S/N ratio at seal unit level	7 - 9 dB	4 - 6 dB

Although the Reflection Intensity attribute displayed acceptable performance in outlining the high amplitude reflections with no further smoothing (Figure 3.22a), lower S/N ratio (hence losing the high frequency end of the spectrum) and acquisition footprints significantly limited the structural/stratigraphic understanding using Chaos and Local Structural Dip attributes. For example in Figure 3.22b, the majority of the poor amplitude fine-grained units were detected as chaotic zones whereas visual inspection of original seismic indicated they are mainly horizontally continuous reflections. The most realistic solution is the generation of a highly smoothed seal risk cube where the dip and chaoticness attributes are computed in a very large neighbourhood ($\sigma > 4$). However, this would be neither a reliable seal textural analysis due to the loss of detail, nor an interactive analysis since the PCA

computations for the large neighbourhood is very time-consuming (in this volume, each PCA-based Local Structural Dip or Chaos calculation with $\sigma = 5$ takes around three hours). As a result, the characterisation difficulty in the North African volume demonstrated the need for high-density seismic data to achieve a robust seismic textural analysis in poorly resolved fine-grained units. In other words, the high-density seismic data in low S/N ratio is required to preserve the high frequencies (by suppressing noise), recover folds and improve the spatial/temporal resolutions (e.g. Bing et al., 2011).

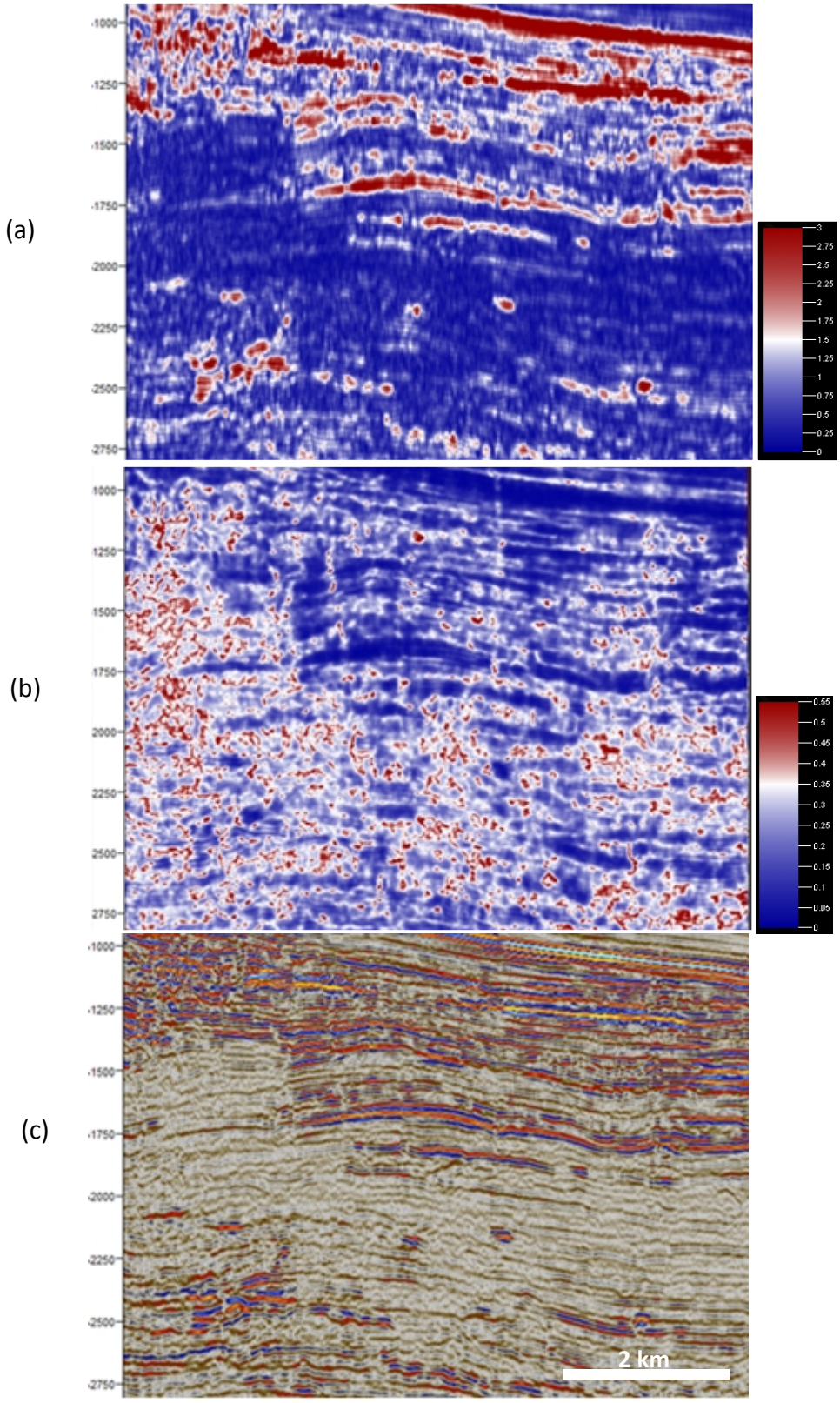

Figure 3.22: *Characterisation efficiency of Reflection Intensity and Chaos attributes in pre-Pliocene fine-grained units in the North African conventional 3D volume. (a) Reflection Intensity attribute was obtained using three-sample computations. The red and blue colours delineate local high and low amplitude events. (b) Chaos attribute was obtained using 3D computation window size of σ = 2. The red and blue colours are supposed to only represent*

local chaotic and organised reflectors. Visual inspection of the original amplitude volume shows that the Chaos attribute is unable to capture the realistic chaotic fine-grained textures in presence low S/N ratio. The detected chaotic textures are often mixed with continuous low amplitude reflections. (c) Original amplitude section.

3.6.3 Seal Risk Factor (SRF) attributes

In order to gain a comprehensive view on seal textural properties, it is necessary to take into account all the seal elements in the proposed texture model. Thus, we combined the effective seal quality component attributes and introduced new attributes which we name Seal Risk Factor (SRF) attributes. Our study focused on the interactive combination of component attributes which was followed by the logfacies validation analysis. Since the interactive combination of attributes is subjective to the geological setting, the following SRF attribute is proposed for seal unit 4:

$$SRF = \text{Reflection Intensity} \times (\text{Chaos} + \text{Dip}) \qquad \text{Equation 3.11}$$

For simplicity, in Equation 3.11, we use the representative attributes for each seal quality component; however, they can also be replaced by other effective attributes of the same seal quality component (i.e. Reflection Intensity can be replaced by Envelope, Sweetness, RMS Amplitude or Magnitude of Gradient attributes; similarly Chaos with Local Flatness, 3D Curvature or Variance). The proposed SRF is an appropriate combination for a seal sequence with a balanced combination of sediment layering, distortion and discontinuities. However, we suggest using a SRF combination with higher weight on dip attribute for a seal unit located in a highly structured context, dominated by the dipping and discontinuity events. Similarly, in the fracture-prone contexts, t* Attenuation attribute or other attributes helping with detecting open fractures can incorporate into the SRF combination. Although the SRF combination is dictated by the seal geological setting, all SRF attributes should follow the proposed schematic seal risk matrix (Table 3.6) and represent a measure of seal risk in terms of three or four components combined into logical, linear equations.

Reflection Intensity has positive values and can go over 100 depending on the amplitude while Chaos and dip values are limited to the range of 0-1 and 0-90°, respectively. Therefore, SRF have positive values with different ranges. Moreover,

the values are not directly comparable, unless they are normalised on the same seismic data.

The characterisation efficiency of SRF (Equation 3.11) has been fully investigated in seal unit 4 in case study A. According to the interrelationship of the SRF attribute with Reflection Intensity and how the other two seal quality components contribute, we can divide seal unit 4 into four seismic texture categories: (I) low Reflection Intensity (<2-3) associated with low chaoticness and verticality: potential continuous muddy strata; (II) moderate Reflection Intensity (3-5) associated with low chaoticness and verticality: potential continuous silt-rich strata; (III) moderate Reflection Intensity (3-5) associated with high chaoticness and verticality: potential distorted silt-rich strata and (IV) high Reflection Intensity (>5): potential sand-rich strata. At the lower range of the Reflection Intensities (<3), the three seal quality components show fairly similar behaviour. This means that low amplitudes are often associated with continuous horizontal reflections in seal unit 4, although we should also consider that the uncertainty in structural and stratigraphic understanding gets higher at very low amplitudes. The latter three seismic texture categories have higher Reflection Intensities (> 3) in which there are greater fluctuations in the SRF-Reflection Intensity relationship due to the independent variation of the chaoticness and dip attributes. This seismic textural categorisation of seal unit 4 is exemplified in the Figure 3.23 where we cross plot Reflection Intensity versus SRF attribute for a composite trace within the analogue seal unit 4 interval at well W31.

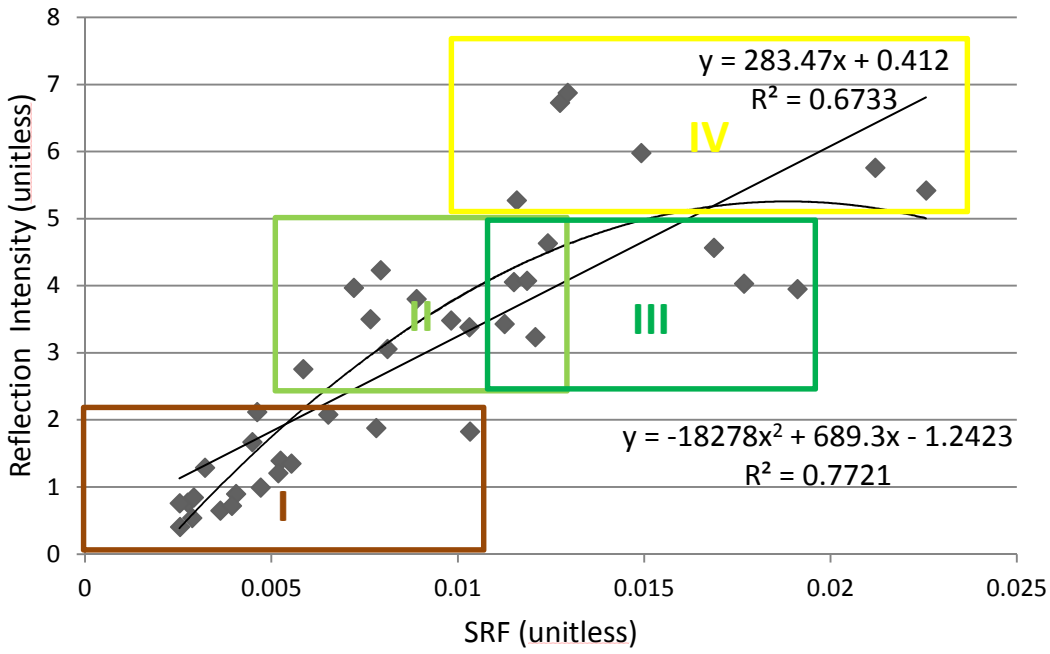

Figure 3.23: *Reflection Intensity and SRF interrelationship for a composite trace within the analogue seal unit 4 interval at well W31. Seal unit 4 can be divided here into four seismic textural categories: 1) low seismic intensity with low chaoticness and verticality (brown box) (ignoring the noise effect within transparent contexts), 2) moderate seismic intensity with low chaoticness and verticality (pale green box), 3) moderate seismic intensity with high chaoticness and verticality (dark green box), 4) high seismic intensity (yellow box).*

The characterisation efficiency of the SRF attribute in seal unit 4 is illustrated with seismic sections and RMS slices in Figures 3.24 and 3.25. In these figures, the red and blue colours represent the most and least local risky seal zones, respectively. The attribute combination process can also randomly boost noises/artefacts from component attributes (Figure 3.24). The red ovals delineate the genuine risky features (faults, dipping layers and build-up of risky textures) whereas the yellow ovals show the possible random noises boosted by attribute combination (here, the boosted random noises are from Local Structural Dip attribute). These boosted random noises can be distinguished by visual inspection of the SRF against the original amplitude and/or component attributes in the section view. This adverse effect is resolved in the RMS slices of SRF which illustrate the spatial distribution of the net effect of attribute in the interval of study (Figure 3.25). The areas detected as low risk (in blue) are considered potential good seal localities (at seismic-scale); however the delineated poor quality areas (in red) need further investigation, such as wellbore data integration, rock physics modelling and AVO analysis, to rule out the

effect(s) of fluid, overpressure or other lithological changes (e.g. carbonate intercalation). As expected, hemipelagite 4 shows better sealing quality (than MTD 4) with some risky anomalies which require more consideration for the exploration purposes (Figure 3.25a). These risky zones are mainly located at the central and NW part of case study A and have moderate amplitude textures with cluttered beddings. In contrast, MTD 4 generally displays the higher risk of leakage, thus in Figure 3.25b, the palette was stretched two times for a better visualisation of the lateral distributions of the SRF attribute. On the other hand, the detected seismic textures in MTD 4 have much more variability than in hemipelagite 4. These range from fairly homogenous transparent contexts (with even better sealing quality than the overlying hemipelagite 4) in the south and central part, to high amplitude distorted textures with lots of dipping events in the NW and NNW part of case study A (Figure 3.25b).

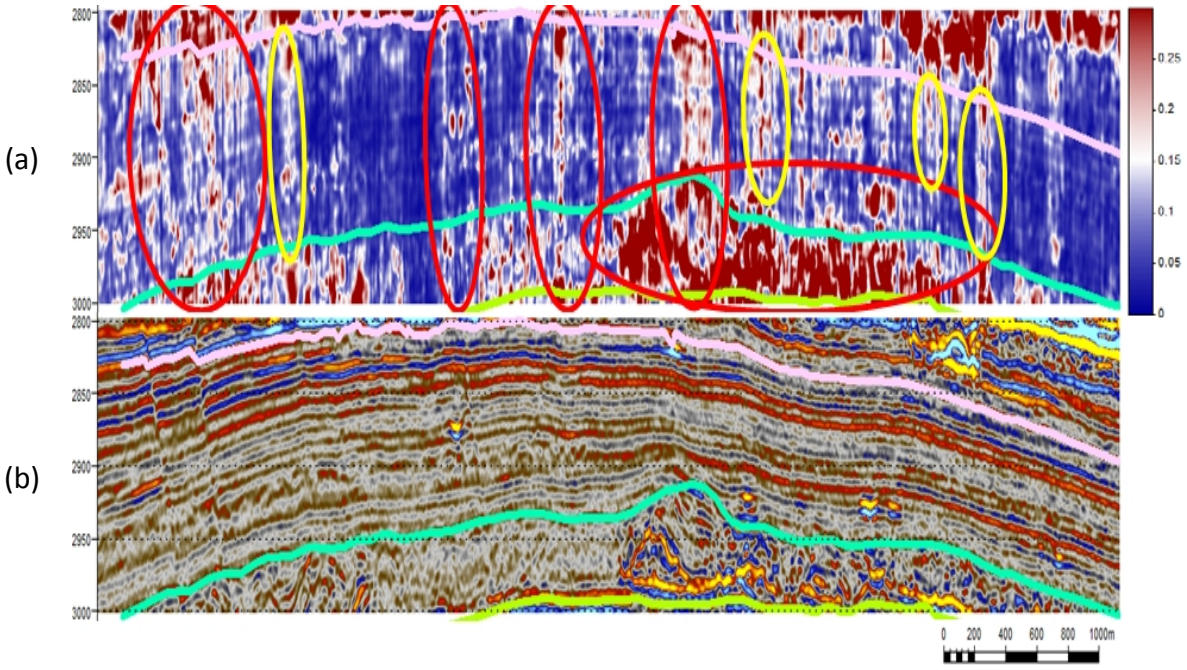

Figure 3.24: *SRF attribute performance in seal unit 4. (a) SRF attribute section. The red and blue colours indicate higher and lower seismic textural risks, respectively. The red ovals mark the genuine risky features related to faults, dipping layers or build-ups of risky textures, whereas the yellow ovals delineate the possible attribute combination artefacts (the boosted random noises from component attributes; they can be distinguished by visual inspection of the SRF against the original amplitude/component attributes). (b) Original amplitude section. The pink, cyan and green interpretation lines are top hemipelagite 4, top MTD 4 and bottom MTD 4, respectively (The section line location is shown in seismic map views in Figure 3.25).*

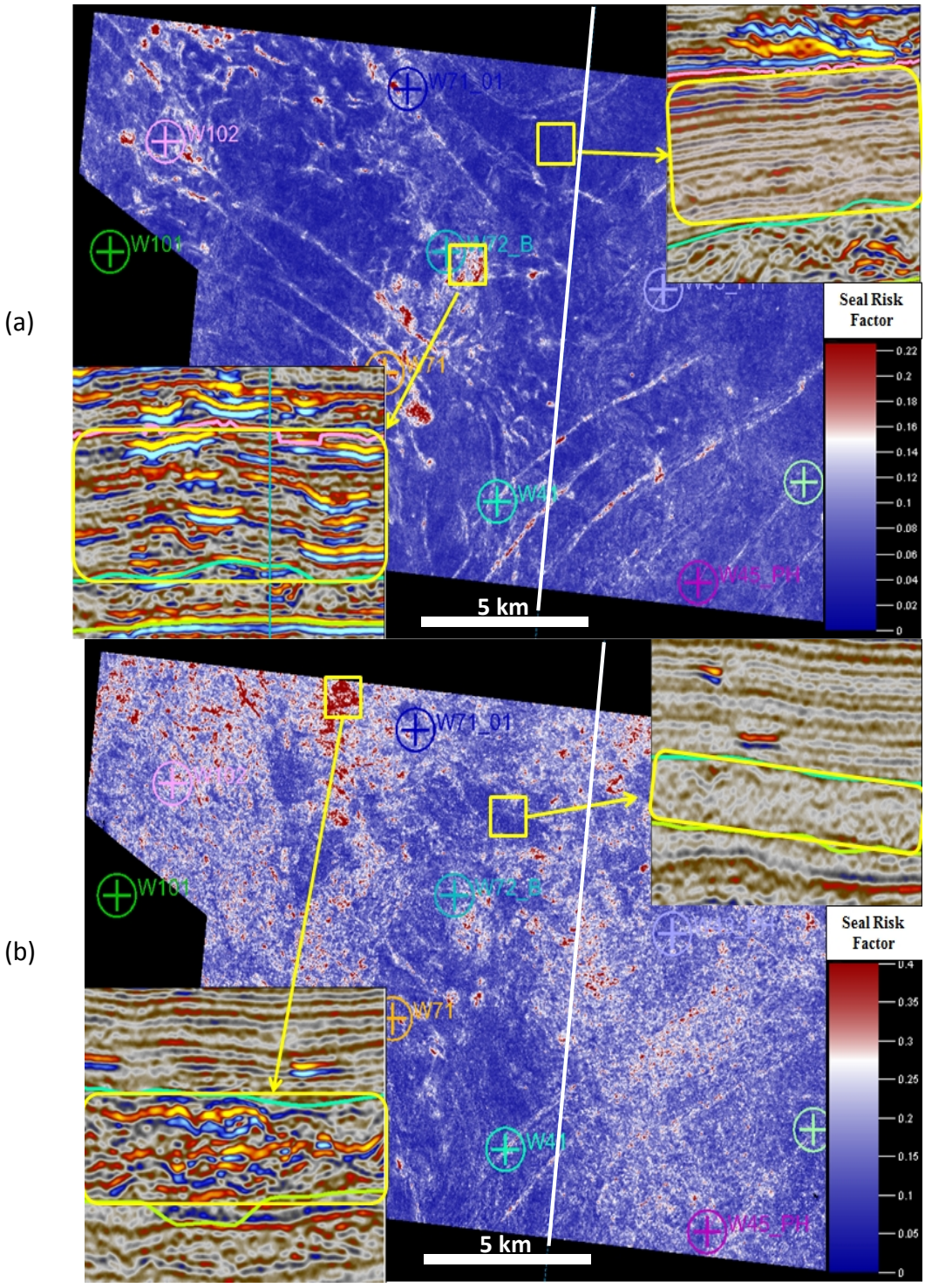

Figure 3.25: *SRF attribute performance in seal unit 4. The red and blue colours indicate higher and lower seismic textural risks, respectively. (a) RMS of SRF in hemipelagite 4 interval. (b) RMS of SRF in MTD 4 interval. The white line indicates the location of seismic section shown in Figure 3.24 (Remark: Due to the detected riskier nature of MTD 4, the colour palette is compressed in (b) for the better visualisation of lateral distributions of SRF attribute).*

3.6.4 Seal Risk Factor (SRF) attribute validation

At the end of the workflow, it is required to validate (based on lithology) the seismic-derived SRF attributes with the available geological information at the seal intervals. In case study A, there are 11 wells, of which five have core data in their reservoir intervals but none of which have core descriptions for the seal unit 4 interval. The only available geological datasets for the validation study were the seal logfacies recognition results derived in Chapter 2. The seal logfacies are considered here to be reliable extrapolations of the core descriptions in the reservoir to the uncored intervals within the seal unit 4. Although we recognised 16 lithological facies in Chapter 2 along the wells, only six facies are fine-grained and dominant in seal unit 4. These fine-grained facies are: "Hemipelagic Shales", "Mud Turbidites UP", "Mud Turbidites LP", "Muddy Debris Flow", "Muddy Sandy-Debris Flow" and "Sandy Debris Flow" facies. The other ten coarser-grained facies were regrouped as "Sands" facies. Moreover, we merged the "Muddy Sandy-Debris Flow" facies into the "Sandy Debris Flow" facies because we were unable to discriminate them in the seismic data. In summary, for achieving a realistic logfacies-seismic integration, the original 16 facies were regrouped into six facies, focusing on the fine-grained facies and the possibility of seismic separability. The facies regrouping is illustrated in Table 3.11, in which the new facies used for validation study are: Hemipelagic Shales, Mud Turbidites UP, Mud Turbidites LP, Muddy Debris Flow, Sandy Debris Flow and Sands facies.

Table 3.11: *Regrouping of the initial 16 fine-grained facies (interpreted by sedimentlogists/petrophysicists of the operating company – a sponsor of Caprocks project -; Insalaco et al., 2001; see Figure 2.2) into six facies, focusing on the fine-grained facies and the possibility of seismic separability. The regrouped facies are used for the SRF validation studies.*

Facies No.	Facies name	Used in validation study	Colour
1	Hemipelagic Shales	Hemipelagic Shales	
2	Mud Turbidites UP	Mud Turbidites UP	
3	Mud Turbidites LP	Mud Turbidites LP	
4	Cross Laminated Silts	Sands	
5	Graded Silts	Sands	
6	Cross Laminated Sands	Sands	
7	Graded Sands	Sands	

8	Massive m-f TB Sands	Sands	
9	Laminated m-f Sands	Sands	
10	Laminated C-Arac TB sands	Sands	
11	Laminated C-Arav sands	Sands	
12	Muddy Debris Flow	Muddy Debris Flow	
13	Muddy Sandy-Debris Flow	Sandy Debris Flow	
14	Sandy Debris Flow	Sandy Debris Flow	
15	Conglomerates	Sands	
16	Sand Injectites	Sands	

The SRF validation study was carried out in the seal unit 4 interval of wells W31 (analogue interval), W41 and W42 since these wells have the most reliable seismic data, log suites and facies recognition results. Furthermore, since the signal/noise ratio is higher in the seal risk cube than in the original seismic amplitude cube, log-seismic integration could proceed more easily. First, the percentages of facies in the seal interval of each well were calculated (Figure 3.26). Initial observations suggest a meaningful relation between the log-derived facies distributions and the average seismic-derived SRF in seal unit 4 (Table 3.12). Higher percentages of "Sands" and "Sandy Debris Flow" facies at well W31 correspond to the highest average SRF. In contrast, well W42, dominated by "Hemipelagic Shales" and "Mud Turbidites UP" facies has the lowest SRF. This promising qualitative correspondence prompted a more quantitative analysis. Therefore, according to the approach described in Section 3.5.4, a linear system of equations was used in order to estimate SRF from a combination of logfacies percentages in seal unit 4 at wells W31, W41 and W42. In this approach, independent, unknown, dependent and weighting variables correspond to the logfacies percentage matrix, logfacies coefficient vector, seismic-derived average SRF vector at well locations and standard deviation of seismic-derived SRF vector at well locations, respectively. As a multivariate analysis, the system of linear equations was solved by a weighted least squares method and Matlab coding. As a result, we obtained the coefficients of logfacies (Table 3.13) and computed the log-estimated SRF for the seal unit 4 interval of each well. Figure 3.27 illustrates the efficiency of this multivariate analysis in estimating seismic SRF by using combination of fine-grained facies percentages in seal unit 4. The overall estimates of SRF from logfacies were

acceptable. The log-estimated SRF tends to have the same general trend as the seismic-derived SRF, especially where there are major variations in the well W31. There are nevertheless mismatches where relatively small or spiky variations occur. These are inevitable because of data resolution difference and the range of parameters which affect both well and seismic records.

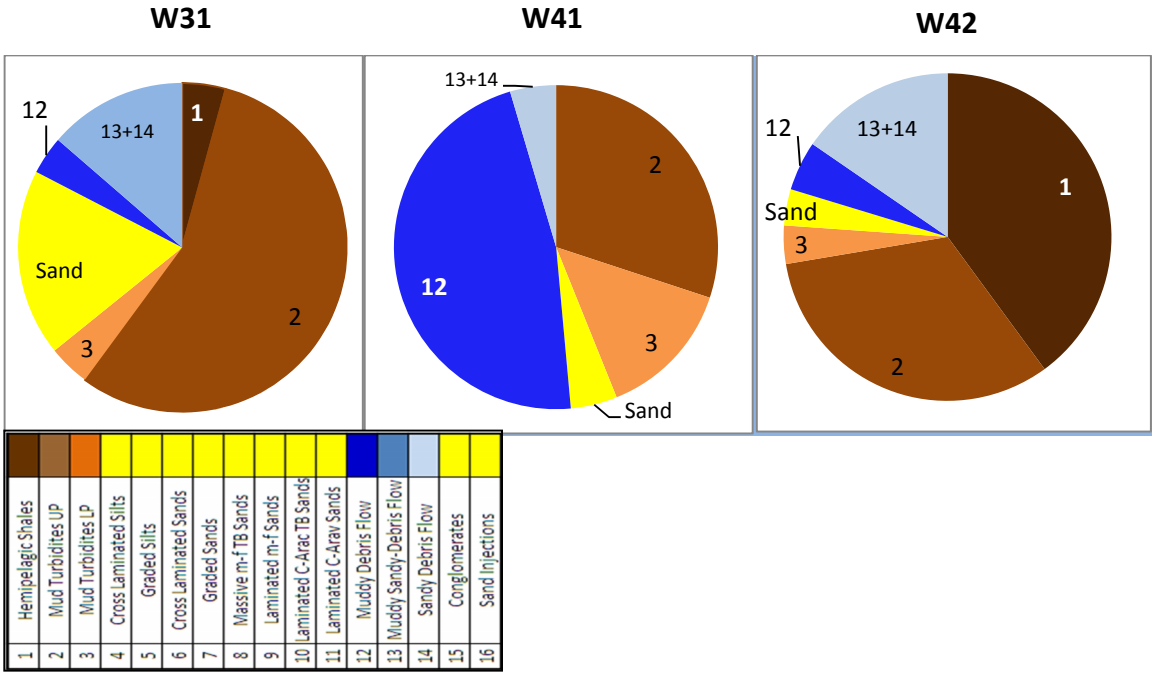

Figure 3.26: *Distribution of fine-grained facies percentages in seal unit 4 in wells W31, W41 and W42 (Note that well W31 does not cross seal unit 4 and an equivalent fine-grained depth-interval of well W31 is used as analogue for seal unit 4; see figure 2.11).*

Table 3.12: *Facies percentages in seal unit 4 of wells W31 (analogue interval), W41 and W42 and their corresponding average seismic SRF. The seismic SRF gradually decreases from W31 to W42 by decrease in Sands.*

Well	Facies1 %	Facies2 %	Facies3 %	Facies12 %	Facies13+14 %	Sands %	Seismic SRF
W31	4.3	55.8	4.1	3.8	13.7	18.4	0.0090
W41	0	30.1	13.8	46.9	4.6	4.6	0.0059
W42	39.9	32.5	3.8	4.9	15.4	3.6	0.0043

Table 3.13: *Facies coefficient matrix derived through weighted least squares solution of Equation 3.10. Multiplication of facies coefficient and facies percentage matrices gives us the log estimation of SRF attribute in seal unit 4 in the vicinity of wells W31 (analogue interval), W41 and W42.*

Facies1 Coefficient	Facies2 Coefficient	Facies3 Coefficient	Facies12 Coefficient	Facies13+14 Coefficient	Sands Coefficient
3.1693E-05	5.253E-05	0.000119916	3.86358E-05	5.13943E-05	0.000190272

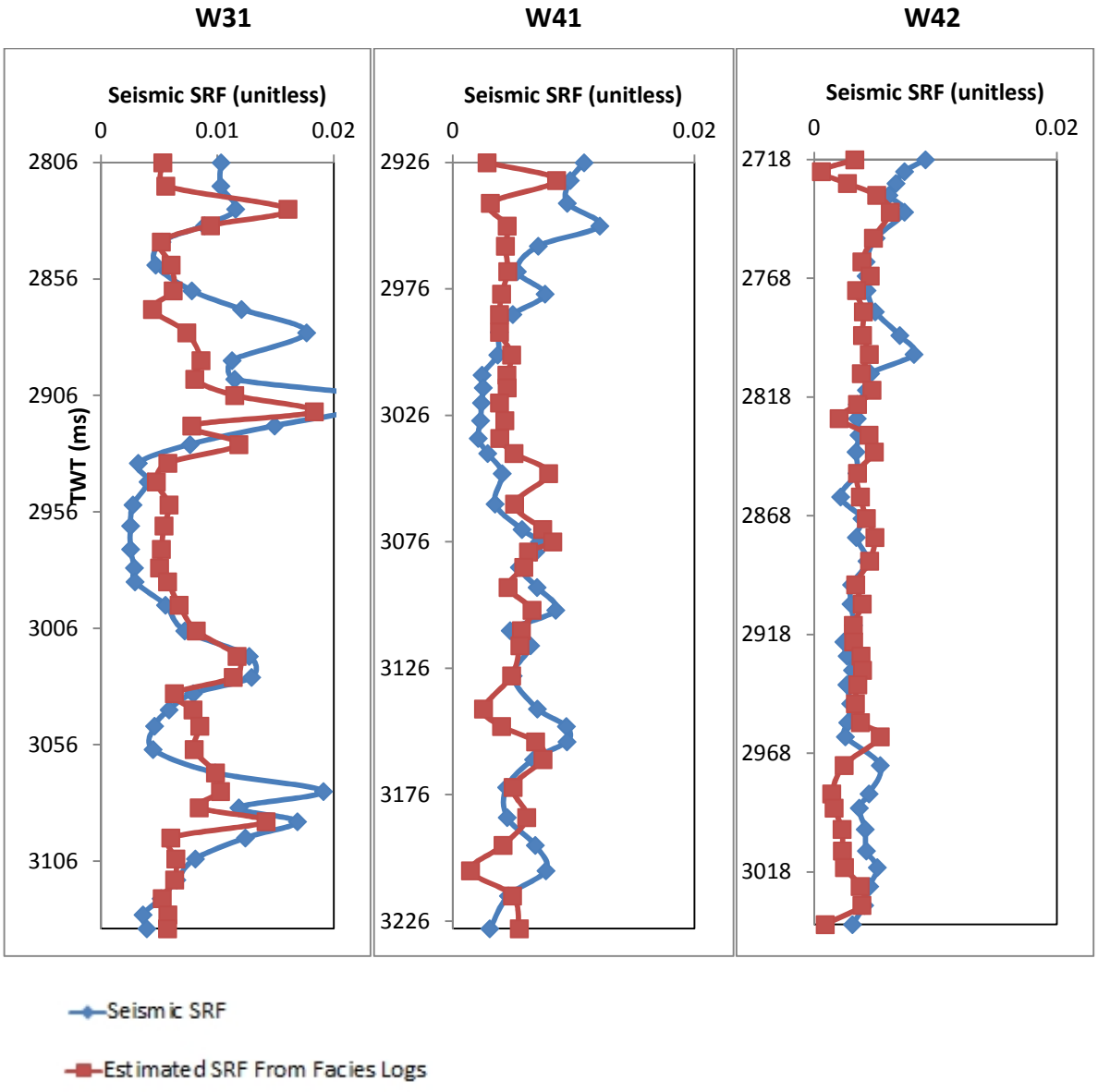

Figure 3.27: *Comparison of seismic SRF attribute and the log-estimated SRF in seal unit 4 of wells W31 (analogue interval), W41 and W42. The overall estimated pattern of the log-estimated SRF follows the seismic SRF. However, some subtle and spiky variations in the log-estimated SRF do not fit with seismic SRF (relative error of estimation for W31, W41 and W42 = 35.5 %, 39.8% and 35.2 %).*

At the end of the validation study, we conclude that the seismically-derived SRF shows a reasonable correspondence to the lithology trends within seal unit 4. High seismic SRFs are often a good approximation for volumes containing a higher percentage of coarser-grained and distorted sediments (riskier facies), and vice versa. In addition, SRF calibration helped us to find the seismic observable grouping of the fine-grained facies and also to calculate proxies for the seismic textural seal risk at the well locations based on logfacies data (i.e. without running into the cumbersome processes of volumetric attributes computation). In the next chapter, we aim to translate the seal risk cube into probabilistic seal litho-cubes.

3.7 Discussion

The textural analysis of reservoir units using seismic attributes is widely discussed in the literature. It includes multi-attribute techniques (Russell et al., 1997) and statistical measures (Vinther et al., 1995; Vinther, 1997; Whitehead et al., 1999; West et al., 2002; Gao, 2003, 2004). These methods have continuously improved their structural/stratigraphic characterisation efficiency by applying advanced techniques such as Principal Component Analysis (Randen et al., 2000; Iske and Randen, 2005). In contrast, there has been limited research on textural analysis for seal characterisation, even though seismic understanding of flow properties in seal units can help with reducing the drilling risk and refining the basin-scale flow simulation. Seal characterisation from seismic data is especially important because log and core data are usually not available within seal intervals. To date, the research in mud-rich context has often been limited to qualitative seismic facies analysis (e.g. Droz et al., 2003; Power et al., 2014), bypass detection (e.g. Meldahl et al., 2001; Tingdahl et al., 2001; Cartwright et al., 2007; Løseth et al., 2009) or semi-quantitative classification at the geobody scale (e.g. Corradi et al., 2009). In this study, we introduced the first quantitative approach for an automated 3D seal textural risk assessment using volumetric attributes. The targets, seismic context, parametrisation and functionality of the attributes in this study are different from the reservoir context, and it is difficult to compare the seal texture results with current literature on reservoir texture analysis, focused on delineating the distribution and connectivity of reservoir pay zones (Carrillat, et al., 2002; Gao, 2007, 2008; de Matos et al., 2011).

The study highlighted the important role of pre-conditioning and post-conditioning of the seismic for increasing the characterisation efficiency of volumetric attributes in seal units. Moreover, primary sensitivity analysis showed most of the commonly used attributes in reservoirs (e.g. Instantaneous Frequency, Dip Deviation, Relative Acoustic Impedance) were inefficient in the seal context, mainly because of their sensitivity to low signal:noise. Consequently, a robust seismic seal characterisation cannot be achieved only by data-driven information, and the interpretation knowledge should contribute to the analysis. Therefore, we interactively combined the seal quality component attributes according to a qualitative seal risk matrix (derived from physical reasoning of leakage probability), and the geological setting. Moreover, the ANN techniques for attribute combination (e.g. Meldahl et al., 2001) have insufficient training sets in the relatively homogeneous seal units (relative to reservoirs).

The proposed approach has a few limitations. Firstly, the calculation of structural and stratigraphic attributes in seal units is very sensitive to signal/noise ratio; they can be more reliably computed on seismic volumes acquired with short shot intervals e.g. high-density seismic data (see Section 3.4). There is no single rule regarding the acceptance criteria for the seismic data; however, we should avoid interpreting these attributes in the marginal part of the cubes, fault shadow zones, around intrusions, gas pockets, etc. Secondly, we cannot directly apply the SRF attribute to the whole seismic cube in one go to investigate the seal textural capacity of all the sequences and to automatically indicate fluid barriers and carriers in the basin. This is because the attributes such as Reflection Intensity and t* Attenuation have depth dependency. In addition to faults and MTDs, deformed channel infills and borders, fluid effects and diagenetic events may also share high chaoticness and dip values. Therefore, dealing with the whole seismic volume needs more consideration. For instance, the high reflectivity of shallow seal units can be adjusted using the shale/sand compaction trend and the sandiness-reflection strength relationship. Moreover, in more complex circumstances, the neural network approach would bring in better attribute combinations because of the variety of seismic textures available for the training. Finally, in the seal texture scheme we assumed a direct link between the geological and seismic characters. This

assumption is thus not valid for the cases of having processing artefacts (e.g. tuning effects, velocity pitfalls, etc.) or fluid effects.

In this study, we also demonstrated the geological dependency of the seismic-derived textural risk using seal logfacies recognitions derived in the Chapter 2. Although subtle logfacies variations did not fit the SRF attribute trend in wells W31, W41 and W42, we found a meaningful link between the logfacies and the seismic texture tendencies; commonly, an increase in the Sands and Sandy Debris Flow facies occurred with high SRF attribute values, and vice versa.

This study was only provided with post-stack time-migrated (PSTM) datasets. So it is recommended also to apply the developed approach on pre-stack or depth-migrated (PSDM) seismic data where a stronger seismic – geology link is promising. For instance, in PSTM seismic, reflection dip angles are apparent and may not be related to geology, which is not the case with PSDM seismic (providing the migration-velocity model honours the subsurface structure). Seal texture characterisation using attributes is currently at the early stage and further studies are essential to reduce the uncertainty of the analysis. We envisage the future work in seal (seismic) texture characterisation on the three following aspects:

1) Signal processing in low amplitude/low signal:noise contexts:

- Thin bed spectral inversion (e.g. Marfurt and Kirlin, 2001; Chopra et al., 2006): to remove the tuning effect in poorly resolved thin-bedded seal units, particularly in hemipelagite seismic facies

- broadband processing techniques (e.g. Zhou et al., 2012): to normalise the spectrum, increase S/N ratio and boost high frequencies to improve our understanding from internal architectures of fine-grained sediments in low S/N ratio areas of a HD3D volume

2) Faults and discontinuities detection in the seal units:

Faults and discontinuities play an important role in hydrocarbon migration. They were partially detected by the chaoticness and verticality component attributes. Since their effect is of higher order in the three seal (textural) quality components, it is better to remove their effect from the seal textural

risk cube and analyse them separately. This can be done through building a normalised bypass cube of seal unit using appropriate edge methods (e.g. ant tracking (Cox and Seitz, 2007; Kolisnyk et al., 2013) and subtract it from a normalised seal textural risk cube. The next question would be the degree of transmissibility of the faults and discontinuities!

3) Open fractures/fluid in the seal units:

Given the importance of the open fractures in sealing capability, an auxiliary attribute can be introduced into the seal quality scheme. This is t* Attenuation attribute which is responsible for the differential loss of high frequencies relative to low frequencies as measured above and below the point of interest. It can be used to identify open fracture zones and fluid movements (Boadu and Long, 1996; Batzle et al., 2006). On the other hand, individual interpretation of t* Attenuation has commonly high uncertainty due to high frequency loss in steep dips and migrated faults (Gardner, 1985). It usually has to be integrated with a proper azimuthal anisotropy studies provided by the wide azimuth dataset (WAZ). In the PSTM cube of case study A, we briefly analysed the t* Attenuation and Local Structural Azimuth attributes. The early observations indicated a series of ambiguous anomalies around the faults in seal unit 4 in the west of case study A, which may be related to open fractures and the reason to have two connected pay zones. However, to establish a valid link between anomalies and open fractures we require further scrutiny including studying dip-meter data and AVO cross-plots.

3.8 Conclusions

This study has contributed to a better understanding of mud-rich sediment sequences at the seismic scale and has introduced the first quantitative assessment of seal risk and internal texture based at the seismic scale. We demonstrated the notable capability of the volumetric attributes in texture detection and signal conditioning of the seal units. We showed that the single attributes are not enough capable to capture a comprehensive seismic perspective of the seal quality. Thus the proposed multiple attribute approach significantly increased the seal texture characterisation by taking into account all the leakage important factors. The detected areas as good seal quality

were considered potential well-sealed localities; however the delineated poor quality areas were required further investigations such as wellbore data integration, AVO analysis, etc. Moreover, the proposed SRF attribute was well correlated with the logfacies at the pilot wellbores in West Africa case study so that the less risky seismic units often occurred with the higher percentage of the muddy facies and vice versa.

In the developed approach we assumed that seismic character is mainly controlled by geological characteristics. On the other hand, the chaoticness and dip attributes calculation showed high sensitivity to signal/noise ratio. Despite these limitations, the application of proposed approach on high-density seismic surveys with high S/N ratio can save days of manual mapping time and can reduce exploration risk by basing decisions on seal texture and their proven link to potential leakage elements.

3.9 References

*Alves, T.M., Kurtev, K., Moore, G.F. and Strasser, M., 2014, Assessing the Internal Character, Reservoir Potential, and Seal Competence of Mass-Transport Deposits using Seismic Texture: A Geophysical and Petrophysical Approach. AAPG Bulletin, 98(**4**), pp 793-824.*

Anstey, N., 2005, Attributes in Color: The Early Years. CSEG Recorder, 30, pp 12-15.

*Aplin, A.C. and Macquaker, J.H., 2011, Mudstone Diversity: Origin and Implications for Source, Seal, and Reservoir Properties. In: Petroleum Systems. AAPG Bulletin, 95(**12**), pp 2031-2059.*

*Bahorich, M. and Farmer, S., 1995, 3-D Seismic Discontinuity for Faults and Stratigraphic Features: The Coherence Cube. The leading edge, 14(**10**), pp 1053-1058.*

Balch, A.H., 1971, Color Sonograms: A New Dimension in Seismic Data Interpretation. Geophysics, 36, pp1074–1098.

*Batzle, M.L., Han, D.H. and Hofmann, R., 2006, Fluid Mobility and Frequency-Dependent Seismic Velocity—Direct Measurements. Geophysics, 71(**1**), N1-N9.*

Bing, L., Hai-bo, W. and Wen-shan, L., 2011, The Application Research on High Density Seismic Exploration in Low SNR Area of Liaohe Peripheral Basin. SPG/SEG Shenzhen 2011 International Geophysical Conference Technical Program. Expanded Abstracts, pp 1295-1302.

*Boadu, F.K., and Long, L.T., 1996, Effects of Fractures on Seismic-Wave Velocity and Attenuation. Geophysical Journal International, 127(**1**), pp 86-110.*

Boardman, M. and Walker, A.R., 1995, The Road to High-Density Seismic. Oilfield Review, Chester (UK), 4, pp 52-60.

Bodine, J.H., 1984, Wave Form Analysis with Seismic Attributes. 54th Annual International Meeting, SEG, session S9.1.

*Brancolini, G., Casula, G., De Cillia, C., Manzella, A., Polonia, A., Rebesco, M. and Seriani, G., 1994, Seismic Modeling of Two Depositional Systems. Anali Di Geofisica, 37 (**5**), pp 899-912.*

Brown, A.R., 2004, Interpretation of Three-Dimensional Seismic Data. AAPG Memoire 42. SEG Investigations in Geophysics, 9.

*Calvert, A., Ekstrand, E., McLain, B., Etgen, J., Billette, F., Sen, V., Regone, C., Byrd, T., Truxillo, M., Young, S. and Cobo, Y., 2003, Pushing the Limits of Resolution at Holstein: A Case History from the Deepwater Gulf of Mexico. The Leading Edge, 22(**9**), pp 897-905.*

Carrillat, A., Randen, T. and Sonneland, L., 2002, Seismic Stratigraphic Mapping of Carbonate Mounds using 3D Texture Attributes. 64th Annual International Meeting, European Association of Geoscientists and Engineers, Z-99.

*Cartwright, J., Huuse, M., and Aplin, A., 2007, Seal Bypass Systems. AAPG Bulletin, 91(**8**), pp 1141-1166.*

*Castagna, J.P., Sun, S. and Siegfried, R.W., 2003, Instantaneous Spectral Analysis: Detection of Low-Frequency Shadows Associated with Hydrocarbons. The Leading Edge, 22(**2**), pp120-127.*

*Chopra, S. and Marfurt, K.J., 2005, Seismic Attributes: A New Historical Perspective, Geophysics, 70(**4**), 3SO–28SO.*

*Chopra, S., Castagna, J. and Portniaguine, O., 2006, Seismic Resolution and Thin-Bed Reflectivity Inversion. CSEG recorder, 31(**1**), pp 19-25.*

Chopra, S. and Marfurt, K.J., 2007, Seismic Attributes for Prospect Identification and Reservoir Characterization. SEG Geophysical Developments Series, 11.

*Churlin, V.V. and Sergeyev, L.A., 1963, Application of Seismic Surveying to Recognition of Productive Part of Gas-Oil Strata. Geologiya Nefti I Gaza, 7(**11**), 363 p.*

Connolly, P., 1999, Elastic impedance. The leading edge, 18, pp 438–452.

*Corradi, A., Ruffo, P., Corrao, A. and Visentin, C., 2009, 3D Hydrocarbon Migration by Percolation Technique in an Alternate Sand–Shale Environment Described by a Seismic Facies Classified Volume. Marine and Petroleum Geology, 26(**4**), pp 495-503.*

Cox, T. and Seitz, K., 2007, Ant tracking Seismic Volumes for Automated Fault Interpretation. In CSPG CSEG Convention, Calgary, Alberta, Canada.

*Dalley, R.M., Gevers, E.C.A., Stampfli, G.M., Davies, D.J., Gastaldi, C.N., Ruijtenberg, P.A. and Vermeer, G.J.O, 1989, Dip and Azimuth Displays for 3D Seismic Interpretation. FirstBreak, 7(**3**), pp 86–95.*

*de Matos, M. C., Yenugu, M., Angelo, S. M. and Marfurt, K. J., 2011, Integrated Seismic Texture Segmentation and Cluster Analysis Applied to Channel Delineation and Chert Reservoir Characterization. Geophysics, 76(**5**), pp 1-21.*

Drews, M., 2012, Modelling Stress-Dependent Effective Porosity-Permeability Relationships of Metre-Scale Heterogeneous Mudstones, PhD Thesis, Newcastle University.

*Droz, L., Marsset, T., Ondras, H., Lopez, M., Savoye, B. and Spy-Anderson, F. L., 2003, Architecture of an Active Mud-Rich Turbidite System: The Zaire Fan (Congo–Angola Margin Southeast Atlantic): Results from Zaango 1 And 2 Cruises. AAPG Bulletin, 87(**7**), pp 1145-1168.*

*Fehmers, G. and Hocker, C., 2003, Fast Structural Interpretation with Structure-Oriented Filtering. Geophysics, 68(**4**), pp 1286-1293.*

Gao, D., 2003, Volume Texture Extraction for 3D Seismic Visualization and Interpretation, Geophysics, 68, pp 1294-1302.

Gao, D., 2004, Texture Model Regression for Effective Feature Discrimination: Application to Seismic Facies Visualization and Interpretation, Geophysics, 69, pp 958-967.

*Gao, D., 2007, Application of Three-Dimensional Seismic Texture Analysis with Special Reference to Deep-Marine Facies Discrimination and Interpretation: Offshore Angola, West Africa. AAPG Bulletin, 91(**12**), pp 1665-1683.*

*Gao, D., 2008, Application of Seismic Texture Model Regression to Seismic Facies Characterization and Interpretation. The Leading Edge, 27(**3**), pp 394-397.*

Gardner, G.H.F., ed., 1985, Migration of Seismic Data. Society of Exploration Geophysicists Monograph Series, 462 p.

Heggland, R., Meldahl, P., Bril, B. and de Groot, P., 1999, The Chimney Cube, An Example of Semi-Automated Detection of Seismic Objects by Directive Attributes and Neural Networks: Part II; Interpretation. In proceeding: 69th SEG Annual Meeting, Houston.

Hocker, C. and Fehmers, G., 2002, Fast Structural Interpretation with Structure-Oriented Filtering. The Leading Edge, 21, pp 238–243.

Insalaco, E., Marion, D., Michel, B. and Rowbotham, P., 2001, Reservoir-Scale 3D Sedimentary Modelling: Approaches and Impact of Integrating Sedimentology into the Reservoir Characterization Workflow. In proceedings: AAPG Annual Meeting.

Iske, A. and Randen, T., 2005, Mathematical Methods and Modelling in Hydrocarbon Exploration and Production. Mathematics in Industry Series, 7, Schlumberger, Springer, 451 p.

Jenkins, F.A. and White, H.E., 1957, Fundamentals of optics. Tata McGraw-Hill Education.

Kearey, P., 2001, Dictionary of Geology, 2nd Edition. Penguin Reference, London, New York, p. 41.

Koehler, F., Taner, M.T., Sheriff, R.E. and Frye, D., 1976, Extraction and Interpretation of the Complex Seismic Trace: Part I. Computational Procedures. Geophysics, 162.

Kolisnyk, A., Castellani, R., de Abreu, E., e Sá, L.T., Pimentel, A., da Cunha, C., da Silva, V., Kraft, R., Silva, C.M.A. and Moraes, D. C., 2013, Connecting Seismic Attributes with Production Performance at Camarupim Gas Field, Espirito Santo Basin, Brazil. 13th International Congress of the Brazilian Geophysical Society & EXPOGEF, Rio de Janeiro, Brazil, pp 1617-1620. (DOI: 10.1190/sbgf2013-331).

Lavergne, M., 1975, Pseudo-Diagraphics de Vitesse en Offshore Profonde. Geophysical prospecting, 23, pp 695–711.

Lindseth, R.O., 1976, Seislog Process Uses Seismic Reflection Traces. Oil & Gas Journal, 74, pp 67–71.

*Løseth, H., Gading, M. and Wensaas, L., 2009, Hydrocarbon Leakage Interpreted on Seismic Data. Marine and Petroleum Geology, 26(**7**), pp 1304-1319.*

Love, P.L. and Simaan, M., 1984, Segmentation of Stacked Seismic Data by the Classification of Image Texture, In proceeding: 54th SEG Annual International Meeting, Session: S7.3.

*Macquaker, J.H. and Howell, J.K., 1999, Small-Scale (< 5.0 m) Vertical Heterogeneity in Mudstones: Implications for High-Resolution Stratigraphy in Siliciclastic Mudstone Successions. Journal of the Geological Society, 156(**1**), pp 105-112.*

*Macquaker, J.H., Taylor, K.G. and Gawthorpe, R.L., 2007, High-Resolution Facies Analyses of Mudstones: Implications for Paleoenvironmental and Sequence Stratigraphic Interpretations of Offshore Ancient Mud-Dominated Successions. Journal of Sedimentary Research, 77(**4**), pp 324-339.*

*Marfurt, K. J. and Kirlin, R.L., 2001, Narrow-Band Spectral Analysis and Thin-Bed Tuning. Geophysics, 66(**4**), pp 1274-1283.*

Meldahl, P., Heggland, R., Bril, B. and de Groot, P., 1999, The Chimney Cube, an Example of Semi-Automated Detection of Seismic Objects by Directive Attributes and Neural Networks: Part II; Methodology. In proceeding: 69th SEG Annual Meeting, Houston.

Meldahl, P., Heggland, R., Bril, B. and de Groot, P., 2001, Identifying Faults and Gas Chimneys using Multiattributes and Neural Networks, The Leading Edge, 20, pp 474–482.

Omeru, T., 2014, Mass Transport Deposits: Implications for Reservoir Seals. PhD Thesis, Cardiff University.

*Pandey, D., Singh, S., Sinha, M. and MacGregor, L., 2007, The Effect of Intra-Trappean Heterogeneities on Seismic Data: A Case Study from the Deccan Traps. Applied Geophysics, 4(**3**), pp 183-193.*

Partyka, G., Gridley, J. and Lopez, J., 1999, Interpretational Applications of Spectral Decomposition in Reservoir Characterization, The Leading Edge, 18, pp 353-360.

Pepper, R. and Bejarano, G, 2005, Advances in Seismic Fault Interpretation Automation. In proceeding: AAPG Annual Convention, pp 19-22.

Picou, C. and Utzmann, R., 1962, La Coupe Sismique Vectorielle: Un Pointe Semi-Automatique. Geophysical prospecting, 4, pp 497–516.

Peyton, L., Bottjer, R. and Partyka, G., 1998, Interpretation of Incised Valleys using New 3D Seismic Techniques: A Case History using Spectral Decomposition and Coherency. The leading edge, 17, pp 1294–1298.

Power, B.A., Covault, J., Sullivan, M. and Posamentier, H., 2014, Bypass-Dominated Mud-Rich Channel-Fill Deposits of the Paleogene Scripps/Ardath Formation at Tourmaline Beach, San Diego, CA: An Analog for Low Net-To-Gross Slope Canyon And Channel Systems. In proceeding: 2014 AAPG Annual Convention and Exhibition, Houston, Texas.

Praeg, D., Ketzer, J.M., Augustin, A.H., Migeon, S., Ceramicola, S., Dano, A., Ducassou, E., Dupré, S., Mascle, J. and Rodrigues, L.F., 2014), Fluid Seepage in Relation to Seabed Deformation on the Central Nile Deep-Sea Fan, Part 2: Evidence from Multibeam and Sidescan Imagery. In Submarine Mass Movements and Their Consequences, Springer International Publishing, pp. 141-150.

Randen, T., Monsen, E., Signer, C., Abrahamsen, A., Hansen, J., Saeter, T. and Schlaf, J., 2000, Three-Dimensional Texture Attributes for Seismic Data Analysis. In proceeding: 70th SEG Annual Meeting, pp 668-671.

Randen, T. and Sønneland, L., 2005, Atlas of 3D Seismic Attributes. Mathematical Methods and Modelling in Hydrocarbon Exploration and Production, Springer, pp 23-46.

*Rijks, E.J.H. and Jauffred, J.C.E.M., 1991, Attribute Extraction: An Important Application in Any Detailed 3-D Interpretation Study. The leading edge, 10(**9**), pp 11-19.*

*Robertson, J.D. and Nogami, H.H., 1984, Complex Seismic Trace Analysis of Thin Beds. Geophysics 49(**4**), pp 344-352.*

Rummerfeld, B., 1954, Reflection Quality, a Fourth Dimension. Geophysics, 19, pp. 684-694.

Russell, B., Hampson, D., Schuelke, J. and Quirein, J., 1997, Multiattribute Seismic Analysis. The Leading Edge, 16, pp 1439-1443.

*Sangree, J.B. and Widmier, J.M., 1979, Interpretation of Depositional Facies from Seismic Data. Geophysics, 44 (**2**), pp 131-160.*

Seebeck, H., Tenthorey, E., Consoli, C. and Nicol, A., 2015, Polygonal Faulting and Seal Integrity in the Bonaparte Basin, Australia. Marine and Petroleum Geology, 60, pp. 120-135.

Sheriff, R.E., Frye, D., Koehler, F. and Taner, M.T., 1976, Extraction and Interpretation of the Complex Seismic Trace: Part II. Geologic Interpretation. Geophysics, 181.

Simpson, S.M., Fink, D. and Treitel, S., 1967, Moveout Averaging Experiments. Geophysics, 32, pp 494–498.

Sonneland, L., Barkved, O., Olsen, M. and Snydea, G., 1989, Application of Seismic Wavefield Attributes in Reservoir Characterization. In proceeding: SEG Annual Meeting.

Taner, M.T., 2001, Seismic Attributes. CSEG Recorder - September 2001, pp 48-56.

*Taner, M.T., and Koehler, F., 1969, Velocity Spectra-Digital Computer Derivation Applications of Velocity Functions. Geophysics, 34(**6**), pp 859-881.*

*Taner, M.T., Koehler, F. and Sheriff, R.E., 1979, Complex Seismic Trace Analysis. Geophysics, 44(**6**), pp 1041-1063.*

Taner, M.T. and Sheriff, R.E., 1977, Application of Amplitude, Frequency, and Other Attributes to Stratigraphic and Hydrocarbon Determination. In: C.E. Payton, ed., Applications to Hydrocarbon Exploration. American Association of Petroleum Geologists Memoir 26, pp 301–327.

Tingdahl, K.M., Bril, A.H. and de Groot, P.F., 2001, Improving Seismic Chimney Detection using Directional Attributes, Journal of Petroleum Science and Engineering, 29, pp 205–211.

*Vail, P.R., Mitchum Jr,R.M. and Thompson III, S., 1977, Seismic Stratigraphy and Global Changes of Sea Level, Part 4, Global Cycles of Relative Changes of Sea Level: In Seismic Stratigraphy Applications to Hydrocarbon Exploration. C.E. Payton, C.E. (ed.), American Association of Petroleum Geologists., Tulsa, OK, Memoir **26**, pp 83-97.*

Vinther, R., 1997, Seismic Texture Classification Applied to Processed 2D and 3D Seismic Data. In proceeding: 67th SEG Annual International Meeting, pp 721-724.

Vinther, R., Mosegaard, K., Kierkegaard, K., Abatzis, I., Andersen, C. and If F., 1995, Seismic Texture Classification: A Computer-Aided Approach to Stratigraphic Analysis. 65th SEG Annual International Meeting, pp 153-155.

West, B., S. May, S., Eastwood, J.E. and Rossen, C., 2002, Interactive Seismic Facies Classification using Textural Attributes and Neural Networks, The Leading Edge, 21, pp 1042-1049.

Whitcombe, D.N., 2002, Elastic impedance normalization. Geophysics, 67, pp 60–62.

Whitehead, P., Fairborn, J. and Wentland, R., 1999, Identifying Stratigraphic Units by Seismic Patterns, 69th SEG Annual International Meeting, pp 942-945.

*Yenugu, M., Marfurt, K.J. and Matson, Sh., 2010, Seismic Texture Analysis for Reservoir Prediction and Characterization. The leading edge, 29(**9**), pp 1116-1121.*

Yilmaz, Ö, 2001, Seismic Data Analysis: Processing, Inversion, and Interpretation of Seismic Data (Volume I). SEG Investigations in Geophysics Series, 10, Tulsa.

*Zhou, Z., Cvetkovic, M., Xu, B. and Fontana, P., 2012, Analysis of a Broadband Processing Technology Applicable to Conventional Streamer Data. First Break, 30 (**10**), pp 77–84.*

4 Probabilistic Prediction of Lithology in Mud-Rich Sediment Sequences using Multivariate Analysis of Seal Quality Attributes and Logfacies Data

4.1 Introduction

The effect of lithology on the flow properties of mud-rich sediment sequences (Ingram et al., 1997; Drews, 2012) makes it very important to develop an approach for translating the seismic seal cube into lithofacies seal cube. More permeable sediments can play an important role in the leakage process. Moreover, the seal lithofacies cube generates a better foundation for dynamic modelling to assess subsurface flow and hydrocarbon migration (Hitchon, 1971; Bjørlykke, 1993, 2010; Aydin, 2000) in sedimentary basins. Lithofacies distribution modelling requires an integrated approach, where data from different sources (such as core, wireline, seismic and outcrop) are used to populate facies away from the wells.

The use of seismic attributes can reduce the uncertainty of spatial modelling and sometimes provides direct information about the distribution of sedimentary bodies such as channels (Biver et al., 2002, 2008; Hass and Formery, 2002) and mass transport deposits (Frey-Martinez et al., 2006; Moscardelli and Wood, 2008; Alves et al., 2010). Discrete facies parameters must therefore be constrained with continuous seismic attribute results. This is conducted by either deterministic or stochastic geostatistical methods which have been widely developed over the last forty years to predict the spatial distribution of geological facies and properties. Deterministic approaches (Doyen et al., 1996; Chiles and Delfiner, 1999; Coleou, 2002) apply kriging principles to interpolate facies data. They are good at honouring the statistics, but often poor at capturing the sedimentary bodies (Amour et al., 2011; Park and Jang, 2014). In contrast, stochastic facies modelling generates models representing more realistic depositional features which honour the existing data and/or a priori model – this is known as conditional simulation (Dubrule et al., 1998, 2003; Miller et al., 2000; Falivene et al., 2006).

Dubrule et al. (1998) described in detail the geostatistical and probabilistic conditional simulation of discrete parameters such as geological facies, lithology, or rock types. Bortoli et al. (1992) and Haas and Dubrule (1994) introduced geostatistical inversion (GI), which generates joint realisations of facies and acoustic-impedance, all directly constrained by seismic data. GI is largely dependent on

seismic quality; thus the algorithm was used in the case of a faulted reservoir (Lamy et al., 1998; Rowbotham et al., 2000) and a salt tectonised region (Shrestha and Boeckmann, 2002) to discriminate facies according to seismic quality variation. Grijalba-Cuenca et al. (2000) and Hegstad and Henning (2001) further developed GI by using a grid by grid rather than a trace by trace algorithm.

Despite these advances in geostatistical simulations, the relatively homogeneous and low amplitude seismic in fine-grained sediment sequences limits the efficiency of GI in modelling seal facies. The alternative conditional simulation approaches are probabilistic and constrained by facies occurrence probabilities derived from seismic attributes at well locations. The algorithms are independent of S/N ratio or assumptions used for statistical relationships between facies and seismic attributes (Dubrule, 2003). MacDonald et al. (1995) and Holden et al. (1998) introduced simulated annealing object-based models to generate facies model realisations by iteratively adding and subtracting channel bodies from the simulated volume. Yarus et al. (2000) also described an application of this method to stochastically model the distribution of bar and channel facies bodies within a shaly background in a Tertiary reservoir in the Gulf of Thailand. Although constraining object-based models with seismic data can effectively capture geological bodies with characteristic geometries such as crevasse splays and channels (Clemesten et al., 1990; Damsleth et al., 1992), it is less useful for predicting more subtle variation of facies in laterally extensive, muddy seal units.

Journel and Gomez-Hernandez (1993) and Doyen et al. (1994) proposed probabilistic pixel-based approaches that generalise the indicator simulation methodology developed for continuous variables for use with discrete variables. These methods are based on constraining a priori, sequential indicator simulation (SIS) realisations using facies likelihood functions derived from seismic data according to Bayes' theorem. Doyen et al. (1994) successfully applied the methodology in the Ness formation of the Oseberg field (North Sea) to find channel deposits using seismic amplitude. Lo and Bashore (1999) proposed a similar approach to obtain a 3D density model and translate it into probabilities of various facies. Insalaco et al. (2001) presented an application of this approach to detailed modelling of a West African turbidite deposit. Due to the increase in interest in shale gas resources, there are also recent case studies utilising similar probabilistic

conditional simulations (Wang and Carr, 2012, 2013) and support vector machines (Wang et al., 2014) to predict shale lithofacies on a regional scale.

In this study, we present a semi-automatic algorithm to predict probabilities of occurrence of fine-grained facies as functions of seismic seal quality attributes within regional seal units. The algorithm extends the conventional probabilistic indicator simulation for channel deposits (Doyen et al., 1994) and turbidites (Insalaco et al., 2001) to fine-grained seal deposits. We incorporate the seal logfacies recognition results in uncored intervals (Chapter 2) and seismic seal quality attributes (Chapter 3), and constrain logfacies predictions by their statistical relationships. Within seal intervals, there are usually limited well log data available, thus variography analysis for generating a priori SIS models is very restricted. We therefore utilise classic multivariate analysis (Fournier and Derain, 1995; Hart and Balch, 2000; Mukerji et al., 2001) and Bayesian (Buland et al., 2008) techniques to establish the likelihood functions of seal facies based on multiple textural attributes with limited well control. This helps to reduce the uncertainty caused by the lack of an a priori model in the seal intervals. The resulting algorithm is used to predict lithology probabilities in three different fine-grained facies classification schemes with different degrees of uncertainty. We believe this is the first attempt to predict different fine-grained facies in non-reservoir mudstones. The strength of the algorithm is that it is generic and benefits from standard seismic attributes as predictors, whilst also compatible with the poorly resolved seismic and limited wireline datasets within seal units.

We have applied the approach to a regional seal from offshore West Africa. No *a priori* model was applied to the prediction algorithm; however, we suggest calibrating the likelihood functions with an a priori model derived from SIS, if sufficient wireline data is available.

4.2 Methods

The conventional seismic conditional simulation of lithofacies, using a probabilistic indicator approach, consists of three main tasks:

1. Calculating the probabilities of facies occurrences (likelihood functions) by seismic-to-well calibration, based on the values of the seismic attributes;

2. Creating a priori probabilities of facies occurrences by running sequential indicator simulation (SIS), based on wells and on the a priori geological model quantified by the variogram;

3. Combining likelihood functions with a priori probabilities using the Bayesian theorem.

The second and third tasks are usually inapplicable to seal intervals where limited wireline data restrict the use of variography analysis, and result in unreliable a priori geological models. In this study, we only focus on the first task. It is based mainly on seismic data and involves the development of a three-step algorithm (Figure 4.1) to derive facies likelihood functions based on multiple seismic seal quality attributes with limited well control. Each step of the algorithm is outlined in detail in Sections 4.2.1 - 4.2.3. In Chapter 2, we proposed a stepwise IPSOM approach to recognise seal facies that honours reservoir core data. Here, therefore, we first determine the best logfacies recognition set which better discriminates sand and mud lithoclasses in the histogram of facies frequency-seismic seal quality attributes. In the second step, we utilise multivariate techniques to predict the probabilities of muds in two muds sub-lithoclasses. Although all facies in the muds lithoclass are by definition mud-dominated, they will have different flow properties (Drews, 2012) and exert different controls on subsurface flow in sedimentary basins. In the last step, we divide the muds sub-lithoclasses into their component facies and derive the likelihood functions by incorporating logfacies distribution controls using Bayes' theorem. The generated seal lithofacies cubes can provide valuable information for appraisal of oil/gas fields and CO2 storage sites, or for flow simulation in sedimentary basins. Considering log and seismic data quality and availability constraints within the seal intervals, we believe this step is at the feasibility borderline of prediction of fine-grained facies from seismic and log data. Finally, we recommend using an SIS a priori model to calibrate the current likelihood functions and reduce uncertainty, should enough well data be available to apply variographic methods.

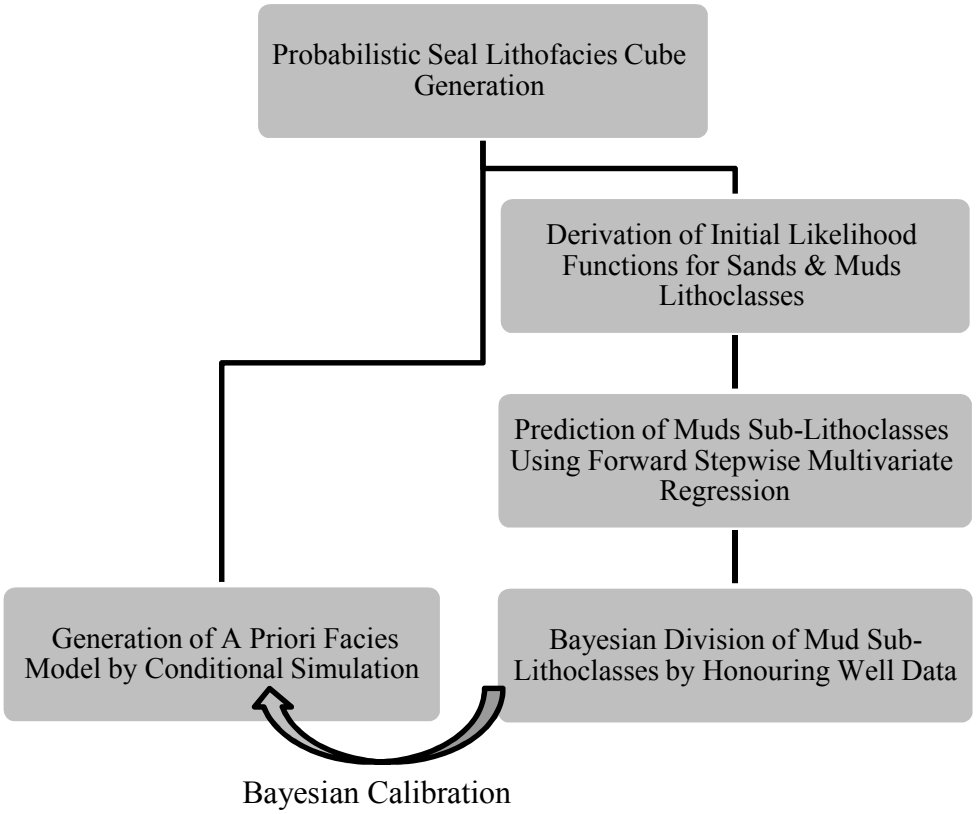

Figure 4.1: *Overview of the approach used to generate probabilistic seal lithofacies cubes.*

4.2.1 Selecting the seal logfacies recognition with the most seismically observable facies distribution/deriving the initial likelihood functions

In order to be able to populate the probabilities of seal facies occurrences as a function of seismic attributes, we first need a description of lithofacies within seal intervals, at the well locations. In Chapter 2, we showed an application of Self-Organising Map (SOM) (Kohonen, 1997, 1998; Malki and Anwar, 2003) for logfacies recognition in uncored seal intervals which was able to recognise fine-grained facies within seal units that were not used for training. We proposed a stepwise SOM approach, in which a range of log curves was used as input neurons. In each recognition operation, logfacies were predicted within seal units based on the interrelationship of log patterns and core descriptions within cored intervals. All seal logfacies recognition results honoured the core descriptions; however they displayed different vertical facies distributions. This can generate different well-to-log calibration results and can avoid achieving consistency in the relationship between facies and seal quality attributes. As a result, we first aim to determine the

recognition operation yielding the most seismically observable seal facies distribution.

4.2.1.1 Defining lithoclasses:

Given the lower resolution of seismic compared to log data, we should group the original sedimentological facies. In West Africa case study, sedimentologists from the operating company defined 16 facies based on reservoir core data (Insalaco et al., 2001; Table 2.2). We classified them into muds and sands lithoclasses, because there is the greatest expected difference between seismic attribute histograms associated with these two lithoclasses (Doyen et al., 1994) and seismic can discriminate between them most easily. All muddy and debris flow facies are included in the muds lithoclass and similarly, all silty, sandy and conglomeratic facies in the sands lithoclass (Table 4.1).

Table 4.1: *Muds and sands lithoclasses definition in seal unit 4 of West Africa case study (see Table 2.2 for the sedimentological descriptions of the individual facies).*

Lithoclass	Facies
Muds	Hemipelagic Shales, Mud Turbidites UP, Mud Turbidites LP, Muddy Debris Flow, Sandy Debris Flow, Sandy Debris Flow
Sands	Cross Laminated Silts, Graded Silts, Cross Laminated Sands, Graded Sands, Massive m-f TB Sands, Laminated m-f Sands, Laminated C-Arac, TB sands, Laminated C-Arav sands, Conglomerates, Sand Injectites

We include all mud-dominated facies in the muds lithoclass because they are expected to exhibit better sealing quality, whereas silty facies are added to the sand lithoclass because their occurrence in seal units increases the risk of capillary breakthrough (Ingram et al., 1997). Moreover, in seal unit 4 of West Africa case study, silty facies are a very low proportion of the logfacies recognition results (Chapter 2) and often coexist with sandy facies. Therefore, there is high uncertainty in their seismic distinction from sandy facies and it is not feasible to introduce a third silt lithoclass.

4.2.1.2 Investigating the log detrending effect on discrimination between lithoclasses in the seal context

As an important log processing technique, detrending is conventionally applied prior to cross-correlation of log data. It can help to capture and compare the wireline characteristic of lithologies, independent of compaction state (Magara, 1986). Log detrending has been commonly applied to reservoir logfacies prediction using statistical methods (Anderberg, 1973; Rao, 1973; Wolff and Pelissier-Combescure, 1982) and neural networks (Delfiner et al., 1987; Roger, 1992). In addition, detrending has been recently used in conjunction with fractal/fluctuation principles to improve the long-range cross correlations between well logs (Dashtian et al., 2011; Marinho et al., 2013).

In Chapter 2 we deployed detrending techniques prior to seal facies recognition from log data. The neuron inputs of the recognition practices varied in type and detrending method of the log curves. Detrending was applied to density, p-wave sonic, s-wave sonic and neutron-porosity logs by implementing linear and segmented non-linear techniques (Chapter 2: Section 2.4.3.2).

Nivlet et al. (2007) tested the efficiency of detrending on recognition of reservoir heterogeneities from seismic-to-log calibration. He used detrended log-derived p- and s-acoustic impedances (I_p and I_s) to compensate for compaction and finally to improve the prediction heterolithic facies of turbidites reservoirs at seismic scale in West Africa case study (Figure 4.2). The detrending was done by filtering out the low-frequency component (0-0-4-8 Hz) of acoustic impedances.

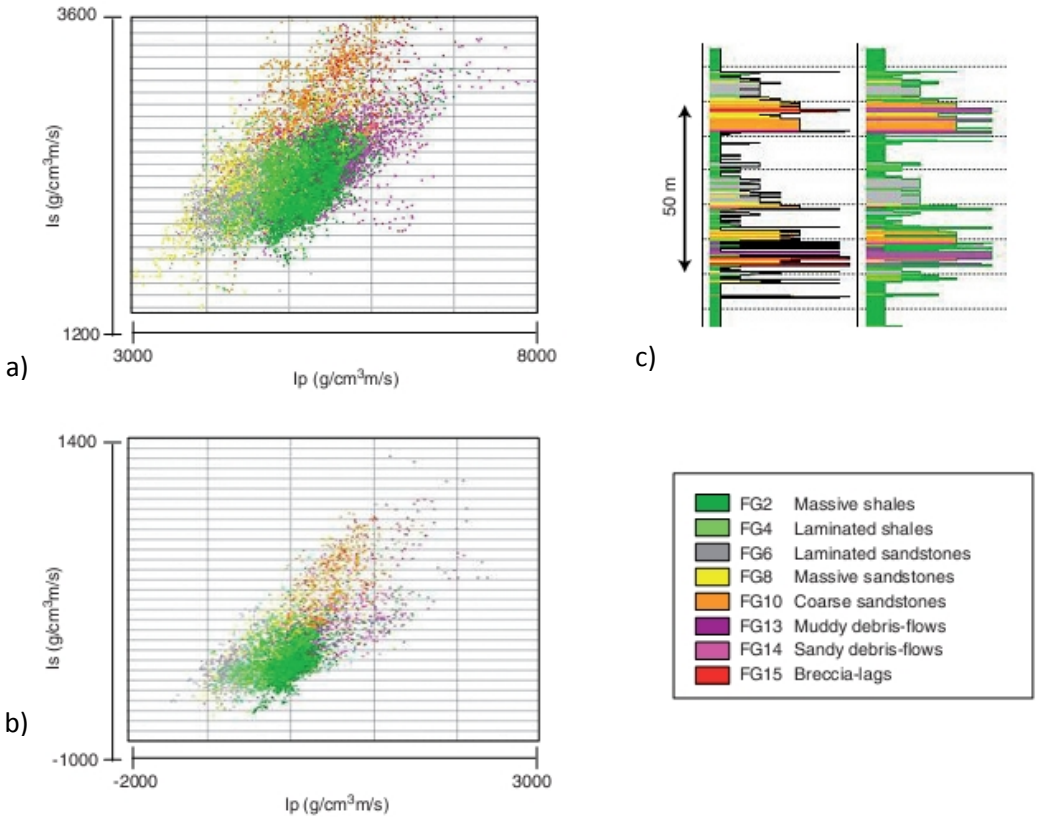

Figure 4.2: *Discrimination of geological facies in Ip-Is crossplot before (a) and after (b) detrending well-log data and comparison between initial and predicted facies log after detrending impedances and grouping heterolithic facies (c) of turbidite reservoir in a West African case study (Nivelt et al.,2007) .*

Although log detrending helps to discriminate between reservoir facies, it should not be applied in seal logfacies prediction. The main reason is that the variability of log responses within mud-rich seal units is very subtle and thus susceptible to being adversely affected by the detrending process, resulting in incorrect facies predictions. In seal unit 4, there is a subtle fining-upward trend which is missed if logs are detrended. On the other hand, seal units have generally very low permeability (μD-nD scale) and hydrocarbon saturation, and field (Geertsma, 1973a; Baldwin and Butler, 1985; de Waal, 1986) and laboratory (Dewhurst et al., 1998) measurements have indicated that tight and dry rocks have lower compaction coefficients than reservoir rocks (assuming compaction equilibrium exists). For example, Revil et al. (2002) suggested average compaction coefficients of 4×10^{-8} Pa^{-1} and 6×10^{-8} Pa^{-1} for shales and sands in compaction modelling.

In order to prove the effect of log detrending on discrimination of logfacies in the seal context, a four-step workflow was followed:

- Depth to time conversion of logfacies recognition results (Chapter 2) based on check-shot data
- Calculation of the average of log facies frequencies at the pick-trough time interval scale (defined by successive peaks and troughs along seismic amplitude traces)
- Qualitative evaluation of conformity of seal quality attributes with logfacies distribution in seal unit 4
- Quantitative evaluation of facies distribution effect on discrimination between muds and sands lithoclasses using facies frequency-seal quality attribute cross-plot analysis

The workflow was applied on logfacies recognition results with RHOB-detrended, PHIT-detrended or non-detrended input logs, since the recognition results showed the best correlation to the reservoir core descriptions (Chapter 2). The approach is similar to the work of Nivelt et al. (2007) and the log detrending effect is analysed by vertical upscaling of seal facies from the log to the seismic scale through log-to-seismic attribute calibration; however, the facies frequency-seal quality attribute cross-plots (instead of I_p-I_s crossplots) are used to discriminate between muds and sands lithoclasses. Better seismic-to-log calibration in the crossplots indicates improvements in discrimination between the lithoclasses in the seal unit. Moreover, the analysis is carried out on the pick-trough time interval scale (in case study A ~ 10 m), the resolution of which is addressed by crosswell seismic profiling (Harris et al., 1995; Yu et al., 2008; Handayani et al., 2011; Neal and Krohn, 2012) as the bridging solution for seismic-log resolution gap.

At the end of the process, the initial likelihood functions are derived from the regression line equations corresponding to the best fitting facies frequency-to-seal quality attribute calibrations. The initial likelihood functions are defined for muds and sands lithoclasses and are based on the seal quality attributes.

4.2.2. Prediction of muds sub-lithoclass probabilities from seal quality attributes using multi-attribute transforms

In this step, we demonstrate a new method to predict muds sub-lithoclass probabilities using multiple seal quality attributes. Hampson et al. (2001) first introduced the application of seismic Multi-Attribute Analysis (MAA) to predict continuous log properties on a sample-by-sample basis. Later, MAA was used to

interpret and detect subtle, seismic-scale lithological features within reservoir formations (e.g. Gray et al., 2006). Recent studies (e.g. Gray, 2011; Archer et al., 2013) also showed that MAA can be beneficial for identifying muds and sands (shale volume) in complex channel reservoirs. In these approaches, continuous lithology logs were derived from wireline data and predicted as "convolutional" weighted sums of seismic attributes within reservoir units. The predictions have been mainly limited to discrimination of muds and sands in reservoirs and have not used core (sedimentary facies) data. In the current study, we extend the MAA approach of Hampson et al. (2001) to the mud-rich seal context and also to predict the probabilities of discrete facies parameters from seismic. Here, lithology logs are discrete, derived from log and core data (Chapter 2) and predicted as ordinary weighted sums of seismic attributes at the pick-trough time interval scale within seal units. The objective is to find data-driven, probabilistic relationships between sets of seal quality attributes and seismically observable muds sub-lithoclasses, and then to use these attributes over a 3D seismic volume to predict the probability of the sub-lithoclasses. The methodology is summarised in the four following main steps and is illustrated in Figure 4.3:

I. Extract seismic attributes at well locations of pilot study
II. Average seismic attributes/calculate logfacies frequencies at the pick-trough time interval scale
III. Correlate multiple seismic attributes and logfacies/lithoclass frequencies using a forward, stepwise, multivariate regression approach
IV. Apply the most robust probabilistic statistical relationship to the seismic volume

In step (I), seismic attributes can be extracted at well locations using industry-standard seismic interpretation packages. Here, we use Hampson-Russell software and apply the composite trace extraction tool. Since volumetric attributes had been previously computed over a 3D neighbourhood (Chapter 3), the composite traces of attributes are extracted in the same neighbourhood along the well trajectories. Moreover, we also extract simple traces of original amplitude at well locations to be able to define the intervals. Each interval is defined as the distance between two successive seismic amplitude peaks and troughs in the time domain.

Steps (II) and (III) are implemented using Matlab programming. In step (II), logfacies recognition results are converted to the time domain using the spline method and available check-shot data, after which their frequencies can be calculated in each interval for different wells. Similarly, seal quality attribute traces are also averaged at the pick-trough time interval scale. The reason we do the correlation at this scale is to bridge the resolution gap between log and seismic data, and also to compare a continuous property (attribute) with a discrete property (facies). It is a geologically relevant upscaling for log data where it is also recognisable by seismic. Each interval is assumed to be an acoustic unit (resolvable by the dominant frequency) with a specific elastic modulus, and thus with a different effective lithology and fluid content.

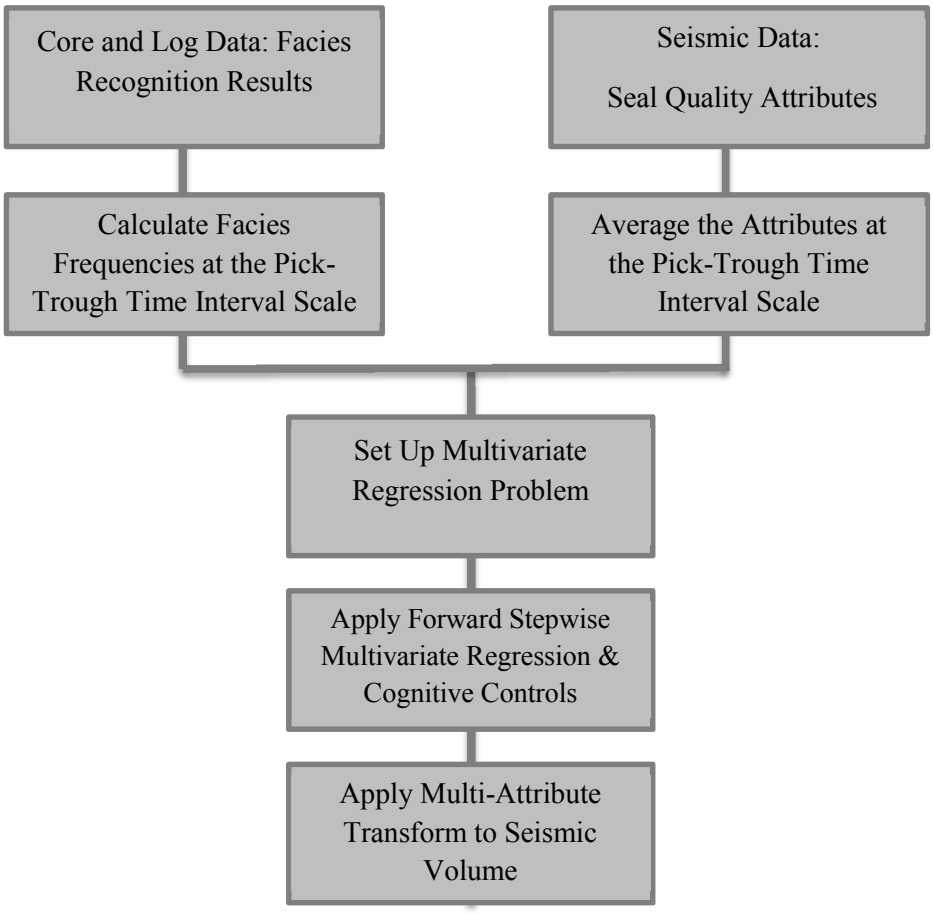

Figure 4.3: *Proposed multivariate regression approach to predict the probability of muds sub-lithoclasses.*

Step III is where we establish data-driven statistical relationships between sets of seal quality attributes and lithoclass frequencies within seal units.

Mathematically, the technique is known as multivariate linear regression, where more than one predictor variable (seal quality attributes) is used to predict multiple outcome variables (lithoclass frequencies) in a form of linear combination. At interval (i), the linear combination that relates seal quality attributes (**Att**) to lithoclass frequencies (**LC**) can be modelled as:

$$\mathbf{LC}(i) = \mathbf{Att}(i)\,\boldsymbol{\beta} + \boldsymbol{\varepsilon}(i) \qquad \text{Equation 4.1}$$

where **LC**(i): a d-by-1 response vector of lithoclass frequencies in *ith* interval (d is the number of lithoclasses to predict)

Att(i): a d-by-K design matrix of seal quality attributes in *ith* interval (K is the number of attributes used for prediction)

β: a K-by-1 coefficient vector of seismic quality attributes (unknown vector; required to find a single coefficient – valid for all intervals - per seismic quality attributes)

ε(i)**:** a d-by-1 error terms vector in *ith* interval which follows multivariate normal distribution (MVN_d) $\overset{i.e.}{\Rightarrow} \varepsilon(i) \sim MVN_d(0, \Sigma)$

Σ: a d-by-d error variance – covariance matrix

If we have n defined intervals in our training set, their measurements are assumed to be independent and the system of equations for n-stacked equation 4.1 is denoted as:

$$\mathbf{LC} \sim MVN_{nd}(\mathbf{Att}\,\boldsymbol{\beta}, \mathbf{I}_d \times \boldsymbol{\Sigma}) \qquad \text{Equation 4.2}$$

where **LC** and **Att** are nd-by-1 vectors of stacked lithoclass frequency response vectors, and nd-by-K matrix of stacked seismic quality attributes design matrices, respectively. To solve this system of equations and fit a multivariate linear regression model, we utilise the *mvregress* tool in the *Statistics Toolbox*^{TM} of *Matlab*. This tool is useful for solving multivariate regression problems with non-parameterised error variance-covariance matrices. Here, we applied the ordinary least squares (OLS) estimation option. The method can provide a multivariate regression model with a diagonal error variance –covariance matrix (**Σ**), assuming $\boldsymbol{\Sigma} = \mathbf{I}_d$. The OLS estimates the coefficient vector ($\boldsymbol{\beta_O}$) in such a way that minimises:

$$\sum_{i=1}^{n} (\boldsymbol{L}(i) - \boldsymbol{A}(i)\,\boldsymbol{\beta_O})' (\mathbf{L}(i) - \mathbf{A}(i)\boldsymbol{\beta_O}) \qquad \text{Equation 4.3}$$

In other words, the OLS coefficient vector ($\boldsymbol{\beta_O}$) can be expressed as:

$$\boldsymbol{\beta_0} = (\mathbf{A}\ '\mathbf{A}\ )^{-1}\ \mathbf{A}\ \mathbf{t}'\ \mathbf{L} \qquad \text{Equation 4.4}$$

The standard errors of $\boldsymbol{\beta_0}$ estimations are also derived from taking the square root of the diagonal of the variance-covariance matrix ($\mathbf{V}$ ($\boldsymbol{\beta_0}$)):

$$\mathbf{V}(\boldsymbol{\beta_0}\ ) = (\mathbf{A}\ '\mathbf{A}\ )^{-1} \qquad \text{Equation 4.5}$$

Furthermore, to compare the residuals with standard errors of estimation, we also compute the mean squared error (MSE) vector:

$$\mathbf{MSE} = \frac{\sum_{i=1}^{n} \boldsymbol{e}\,(i)\,e'(i)}{n-K} \qquad \text{Equation 4.6}$$

where $\mathbf{e}(i) = (\mathbf{LC}\,(i) - \mathbf{Att}\,(i)\,\boldsymbol{\beta_0}\ )'$.

Lastly, in order to resolve the wavelet effect (which smears the effect of log measurements over a range of seismic samples), the multivariate problem is solved at ±2 and ±1 shifted intervals for each attribute. This approach has been used in classic convolutional models and analogues to the application of convolutional operators for the prediction of continuous properties (Hampson et al., 2001).

Having defined the framework for the multivariate regression problem, we design and infill the system of equations with seismic attributes and logfacies measurements. In Chapter 3, we found ten effective seal quality attributes which have been classified into three groups based on their efficiency in characterising seal quality elements, and sixteen logfacies recognised from core descriptions and well data, including six mud-rich facies. In Section 4.2.1, the logfacies were grouped into two lithoclasses of muds and sands and their statistical relationship to single seal quality attributes were derived by cross-plotting analysis. Since facies within the mud lithoclass have different flow properties, here we are interested in subdividing the mud lithoclass and finding a combination set of seal quality attributes and muds sub-lithoclasses which provides the best correlation, and thus the maximum lithology prediction efficiency. Combinatorial mathematics (Ryser, 1963; Mazur, 2010) states that the number of combinations of n things taken k at a time without repetition and irrespective of selection order is equal to:

$$\frac{n!}{k!(n-k)!} \qquad \text{Equation 4.7}$$

whenever $k \leq n$. The total number of combinations of muds sub-lithoclasses to check is therefore 57 (in a form of multiplets with one to five members). According to the same rule, seal quality attributes can also have 1013 forms of combination in the prediction process where each form has to be solved with five different shifted intervals. Thus, an overall $1013 \times 57 \times 5 = 288{,}705$ multivariate regression problems are required to be solved to determine the best combination set in the seal pilot study.

Although correct type and number of predictor seismic attributes can be determined by cross-validation (e.g. Kalkomey, 1997), a reliable validation study requires a rich wireline database (Leonard et al., 1992). In Chapter 3, we determined ten effective volumetric attributes for seal textural quality prediction; and here we can limit them to three representative attributes (i.e. Reflection Intensity, Chaos and Local Structural Dip) in order to avoid the excessive calculation of linearly dependent attributes which are unlikely to improve correlations significantly. Instead, we add seal risk factor (SRF), as a non-linear transform between representative attributes, to increase the regression prediction efficiency. This approach can readily be used in seal studies where wireline data is scarce.

Furthermore, we also utilise stepwise regression analysis in defining muds sub-lithoclasses. Stepwise regression was initially introduced by Draper and Smith (1966) and was later used by Hampson et al. (2001) to predict reservoir porosity from seismic attributes. Hampson et al. (2001) used the approach to find the best set of attributes to predict a single, continuous log property. We extend Hampson et al.'s (2001) approach to predict multiple discrete parameters (i.e. lithoclass frequencies) from multiple volumetric seismic attributes. This procedure assumes that the best combination of N+1 lithoclasses should include the previous best N lithoclasses as members. In order to subdivide the mud lithoclasses, we use a stepwise regression, with a maximum of five steps.

First, we find the facies frequency showing the best correlation with seal quality attribute sets. The multivariate problems are thus solved for a combination of sand lithoclass and six mud facies, and the corresponding standard errors and MSE are derived according to Equations 4.5 and 4.6. The facies with the lowest errors is considered as the best singlet muds sub-lithoclass.

In the next step, we create doublet lithoclasses by adding the other mud facies to the best singlet lithoclass, and solve the multivariate problems accordingly. The best doublet muds sub-lithoclass is assigned to the estimation with the lowest errors.

Similar procedures are followed for triplet, quartet and quintet muds sub-lithoclasses. If, at step X+1, the addition of new facies to the multiplet muds sub-lithoclass does not improve the estimation, then the muds lithoclass subdivision at step X is considered favourable and the procedure stops. As a result, we achieve the optimum multiattribute transforms for the prediction of the sands lithoclass and two muds sub-lithoclasses; the transforms can then be applied to 3D seismic data to make predictions away from wellbores. Depending on the required threshold for prediction efficiency, each sub-lithoclass can also be subdivided using the same approach.

Optimum multiattribute transforms are achieved by limiting seal quality attributes, adding a nonlinear term and applying stepwise regression. Although the transforms are not necessarily the best solutions with the lowest prediction errors, the approach saves an enormous amount of time, results in stepwise refinement of predictions, avoids excessive computation of the contributions of linearly dependent variables, and is more practical than exhaustive regression in terms of real-world hydrocarbon prospectivity studies. In this approach, the maximum number of multivariate regression problems to be solved is $(6+5+4+3+2) \times 5 = 100$ problems, which is 288,605 problems fewer than exhaustive regression analysis.

We note that there are alternative probabilistic approaches to predict log values from seismic attributes, including neural networks (Specht, 1991; Hampson et al., 2001). However, their estimation consistency is strongly dependent on the availability of suitable wireline training sets, which is not often the case in seal analysis.

4.2.3 Prediction of fine-grained logfacies probabilities from estimated muds sub-lithoclasses using Bayesian probability calculations

In the previous step, mathematical models (transforms) were developed to translate seal quality attributes into frequencies of one sand lithoclass and two muds sub-lithoclasses. Each muds sub-lithoclass comprises a group of fine-grained facies which exhibit different flow properties (permeability and capillary entry pressure).

Therefore, the seal flow behaviour may not be directly inferred from a lithology cube with only three lithoclass members. Moreover, we are unable to integrate the current lithology model with log-scale flow properties because the majority of log -scale flow property models (e.g. Costa, 2006; Chehrazi and Rezaee, 2012; Drews, 2012) have been developed for specific sedimentological units (either logfacies or petrofacies). As a result, it is important to elaborate further the multiattribute transforms in order to be able to subdivide the estimated muds sub-lithoclass frequencies into their component facies.

Regarding differences between seismic and log resolution and - more importantly – the low signal content in mud-rich sediment sequences, we believe that seal quality attributes derived from high-density post-stack seismic data, are only able to discriminate between *groups* of fine-grained facies in the seal units. Therefore, further application of MAA cannot robustly and accurately subdivide muds sub-lithoclasses. In order to capture the probability of fine-grained logfacies away from wellbores, there are two possible options which have also been used to predict sub-seismic features in reservoir context: i) post-processing filtration on post-stack seismic data such as Kalman filtering (Sayman, 1992; Rocha et al., 2007) and spectral analysis (Chakraborty and Okaya, 1995; Marfurt and Kirlin, 2001; Sinha et al., 2005; McArdle and Ackers, 2012), accompanied by forward modelling analysis such as wedge models or ii) subdivision of estimated muds sub-lithoclass probabilities into their logfacies components by the use of Bayesian probabilities derived from wellbore data.

Despite the important role of post-processing in the seismic characterisation of mud-rich sediment sequences, there is no significant literature on this topic. Here therefore, in order to keep consistency in the workflow, the Bayes theorem is used to predict logfacies probabilities from estimated muds sub-lithoclasses. Mathematically, the Bayes theorem gives the relationship between the probabilities of A and B, P(A) and P(B) and the conditional probabilities of A given B and B given A, P(A|B) and P(B|A). In this study, P (A) and P (B) are the probability of occurrence of a specific fine-grained log facies and the probability of occurrence of any component of a specific muds sub-lithoclass in the interval of study, respectively. According to the Kolmogorov definition, the joint probability of event A and B can be expressed as an axiom of probability (Lee, 2012):

$$P(A \cap B) = P(A|B) \,.\, P(B) \qquad \text{Equation 4.8}$$

$$= P(B|A) \,.\, P(A) \qquad \text{Equation 4.9}$$

Values of P(A|B) are calculated from logfacies recognition results in seal intervals within all pilot study wellbores, whereas values of P(B) were seismically derived in step II by the use of multiattribute transforms. In other words, according to Equation 4.8, well-based conditional probabilities of facies, P(A|B), can be incorporated into the multiattribute transforms as coefficients in order to be able to predict the probability of occurrence of individual fine-grained facies. In this way, we end up with six multiattribute transforms corresponding to six fine-grained facies and one multiattribute transform to predict the sand lithoclass. Since there are considerable limitations in seismic resolution and wireline availability within the seal context, we hierarchically used seismic and log data to avoid augmenting uncertainties in lithology predictions due to single source application.

In geostatistics, our derived probabilistic mathematical relationships are called likelihood functions. Doyen et al. (1994) suggest calibrating the likelihood functions with an *a priori* model generated by Sequential Indictor Simulation (SIS). SIS is a variogram-based facies modelling which can generate a facies model conditioned to both seismic and log data, but it is not effective in capturing realistic architectures (Strebelle, 2000, 2002), particularly within seal units. This is because of the limitations of two-point statistics in modelling curvy textures (e.g. debris flow facies) and long-range continuous bodies (e.g. *Hemipelagic Shales*). It can be even more problematic, since well data are very sparse in seal sections. Moreover, the poor delineation of facies architecture in an SIS a priori model places major constraints on the construction of a conditioned facies model, because the seal likelihood functions are derived from the correlation of seismic textures and facies. On the other hand, object-based facies models (Lia et al., 1996; Viseur, 1999) are able to honour the geometries involved in the seal units, but are still unable to integrate seismically-derived seal likelihood functions.

There is ongoing research to improve the traditional geostatistical simulation and solve the problem of facies architecture modelling while keeping the integration of a priori models with soft constraints (i.e. likelihood functions). For example, in multiple-point statistics (MPS) simulations (Guardiano and Srivastava, 1993;

Strebelle, 2000, 2002; Strebelle and Levy, 2008) the facies are modelled based on multi-point statistics moments (with order higher than two, unlike traditional two-point variography) derived from a training 3D conceptual model. The multi-point statistics moments allow us to better capture nonlinear or long-range facies geometries. The other innovative approach is event-based facies modelling which benefits from nonstationary statistics and conditions facies models by interactive rules developed through the analysis of relationships between texture and reservoir. Pyrcz et al. (2012) successfully applied the method on complex channel context with sparse well data setting. Despite the promising development in conditional facies simulation, the methods mostly address issues specific to the architectures of siliciclastic reservoirs such as channels and levees. Therefore, we recommend the application of MPS and event-based conditional facies simulation in mud-rich seal environment for further studies, since having a reliable a priori model is essential for calibrating seal likelihood functions and generating realistic seal lithology models in sparse data settings.

4.3 Data

Similar to Chapter 3, the developed probabilistic facies prediction methodology is demonstrated on regional seal unit 4, in West Africa case study. The interval of study covers both seismic facies, i.e. hemipelagite 4 and MTD 4. Although 11 wells are available in the case study, we only use three of them: W31, W41 and W42. This is because they have reliable seal facies recognition results to integrate with the seismic analysis. The reliability of the facies recognition results from their complete conventional log suite (gamma-ray, p-sonic, density and neutron porosity) in both seal and reservoir intervals, and also the availability of reservoir cores to train the facies recognition algorithm. The other wells suffer either from a shortage of wireline data within the seal interval or core data for training, or both.

4.4 Results

The methodology is applied on a high-density seismic cube from offshore West Africa. The interval of study is a lower Miocene (Aquitanian) heterogeneous mud-rich deposit, the so-called seal unit 4. Seal unit 4 is relatively flat and extends laterally throughout the seismic cube. On average, the top of seal unit 4 is located at

a depth of around 2257 mbsl (2839 TWT ms/msl) with a thickness of 195 m (178 TWT ms). It has a heterogeneous seismic texture with low to moderate seismic amplitudes (-1000<amplitude<1000). The upper part of seal unit 4 contains relatively flat and continuous reflections, whereas a great proportion of chaotic textures occur within the lower part. Whilst these textures correspond to the interpreted Hemipelagite 4 and MTD 4 seismic facies, there are several non-conforming anomalies within these seismic facies that may impact seal risk. The objective is here to find statistical relationships between the seal quality seismic attributes and the fine-grained logfacies and to use multiattribute transforms as an automated tool to predict lithology variations within seal unit 4.

4.4.1 Derivation of the initial likelihood functions for the sands and muds lithoclasses

Each well contains several sets of logfacies within seal unit 4 interval, which differ according to input logs and detrending method used for their recognition. In Chapter 2, three approaches resulted in good fits with core descriptions at wells W31, W41 and W42: a) recognition with detrended total neutron-porosity (PHIT) log, b) recognition with detrended bulk density (RHOB) log and c) recognition with no detrending of input logs. Although the fit to core descriptions is similar in each case (Chapter 2), the recognition results have different spatial distributions within seal unit 4. We therefore first investigate the effect of log detrending on the recognition of fine-grained facies and their subsequent fit with seismic seal quality attributes. This is because we believe that standard log detrending approach may diminish or remove variations in log responses within seal intervals, which are usually subtle (Section 4.2.1). Figure 4.4 shows three sets of logfacies recognition along the wells within the Seismic SRF sections. Note that well W31 is not crossing the seal unit-4 and an equivalent fine-grained depth-interval is used as an analogue for seal unit-4. The Seismic SRF volume has been generated using the *Volumetric Attributes* tool in Petrel and according to equations in Table 3.9 and recommended parameters in Chapter 3. Note that the range of Seismic SRF colorset is deliberately kept wide in order to discriminate better seal unit 4 and reservoir intervals.

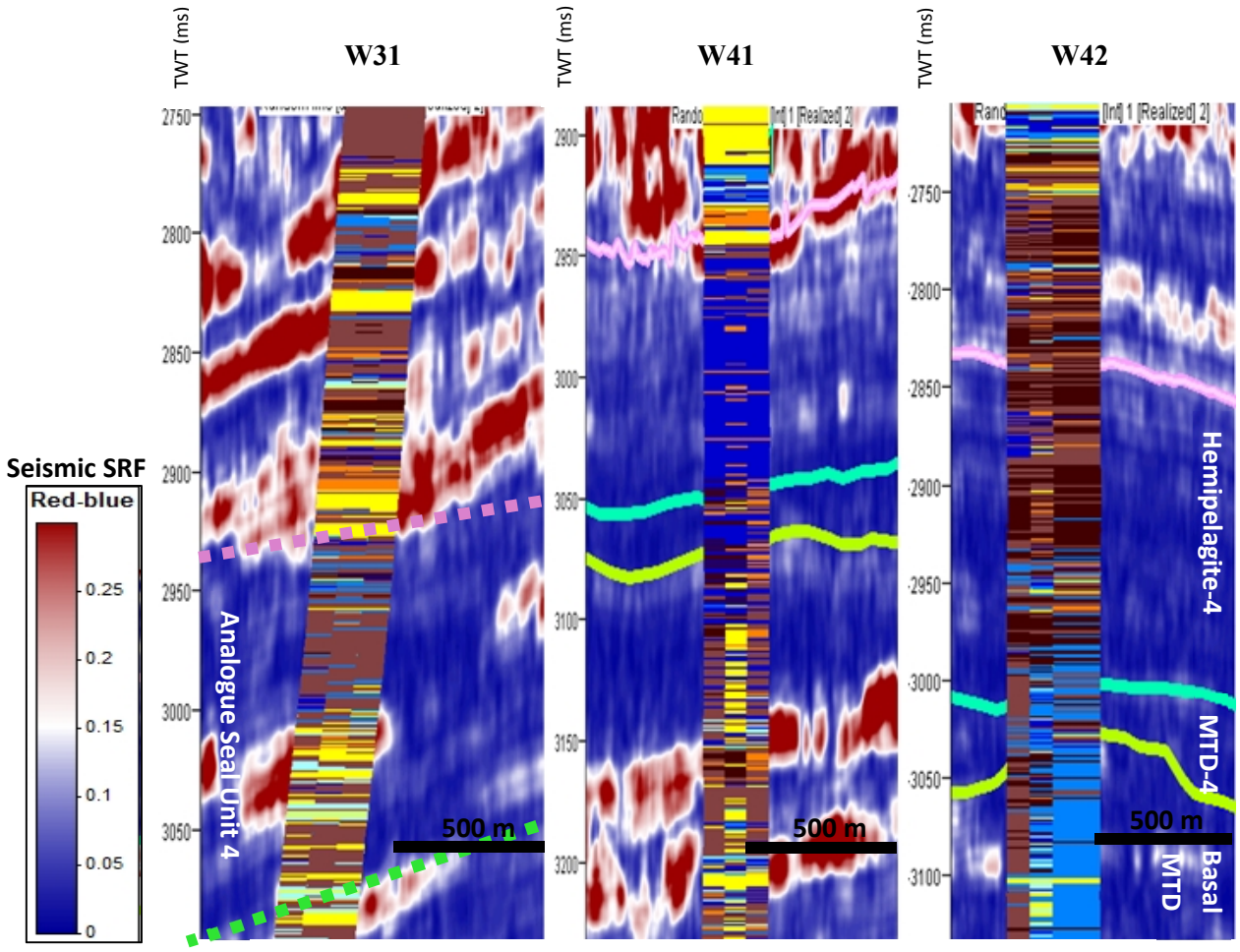

Figure 4.4: *Comparison of Seismic SRF-logfacies fit for three different logfacies recognitions within seal unit 4 of well W31 (analogue interval), W41 and W42. Recognitions from left to right: recognition with detrended PHIT log, recognition with detrended RHOB log, recognition with no log detrending. Logfacies recognitions without detrending display the better fit with Seismic SRF. Red and blue colours indicate the higher and lower Seismic SRF (seismic-derived leakage risk)*

Facies No.	Facies Name	Colour
1	Hemipelagic Shales	
2	Mud Turbidites UP	
3	Mud Turbidites LP	
4 – 11, 15-16	Sands	
12	Muddy Debris Flow	
13	Muddy-Sandy Debris Flow	
14	Sandy Debris Flow	

Qualitative inspection shows that the logfacies recognition using the detrended PHIT log unrealistically predicts more *Hemipelagic Shales* and *Mud Turbidites* within MTD-4 and basal MTD intervals (the intermediary deposits between seal unit 4 and lower reservoir) at W41 and W42. Moreover, the logfacies recognition using the detrended RHOB log also predicts highly sand dominated MTD-4 and basal MTD at W41, which is not consistent with their low seismic

amplitude/SRF. These observations are in contrast with the result of logfacies recognition with non-detrended logs where logfacies show a consistent agreement with the interpreted seismic facies at W41 and W42. Therefore, we qualitatively expect a better correlation between Seismic SRF (or other seal quality component attributes) and logfacies from non-detrended logs at wells W41 and W42.

At well W31, the difference between recognition results within the analogue seal interval is subtle, so that a quantitative approach has been taken to compare how they agree with the Seismic SRF attribute. This has been done through conventional cross-plot analysis. We have firstly calculated the logfacies frequencies from each recognition within the analogue seal unit 4 interval in well W31 (Table 4.2). Table 4.2 shows that relatively similar amounts of logfacies have been predicted in all three recognitions; however, their vertical distributions are slightly different. As explained in Section 4.2.1.1, at this step six fine-grained logfacies have been grouped into a single mud lithoclass due to limited fitting capability of univariate regression in conventional cross-plotting.

Table 4.2: *Logfacies frequencies (%) at analogue seal unit 4 interval in well W31, derived from three different recognitions in Chapter 2.*

Logfacies	Logfacies frequencies% within analogue seal unit 4 interval in well W31		
	Recognition with PHIT-detrended	Recognition with RHOB-detrended	Recognition with no log detrending
Hemipelagic Shales	6.03	4.68	4.25
Mud Turbidites UP	55.11	54.89	55.84
Mud Turbidites LP	4.33	5.38	4.11
Sands	16.71	19.33	18.38
Muddy Debris Flow	4.36	2.47	3.75
Muddy-Sandy Debris Flow	5.28	6.17	5.50
Sandy Debris Flow	8.17	7.09	8.17

On the other hand, composite traces of seismic amplitude and SRF have been extracted from their corresponding seismic attribute volumes along the trajectory of well W31. This was done by averaging the nine nearest traces around the borehole. Then lithology logs (logfacies recognition) were converted from depth to time using check-shot data and vertically averaged at the pick-trough time interval scale according to the timing of successive peaks and troughs in the amplitude composite trace. The same vertical averaging was performed on Seismic SRF composite trace to obtain similar sampling rates as the lithology logs.

We plotted seismic attribute values against logfacies frequencies. Figures 4.5 and 4.6 show cross-plots of mud and sand lithoclass frequencies against Seismic SRF values in well W31 for each of the three logfacies recognitions. In both muds and sands cross-plots, recognition with non-detrended logs has the highest coefficients of determination (R-squared), and thus indicates a better correlation with the Seismic SRF values. The same cross-plot analysis was repeated for the Reflection Intensity attribute and also for the two other wells and their correlation results are shown in Table 4.3. In all these cases, R-squared values affirm better seismic attribute-logfacies correlations when using the recognition with non-detrended logs. In addition, the outcome of cross-plot analysis agrees with the visual inspection at W41 and W42. Comparison between R-squared values also illustrate that Seismic SRF is a more effective predictor of mud lithoclass frequencies (because of contribution of structural and stratigraphic attributes), whereas Reflection Intensity can better delineate sand lithoclass frequencies.

In summary, both qualitative and quantitative comparisons of seismic attributes and logfacies illustrate that the conventional log detrending approach should not be applied for logfacies recognition within seal unit 4 because variations in log responses are subtle and can be unrealistically diversified or smoothed by detrending. In addition, there are reasonable linear relationships between mud/sand lithoclass frequencies and Seismic SRF and Reflection Intensity. In other words, more risky seismic intervals contain higher percentages of sand lithoclass and vice versa (Figure 4.7). Therefore, as the initial likelihood functions, we expect the Seismic SRF attribute to give relatively reliable predictions of sandiness within seal

unit 4 away from wellbores. Above all, these univariate relationships also support the next step - multivariate analysis.

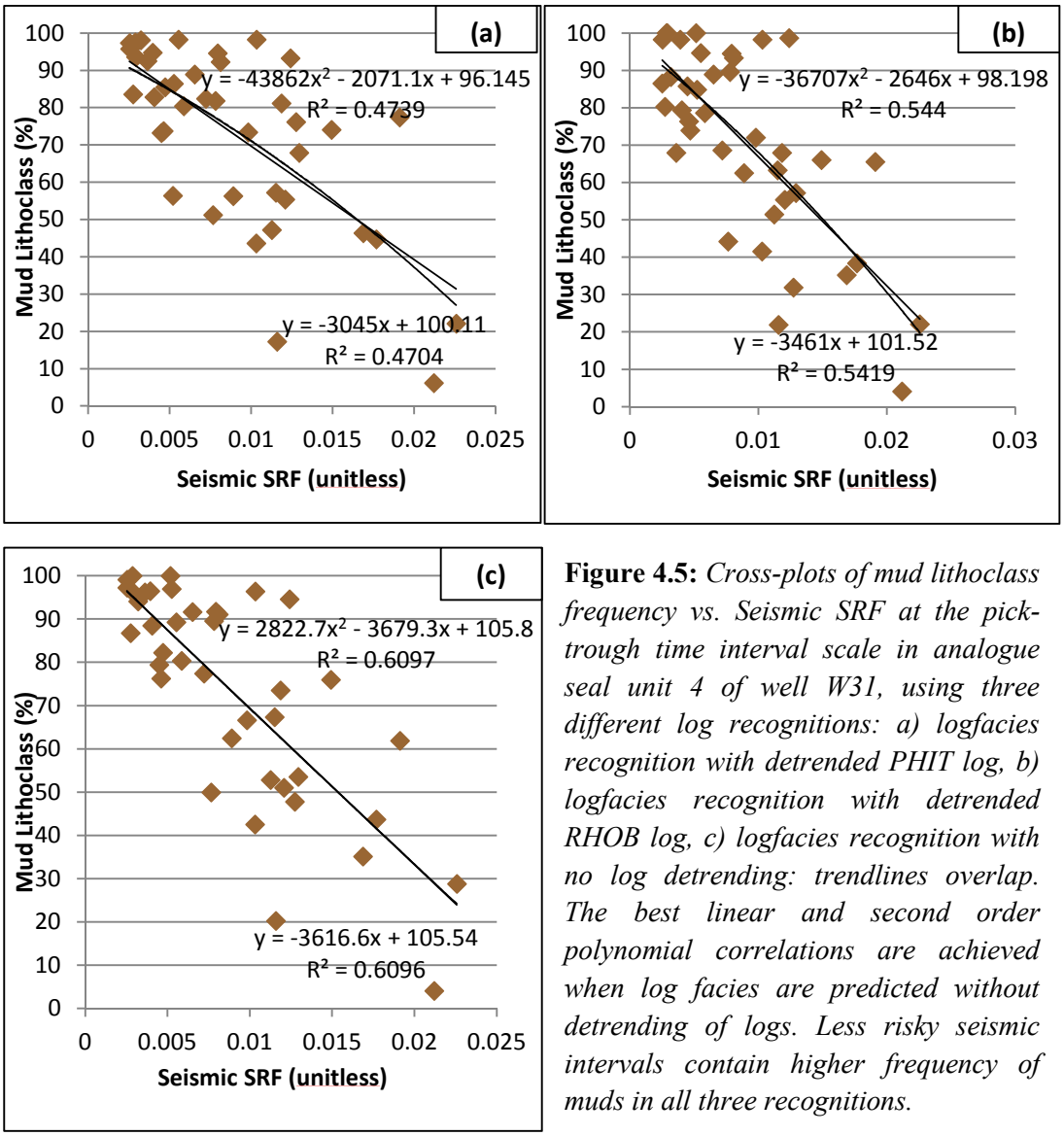

Figure 4.5: *Cross-plots of mud lithoclass frequency vs. Seismic SRF at the pick-trough time interval scale in analogue seal unit 4 of well W31, using three different log recognitions: a) logfacies recognition with detrended PHIT log, b) logfacies recognition with detrended RHOB log, c) logfacies recognition with no log detrending: trendlines overlap. The best linear and second order polynomial correlations are achieved when log facies are predicted without detrending of logs. Less risky seismic intervals contain higher frequency of muds in all three recognitions.*

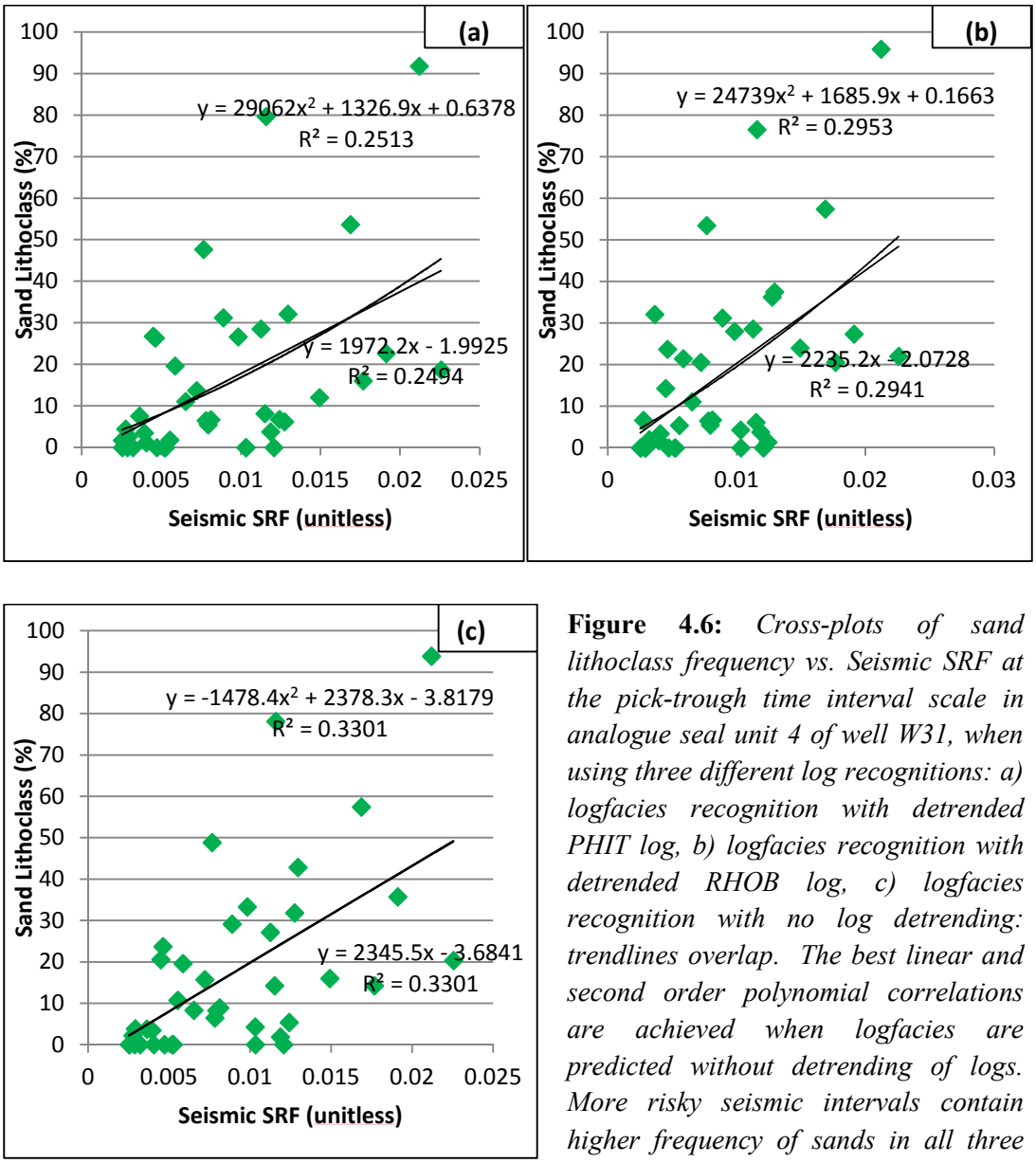

Figure 4.6: *Cross-plots of sand lithoclass frequency vs. Seismic SRF at the pick-trough time interval scale in analogue seal unit 4 of well W31, when using three different log recognitions: a) logfacies recognition with detrended PHIT log, b) logfacies recognition with detrended RHOB log, c) logfacies recognition with no log detrending: trendlines overlap. The best linear and second order polynomial correlations are achieved when logfacies are predicted without detrending of logs. More risky seismic intervals contain higher frequency of sands in all three recognitions.*

Table 4.3: *R-squared (R^2) values of univariate linear regression between frequencies (%) of muds/sands lithoclasses and Seismic SRF/Reflection Intensity in seal unit 4 at wells W31, W41 and W42*

Seismic Attribute	Well	PHIT-Detrended		RHOB-Detrended		No Log Detrending	
		Muds R^2	Sands R^2	Muds R^2	Sands R^2	Muds R^2	Sands R^2
Reflection Intensity	W31	0.37	0.28	0.50	0.37	0.55	0.41
	W41	0.51	0.37	0.46	0.29	0.58	0.43
	W42	0.49	0.25	0.45	0.31	0.51	0.35

Seismic SRF	W31	0.47	0.25	0.54	0.30	0.61	0.33
	W41	0.53	0.26	0.51	0.21	0.63	0.37
	W42	0.48	0.22	0.51	0.25	0.55	0.30

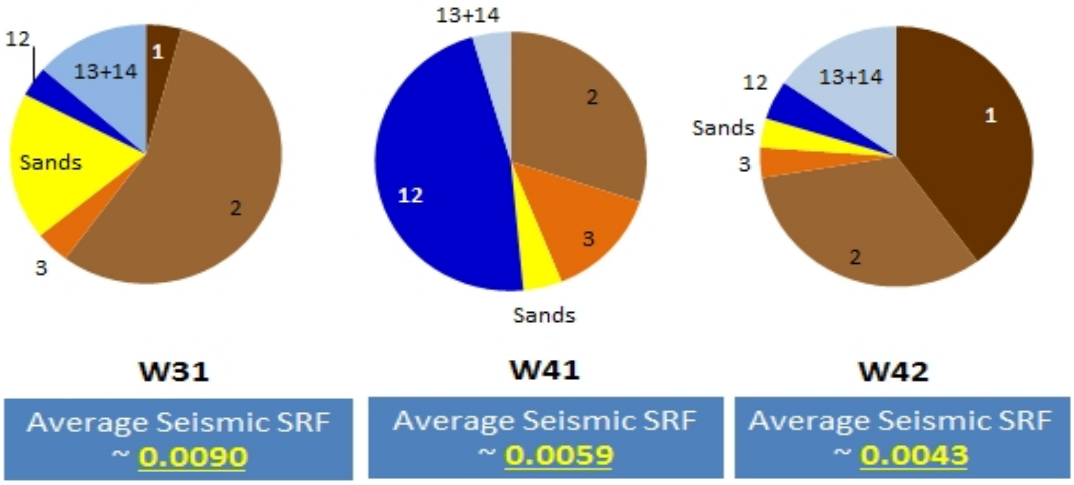

Figure 4.7: *Relationship between overall facies distribution and average Seismic SRF within seal unit 4 at wells W31, W41 and W42. Average Seismic SRF in seal unit 4 shows a direct relationship with the frequency of coarser-grained facies i.e. sand lithoclass and debris flow facies of 12, 13 and 14.*

Facies No.	Facies Name	Colour
1	Hemipelagic Shales	
2	Mud Turbidites UP	
3	Mud Turbidites LP	
4 – 11, 15-16	Sands	
12	Muddy Debris Flow	
13	Muddy-Sandy Debris Flow	
14	Sandy Debris Flow	

4.4.2 Prediction of the muds sub-lithoclasses using forward stepwise multivariate regression

Knowing the univariate correspondence between muds lithoclass frequency and Seismic SRF attribute, we have attempted to translate Seismic SRF into muds sub-lithoclass frequencies through the use of multivariate analysis. Note that the prediction of six individual fine-grained logfacies from seismic quality attributes is not feasible due to the limitations of seismic resolution. The seal quality attributes available for the multiattribute analysis consist of ten volumetric attributes classified into three groups (Table 3.8) plus the Seismic SRF attribute. To avoid overtraining and excessive calculations of linearly dependent attributes, only the representative attribute of each group has been considered, thus we have reduced the number of attributes to four: Reflection Intensity, Chaos, PCA-based Local Structural Dip and SRF.

The multiattribute analysis consists of utilising forward stepwise regression at the pick-trough time interval scale as described earlier in Section 4.2.2. The average of calculated pick-trough time intervals at W31, W41 and W42 are 8.4 ms, 7.9 ms and 8.2 ms. The interval size is a function of the dominant seismic frequency within the seal interval at each well location and is thus proportional to the rate of vertical sedimentological variation. The systems of equations have been solved by use of computer programming at seal unit 4 of W31, W41 and W42 which returned ordinary least-squares solutions (OLS) given a known covariance. The results are shown in Tables 4.4 and 4.5, and give two types of prediction error: the average relative absolute error (%) and the average of relative absolute error and OLS standard error (%) (Equation 4.5). In the first columns, the average of prediction errors for each single facies and its complementary muds sub-lithoclass has been given. At the first step, *Mud Turbidites UP* and its corresponding complementary muds sub-lithoclass possess the best seismic quality attribute fit with average prediction errors of 49.5% and 42.5%. As we go to the right, the error values in the columns show how integrating logfacies at each step influences the prediction error of the best muds sub-lithoclass in the previous step. Therefore, in step 2, the results indicated that OLS error is reduced by integrating *Mud Turbidites UP* and *Mud Turbidites LP*, and similarly in step 3 by adding *Muddy Debris Flow* to their combination. The process is stopped at the point where an increasing number of logfacies decreases the prediction efficiency (i.e. step 3).

Table 4.4: *Average of overall relative absolute error (%) for prediction of two divided muds sub-lithoclasses at different steps of forward multivariate regression. The process stops at step 3 due to increment of average relative absolute error in the fourth step.*

Logfacies	**Average relative absolute error (%) for two divided muds sub-lithoclasses**				
	Primary muds sub-lithoclasses				
	Step 1: singlet	**Step 2: doublet**	**Step 3: triplet**	**Step 4: quartet**	**Step 5: quintet**
Hemipelagic Shales	74.9	54.7	58.1	64.5⊗	
Mud Turbidites UP	**49.5**				
Mud Turbidites LP	56.5	**49.9**			
Muddy Debris Flow	72.4	53.8	**48.3**		
Muddy-Sandy Debris Flow	72.1	50.7	52.1	65.0⊗	

Sandy Debris Flow	73.9	51.3	52.0	68.4⊗	

Table 4.5: *Average of overall relative absolute error and OLS standard error (%) for prediction of two divided muds sub-lithoclasses at different step of forward multivariate regression. Again the process stops at step 3 and similar classification for muds sub-lithoclasses is obtained.*

Logfacies	**Average of relative absolute error and OLS standard error (%)**				
	Primary muds sub-lithoclasses				
	Step 1: singlet	**Step 2: doublet**	**Step 3: triplet**	**Step 4: quartet**	**Step 5: quintet**
Hemipelagic Shales	76.9	43.5	47.8	70.5⊗	
Mud Turbidites UP	**42.5**				
Mud Turbidites LP	73.4	**41.9**			
Muddy Debris Flow	75.4	44.4	**39.8**		
Muddy-Sandy Debris Flow	89.6	42.7	44.7	62.0⊗	
Sandy Debris Flow	106.2	44.0	45.2	61.2⊗	

The stepwise multiattribute analysis illustrates that a combination of *Mud Turbidites LP/UP facies* with *Muddy Debris Flow facies* gives the lowest prediction errors of 48.3% and 39.8%. In other words, the four seal quality attributes can better discriminate between two muds sub-lithoclasses in seal unit 4 as defined below:

Muds Sub-lithoclass I: Mud Turbidites UP+Mud Turbidites LP+Muddy Debris Flow

Muds Sub-lithoclass II: Hemipelagic Shales+Muddy Sandy Debris Flow+Sandy Debris Flow

This classification is also consistent with the seismic characters of the logfacies within seal unit 4. As shown in Figure 4.8, the facies of muds sub-lithoclass II typically occur within poor/moderate amplitude, chaotic seismic contexts in seal unit 4, whereas the facies of muds sub-lithoclass I often occur within moderate amplitude, layered seismic textures. In terms of seismic character, we have therefore called muds sub-lithoclasses I and II *non-distorted* and *distorted muds*, respectively. Note that *Hemipelagic Shales* have been recognised in the intervals in which seismic is at its lowest amplitude and a chaotic texture (contrary to the geologically layered structures of hemipelagites). This is likely due to the seismic frequency limit, and the subtle and rapid changes in acoustic impedances within these sediments.

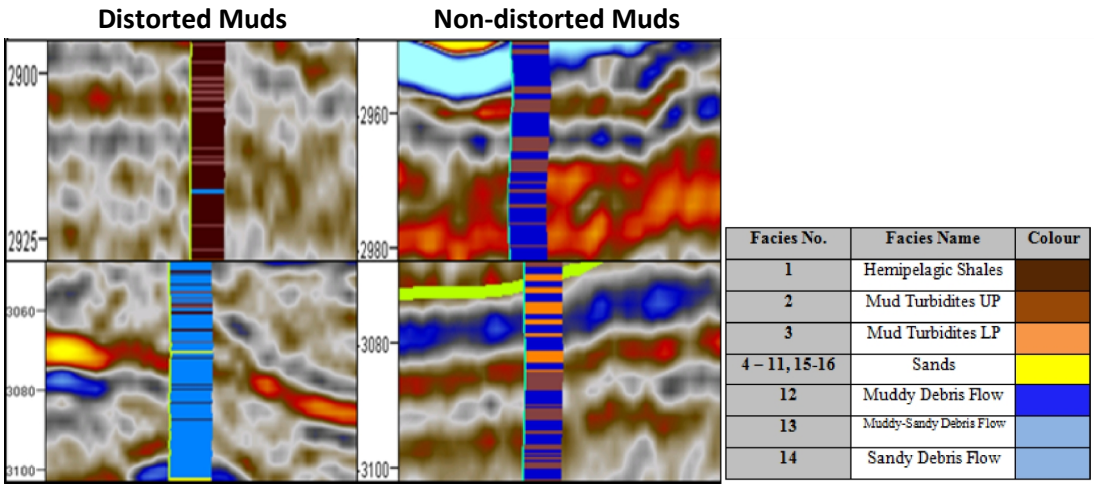

Figure 4.8: *Comparison of muds sub-lithoclass classification derived from multivariate analysis with seismic characters. Non-distorted muds often occur within moderate amplitude, layered seismic textures in seal unit 4 and vice versa for distorted muds.*

According to the OLS solutions of the multivariate analysis, the frequencies of distorted, non-distorted muds and sands can be predicted as linear combinations of the four seal quality attributes with known coefficients and an intercept. The derived multiattribute transforms based on seal unit 4 of W31, W41 and W42 are as follows:

Non-distorted Muds%= -1.13 **SI** - 12.39**SC**+0.8**LD** - 452.87 **SRF**+60.06 Equation 4.10a

Distorted Muds%= -2.61 **SI** + 22.11 **SC** - 0.69 **LD** - 783.41 **SRF** + 43.09 Equation 4.10b

Sands%= 3.74 **SI** - 9.72 **SC** - 0.11 **LD** + 1236.28 **SRF** - 3.15 Equation 4.10c

where SI, SC, LD and SRF are Reflection Intensity, Chaos, PCA-based Local Structural Dip and Seal Risk Factor, respectively (Chapter 3). We interpret the formulae to mean that the frequency of non-distorted muds is directly proportional to Seismic SRF or leakage risk and vice versa for distorted-muds and sands. The predictions of the multiattribute transforms in seal unit 4 of W31 and W41 are displayed graphically in Figure 4.9, in which measured frequencies of lithoclasses are shown as dotted lines and predicted frequencies as solid lines. The generally good agreement between measured and predicted values suggests a promising predictive power of the seal quality attributes for a more detailed discrimination of lithologies in seal unit 4 when using the multivariate approach. However, it also shows that seismic data has a very limited capability to predict (a) isolated log-scale lithological variations (here ~ < 10 m) and (b) lithologies with small contributions to

the total section (e.g. distorted muds in well 41). In summary, multivariate analysis using the four seal quality attribute predictors has enabled us to make reasonable predictions of the percentages of three lithology groups in seal unit 4.

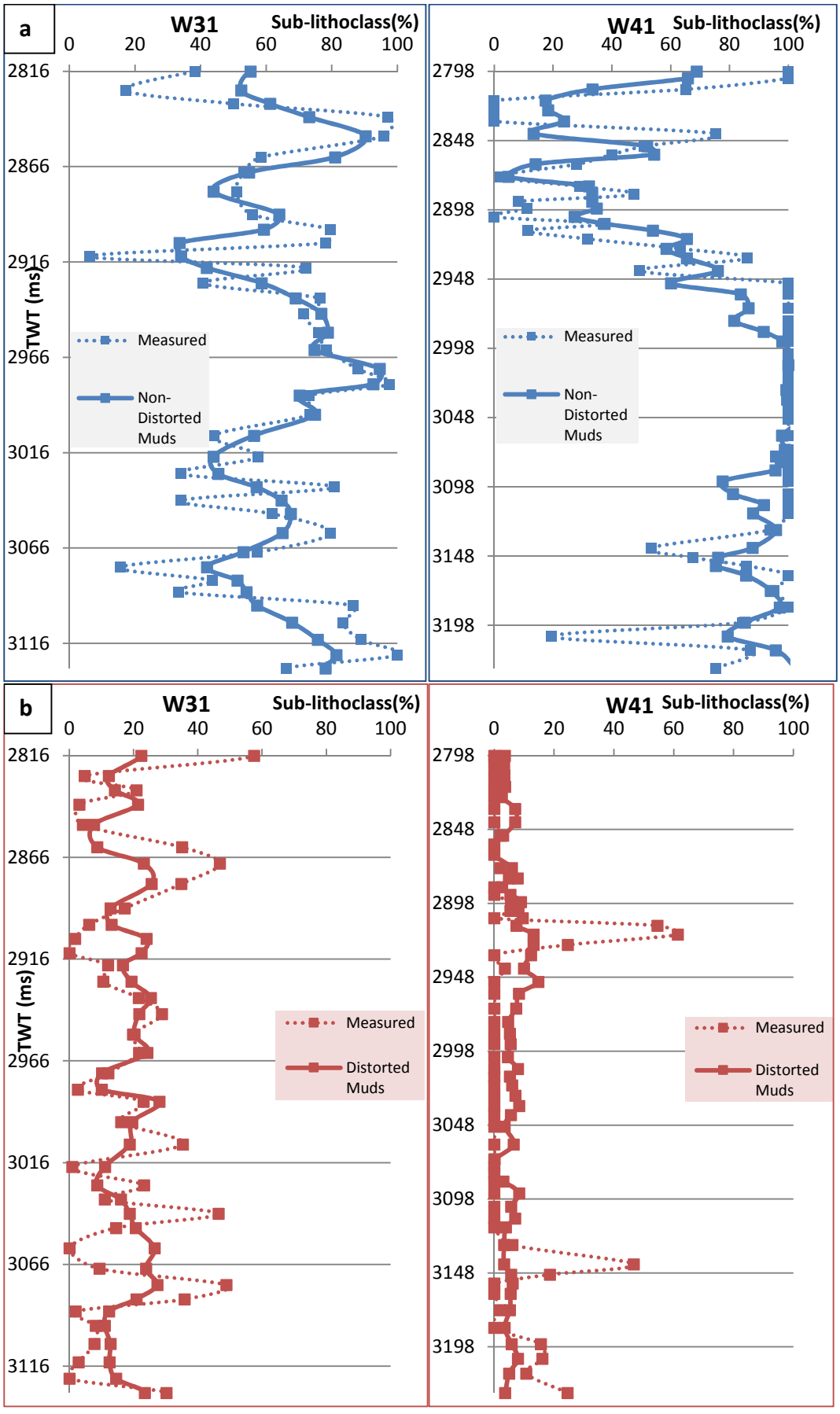
a
W31
Sub-lithoclass(%)
0
20
40
60
80
100
2816
2866
2916
2966
3016
3066
3116
TWT (ms)
Measured
Non-Distorted Muds
W41
Sub-lithoclass(%)
2798
2848
2898
2948
2998
3048
3098
3148
3198
b
Distorted Muds

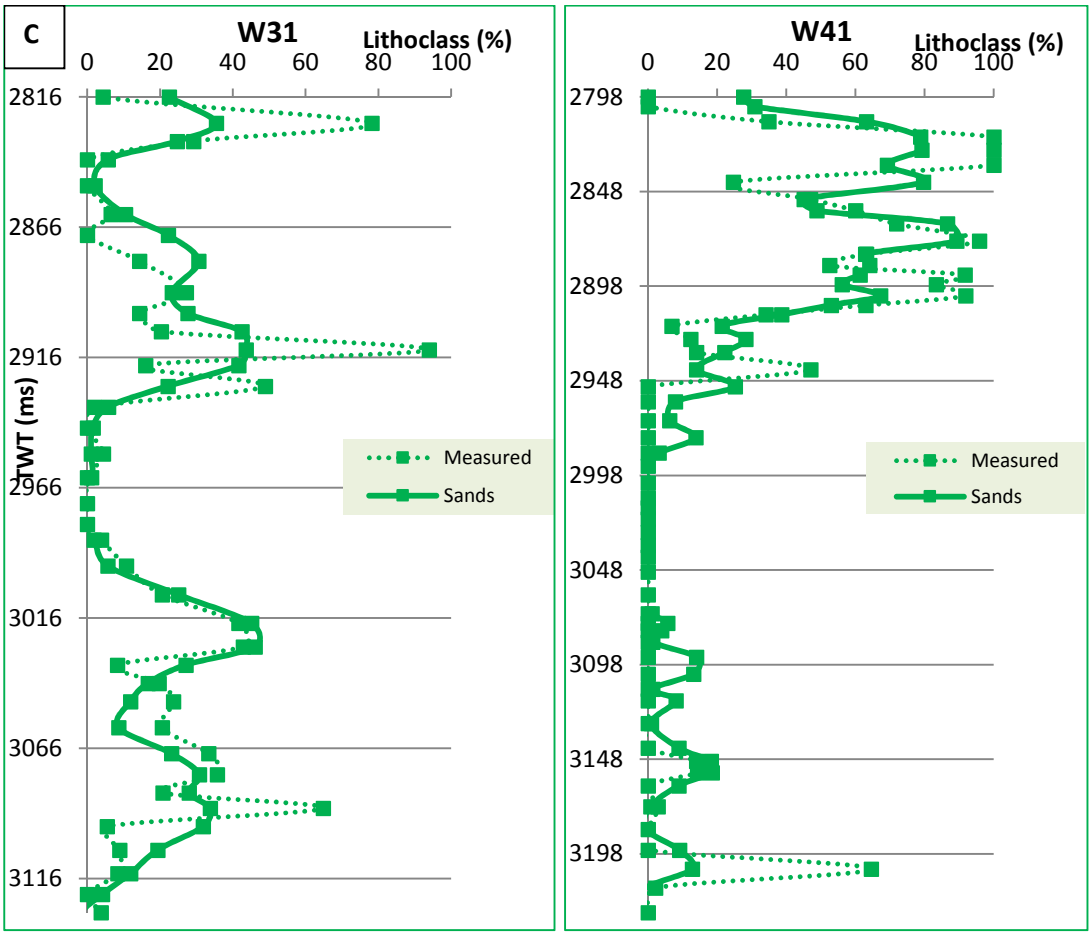

Figure 4.9: *Prediction of muds sub-lithoclass frequencies based on the developed multiattribute transforms (Equations 4.10) in wells W31 and W41: a) non-distorted muds, b) distorted muds and c) sands. The predicted and measured frequencies are shown as solid and dotted lines, respectively. The multiattribute transforms were derived according to stepwise multivariate regression between four seismic seal quality attributes and non-detrended logfacies recognitions at the pick-trough time interval scale within seal unit 4 in wells W31, W41 and W42.*

4.4.3 Bayesian division of the muds sub-lithoclasses by honouring well data statistics

Since the facies in the muds sub-lithoclasses have different flow/sealing properties, we have tried to divide the muds sub-lithoclasses into their component facies (as illustrated in Figure 4.10) by applying Bayesian probabilities derived from the well data. Bayesian division of the muds sub-lithoclasses consists of calculating conditional probabilities of component facies at different ranges of muds sub-lithoclass frequencies (Equation 4.8). The derived conditional probabilities (P(A|B)) have been multiplied by predicted muds sub-lithoclass frequencies (P(B)) (calculated in Section 4.4.2), to obtain probabilistic frequencies of component facies (P(A∩B))

at each interval. As described in Section 4.2.3, probabilities P(A|B) have been directly derived from the logfacies recognition results in wells W31, W41 and W42 and are shown in Tables 4.6 and 4.7. The second column, for example, shows the probabilities of occurrence of *Mud Turbidites UP* facies having predicted different ranges of non-distorted muds from the seal quality attributes. On the right side of the Tables, relative standard deviations of conditional probabilities, σ(P(A|B)), are given at each interval. Assuming a proper sample space for Bayesian calculation, σ(P(A|B)) can represent the measure of uncertainty in our conditional probabilities. As expected, the Bayesian division gives much more reliable results for non-distorted muds. The average relative standard deviation for non-distorted muds is 12.1%, while for distorted muds is 32.2%. Moreover, the facies of neither non-distorted muds nor distorted muds show meaningful trend/relationship with variations in sub-lithoclass frequencies. In other words, the component facies within both sub-lithoclasses maintain relatively consistent proportions throughout the intervals, within an average standard deviation of 11%. This consistent facies distribution in seal unit 4 further supports the use of Bayesian calculations.

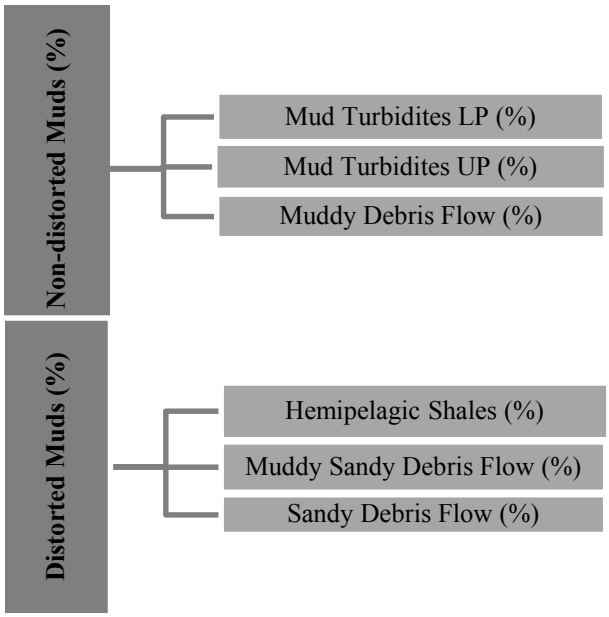

Figure 4.10: *Overview of component facies for the two muds sub-lithoclasses: Bayesian probabilities were utilised to divide muds sub-lithoclasses predictions (derived from multivariate analysis, Section 4.4.2) to their component facies.*

Table 4.6: *Bayesian (conditional) probabilities P(A|B) derived for component facies of non-distorted muds at different ranges of sub-lithoclass frequencies (event B); P(A|B)s are based on distributions of facies from non-detrended logfacies recognitions within seal unit 4 in wells W31, W41 and W42.*

Non-distorted muds						
B: Non-distorted muds range %	**P(A|B) %**			**σ (P(A|B)) %**		
	Mud Turbidites UP	**Mud Turbidites LP**	**Muddy Debris Flow**	**Mud Turbidites UP**	**Mud Turbidites LP**	**Muddy Debris Flow**
95-100	28.0	13.1	58.9	29.6	15.6	32.2
90-95	84.0	4.1	11.9	14.1	6.3	9.7
85-90	92.8	0.5	6.8	2.6	0.5	2.1
80-85	70.1	18.3	11.6	26.2	25.3	15.8
75-80	79.5	17.3	3.2	23.1	24.9	3.0
70-75	86.7	8.4	5.0	15.2	12.2	3.8
65-70	82.5	4.4	13.1	6.7	3.4	10.0
60-65	61.7	6.7	31.7	28.1	7.6	26.1
55-60	85.0	8.4	6.7	11.2	7.6	9.4
50-55	76.9	2.9	20.1	22.2	3.2	20.6
45-50	66.8	18.3	14.9	22.4	7.1	18.2
40-45	91.3	8.7	0.0	4.3	4.3	0.0
35-40	78.9	12.5	8.6	3.9	12.5	8.6
30-35	96.5	3.5	0.0	5.0	5.0	0.0
Average	77.2	9.1	13.7	15.3	9.7	11.4
				12.1		

Table 4.7: *Bayesian (conditional) probabilities P(A|B) derived for component facies of distorted muds at different ranges of sub-lithoclass frequencies (event B); P(A|B)s are based on distributions of facies from non-detrended logfacies recognitions within seal unit 4 in wells W31, W41 and W42.*

Distorted muds						
B: Distorted muds range %	**P(A|B) %**			**σ (P(A|B)) %**		
	Hemipelagic Shales	**Muddy Sandy Debris Flow**	**Sandy Debris Flow**	**Hemipelagic Shales**	**Muddy Sandy Debris Flow**	**Sandy Debris Flow**
30-35	21.8	17.1	61.1	37.8	12.3	37.3
25-30	13.3	49.3	37.3	18.9	40.8	44.6
20-25	-	41.4	58.7	0.0	38.4	38.4
15-20	9.6	59.2	31.3	12.0	32.5	35.5
10-15	18.3	46.6	35.1	36.7	31.1	30.2
5-10	3.1	33.6	63.3	5.9	37.4	41.1
0-5	18.1	35.4	46.5	33.0	42.0	46.3
Average	14.0	40.4	47.6	24.0	33.5	39.1
				32.2		

Figure 4.11 shows graphically the result of applying the Bayesian probabilities within seal unit 4 of wells W31 and W41. The thicker curves are muds sub-lithoclass frequencies predicted by stepwise multivariate analysis and the other curves represent Bayesian frequencies of component facies. The *Mud Turbidites UP* facies dominates throughout the most of seal unit 4 at W31, but makes a high contribution only in the lower part of seal unit 4 (i.e. basal MTD) at W41. At W31, there is a greater proportion of the *Hemipelagic Shales* facies in the upper part of the seal interval (i.e. hemipelagite 4) while *Sandy Debris Flow* and *Muddy Sandy-Debris Flow* facies prevail in the lower parts (i.e. MTD 4 and basal MTD). Table 4.8 also shows average relative absolute errors for the Bayesian prediction results at these two wells. Similar to Section 4.4.2, smaller contribution of distorted muds in seal unit 4 decreased the reliability of prediction results (with average relative absolute error: 54.8%). Thereby, with current sample space (seal unit 4), we do not recommend use of Bayesian calculations for prediction of component facies frequencies in non-distorted muds and stay with sub-lithoclass frequencies derived from multivariate analysis. Despite the high degree of uncertainty for prediction of component facies in distorted muds, prediction efficiency significantly improved for non-distorted muds and average relative absolute error is reduced from 40.2% (multivariate analysis, Section 4.4.2) to 17.1% (Bayesian division, 4.4.3).

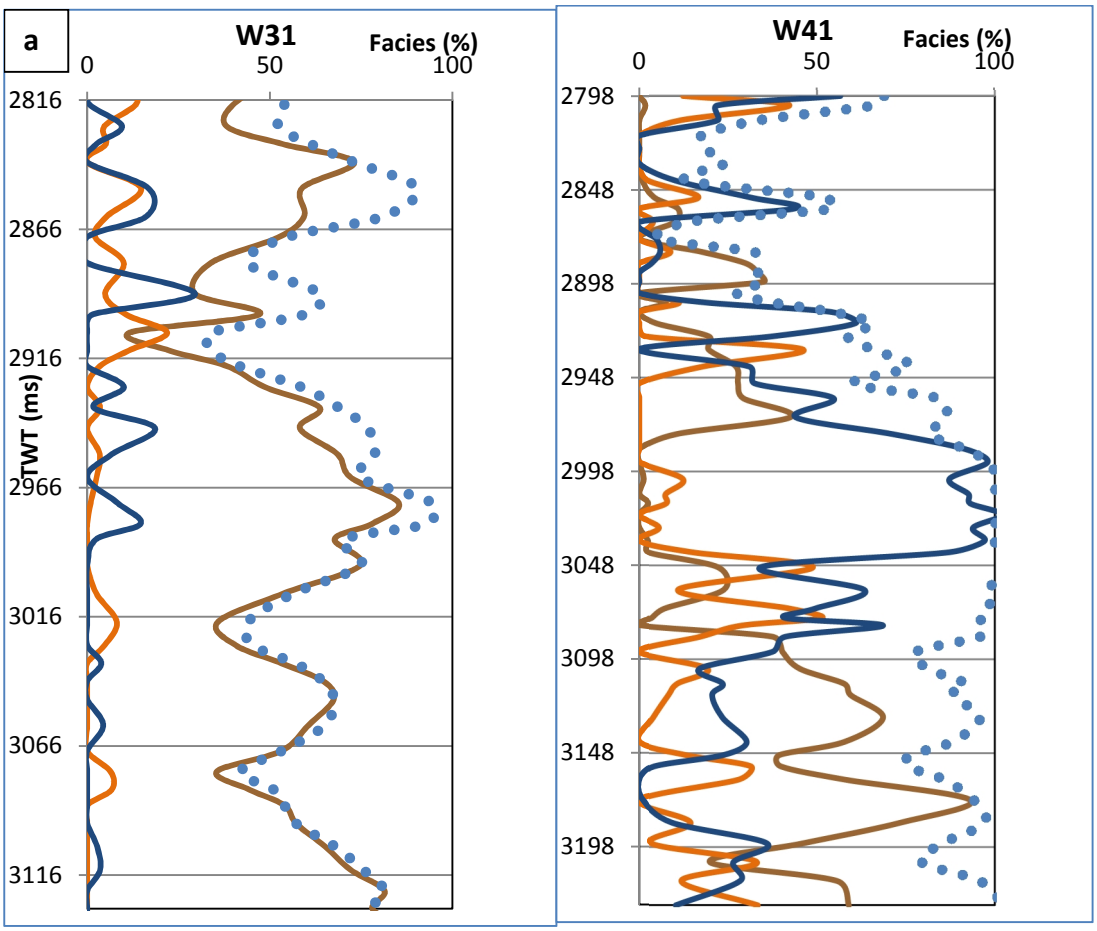
a
W31
Facies (%)
0
50
100
TWT (ms)
2816
2866
2916
2966
3016
3066
3116
W41
Facies (%)
0
50
100
2798
2848
2898
2948
2998
3048
3098
3148
3198

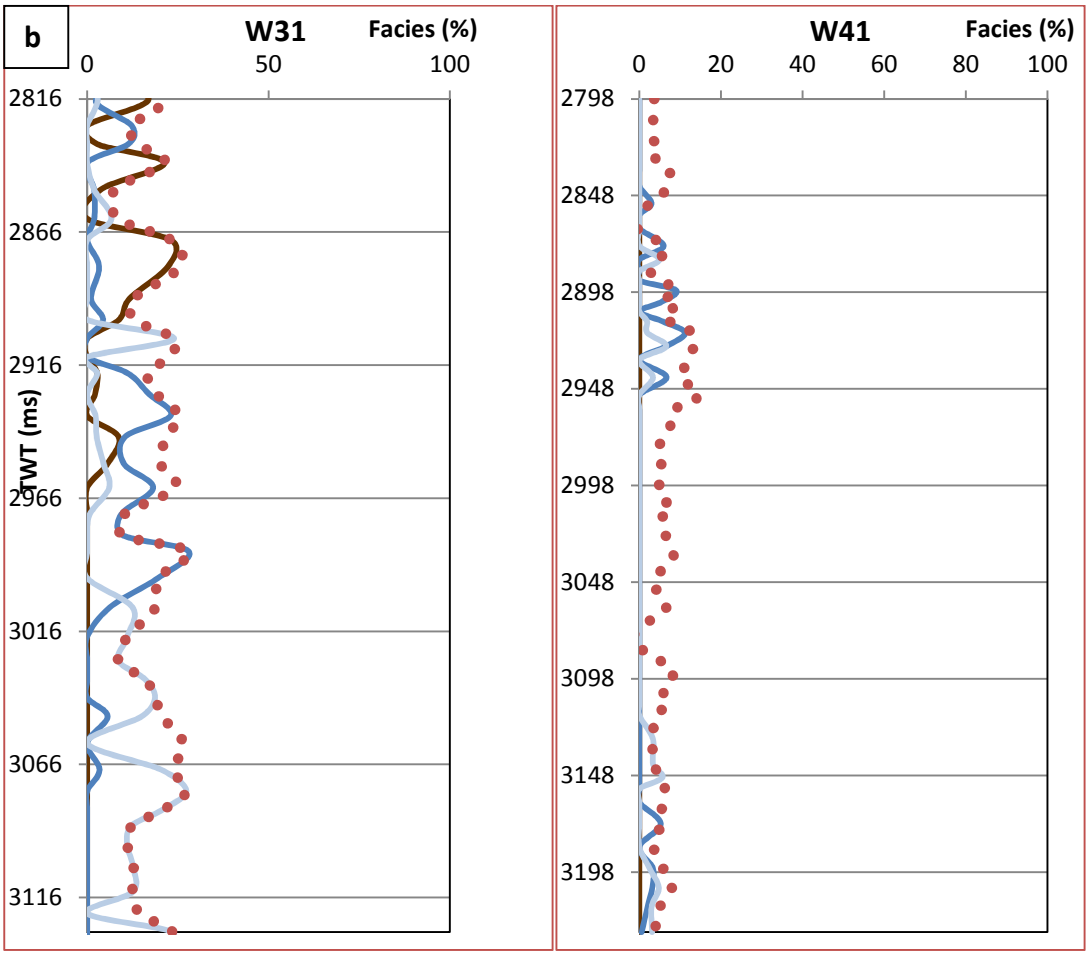

Facies No.	Facies Name	Colour
1	Hemipelagic Shales	
2	Mud Turbidites UP	
3	Mud Turbidites LP	
4 – 11, 15-16	Sands	
12	Muddy Debris Flow	
13	Muddy-Sandy Debris Flow	
14	Sandy Debris Flow	

Figure 4.11: *Predicted frequencies of component facies from Bayesian probability calculations within seal unit 4 of wells W31 and W41: for a) non-distorted muds and b) distorted muds. The dotted lines represent the sub-lithoclass frequencies, whilst the solid three lines show the predicted frequencies of the component facies. Note that Bayesian calculation depends on both facies frequency and distribution. For example, seal unit 4 within well W41 is dominated by non-distorted muds so that Bayesian division of distorted muds is not feasible.*

Table 4.8: *Overall average relative absolute errors for predicted frequencies by Bayesian probability calculations at different resolution levels (calculated for seal unit 4 in wells W31, W41 and W42)*

Average relative absolute error %	Non-distorted muds			Distorted muds		
	Mud Turbidites UP	Mud Turbidites LP	Muddy Debris Flow	Hemipelagic Shales	Muddy Sandy Debris Flow	Sandy Debris Flow
For each facies	19.3	10.0	22.0	54.8	42.0	67.5
For each muds sub-lithoclass	17.1			54.8		

4.5 Discussion

The seismically constrained geostatistical approaches used in reservoir facies modelling are not easily applicable in the relatively poorly-resolved and low amplitude context of seal rocks. Therefore the purpose of this study was to develop an integrated, probabilistic approach for translating seal seismic responses into lithological values. The results suggest that a stepwise approach is required, in which at different levels of resolution, different probabilistic methods should be applied to establish the link between seal logfacies and seismic attributes. Conventional cross-plotting was only effective in discriminating between sand and mud lithoclasses by use of Seismic SRF or Reflection Intensity, with R-squared values of 50% - 60%. This is mainly due to limitation of univariate cross-plotting and the fact that a single seal quality attribute cannot define the characteristics of the fine-grained logfacies. At finer resolution, the application of stepwise forward multivariate regression resulted in robust, multiattribute transforms to estimate the frequencies of two muds sub-lithoclasses, suggesting that we can effectively predict the probability of three different lithologies - distorted muds, non-distorted muds and sands (Equation 4.10) - away from wellbores. When high-density post-stack time-migrated seismic volumes are available, we believe that the prediction of these three lithologies is the practical optimum predictive power of seismic seal quality attributes for seal lithology identification. Thus, further division of muds sub-lithoclasses into facies frequencies was performed by Bayesian analysis which honoured wellbore statistics. In particular, prediction errors considerably reduced for facies of non-distorted muds. Although this step was not directly guided by seismic attributes and Bayesian probabilities derived at well locations, the consistent distribution of facies at all wellbore locations reasonably acknowledged the use of Bayesian probabilities away from wellbores. In the ideal case, results should be calibrated with an a priori lithofacies model derived by conditional simulations such as sequential indicator simulations (SIS). However, as mentioned earlier, running conditional simulations within mud-rich sediment sequences are often not feasible due to the limitations in seismic data quality (low signal:noise) and wellbore data availability within seal intervals.

Our findings integrate and extend the approaches taken by Doyen et al. (1994) and Hampson et al. (2001), who used a single attribute to predict sandiness, and multiple attributes to predict a continuous property (i.e. porosity) in clastic reservoirs. In this study we took a step in the direction of hierarchically applying 3D attribute analysis to predict a categorical property (i.e. facies) at different resolution of interest within mud-rich sediment sequences, while replacing the convolutional operator with multiple shifted pick-trough time intervals calculations.

There were two main conflicting points between the findings and theories/literature. First, the cross-plotting results suggested that conventional detrending techniques may not be suitable for facies recognition in the seal intervals. This is in contrast to the work of Nivlet et al. (2007) who achieved improved seismic-well tie when using detrended logs in turbidite reservoirs of a West African case study. The possible explanation would be the relatively lower compaction coefficient in mud-rich sediments with low porosities (e.g. Revil et al., 2002) and also sensitivity of log curves to detrending due to subtle variation of log response within these sediments.

In the other conflicting point, the data-driven classification of facies within muds sub-lithoclasses (Section 4.4.2) is not in agreement with sedimentology of the facies: the *Hemipelagic Shales* facies with excellent sealing quality was grouped with coarser grained *Sandy/Muddy-Sandy Debris Flow* facies with higher risk of leakage. This illustrates the fact that seismic attributes calculated at full seismic bandwidth are not able to genetically discriminate between seal facies. In other words, we have deposition of fine-grained facies with slightly different acoustic properties in the seal intervals, thus sub-seismic variations of facies do not exert much influence on seismic responses in this seismic bandwidth (a seismic volume with a higher resolution is required to resolve the individual seal facies). The factors that make seismic attributes impotent are geometry and reflectivity differences between seismic-scale, mud-rich sedimentological settings with different frequencies and arrangements of fine-grained facies.

The advantage of the developed approach is that it is relatively generic and is easy to apply to other datasets. It is a data-driven, interpreter-guided approach which returns a quantitative, fast and objective overview of seal lithology variations while

honouring manual interpretations/mappings and geological contexts. Moreover, the approach can work with limited wireline datasets. On the other hand, as one of the very first quantitative approaches for seal lithology analysis at the seismic scale, the approach has some limitations. Firstly, since seismic and log data were correlated over a time window, the approach always requires an accurate depth-to-time conversion based on check-shot data. It also has a very limited ability to capture spiky (log-scale) variations of logfacies. This is partly caused by the need to work with the full seismic bandwidth within low S/N ratio seal context. Similar to soft computing techniques, the reliability of predictions of logfacies depends on their frequency and spatial organisation. For example, high uncertainty is expected for prediction of logfacies/group of logfacies which make(s) up a small proportion of the seal interval. Moreover, the use of Bayesian division can be only justified if consistent proportional distributions of logfacies exist within the seal interval at all wells. Our approach needs be replicated in other case studies which have substantial well data, so that results can be calibrated with conditional simulations. It may then be possible to recommend the general use of Bayesian multiattribute transforms for lithology prediction within seal intervals. Finally, the incorporation of image logs and dip information into the log recognition process as well as the use of post-stack depth-migrated volumes have the potential to improve local structural dip-to-facies calibration, and hence to increase the reliability of derived multiattribute transforms.

4.6 Conclusions

We have developed a three-step approach to build a mathematical model for converting seismic seal quality attributes into frequencies (probabilities) of six different fine-grained logfacies in seal intervals. This cube translation generates useful information about the frequency and distribution of risky/non-risky lithologies throughout the seal unit. Since the approach is based on standard volumetric attributes and logfacies recognition processes, it is readily applicable on case studies with high-density 3D seismic volumes and with limited wireline data.

From a hydrocarbon exploration point of view, the quantification of seal lithology probabilities can help to mitigate risk in exploration and appraisal phases of new ventures. The approach outlined in this study can help to make more informed, seismically-driven decisions regarding well locations with lower risk of seal

breaching. The approach can also have similar application in other fields such as waste disposal and carbon capture storage.

Secondly, the derived litho-probability cubes provide a platform for flow property modelling within mud-rich sediment sequences and can help basin modellers with running more realistic flow simulations which honour heterogeneities within these sediments. And finally, litho-probability cubes can be also used as objective, data-driven and seismic-scale inputs for hydrocarbon/flow migration packages such as Permedia.

4.7 References

Amour, F., Mutti, M., Christ, N., Immenhauser, A., Agar, S.M., Benson, G.S., Tomás, S., Always, R. and Kabiri, L., 2012, Capturing and modeling metre-scale spatial facies heterogeneity in a Jurassic ramp setting (Central High Atlas, Morocco). Sedimentology, 59, pp 1158-1189.

Anderberg, M. R., 1973, Probability and mathematical statistics.

Archer, S. H., Du, X. and Fletcher, R. P., 2013, June, Amplitude inversion of depth-imaged seismic data from areas with complex geology. In 75th EAGE Conference & Exhibition incorporating SPE EUROPEC 2013.

*Aydin, A., 2000, Fractures, faults, and hydrocarbon entrapment, migration and flow. Marine and Petroleum Geology, 17(**7**), pp 797-814.*

*Baldwin, B. and Butler, C. O., 1985, Compaction curves. AAPG Bulletin, 69(**4**), pp 622-626.*

*Biver, P., Haas, A. and Bacquet, C., 2002, Uncertainties in facies proportion estimation II: application to geostatistical simulation of facies and assessment of volumetric uncertainties. Mathematical geology, 34(**6**), pp 703-714.*

Biver, P., Allard, D. and D'or, D., 2008, Litho-type modeling using soft probabilities from seismic attributes and other sources of information. In International geostatistics congress.

*Bjørlykke, K., 1993, Fluid flow in sedimentary basins. Sedimentary Geology, 86(**1**), pp 137-158.*

Bjørlykke, K., 2010, Petroleum geoscience: From sedimentary environments to rock physics. Springer.

Bortoli, L.J., Alabert, F., Haas, A. and Journel, A.G., 1992, Constraining stochastic images to seismic data. In Soares A., Ed., In proceeding: International Geostatistics Congress, Troia, Kluwer Academic Publication.

Buland, A., Kolbjørnsen, O., Hauge, R., Skjæveland, Ø. and Duffaut, K., 2008, Bayesian lithology and fluid prediction from seismic prestack data. Geophysics, 73(3), pp C13-C21.

*Chakraborty, A. and Okaya, D., 1995, Frequency-time decomposition of seismic data using wavelet-based methods. Geophysics, 60(**6**), pp 1906-1916.*

Chehrazi, A. and Rezaee, R., 2012, A systematic method for permeability prediction, a Petro-Facies approach. Journal of Petroleum Science and Engineering, 82, pp 1-16.

Chiles, J. P. and Delfiner, P., 1999, Modeling spatial uncertainty. Geostatistics, Wiley Series in Probability and Statistics. New York: Wiley Interscience.

Clemetsen, R., Hurst, A.R., Knarud, R. and Omre, H., 1990, A computer program for evaluation of fluvial reservoirs, North Sea Oil and Gas Reservoirs II: Graham and Trotman. Springer Netherlands. pp 373-385.

Coleou, T., 2002, May, Time-lapse filtering and improved repeatability with automatic factorial co-kriging. AFACK. In 64th EAGE Conference & Exhibition.

*Costa, A., 2006, Permeability-porosity relationship: A reexamination of the Kozeny-Carman equation based on a fractal pore-space geometry assumption. Geophysical research letters, 33(**2**).*

*Damsleth, E., Tjolsen, C.B., Omre, H. and Haldorsen, H.H., 1992, A two-stage stochastic model applied to a North Sea reservoir. Journal of Petroleum Technology, 44(**4**), pp 402-486.*

*Dashtian, H., Jafari, G. R., Lai, Z. K., Masihi, M. and Sahimi, M., 2011, Analysis of cross correlations between well logs of hydrocarbon reservoirs. Transport in porous media, 90(**2**), pp 445-464.*

de Waal, J. A., 1986, On the rate type compaction behaviour of sandstone reservoir rock. Technische Hogeschool Delft.

*Delfiner, P., Peyret, O. and Serra, O., 1987, Automatic determination of lithology from well logs. SPE Formation Evaluation, 2(**03**), pp 303-310.*

*Dewhurst, D. N., Aplin, A. C., Sarda, J. P. and Yang, Y., 1998, Compaction-driven evolution of porosity and permeability in natural mudstones: An experimental study. Journal of Geophysical Research: Solid Earth (1978–2012), 103(**B1**), pp 651-661.*

Doyen, P. M., Psaila, D. E. and Strandenes, S., 1994, January. Bayesian sequential indicator simulation of channel sands from 3-d seismic data in the Oseberg field Norwegian North Sea. In SPE Annual Technical Conference and Exhibition. Society of Petroleum Engineers.

Doyen, P., Den Boer, L. and Pillet, W., 1996, June. Seismic porosity mapping in the Ekofisk Field using Bayesian stochastic simulation. In 58th EAEG Meeting.

Drews, M., 2012, Modelling stress-dependent effective porosity-permeability relationships of metre-scale heterogeneous mudstones. PhD Thesis, Newcastle University, 164 p.

*Dubrule, O., Thibaut, M., Lamy, P. and Haas, A., 1998, Geostatistical reservoir characterization constrained by 3D seismic data. Petroleum Geoscience, 4(**2**), pp 121-128.*

Dubrule, O., 2003, Geostatistics for seismic data integration in Earth models. 2003 Distinguished Instructor Short Course (No. 6), SEG Books.

*Falivene, O., Arbués, P., Howell, J., Muñoz, J. A., Fernández, O. and Marzo, M., 2006, Hierarchical geocellular facies modelling of a turbidite reservoir analogue from the Eocene of the Ainsa basin, NE Spain. Marine and Petroleum Geology, 23(**6**), pp 679-701.*

*Fournier, F. and Derain, J. F., 1995, A statistical methodology for deriving reservoir properties from seismic data. Geophysics, 60(**5**), pp 1437-1450.*

*Frey-Martínez, J., Cartwright, J. and James, D., 2006, Frontally confined versus frontally emergent submarine landslides: a 3D seismic characterisation. Marine and Petroleum Geology, 23(**5**), pp 585-604.*

*Geertsma, J., 1973. Land subsidence above compacting oil and gas reservoirs. Journal of Petroleum Technology, 25(**6**), pp 734-744.*

*Gray, F. D., Anderson, P. F. and Gunderson, J. A., 2006, Prediction of shale plugs between wells in heavy oil sands using seismic attributes. Natural Resources Research, 15(**2**), pp 103-109.*

Gray, D., 2011. Oilsands: Not your average seismic data. CSEG abstract.

Grijalba-Cuenca, A., Torres-Verdin, C. and van der Made, P., 2000, Geostatistical inversion of 3D seismic data to extrapolate wireline petrophysical variables laterally away from the well. In proceedings: SPE Annual Technical Conference and Exhibition. 63283.

Guardiano, F.B. and Srivastava, R.M., 1993, Multivariate geostatistics: beyond bivariate moments. In Geostatistics. Springer Netherlands.ith efficiency. In SPE annual technical conference Troia'92, pp 133-144.

*Haas, A. and Dubrule, O., 1994, Geostatical inversion-a sequential method of stochastic reservoir modelling constrained by seismic data. First Break, 12(**11**).*

*Haas, A. and Formery, P., 2002, Uncertainties in facies proportion estimation I. Theoretical framework: the Dirichlet distribution. Mathematical geology, 34(**6**), pp 679-702.*

*Hampson, D. P., Schuelke, J. S. and Quirein, J. A., 2001, Use of multiattribute transforms to predict log properties from seismic data. Geophysics, 66(**1**), pp 220-236.*

Handayani, T., Irwanzah, Z., Taslim, M., Kurniadi, D., Dogra, S., Nalonnil, A. and Carillo, P., 2011, Exploring the interwell reservoir space with crosswell imaging and interpretation: an example of multi scale data integration from Indonesia. In International Petroleum Technology Conference. International Petroleum Technology Conference.

Harris, J.M, Nolen-Hoeksema, R.C., Langan, R.T., Van Schaack, M., Lazaratos, S.K. and Rector, III, J.W., 1995, "High-resolution crosswell imaging of a west Texas carbonate reservoir: Part 1—Project summary and interpretation." High-resolution crosswell imaging of a west Texas carbonate reservoir: Part 1—Project summary and interpretation 60, special issue, pp 667-681.

*Hart, B. S. and Balch, R. S., 2000, Approaches to defining reservoir physical properties from 3-D seismic attributes with limited well control: An example from the Jurassic Smackover Formation. Alabama. Geophysics, 65(**2**), pp 368-376.*

*Hegstad, B.K. and Henning, O., 2001, Uncertainty in production forecasts based on well observations, seismic data, and production history. SPE Journal, 6(**4**), pp 409-424.*

*Hitchon, B. and Hays, J., 1971, Hydrodynamics and hydrocarbon occurrences, Surat Basin, Queensland, Australia. Water Resources Research, 7(**3**), pp 658-676.*

*Holden, L., Hauge, R., Skare, Ø. and Skorstad, A., 1998, Modeling of fluvial reservoirs with object models. Mathematical Geology, 30(**5**), pp 473-496.*

Ingram, G. M., Urai, J. L. and Naylor, M. A., 1997, Sealing processes and top seal assessment. Norwegian Petroleum Society, Special Publications, 7, pp 165-174.

Insalaco, E., Marion, D., Michel, B. and Rowbotham, P., 2001, Reservoir-scale 3D sedimentary modelling: Approaches and impact of integrating sedimentology into the reservoir characterization workflow. In proceedings: AAPG Annual Meeting.

*Journel, A.G., and Gomez-Hernandez, J.J., 1993, Stochastic imaging of the Wilmington clastic sequence. SPE formation Evaluation, 8(**1**), pp 33-40.*

*Kalkomey, C. T., 1997, Potential risks when using seismic attributes as predictors of reservoir properties. The Leading Edge, 16(**3**), pp 247-251.*

Kohonen, T., 1997, Learning vector quantization. In Self-Organizing Maps. Springer Berlin Heidelberg. pp. 203-217.

*Kohonen, T., 1998, The self-organizing map. Neurocomputing, 21(**1**), pp 1-6.*

Lamy, P., Swaby, P.A., Rowbotham, P.S., Dubrule, O. and Haas, A., 1998, From seismic to reservoir properties using geostatistical inversion. In proceedings: SPE annual technical conference, pp 535-545.

Lee, P. M., 2012, Bayesian statistics: an introduction. John Wiley & Sons.

Leonard, J. A., Kramer, M. A. and Ungar, L. H., 1992, Using radial basis functions to approximate a function and its error bounds: IEEE Trans. on Neural Networks, 3, pp 624–627.

Lia O., Tjelmeland H. and Kjellesvik L.E., 1996, Modeling of facies architecture by marked point models. In: Baafi E, Schofield N (eds) Geostatistics Wollongong'96, 1, Kluwer Academic, Dordrecht, pp 386–387.

Lo, T.W. and Bashore, W.M., 1999, Seismic constrained facies modeling using stochastic seismic inversion and indicator simulation a North Sea example. In proceedings: 1999 SEG Annual Meeting. Society of Exploration Geophysicists.

MacDonald, A.C., Berg, J.I., Skare, Ø. and Holden, L., 1995, Constraining a stochastic model of channel geometries using seismic data. In proceeding: 57th EAEG Meeting.

*Malki, H.A. and Anwar, M.S., 2003, Determination of lithofacies from well logs using unsupervised neural network model. The Technology Interface. Electronic Jour. Eng. Tech., 5(**1**), pp.947–964*

Magara, K., 1986, Geological models of petroleum entrapment. Springer.

*Marfurt, K. J. and Kirlin, R. L., 2001, Narrow-band spectral analysis and thin-bed tuning. Geophysics, 66(**4**), pp 1274-1283.*

*Marinho, E.B.S., Sousa, A.M.Y.R. and Andrade, R.F.S., 2013, Using detrended cross-correlation analysis in geophysical data. Physica A: Statistical Mechanics and its Applications, 392(**9**), pp 2195-2201.*

Mazur, D R., 2010, Combinatorics: a guided tour. MAA Textbooks.

*McArdle, N. J. and Ackers, M. A., 2012, Understanding seismic thin-bed responses using frequency decomposition and RGB blending. First Break, 30(**12**).*

*Moscardelli, L. and Wood, L., 2008, New classification system for mass transport complexes in offshore Trinidad. Basin Research, 20(**1**), pp 73-98.*

*Mukerji, T., Jørstad, A., Avseth, P., Mavko, G. and Granli, J. R., 2001, Mapping lithofacies and pore-fluid probabilities in a North Sea reservoir: Seismic inversions and statistical rock physics. Geophysics, 66(**4**), pp 988-1001.*

Neal, J. and Krohn, C., 2012, Higher Resolution Subsurface Imaging, Article 5 in R&D Grand Challenges-JPT Article Series. Paper SPE 163061. SPE Journal of Petroleum Technology, pp 44-53.

*Nivlet, P., Lefeuvre, F. and Piazza, J. L., 2007,3D seismic constraint definition in deep-offshore turbidite reservoir. Oil & Gas Science and Technology-Revue de l'IFP, 62(**2**), pp 249-264.*

Park, N.W. and Jang, D.H., 2014, Comparison of geostatistical kriging algorithms for intertidal surface sediment facies mapping with grain size data, The Scientific World Journal, 2014, 11 p.

*Pyrcz, T. W. and Garlacz, R., 2012, The presence–absence situation and its impact on the assemblage structure and interspecific relations of Pronophilina butterflies in the Venezuelan Andes (Lepidoptera: Nymphalidae). Neotropical entomology, 41(**3**), pp 186-195.*

Rao, C. R., 1973, Linear statistical methods and its applications. Second Edition, Wiley Series in Probability and Statistics.

*Revil, A., Grauls, D. and Brévart, O., 2002, Mechanical compaction of sand/clay mixtures. Journal of Geophysical Research: Solid Earth (1978–2012), 107(**B11**), ECV-11.*

*Rocha, M. P., Leite, L. W., Santos, M. D. L. and Farias, V. J. D. C., 2007, Attenuation of multiple in reflection seismic data using Kalman–Bucy filter. Applied mathematics and computation, 189(**1**), pp 805-815.*

Rogers, S.J., Fang, J.H., Karr, C.L. and Stanely, D.A., 1992, Determination of lithology from well logs using neural networks. AAPG Bulletin, 76, pp.731–739.

Rowbotham, S.P., Marion, D., Lamy, P., Swaby, P.A. and Rabary, G., 2000, Detailed reservoir characterisation of the Elgin Field using geostatistical inversion. In proceeding: 62nd EAGE Conference and Exhibition.

Ryser, H. J., 1963, Combinatorial mathematics. MAA Textbooks, New York.

*Sayman, A., 1992, Application of Kalman filter to synthetic seismic traces. Jeofizik, 6(**2**), pp 67-75.*

Shrestha, R. K., and Boeckmann, M., 2002, January, Stochastic seismic inversion for reservoir modeling. In 2002 SEG Annual Meeting. Society of Exploration Geophysicists.

*Sinha, S., Routh, P. S., Anno, P. D. and Castagna, J. P., 2005, Spectral decomposition of seismic data with continuous-wavelet transform. Geophysics, 70(**6**), P19-P25.*

*Specht, D. F., 1991, A general regression neural network. Neural Networks. IEEE Transactions on, 2(**6**), pp 568-576.*

Strébelle S. and Journel, A.G., 2000, Sequential simulation drawing structures from training images. In: Kleingeld, W.J. and Krige, D.G. (eds), Geostatistics 2000, 6th international geostatistics congress, Geostatistical Association of Southern Africa, Cape Town, South Africa, pp 381–392.

*Strebelle, S., 2002, Conditional simulation of complex geological structures using multiple-point statistics. Mathematical Geology, 34(**1**), 1-21.*

*Strebelle, S. and Levy, M., 2008, Using multiple-point statistics to build geologically realistic reservoir models: the MPS/FDM workflow. Geological Society, London, Special Publications, 309(**1**), pp 67-74.*

Viseur, S., 1999, Stochastic boolean simulation of fluvial deposits: a new approach combining accuracy and efficiency. In Proceedings: SPE annual technical conference and exhibition, Houston.

Wang, G. and Carr, T.R., 2012, Methodology of organic-rich shale lithofacies identification and prediction: a case study from marcellus shale in the Appalachian basin. computers and geosciences, 49, pp 151-163.

*Wang, G. and Carr, T.R., 2013, Organic-rich Marcellus Shale lithofacies modeling and distribution pattern analysis in the Appalachian Basin. AAPG bulletin, 97(**12**), pp 2173-2205.*

Wang, G., Carr, T.R., Ju, Y. and Li, C., 2014, Identifying organic-rich Marcellus Shale lithofacies by support vector machine classifier in the Appalachian basin. Computers & Geosciences, 64, pp 52-60.

Wolff, M., and Pelissier-Combescure, J., 1982, Faciolog—automatic electrofacies determination.in Transactions, 23rd annual logging symposium, paper FF, Society of Professional Well Log Analysts, Houston, 23 p.

Yarus, J.M., Yang, K., Sriisraporn, S., Chuemthaisong, N. and Sangwongwanich, K., 2000, Integrating 3d seismic and geostatistics; building a 3D model of a Tertiary deltaic and shallow marine deposit Malay Basin Offshore Gulf of Thailand. In proceeding: Offshore Technology Conference.

*Yu, G., Marion, B., Bryans, B., Carrillo, P., Wankui, G., Yanming, P. and Fanzhong, K., 2008, Crosswell seismic imaging for deep gas reservoir characterization. Geophysics, 73(**6**), pp B117-B126.*

5 Summary and Conclusions

5.1 Summary and key results

The key results of this research should be seen in the light of the case study used. Although West Africa case study has high-density post-stack time migrated (PSTM) seismic data with good quality log suites and variable mud-rich sediment sequences, the derived correlations might be different for other seismic data sets and sedimentary basins. Hereby, the developed approach should be considered as a basis/starting point for a generic quantitative log and seismic analysis, thus facies modelling, in heterogeneous mud-rich sediments. Application of other seismic volumes (e.g. pre-stack, post-stack depth migrated (PSDM), and multi-component) and logs (e.g. image log, dip meter, and dipole sonic) can refine the workflow and improve the efficiency of predictions, but the templates, schemes and key steps can be applicable to any case study, where limited conventional log and reservoir sample/core data are available with a high-density seismic volume.

In the framework of logfacies recognition, we found that the majority of conventions for log processing and design factors are not applicable to mud-rich sediment sequences. Thus a new logfacies recognition approach was introduced in which the generic IPSOM engine was supplied with series of new pre-processing, design constraints and validation techniques. In West Africa case study, the new approach led to recognising seal logfacies based on the conventional log suite and to extrapolating core descriptions from the reservoir to the fine-grained seal unit.

We showed that the recognition accuracy is irrespective of electrofacies classification scheme, log detrending or logging tool calibration, and mainly controlled by IPSOM design parameters, knowledge derived from supporting data (such as seismic) and input log types. In West Africa case study, the overall recognition accuracy in local calibration cases reached up to 80-90% in the pilot wells. Although few pilot wells were provided for the blind recognition, the recognition accuracy significantly improved using the seismic guide so that the similarity of seismic characters along the seal formation used as the selection criteria for training well(s). We concluded that in mud-rich sediment sequences the degree of heterogeneity of vertical distribution of logfacies can be considered as a good proxy for the level of seismic amplitude and frequency at well locations.

In the seismic attribute analysis, we have developed the very first quantitative approach for textural seal risk assessment based on volumetric seismic attributes. Application of the proposed approach on modern seismic surveys can save days of manual mapping time and reduce exploration risk by basing decisions on seal texture and their proven link to leakage elements. By defining the seal risk factor (SRF) attribute we were able to take into account all three leakage important characters (i.e. sandiness, chaoticness and verticality) according to the proposed seal texture model. At the pick-trough time interval scale (in case study A ~ 10 m), we showed that synthetic SRF curve can be estimated from a linear combination of multiple logfacies frequencies within a mud-rich section and the less risky seismic units often occur with higher percentage of muddy facies and vice versa. The SRF can effectively detect areas with good seal quality; however, delineated areas with high SRF need further investigations (e.g. wellbore data integration and AVO analysis) before making conclusive interpretation. The functionality of the SRF can be improved if the component attributes extract from other 3D seismic sources (e.g. pre-stack or PSDM seismic volumes) or introduce fractures into the seal texture model using azimuthal-stack data.

In a final step, the seismic attribute analysis result has been integrated with the logfacies recognition to generate lithofacies models within mud-rich sediment sequences. The mud lithofacies model allows us to make informed seismically-driven decisions about well locations with lower risk of seal breaching or to take into account lithological distributions and heterogeneities within mud-rich sediment sequences in basin flow simulation, CO2 sequestration or waste disposal studies. In this study, a three-step approach was proposed to build mathematical models for translating seal quality attributes into frequency/probability of six different fine-grained lithofacies within seal unit-4 in West Africa case study. A combination of cross-plotting, forward multiattribute regression and Bayesian techniques has been applied at the pick-trough time interval scale to estimate the probabilistic mud-rich facies frequencies. We kept the same reflection interval selections as conducted earlier in this thesis. We showed that a single seismic seal quality attribute can reliably discriminate sand and mud lithoclasses through nonlinear relationships. At the next level, forward multiattribute regression analysis has been implemented to split the mud lithoclass into distorted and non-distorted muds. Non-distorted muds

include the group of mud facies with layered and organised seismic texture, hence lower leakage risk. However, hemipelagic shale-dominated intervals with good seal quality often occurred with poorly resolved and distorted seismic texture. This could indicate the limitation of seismic resolution in high-density seismic at full seismic bandwidth, which should alarm geomodellers dealing with mud-rich sediment sequences dominated by hemipelagic shale facies. Mud sub-lithoclasses have been divided into their logfacies components using Bayesian analysis so that the prediction significantly relied on the wellbore and recognition results rather than seismic data. The lithology predicted in three lithological levels/resolutions associated with different level of uncertainty. The developed approach is generic and can be applied to other siliciclastic seal sequences as long as a high-density 3D seismic volume, conventional log suites (at reservoir and seal intervals) and reservoir core/sample data are provided.

5.2 Limitations and future work

Despite the growing importance of mud-rich sediments, their seismic-log characterisation is still at the early stage so that substantial future work can be considered for the current study:

- Although the developed approach can work with any high-density seismic amplitude cube, the entire seal quality component attributes have been computed on PSTM seismic amplitude cubes only. Applying different seismic amplitude cubes such as pre-stack and PSDM cubes might give different results and should be addressed/compared in future studies, in particular with regard the relations between seismic amplitude and sandiness (in a pre-stack amplitude cube) and seismic local structural dip and sediment verticality (in a PSDM amplitude cube).
- In addition, in this study SRF only includes three seal quality component attributes. The fourth seal quality component attribute, fracture, should be considered in future studies, providing that seismic azimuthal-stack data are available for azimuthal anisotropy analysis (AVAZ). Fractures can play an important role in the fluid flow within mud-rich sediments; however, their seismic interpretation can be tricky and misleading using PSTM data.

- In Chapter 3, the results were based on the assumption that seismic characters in mud-rich seal units are mainly controlled by their corresponding geological characteristics. This may only be valid in siliciclastic mud-rich sediment sequences with relative lateral continuity and low hydrocarbon saturation. The assumption is no longer valid when a mud-rich sediment sequence is associated with calcareous sediments or if the seismic reflections are significantly affected by pore fluid content (e.g. gas pocket). Therefore, further studies should include mud-rich overburden sediment sequences with a wider range of lithology and geological settings in order to achieve more generic log-seismic lithology predictions.
- The application of SRF to the whole seismic volume should be treated with care for depth dependency of the seismic attributes because relative acoustic responses from muds and sands vary with depth. Furthermore, given the whole seismic volume, there are other sedimentary units than seals which may share similar seismic characteristics, and hence be difficult to discriminate using an interactive attributes combination. It is, therefore, recommended to calculate a feature-based seismic SRF using neural network training.
- Seismic quality strongly controls the extent to which structural/stratigraphic interpretations can be made in low amplitude mudstones. In the current research, we did not undertake any post-processing of the seismic data but recognise that this could help to improve signal:noise ratio and thus reduce uncertainties in the quantitative interpretations and seismic-well ties. This could involve improvement of routine filtering such as tuning effect removal by wedge methods in hemipelagic seismic facies or more complicated seismic processing like Kalman filters.
- This study is mainly focused on the evaluation of seal risk based on the internal texture and using volume attributes. Although chaoticness and dip attributes do help to detect faults and other discontinuities, the potential importance of vertical conduits for leakage means that a bypass cube would be a sensible, complementary volume for our established SRF volume. In

addition, RMS slices of SRF can be compared / calibrated with the textures detected by seismic surface attributes.

- Finally, image log and dip-meter log data have not been used in the logfacies recognition process. Since core data are rare in seal intervals, these log data can be used not only to cross-validate the logfacies recognition results, but also to quality control the attribute computation results (e.g. dip attribute), and finally improve the robustness of the lithology prediction results.